Master Thesis

Retrofitting of Unreinforced Masonry Buildings with Timber Elements

Earnest Alderliesten

TU Delft

abt

Retrofitting of Unreinforced Masonry Buildings with Timber Elements

Master thesis

by

Earnest Alderliesten

to obtain the degree of Master of Science
at the Delft University of Technology,
to be defended publicly on Wednesday October 16, 2019 at 4:00 PM.

Student number:	4225430	
Project duration:	September, 2018 – October, 2019	
Graduation committee:	Prof. dr. ir. J. W. G. van de Kuilen,	TU Delft, Chairman
	Dr. ir. G. J. P. Ravenshorst,	TU Delft
	Dr. ir. K. C. Terwel,	TU Delft
	Ir. H. G. Krijgsman RO,	ABT bv

Preface

Before you lies the Master Thesis ”Retrofitting of Unreinforced Masonry Buildings with Timber Elements”. The research has been completed in the time period from September 2018 until October 2019 in order to obtain the Master of Science degree in Building Engineering at the Faculty of Civil Engineering and Geosciences at Delft University of Technology.

First of all, I want to thank my graduation committee: Han Krijgsman, Jan-Willem van de Kuilen, Geert Ravenshorst and Karel Terwel for their guidance, assistance and advice during the whole research period. I would like to thank ABT for giving me the opportunity to conduct this research in their name and providing me with excellent facilities during the thesis. Furthermore, I thank all my colleagues from both BORG and ABT for answering questions, giving advice and the overall pleasant working environment. Special thanks goes to Ersan Erdogan, for always being there to help me when I got stuck.

Lastly, special thanks to family, friends and Marianna for their support and presence throughout this challenging period.

Earnest Alderliesten
Delft, October 2019

Abstract

Due to gas extraction, seismic activity has become a major problem in the province of Groningen. Existing buildings are not designed to withstand seismic loads and are likely to be structurally unsafe. Two storey terraced houses with concrete floors and large openings in the ground floor façade walls are considered vulnerable, since the in-plane behaviour of these walls is weak. This research aims to investigate the possibilities of enhancing the seismic in-plane performance of this building type with the application of timber elements.

Non-linear static pushover analyses are performed to assess the in-plane behaviour according to the Dutch guidelines for the Near Collapse limit state using a macro-element modelling approach in ETABS, a 3D non-linear analysis software. Variants of the typology are studied to investigate the sensitivity to certain geometrical and structural parameters, such as the height, width and depth of a building and the applied masonry type. Based on the results, a timber strengthening design is proposed and the effect on the behaviour is studied.

The majority of the un-strengthened buildings presents rocking behaviour caused by the slenderness of masonry piers due to the large openings in the façade walls. This ductile behaviour ensures relatively large lateral displacement capacities, often resulting in the satisfaction of the safety standards. Moreover, results show that structures with wide masonry piers, calcium silicate element masonry and extremely large openings at ground floor level (up until 70% of opening) are likely to be unsafe. Therefore, strengthening is required. Global capacity of the numerical models depends heavily on prescribed drift limits. Therefore, establishing the appropriate limits for each model is essential. The analysis indicates that assessment according to other guidelines, can lead to different outcomes.

The proposed retrofit design consists of a timber framework connected to the inner masonry piers, with an OSB panel nailed on top of it to increase the stiffness. The retrofit is attached to the foundation by tension anchors. Gravity loading of the structure is mainly carried by the masonry elements. Implementation results in stable rocking behaviour of the piers, which ensures higher displacement capacities. Analysis demonstrates that the application of the timber retrofit leads to the satisfaction of the Near Collapse limit state, when higher drift limits can be prescribed. Furthermore, applying the reinforcement results in a change from unfavourable shear behaviour to rocking behaviour. However, increase of strength is limited, since the resistance of the anchors to the lateral forces is largely depending on the design of the foundation and structural elements to which they are attached. Therefore, the retrofit is not suitable for significantly increasing lateral resistance, which is required for structures with extremely large openings in the façade walls. Experimental testing is recommended to quantify the increase of drift limits. An overall consistent definition of capacity values and corresponding drift limits for each possible failure mechanism is essential for reliable evaluation of the in-plane response, especially when buildings are assessed using non-linear analyses.

Contents

List of Figures

List of Tables

1. Introduction

1.1 Context

In 1959, during a quest for oil, natural gas was discovered near Kolham in Groningen. Since the sixties natural gas has been extracted from the bottom in the Northern part of Holland by the NAM (Dutch Petroleum Company). The Groningen gasfield is among the largest in the world and its discovery has therefore been of great importance to the Dutch economy.

The extraction takes place at a depth of 3 kilometers, where a layer of sandstone is present. The downside of the activity is the clinging of this sandstone layer, which causes fractures. Along these fractures a tension difference is created, which leads at certain moments to a sudden shift, also known as induced earthquake. Such an earthquake is the result of human activities. The first of this type took place in 1986 near Assen. Since then a lot more followed. The amount of earthquakes with a magnitude higher than 1.5 on the Richter Scale differs every year, ranging from 30 in 2013 to 15 in 2018 [1], see Figure 1.1. The heaviest induced earthquake observed took place in 2012 in Huizen and had a magnitude of 3.6 on the Richter Scale.

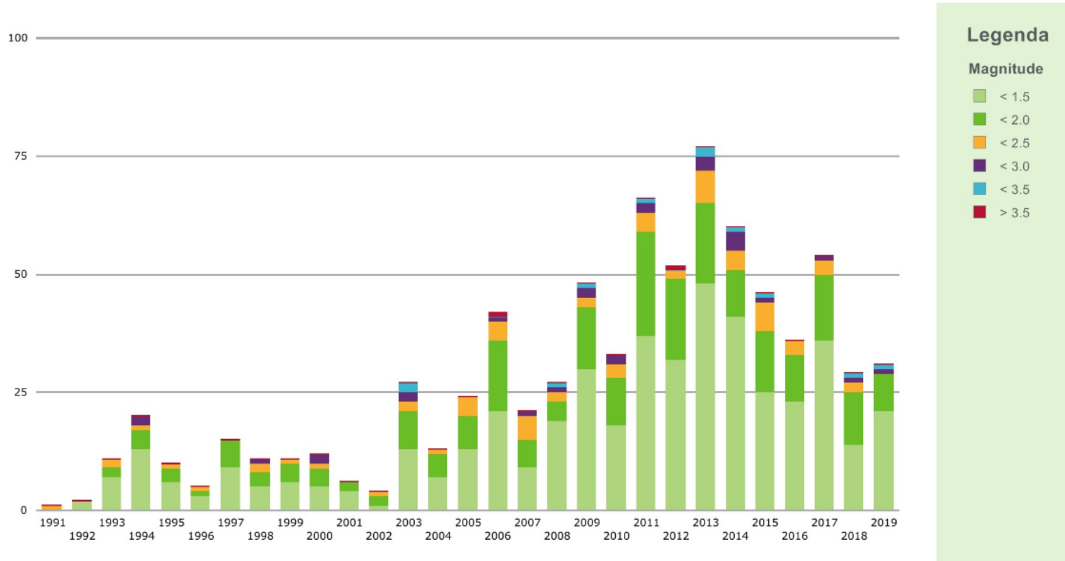

Figure 1.1: Number of earthquakes per year with a magnitude higher than 1.5 on the Richter Scale (Source:[1])

In contrast to a tectonic earthquakes, which occur at depth of 15 to 700 km below surface, induced earthquakes occur at a shallow depth, around 3 km below the surface. The hypocentral and epicentral distance of induced earthquakes to the ground surface is shorter and therefore a smaller area on the surface is affected, causing relatively less damage. Next to that, the spectrum of induced earthquakes is based on a single source with a relatively small magnitude, thus resulting in reduced energy and reduced amplification in the longer response period range.

Seismicity is a relatively new problem in the Netherlands. Up until 2012 there was not a seismic guideline in the Netherlands. Even though induced earthquakes usually cause less damage compared to tectonic earthquakes, the existing buildings in immediate vicinity of the gas fields in Groningen are not able to withstand these seismic loads. The structural safety of a large part of the building stock in this area cannot be guaranteed. Some of the existing houses are now strengthened with temporary measures, such as timber strut constructions, see Figure 1.2. A more permanent solution needs to be found. Although it can be argued that in the long term demolition and rebuilding is a more effective option, the replacement of all unsafe unreinforced masonry buildings is not desirable. Retrofitting existing structures in Groningen is and is going to be a big challenge. More research within this field is needed to find an adequate, sustainable and economical solution for the Groningen region.

Figure 1.2: Temporarily strengthened house in Groningen (Source: Kees van de Veen)

1.2 Problem statement

Based on previous assumptions about the future level of gas extraction and on the NPR 9998:2015, around 20.000 houses were thought to be structurally unsafe. However, in March 2018, the government decided that the extraction in Groningen will gradually be reduced and eventually be stopped in 2030 at the latest. This leads to a reduction of seismicity of the area. In a consultancy report about the safety risks and reinforcement task in Groningen from the Mijnraad [2], it was concluded that therefore less houses have to be reinforced. Instead of the aforementioned 20.000 houses approximately 1.500 houses (7.200 with margin of uncertainty) need to be strengthened.

The Meijdam Committee has recommended the safety standard 10¯5 per year, which prescribes the maximum acceptable chance that someone dies due to the consequences of an earthquake per year. When this safety standard is not reached, strengthening is needed. The amount of houses that needs to reinforced continues to decrease as a function of time. Eventually, all buildings meet the safety standard without any intervention (see the yellow line in Figure 1.3). The best strengthening strategy of the houses in Groningen is debatable. Either extensive retrofit measures are implemented, by which the safety standard is reached immediately (see blue line in Figure 1.3). Or more simple strengthening measures are implemented, which reduce the risk, so the safety standard is reached earlier in time compared to doing nothing (see green line in Figure 1.3).

Extensive retrofit plans demand more preparation time and ensure higher investments, however, the structure directly meets the safety standards. Furthermore, this kind of intervention requires extensive structural changes, which have more impact on the owners, due to higher costs and possibility of complete change of interior. At the time of implementing the risk is already further reduced, therefore the efficiency is questionable. More simple strengthening measures require less engineering time and can therefore be implemented earlier. Although they do not provide the required safety level at once, the risk is significantly reduced. The challenge is to make a trade off between the severity of strengthening and the preparation and implementation time needed to strengthen unsafe buildings in Groningen.

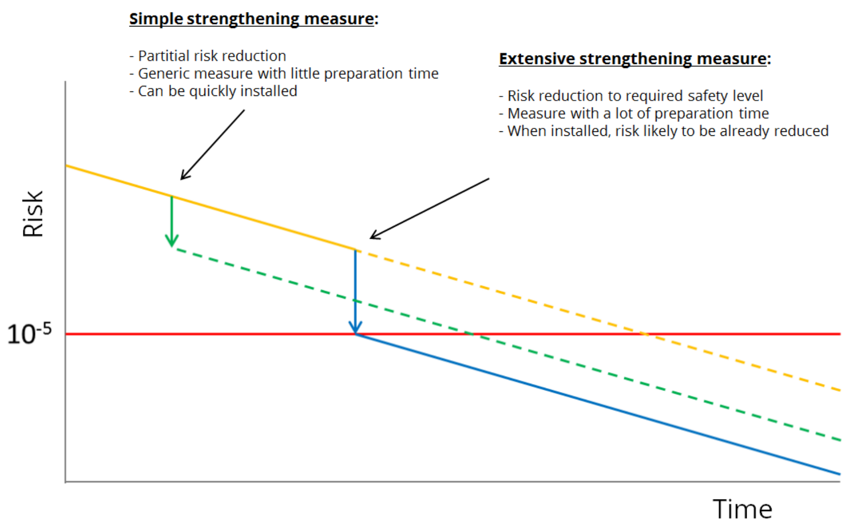

Figure 1.3: Risk vs time (Source: Adaptation of Appendix B4_1 of [2])

1.3 Objectives and research questions

The challenge for the Groningen region is to strengthen the most vulnerable existing buildings in an adequate, sustainable and economical way. Furthermore, a trade off between the level of strengthening and the preparation and implementation time has to be made, since the seismic hazard decreases in time.

The objectives of this research are the following:

- Investigate the characteristics of the most vulnerable building typology in Groningen
- Investigate the governing failure mechanisms of the most vulnerable building typology with the help of a numerical model
- Investigate and evaluate the options for strengthening measures by using timber elements
- Study the effect of the retrofit measures on the seismic performance of the chosen building typology with a numerical model

The objectives mentioned before lead to the following main research question:

“In what way could timber elements be used as an effective measure to improve the in-plane strength and therefore enhance the seismic performance of typical low-rise URM buildings in the Groningen area to satisfy the Near Collapse limit state?”

This question is approached with the help of the following sub questions:

- Which building typologies are typical for the Groningen area?
- What are the characteristics of the most vulnerable building typology?
- What are the governing failure mechanisms for geometric variants of the vulnerable building typology?
- Which seismic retrofit techniques regarding timber elements are accessible and integrable to strengthen URM buildings in-plane?
- What is the effect of the chosen retrofit measures on the seismic in-plane performance of the structure?
- Which strengthening measures are the most beneficial based on the effectiveness and provided structural safety?

1.4 Scope of thesis

A lot of research is done to find adequate, sustainable and economical solutions to strengthen the structurally unsafe existing buildings in Groningen. It is a complex problem with a lot of possible solutions. Narrowing down the scope helps to clarify the problem and study it at greater depth. The focus on this research is on the following subjects:

- One of the most vulnerable building typologies of the Groningen area; consisting of a two storey terraced house with concrete floors and large openings in the ground floor façade walls.
- Global in-plane failure mechanisms of the structure
- Use of non-linear pushover analysis for the structural analysis
- The use of timber as strengthening material

1.5 Reader's guide

In order to answer the research question and to be able to reach the stated objectives, the research is divided in several parts. The parts are described below.

Introduction
The introduction provides context and the problem statement. Furthermore, the objectives, outline, scope and limitations of the research are presented.

Part I: Literature study
The literature study provides background information on several topics to create a clear image of the problem. It addresses the following topics to obtain theoretical knowledge:

- Building typologies
- Seismic behaviour of URM structures
- Analysis strategy

Part II: Structural sensitivity analysis
In this part, a numerical model of the most vulnerable building typology is set up. A sensitivity analysis is performed to assess the seismic in-plane behaviour and determine which failure mechanisms are governing. This is done by a variant study, which gives a better insight in the overall behaviour of the analysed typology. The model is validated before starting the numerical analyses. Finite element program ETABS is used, which is applicable for modelling unreinforced masonry structures and the timber strengthening and able to perform non-linear pushover analyses. The most notable outcomes of the sensitivity analysis are discussed in detail.

Part III: Design and assessment of strengthening measures
In this part, the seismic performance of timber construction is studied. After, strengthening measures are designed to account for the established failure mechanisms in the sensitivity analysis. The effect of the proposed retrofit design on the behaviour of the buildings is analysed by implementing the measures in the numerical model. The most effective retrofit measures are discussed in more detail.

Part IV: Conclusions and Recommendations
In this part overall conclusions are discussed, followed by recommendations based on the findings and for further research.

Part I

Literature study

2. Description of houses in Groningen

To get more insight in the characteristics of buildings in the Groningen region, the building stock is described and analysed based on structural system, materials and height. The building type most vulnerable to the seismic loads is described in more detail, since this is used as a basis for the numerical model. The study area is shown in Figure 2.1. It represents a 5 km band beyond the extent of the Slochteren gas field. In this area of approx. 1475 km^2, around 275.000 buildings exist, with all different shapes and sizes.

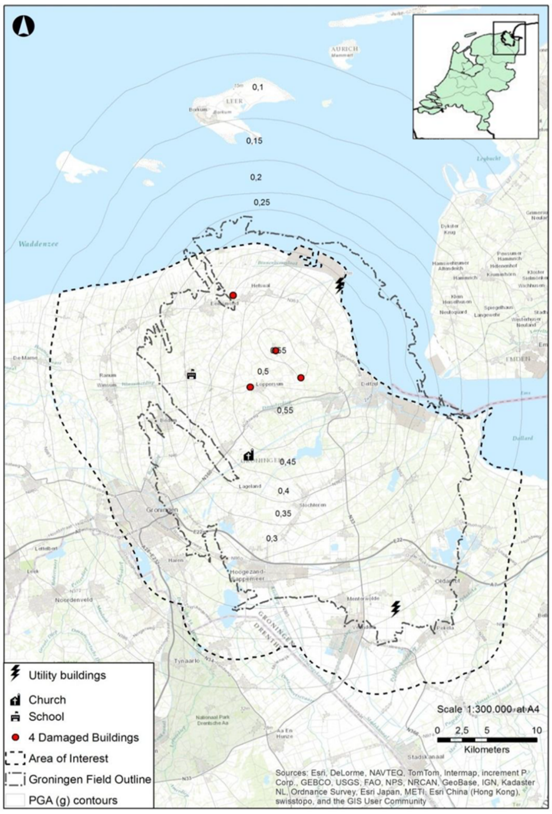

Figure 2.1: Hazardmap with investigated building locations (Source:[3])

2.1 Building typologies

The building stock is divided in several typologies. In this way not all structures have to be analysed individually and time is saved. A typology is representative for a significant proportion of the building stock, so strengthening measures can be designed for a larger amount of structures at once. This is both convenient for the engineers and the residents.

The Groningen building stock is categorized in four main typologies, based on research of Arup [3]:

- **Typical buildings** – These represent the largest proportion of buildings and can be divided into a number of sub-typologies representative of the majority of the total building stock in the region:
  - Terraced house
  - Semi-detached house
  - Detached house

  - Labourer's cottage
  - Mansion
  - Villa

- **Damaged buildings** – This are buildings where damage has been reported in the past and where a damage survey has been conducted. These buildings are in a 'critical condition'.
- **Historic heritage buildings** – They often comprise large masonry elements attracting high seismic loads and use different structural systems than domestic-scale buildings.
- **Other buildings** – are a mixed group with different materials or combinations of materials structural typologies. Schools, hospitals and utility buildings fall into this category.

The most common buildings in the area are resembled by terraced, semi-detached and detached houses, primarily consisting of two storey high unreinforced masonry, see examples in Figure 2.2, based on the Arup report [3].

(a) Terraced house (b) Semi-detached house (c) Detached house

Figure 2.2: Examples of most common buildings in the area (Source: funda.nl)

Exposure database

An exposure database (EDB) is developed by Arup commissioned by the NAM, to get an overview of the structural systems of the building typologies in Groningen. For more information on how this database is developed see the database documentation of Arup [35]. In this database several existing public and proprietary datasets are used, containing information related to the buildings and population of the studied area. The datasets include:

- Basisregistratie Adressen en Gebouwen (BAG) (Kadaster – Dutch Land Register)
- AHN Actueel Hoogtebestand Nederland (Heights of buildings)
- DataLand address usage data
- CBS StatLine - Inhabitants per hectare 2014/ Education per municipality 2014 - 2015/ Time use data
- LISA – Landelijk Administratiesysteem Arbeidsplaatsen/ Number of jobs per category per postcode

The data is merged into a Geographical Information System (GIS). The buildings are grouped into categories as a function of their expected seismic performance. The most important characteristic for that is the "lateral load resisting system", made up by the construction material of the walls, frames and floors. The construction materials are divided in unreinforced masonry (URM), steel (S), reinforced concrete (RC) and wood (W).

Since there is no information on the construction material and the system for each individual property, inspections of the buildings have been carried out to establish the main characteristics of the buildings without entering.

To classify the different structural systems for the buildings the GEM building taxonomy is used. This is a global classification scheme for buildings, able to capture all different types that exist around the globe and describe and classify them in an uniform manner. The classification is based on a combination of:

- Lateral load resisting system (LLRS)
- Material of the lateral load resisting system
- External wall presence
- Floor material
- Height (<3 and >= 3 storeys)

For the Groningen area, 54 different structural systems are used to categorize the existing buildings, see for a short description of each of the systems Figure A.1 in Appendix A. Of these 54, 15 are constructed with unreinforced masonry. There are around 150.000 regularly populated buildings in the database, and over 85% of the buildings is constructed with unreinforced masonry [4]. Figure 2.3 presents which structural system is most used in the area on the left hand. The structural system with the code URM3L is most common in the Groningen area. It is a unreinforced masonry low-rise building with cavity walls and concrete floors. The right hand of Figure 2.3 shows which structural system has the most occupants. A large portion of the population lives in concrete high rise buildings, such as the typology with code RC4M.

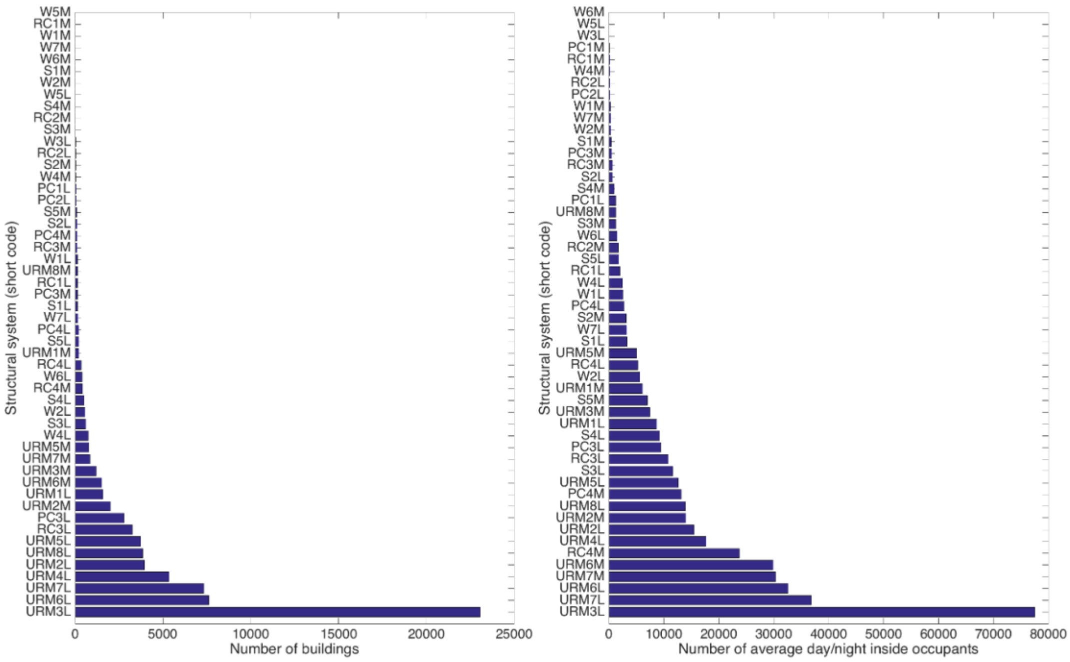

Figure 2.3: The frequency distribution of buildings and average day/night inside occupants within each structural system taxonomy class (Source:[4])

Furthermore, the most common URM structure is more evenly distributed across the area, see Figure 2.4 on the left. The high rise buildings are mainly concentrated in the city of Groningen, see Figure 2.4 on the right.

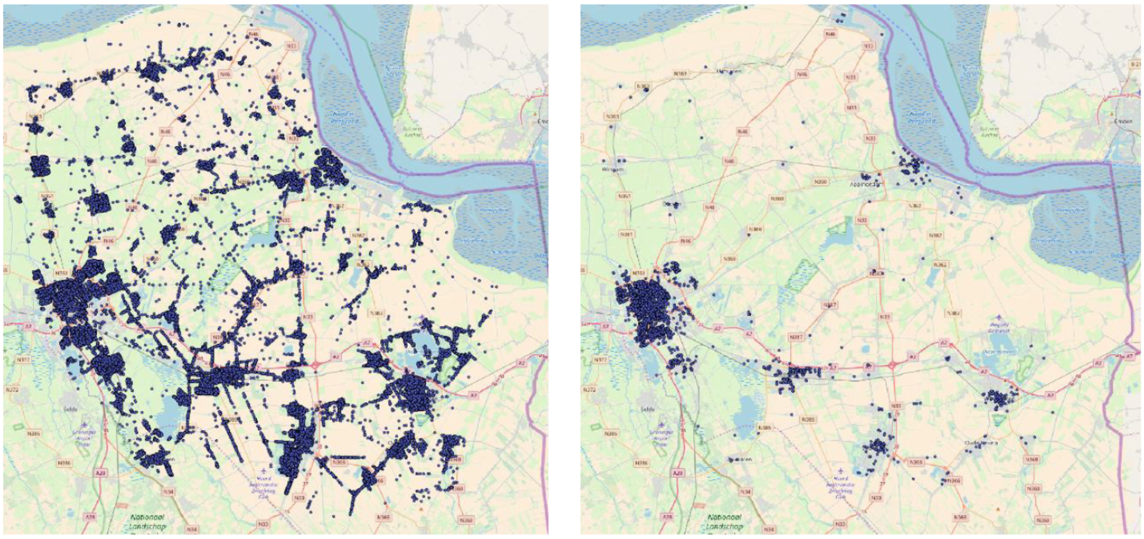

Figure 2.4: Left: the distribution of the structural system URM3L within the exposure model. Right: the distribution of the structural system RC4M (Source:[4])

2.2 Description of most vulnerable building typology

Due to the announced stop of the gas extraction in the Groningen region in 2030, less buildings need strengthening, see Chapter 1. Before, 46% of the houses that needed strengthening consisted of one typology, namely the URM4L, see Figure 2.5. This building type is a low-rise terraced house that consists of unreinforced masonry with cavity walls and large openings on both ground floor walls. In the case of the reduced seismic risk, this typology covers an even larger proportion (in the future up to 80 %) of the total number of houses that does not meet the safety standard, according to [2]. The second most vulnerable typology in Groningen, with code URM8L, is a low-rise terraced house consisting of unreinforced masonry with cavity walls and timber floors.

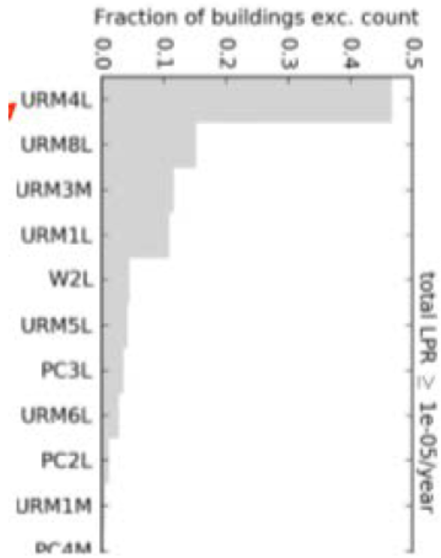

Figure 2.5: Fraction of each of the typologies that need strengthening based on the Seismic Hazard and Risk Assessments (SHRA's) from November 2017 drawn up by the NAM (Source:Appendix B3 of [2])

From building to building several differences are present within the typology. However, it is characterised by certain aspects. Typically it is a two storey structure, with a narrow floor plan being approximately 5,5 to 7 m in width and 6 to 9 m in depth [17]. The inter-storey height varies typically between 2.6 and 2.8 m [17]. Because it is a terraced house, it is usually composed of 5 to 10 adjoining housing units, sharing the party walls. Furthermore, the construction is characterised by a weaker longitudinal direction due to the presence of large daylight openings in both façades. The transversal direction with large gable walls is much stiffer. Figure 2.6 presents an example of such a structure.

Figure 2.6: Drawing of a typical terraced house with large openings on ground floor walls (URM4L)

Building elements

The structural differences within the typology can have a significant impact on the seismic behaviour of the structure. This section gives a brief overview of the similarities and variations within those aspects. The connection details are based on similar tested building specimens, which represent the end-unit of a URM cavity-wall terraced house [36, 17].

Foundation

Generally, the houses in Groningen are founded on shallow foundations. Depending on the construction period, several different methods could have been used. The spread footing, consisting of strips or pads of concrete, is commonly applied. The spread footing can consist of masonry, see Figure 2.7. The footings are placed underneath the walls and are often embedded into the soil, improving the bearing capacity. The shallow subsurface mainly consists of sand and clay, which for most buildings has reached the end of the consolidation period. Pile foundation is less used in this area.

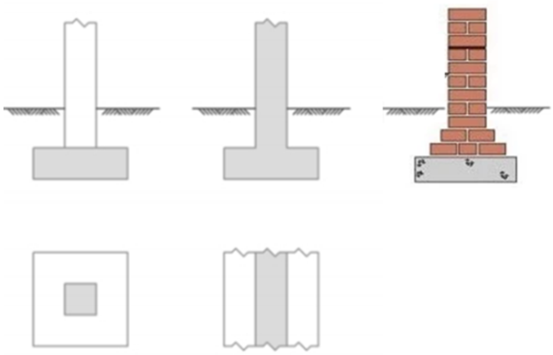

Figure 2.7: Schematisation of spread footings used in the area. (Source: adaptation from [5] and [6]).

Walls

The walls of this typology are composed of façade walls with large perforations and long transversal walls without openings. The walls are primarily cavity walls, with two leaves of around 100 mm thick and one cavity of around 100 mm. To a lesser extent the transversal party walls can consist of solid walls of about 200 mm thick. Cavity walls are either coupled or uncoupled depending on the presence of steel anchors within the cavity wall. The inner leaf is usually load bearing. The longitudinal façade walls contain large openings, especially on ground floor level, resulting in the presence of slender masonry pier elements, see Figure 2.9a. The façade walls consist usually of three piers per wall.

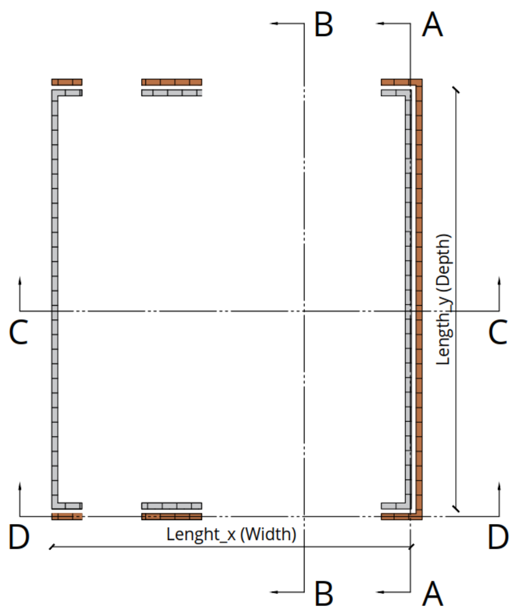

Figure 2.8: Plan view of a unit

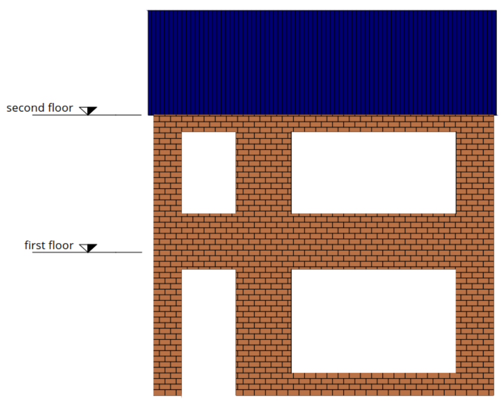

(a) Schematisation of a typical front façade of a masonry terraced house unit (Section D of Figure 2.8)

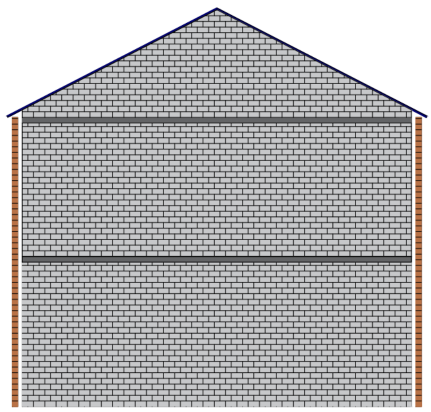

(b) Schematisation of the side view of a typical terraced masonry house.

Figure 2.9: Front and side view of a typical terraced masonry house.

The floors are either supported by the transversal walls only or by both walls, depending on the material and structural detail of the floor slabs. The slender piers in the façades carry a percentage of the load, but the majority of the load is carried by the long transversal walls.

Differences in the construction of the walls are found within materials and the detailing. During different periods, other masonry materials are used. Usually solid clay or calcium silicate brick masonry is used for the inner leaf and solid or perforated clay for the outer leaf. It consists of either larger elements or bricks, joint together by certain mortar. The properties of various masonry types are discussed in Chapter 3.

Floors

Generally, the first floor consists of a reinforced concrete slab, either cast in place or prefab. They span either one single housing unit or multiple units. The second floor is either a reinforced concrete slab or a timber diaphragm. For this research both first and second floor are considered to have a reinforced concrete slab, acting as a rigid diaphragm, similar to the building specimen tested in Italy, representing an end-unit of a URM cavity-wall terraced house [36]. The roof usually is a gable roof, consisting of a timber framework of a ridge beam, rafters and purlins built into the gable wall to provide added support, covered with roof tiles. Depending on the construction details, the floor slabs are either one-way or two-way spanning.

Building connections

The connections between wall-floor and wall-wall can differ within the building typology. Figures 2.10a and 2.10b show the main connections of floors and walls within this building typology.

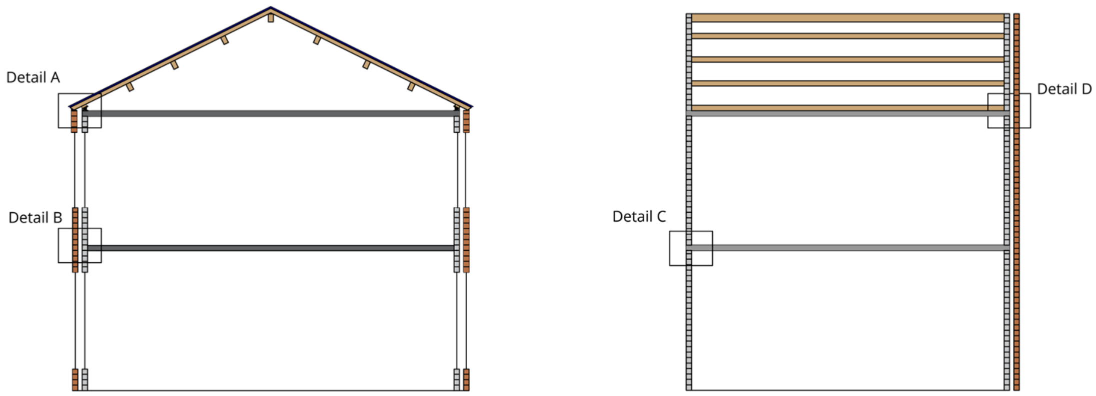

(a) (Section B of Figure 2.8)

(b) Floors carried by transversal walls (Section C of Figure 2.8)

Figure 2.10: Sections of a typical terraced masonry house of Figure 2.8)

The floors lay upon the inner leaf of the transversal walls, since they are the main load bearing walls. Figures 2.11a and 2.11b show the connection between floor and transversal wall on both storey levels. Floor slabs are either one-way or a two-way spanning, depending on the kind of connection between the floor and the longitudinal wall.

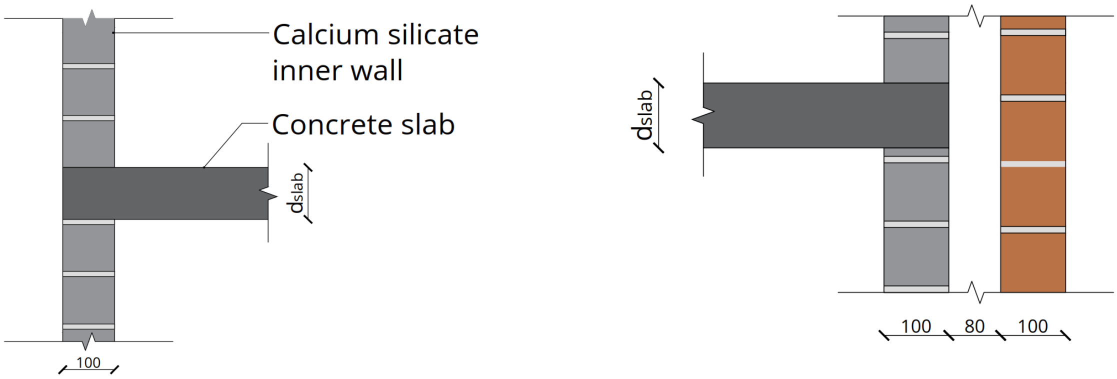

(a) Detail of wall-floor connection at first floor. Detail C of Figure 2.10b

(b) Detail of wall-floor connection at second floor. Detail D of Figure 2.10b

Figure 2.11: Connection details of a typical terraced masonry house of Figure 2.10b.

The longitudinal façade walls usually do not carry the weight of the first floor and only part of the weight of the second floor. Figure 2.12a shows the connection at first floor when the façade wall does not carry the floor. The connection of the first floor slab with the inner leaf is ensured by means of anchors. These anchors are commonly used for horizontal buckling or wind load support of the pier, not designed to withstand any vertical load [17]. When the longitudinal wall is load bearing, the floor lays upon the inner wall of the longitudinal wall, similar to the connection of the floor to the transversal wall, see Figure 2.12.

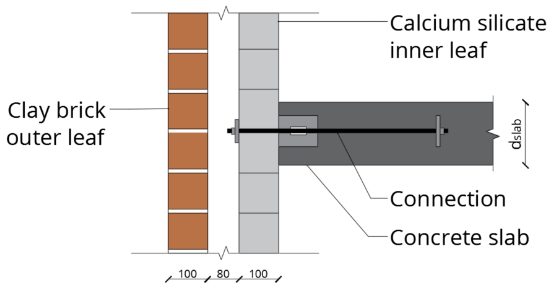

(a) Detail of longitudinal wall-floor connection at first floor. Detail B of Figure 2.10a

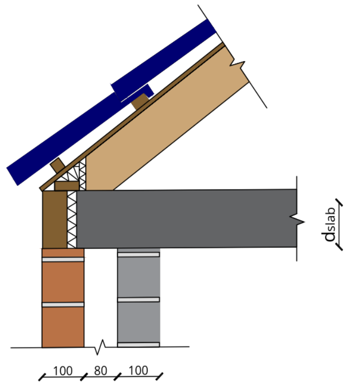

(b) Detail of longitudinal wall-floor connection at second floor. Detail A of Figure 2.10a

Figure 2.12: Details of longitudinal wall-floor connections of a typical terraced house from Figure 2.10a

3. Unreinforced masonry

This chapter addresses the properties, the seismic behaviour and the modelling of masonry, with the focus on Dutch unreinforced masonry which is typical for the Groningen region.

3.1 Classification

Masonry is one of the oldest building materials known to mankind. It is a heterogeneous composite building material that consists of masonry units held together with mortar. The units are made from clay, compressed earth, stone, concrete and even glass and come in different shapes, mostly rectangular. Mortar is composed of binders, aggregates and water in various proportions. It is often based on cement and/or lime, sand and water with or without additives.

Construction methods

Construction of masonry is done by bricklayers or masons, depending on the skill level. Even though the construction is relatively simple and cheap, it is labour-intensive work. In certain cases bricklaying requires highly skilled labour. There are several ways to construct with masonry and it can be classified in categories depending on the construction method followed.

- **Unreinforced masonry** – Solely built with masonry units held together with mortar, as traditional.
- **Reinforced masonry** – Masonry construction in which reinforcement is embedded in such a manner that the two materials act together in resisting forces. The reinforcement can take various forms, such as internal steel or wooden rods or bars grouted into masonry units or laid in horizontal mortar courses.
- **Confined masonry** – Masonry construction where masonry walls are first laid and then horizontal and vertical reinforced concrete confining elements are cast.
- **Infilled frame** – In this case masonry is used as infill for a framework of beams and columns. Due to the strength and stiffness in plane, infill masonry walls do not allow beams and columns to bend under horizontal loading.

In the Groningen region the majority of the structures is built with unreinforced masonry.

Dutch masonry

The mechanical properties of masonry depend on the properties of the mortar and the masonry units. Properties vary a lot, therefore, it is hard to predict masonry behaviour by solely knowing the characteristics of the individual elements. Experiments are essential to correlate the strength characteristics of individual components with the overall characteristics of masonry.

A first categorization is based on the material of brick units. The two main materials in the region are clay and calcium silicate (CaSi). A second categorization is based on the construction period. For clay units including solid, perforated and frogged units, two different time periods are considered: pre-war period (until 1945) and post-war period (after 1945). Regarding the CaSi units two other time periods are considered: before 1985, when smaller bricks and mortar was used, and after 1985, when larger glued elements were mostly used. Almost 25% of the building stock consists of pre-war clay bricks and 12% consists of post-war clay bricks, according to Arup's Exposure Database [35]. Regarding the calcium silicate bricks, almost 20% of the buildings are made with pre 1985 units, while 13% consists of newer CaSi bricks from after 1985.

To accurately assess the behaviour of the buildings in the Groningen area, a characterization of the masonry properties is required. A campaign on the material characterization of existing buildings was performed in 2015, as part of the larger project concerning the seismic hazard in Groningen. This campaign included laboratory and in-situ testing of masonry walls typical for the region. Properties for the characterization of the masonry in compression, bending and shear were investigated [37, 38]. The characteristic mean values for the masonry properties for the different types of masonry are given in the Dutch guideline NPR 9998:2018 Table F.2.

The mean values for the masonry properties are used in this thesis for the assessment of the terraced houses, since the focus is on the typology as a whole.

3.2 Seismic behaviour

Seismic response of masonry buildings can be characterized based on two different classes of mechanisms: out-of-plane and in-plane mechanisms [39]. When a building is subjected to seismic forces, the structure inevitably experience a combination of in-plane and out-of-plane response. Since the identification of a combined in-plane and out-of-plane failure mode is very complicated, the failure modes are generally attributed to either in-plane or out-of-plane failure. Adequate seismic performance can be attained if out-of-plane collapse is prevented and in-plane strength and deformation capacity of the shear walls are fully used. Both are discussed in more detail.

Out-of-plane behaviour

Out-of-plane failure is a common phenomenon. Often it is a result of insufficient connections between walls to walls and walls to floors. Observations after several strong earthquakes show that out-of-plane failure probably causes the most serious life-safety hazard. The unstable out-of-plane failure endangers the gravity-load-carrying capacity of a wall, whereas for in-plane failure this is less likely to happen, unless for extremely severe shaking. D'Ayala and Speranza [8] have defined some typical out-of-plane collapse mechanisms for masonry buildings based on post earthquake damage inspections, see Figure 3.1.

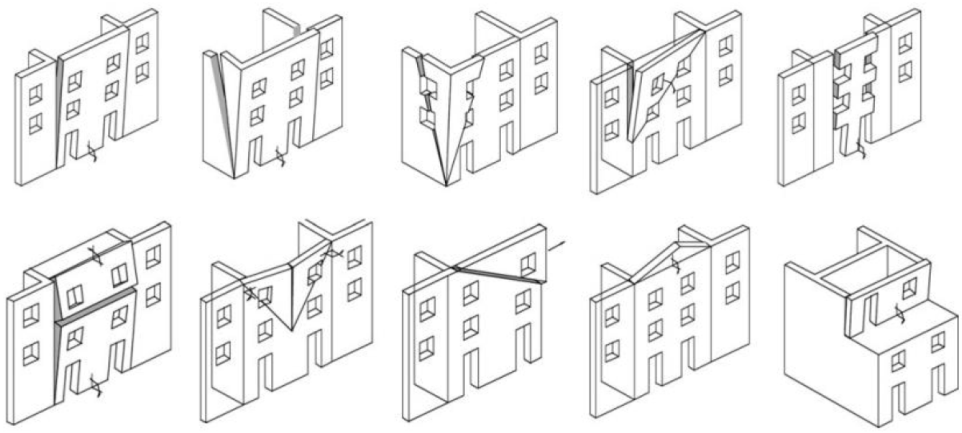

Figure 3.1: Examples of out-of-plane failure mechanisms of unreinforced masonry(Source: [7] adjusted from [8])

The collapse modes and resulting analytical models account for connections, loading and restraint effects of horizontal structures and presence of strengthening devices, such as ties and ring beams. The equivalent shear capacity for each façade wall and for each collapse mechanism is calculated and the governing mechanism, with the lowest capacity, is identified.

In-plane behaviour

The main in-plane failure mechanisms of unreinforced masonry walls can be summarized as follows [9]:

- Shear failure
- Sliding failure
- Rocking and toe crushing failure

The shear failure mode is typically found in walls with high axial loads and a low height to length ratio, leading to diagonal or X-cracking in the direction of the wall lengths, as depicted in Figure 3.2a. These cracks pass either through the mortar joints or through the masonry units, depending on the relative strength of the components. Perforations in a structure facilitate in-plane cracking, since a greater concentration of stress is present at the edges of the openings.

In case of a low friction coefficient or low vertical loads, the horizontal cracks in the bed joint can cause a sliding plane extending along the wall. In that way the upper part of the wall can slide on the lower part, causing shear sliding failure, as demonstrated in Figure 3.2b. This sliding plane is typically formed at the base of a wall.

Rocking or toe crushing failure occurs in case of high moment to shear ratio or enhanced shear resistance, depending on the level of the applied normal force, see Figure 3.2c and 3.2d. Generally, failure initiates with large flexural cracks developing at the bottom and the top of the element. A rotation mechanism can be activated if the displacement increases.

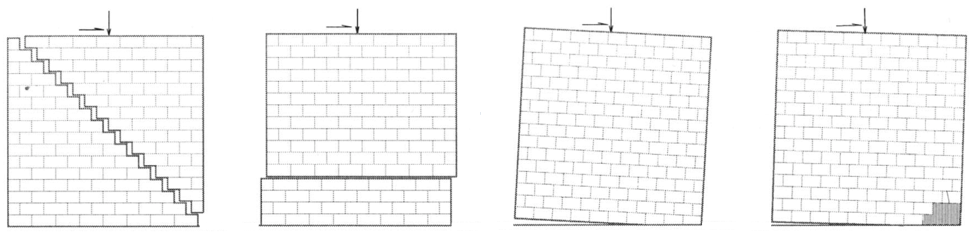

(a) Shear failure (b) Sliding failure (c) Rocking failure (d) Toe crushing failure

Figure 3.2: Main in-plane failure modes (Source: [9])

3.3 Modelling of unreinforced masonry

Masonry is a composite material with different properties depending on the properties of its constituents (masonry units and mortar) and the cohesion between them. Therefore, modelling of masonry can be complicated. There are several different ways to model masonry. Each method has its advantages and disadvantages.

The main differences are based on the scale of analysis and on how connectivity of the masonry is described. Depending on the desired level of accuracy, simplicity and required time of the modelling, there are generally two principal strategies: micro-modelling and macro-modelling. It is also possible to model on a scale in between these two, namely simplified micro-modelling or meso-modelling [40]. In Figure 3.3 a schematisation of the different modelling approaches is presented.

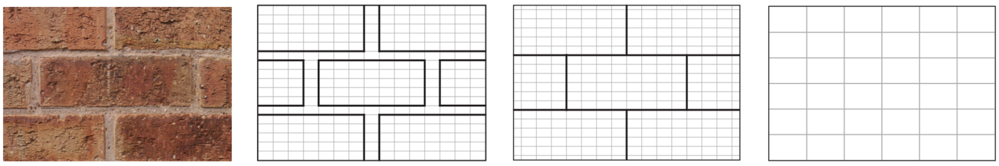

(a) Masonry sample (b) Detailed micro-model (c) Simplified micro-model (d) Macro-model

Figure 3.3: Masonry modelling strategies (Source: Adapted from [10])

Micro-modelling

Since the beginning of the modelling of masonry, micro-models are used. It basically consists of modelling brick by brick. The masonry units, the mortar and their interface are modelled separately.There are two ways to use a micro-modelling approach [10]:

- ***Detailed micro-modelling*** – The masonry constituents are represented by continuum elements. The interface of the mortar and the masonry units is described by discontinuous elements, representing possible planes of failure. The characteristic non-linear behaviour of masonry is predominantly modelled in the interfaces. This model should be able to describe all failure mechanisms.
- ***Simplified micro-modelling or meso-modelling*** – The units are represented by continuum elements. However, the mortar is scaled down to zero-volume interface elements. The masonry units are expanded so the geometry of the masonry is ensured. The units are separated by discontinuous elements that simulate the behaviour of the mortar and the interface of units and mortar.

A disadvantage of micro-modelling is that it is time consuming. Furthermore, all the properties of the constituents have to be known, which can be difficult to obtain, especially for existing structures. Therefore a micro-model is mostly used for studying the behaviour of a single structural element rather than a complete structure.

Macro-modelling

Knowledge of the interaction between units and mortar is, in practice and for extensive analyses. Generally, it is negligible for the global structural behaviour. In these cases a macro-modelling approach can be adopted [41]. In a macro-model the masonry units and the mortar are not described separately, but they are considered as homogeneous and anisotropic continuum material. Therefore, all aspects of the behaviour are smeared out over the material. Masonry stress-strain relationships are derived by performing tests on masonry, where combined brick and mortar behaviour is analysed.

The modelling process of macro-models is less complex and the calculation time is significantly lower than micro-modelling. On the other hand, this method only reproduces a more general structural behaviour. Macro-models can be seen as a compromise between accuracy and computational speed. The models are mostly used to study the behaviour of a whole structure rather than a single component.

To connect the macro-model to the actual masonry behaviour, assumptions are made. The step from micro to macro-models is called homogenisation. Important aspects of homogenisation include periodic geometry, non-linearity, bond and/or damage-induced anisotropy.

Furthermore, there are structural element models. The most essential structural elements are defined and the constitutive laws are provided in terms of internal forces such as shear force or bending moment, rather than in terms of stresses and strains. An example of such a model is given by the equivalent frame method, which is described below.

Equivalent frame modelling

The equivalent frame model is one of the most widely used structural element modelling strategies. The strategy is based on the identification of macroscopic structural elements, usually two main structural components are identified: piers and spandrels. The deformation and the non-linear response are concentrated within these elements[11]. Generally, cracks and failure modes are concentrated there. The panels are connected by rigid portions that are usually not subjected to damage, referred to as rigid nodes. Figure 3.4 sows an example of this equivalent frame idealization process.

Piers are the main resistant elements, carrying both vertical and lateral loads. The spandrels, which are the parts between two piers, couple the response of those piers in the case of lateral loads.

The approach requires a limited number of degrees of freedom in order to allow the analysis of complex three dimensional models of URM structures, obtained by assembling its walls and floors. This modelling approach is applied in the program TreMuri, which is a frequently used program in earthquake modelling of masonry, usually to perform non-linear pushover analyses.

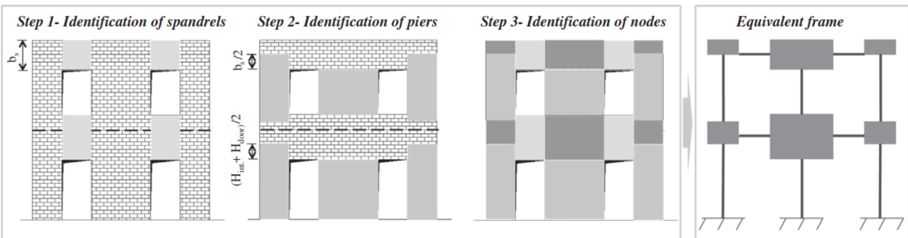

Figure 3.4: Example of an equivalent frame idealization (Source: [11])

Simple Lateral Mechanism Analysis (SLaMA)

Another macro modelling approach, is the Simple Lateral Mechanism Analysis or SLaMA method. This is a simplified non-linear calculation method, which determines the global capacity of the structure by the summation of the capacities of identified individual mechanisms for elements or members. It is considered to be a relatively easy way of obtaining an estimate of the non-linear pushover relationship of fairly complex structures.

According to New Zealand guidelines [42], the key steps for performing a SLaMA are:

- Assess the structural configuration and the load paths in order to identify the essential structural elements and the potential structural weaknesses.
- After these elements are identified, the probable in-plane capacities for various failure mechanisms of the individual elements have to be determined.
- Compare the element capacities and determine the governing failure mechanisms and therefore the hierarchy of strength.
- Assess the sub-system inelastic mechanisms by extending local to global behaviour.
- Combine the various individual mechanisms and the capacities and calculate the base shear and global displacement capacity.
- After that the equivalent SDOF system has to be determined together with the seismic demand in order to plot an ADRS curve.

- Next to that, the the diaphragm connection to the walls has to be assessed and the put-of-plane response has to be assessed as well.

The SLaMA method provides a good insight in the seismic behaviour especially for low-rise structures, since their first mode response is dominant and therefore higher mode amplification can be neglected. Due to the clarity of the simplistic representation of the structure, the SLaMA method often provides a useful understanding of the structure's behaviour. A disadvantage is the potential to overestimate the capacity of an element by missing the mechanism that has the lowest strength and displacement capacity and therefore overestimating the overall strength and displacement capacity.

4. Analysis strategy

4.1 Analysis methods

The aim of a structural seismic analysis is to compute the forces and displacements of the structural elements and the entire system. The main analysis methods appropriate for evaluating the seismic behaviour are: the lateral force analysis, the modal response spectrum analysis, non-linear static pushover analysis and the non-linear time history analysis. These methods can be divided into linear or non-linear and static or dynamic, as presented in Table 4.1.

Method	**Procedure**
Lateral Force Analysis	Linear Static
Modal Response Spectrum Analysis	Linear Dynamic
Non-linear Pushover Analysis	Non-linear Static
Non-linear Time History Analysis	Non-linear Dynamic

Table 4.1: Analysis methodologies

Moving from linear to non-linear analysis and from static to dynamic analysis, the procedure provides a more accurate model of the actual seismic performance of a building, but the processing time and the computational effort increases. Generally, national standards and guidelines use more simplified analysis methods to be on the conservative side concerning safety. When modelling becomes more detailed,the mathematical representation of the actual structural behaviour increases and therefore the accuracy of the analysis, resulting in less-conservative outcomes.

In this section, the calculation methods and the differences between them are described briefly. After, the main method used during this research is determined and described in more detail.

Lateral force analysis

The lateral force analysis (LFA) is a linear static calculation method. It is a simplified method that substitutes the effect of dynamic loading by distributing static forces laterally on a structure. The main assumptions are the response in its fundamental lateral mode and the simple approximation of the shape of the mode. The structure must be able to resist the lateral forces in either direction, not simultaneously in both. The lateral force method is relatively easy and fast and little amount of input is required. A number of assumptions has to be made, which reduce the accuracy of the method. Dynamic effects, non-linear material behaviour and ductility is not taken into consideration and the contribution of higher mode shapes is ignored. Furthermore, rigid diaphragms are assumed. The method is useful for an easy and fast estimation of the structural behaviour of regular low-rise buildings which are dominated by their first mode shape.

Modal analysis

This analysis method is a linear dynamic analysis of a structure subjected to earthquake excitation. It is the most used method to accommodate the stochastic nature of seismic events. It is performed to identify the eigenvalues, the frequencies, the mode shapes and the periods of the structural system. The seismic input is given in terms of a response spectrum, usually an acceleration response spectrum. Unlike the lateral force method, contribution of higher mode shapes is taken into account. Therefore, it is applicable for more complex geometries and shapes. Additionally, the modal analysis includes dynamic effects. Similar to the lateral force method, it is a linear method, thus non-linear material behaviour and ductility is not directly taken into account

Non-linear pushover analysis

The non-linear pushover (NLPO) analysis is a commonly used non-linear analysis method for seismic assessment of existing structures. A structure is subjected to gravity loading and a monotonic displacement-controlled lateral load pattern which is continuously increased through elastic and inelastic behaviour until the ultimate capacity is reached [43]. The lateral load is usually applied in a load vector that approximates the relative acceleration associated with the fundamental and dominant mode of vibration. Basically, the building is pushed until its maximum capacity to deform is reached. It gives an idea of the maximum base shear that the structure is capable of resisting. The output of the analysis is a static-pushover curve which plots a strength-based parameter against deflection, giving the expected lateral force capacity and therefore registering the structural response. Results provide insight into the ductile capacity and indicate the mechanism, load level, and deflection at which failure occurs.

The pushover analysis is an attractive method for seismic analysis since it allows the explicit consideration of the non-linear structural behaviour without the need to define the often complex characteristics of the structural elements and therefore maintaining the simplicity of a static analysis. Furthermore, it gives good insight into the propagation of damage and accounts for second order effects. Disadvantages of the pushover method are the use of only a first mode shape (SDOF system), the lack of dynamic effects and the use for solely in-plane analysis. Next to that, it is hard to obtain useful results for structures with flexible diaphragms, since the method is initially developed considering rigid diaphragms, according to [44].

Non-linear time history analysis

The time history analysis is a dynamic non-linear method. From the aforementioned analysis methods, this is the most complete form of analysis. It accounts for non-linear behaviour and ductility, second order effects, a combination of in-plane and out-of-plane loading and it accounts for dynamic effects. The downside is the necessity of large amounts of input information which is essential for the accuracy of the method. Results are very sensitive to the input and therefore it is hard to interpret the accuracy. During an earthquake, the ground acceleration changes and therefore the applied forces on the structure change over time. By solving the equation of motion for every time step, the internal forces and displacements are calculated for every element in the structure. For a typical building, this requires solving many equations simultaneously. Therefore, it is very time consuming. On the other hand it provides more detailed information regarding the seismic behaviour.

Conclusion

In this research the focus is mainly on buildings with relatively simple geometries with rigid diaphragms, of which the structural behaviour is predominantly governed by their first mode shape. A good insight in the propagation of the failure mechanisms is important, just as the application of second order effects. Since relatively simple buildings are analysed, there is no need for the extensive and time consuming non-linear dynamic time history analysis. Therefore, the focus in this research is on the non-linear static pushover analysis.

4.2 Non-linear pushover analysis

There are generally two main approaches to the pushover analysis: The capacity spectrum method and the displacement coefficient method. In this research the capacity spectrum method, also prescribed in the Dutch guidelines NPR 9998:2018, is used. This guideline, gives a basis for new construction as well as for strengthening existing building constructions with insufficient safety. It is based on Eurocode 8 and it gives several methods to determine the structural safety and the seismic action.

In this method, a capacity (or pushover) curve of the structure is generated by subjecting the detailed non-linear structural model to the fundamental mode inertia load vector. The curve is given in terms of base shear force versus displacement of the target point chosen, in this case the roof displacement. The capacity curve approximates how structures behave after they exceed their elastic limit. After generation of the capacity curve, it is converted the multi degree of freedom (MDOF) system into an equivalent Single Degree Of Freedom (SDOF) system, as presented by Figure 4.1. By doing so, values for the roof displacement and the base shear on the pushover curve are converted to the corresponding spectral displacement and spectral acceleration.

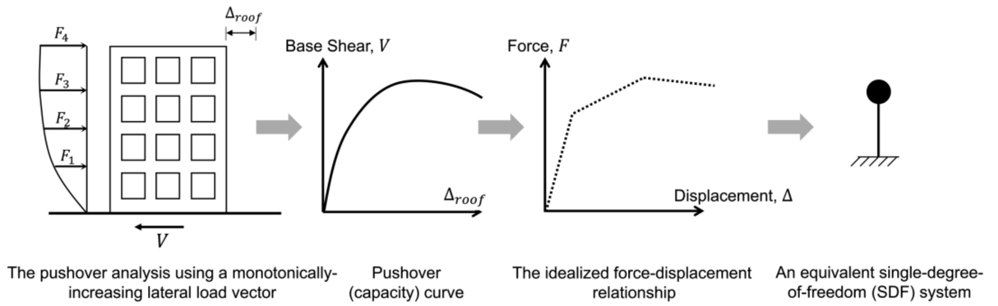

Figure 4.1: Conversion of a more detailed structural model into an equivalent SDOF system (Source: [12])

The seismic demand is converted to an Acceleration-Displacement Response Spectrum (ADRS), also referred to as a demand spectrum. The capacity spectrum and ADRS are compared. The intersection point of these curves is called the performance point, which is an estimate of the expected maximum displacement. With this so called target displacement the structural performance is checked by comparing the displacement to the displacement capacity of the structure. In Figure4.2 the process is illustrated.

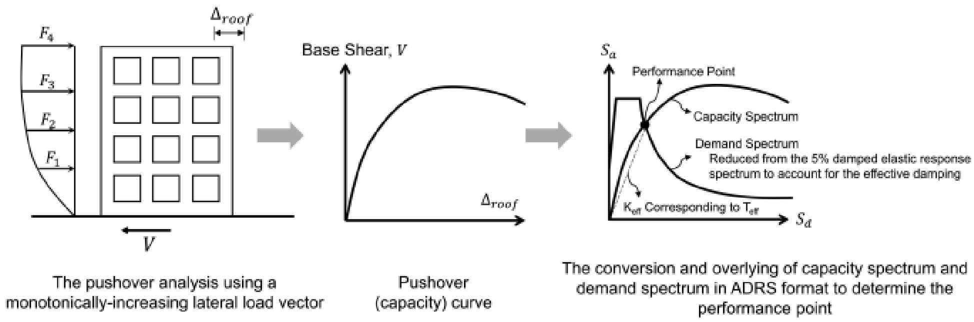

Figure 4.2: Process of capacity spectrum method (Source: [12])

The application of the NLPO procedure generally involves four main phases:

1. Define the structural model with the non-linear force-deformation relationships for the various components/elements
2. Define a suitable lateral load pattern and use the same pattern to define the capacity of the structure
3. Define the seismic demand
4. Evaluate the performance of the building

Phase 1

For this research, the definition of the structural model with the non-linear force-deformation relationships for the various structural elements is explained and described in Chapter 5 according to the NPR 9998:2018.

Phase 2

To perform a pushover analysis a lateral load pattern, equivalent to the earthquake load is required. Regulations are mostly focused on a monotonic lateral load pattern which pushes the structure till the capacity is reached. The loads are in proportion to the distribution of inertia forces in the plane of each floor diaphragm. According to the NPR 9998:2018 at least two vertical distributions of lateral load patterns should be applied. In this case, the following load pattern are used for the pushover analyses:

- a so-called uniform load pattern, which is proportional to the story masses.

- a triangular load pattern based on a first mode dominant response, which is proportional to the story masses

The choice of the load pattern plays a significant role, because certain deformation modes are triggered by a particular load pattern while other modes are therefore missed. Since the loads are increased for each step of the pushover curve, the initial magnitude of the lateral forces is less important. The ratio between the lateral forces is more relevant. Figure 4.3 shows the ratio for both applied load patterns.

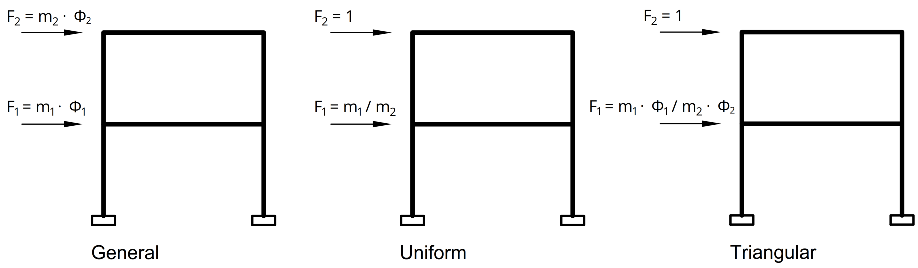

Figure 4.3: Ratio of pushover forces for the first and second floor for uniform and triangular lateral load pattern.

The lateral load on the first floor is related to the load of the second floor, which is set at a value of 1 kN. For a uniform load pattern $\phi_1 = \phi_2 = 1$. For a triangular load pattern, ϕ is calculated according to 4.3.3.2 of NEN-EN 1998-1:

$$\phi = \frac{h_i \cdot m_i}{\sum h_j \cdot m_j} \tag{4.1}$$

Where:

h_i, h_j: are the heights of the masses m_i, m_j above the level of application of the seismic action

Phase 3

The seismic demand is represented by an elastic design spectrum. For the Groningen situation, the NPR 9998:2018 uses response spectra based on predictive values from theoretical models. Models are based on a single earthquake source with a relatively low magnitude and therefore an amplification for longer response periods. This is typical for induced earthquakes. A tool is used, to gain insight into the predicted ground movements with a self-chosen return period at a self-chosen specific location. The tool presents an elastic response spectrum at the chosen location. Figure 4.4 shows a typical shape of a response spectrum taken from the NPR web-tool.

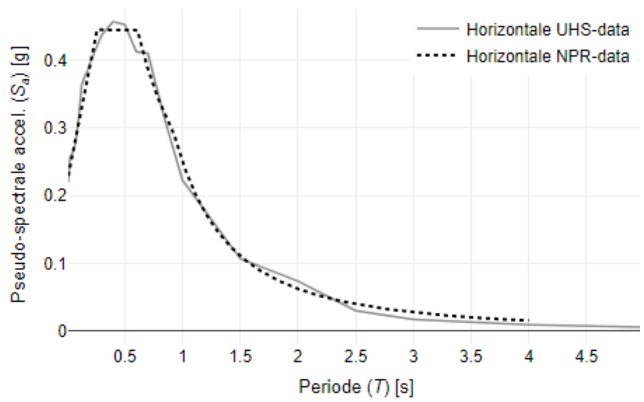

Figure 4.4: Shape of elastic response spectrum taken from the webtool (Source: [13])

For each location in Groningen the values for T_B, T_C, T_D, p and $a_g S$ are given. The value for $a_{g;d}$ follows from multiplying $a_g S$ with an importance factor. For existing structures the value for the importance factor is 1.0, according to Table 2.4 of the NPR 9998:2018. With these parameters an elastic response spectrum is constructed, see Appendix C.

In Groningen the degree of damage to a structure is distinguished by three limit states:

1. **Near Collapse** - the load bearing structure is about to collapse and would probably not survive another earthquake. This level is achieved corresponding to a seismic action with probability of exceedance of 2% in 50 years, which is a return period of 2475 years.

2. **Significant Damage** - the load bearing structure is significantly damaged with some residual lateral strength and stiffness, vertical elements are still capable of sustaining vertical loads. Seismic action corresponding to a 10% probability of exceedance or a return period of 475 years.

3. **Damage Limitation** - the load bearing structure is only slightly damaged retaining its strength and stiffness properties. This limit state corresponds to a seismic action with probability of exceedance of 20% in 50 years or a return period of 225 years.

In practice, buildings are assessed according to the Near Collapse (NC) limit state in Groningen, as is done for this research. Most seismic standards in the world use the Significant Damage limit state, which accounts for a lower return period.

To account for energy dissipation of the system, the seismic demand spectra are adjusted by a spectral reduction factor, based on the equivalent viscous damping of the system, see Appendix C. For unreinforced masonry walls that show ductile behaviour, a hysteretic damping of $\xi_{hys} = 0,15(15\%)$ can be applied as a conservative assumption when loaded in-plane, according to Table G.3 of NPR 9998:2018 [34]. For walls showing brittle behaviour, a hysteretic damping of $\xi_{hys} = 0(0\%)$ should be applied. However, in practice it is depending on the masonry properties and overall structural condition.

Phase 4

In this phase the performance of the structure is evaluated. In order to compare the capacity curve with the seismic demand, the MDOF system is converted into an equivalent SDOF system. This transformation is described in Appendix D according to the NPR 9998:2018 [34].

After, the capacity curve is presented into to the same format as the seismic demand, an acceleration-displacement curve. To do so, the base shear is divided by the the effective mass of the system, as explained in Appendix D. The capacity spectrum and ADRS are compared. The intersection of these two curves is called the performance point, which is an estimate of the expected maximum displacement. If the curves do not cross, the structure needs seismic strengthening.

Part II

Structural sensitivity analysis

5. Numerical model

The purpose of this research is to design certain timber seismic strengthening measures for one of the most vulnerable building typologies in the Groningen area. To simulate and test the proposed strengthening measures, first a numerical model of the building typology has to be created. This model is based on certain assumptions on the behaviour of the existing masonry structures. Chapter 4 presents the analysis strategy used, namely the non-linear pushover analysis. Phase 1, the definition of the structural model with the non-linear force-deformation relationships for the various elements, is described in this Chapter.

5.1 Modelling assumptions

There are several ways to model masonry, as addressed in Chapter 3. In this research, it is chosen to model the building typology according to a macro-modelling approach. It is modelled using ETABS17, a 3D non-linear analysis software developed by Computers and Structures Inc. (CSi) California. The approach used is a mechanism based analysis, similar to the SLaMA method described in section 3.3. However, ETABS takes 3D and second order effects into account. It provides a good insight in the seismic behaviour especially for low-rise structures, since their first mode response is dominant and therefore higher mode amplification can be neglected. The modelling process of macro-models is less complex and the calculation time is significantly lower than micro-modelling. This is preferable, because in this research a range of geometric variants of the same building typology are tested, instead of a single component of the structure. Therefore, it is a compromise between accuracy and computational speed. Furthermore, this approach is used in combination with the non-linear pushover analysis.

For URM buildings, the main structure is composed of piers, spandrels and elements that connect them, as can be seen in Figure 5.3. The computation of the capacities of the individual structural components is done according to the recommendations of the Dutch guideline NPR 9998:2018, §G.10 (Appendices E and F). The governing failure mechanism for each element is determined separately. The capacities are based on the mean properties of the masonry used, the geometry and the structural elements and the loads within and on the structure.

The mechanisms that are considered for the pier elements are the following:

- Rocking or flexural mechanism, which accounts for both rocking and toe crushing (respectively a) and b) in Figure 5.1)
- Shear sliding mechanism (see d) in Figure 5.1)
- Shear limit or cracking of bricks (shear tension)

In contrast to the NPR 9998:2017, the diagonal tension failure does not have to be checked for. Instead, the cracking of bricks is taken into account by applying a drift limit for the shear failure.

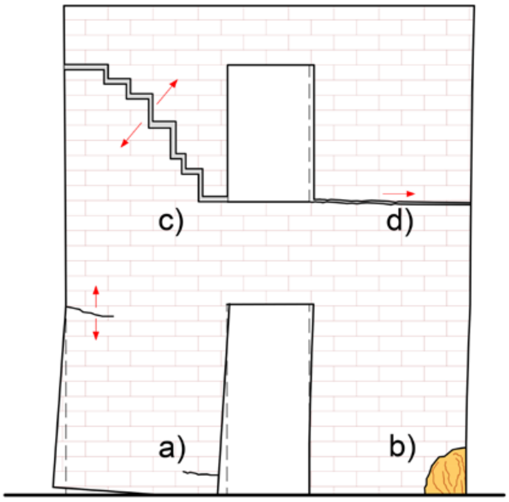

Figure 5.1: In-plane failure mechanisms of masonry piers: a) cracks due to rocking; b) toe crushing cracks; c) shear- diagonal cracks along the mortar bed joints; d) shear-sliding cracks (Source:[14]).

For spandrel elements, two different failure mechanisms are accounted for, namely:

- Flexural failure
- Shear failure

Next to these assumptions, the following assumptions to the overall model of the studied structure have been made:

- The roof diaphragm, gable walls and the clay brick veneer have not been modelled. Instead, mass and weight have been added to the model to account for these elements.
- The foundation is assumed to be fixed.
- Second order effects are checked for.
- The out-of-plane performance of the walls is not modelled in ETABS.
- Only one unit is modelled, therefore pounding effect is not taken into account. Since the structural system of the adjacent units of terraced houses have the same structural system, the effect is likely to govern.

Second order effects

The P-delta effect is a destabilizing moment equal to the force of gravity multiplied by the horizontal displacement a structure undergoes when loaded laterally. To examine if these second order effects should be incorporated in the model, a check according to the NPR 9998:2018 is performed. These effects do not have to be taken into account when for each storey the following applies:

$$\theta = \frac{P_{tot} \times d_r}{V_{tot} \times h} \leq 0,10 \tag{5.1}$$

Where:

θ	is the coefficient for the sensitivity to the relative displacement of floors;
P_{tot}	is the mass on and above the considered floor ;
d_r	is the relative displacement between floors;
V_{tot}	is the total seismic base shear at the considered floor;
h	is the height between floors considered.

When $0,1 < \theta \leq 0,2$, second-order effects can be approximated by multiplying the relevant seismic demand by a factor of $1/(1-\theta)$. The θ value can not exceed 0,3. In that case, either the model needs strengthening or a more complex assessment has to be performed with for example a time history analysis to assess the model in a more accurate way.

5.2 Model of URM building

A typical unreinforced masonry terraced house, as shown in Figure 5.2, is divided in the most essential structural elements. The main structure is composed of piers, spandrels and elements that connect them. Figure 5.3 shows the identification of piers and spandrels of a typical terraced house with large openings on ground level. Together with the connections between them, these elements make up the numerical macro model. In order to speed up the creation of the model and the computational time, the model is simplified, by the of the piers and spandrel element, as demonstrated in 5.3d. A 3D representation of the model in ETABS, is presented in Figure 5.4. It is chosen to model only an end unit of a terraced house.

Figure 5.2: Typical terraced house in Uithuizen, Groningen (Source:[15]).

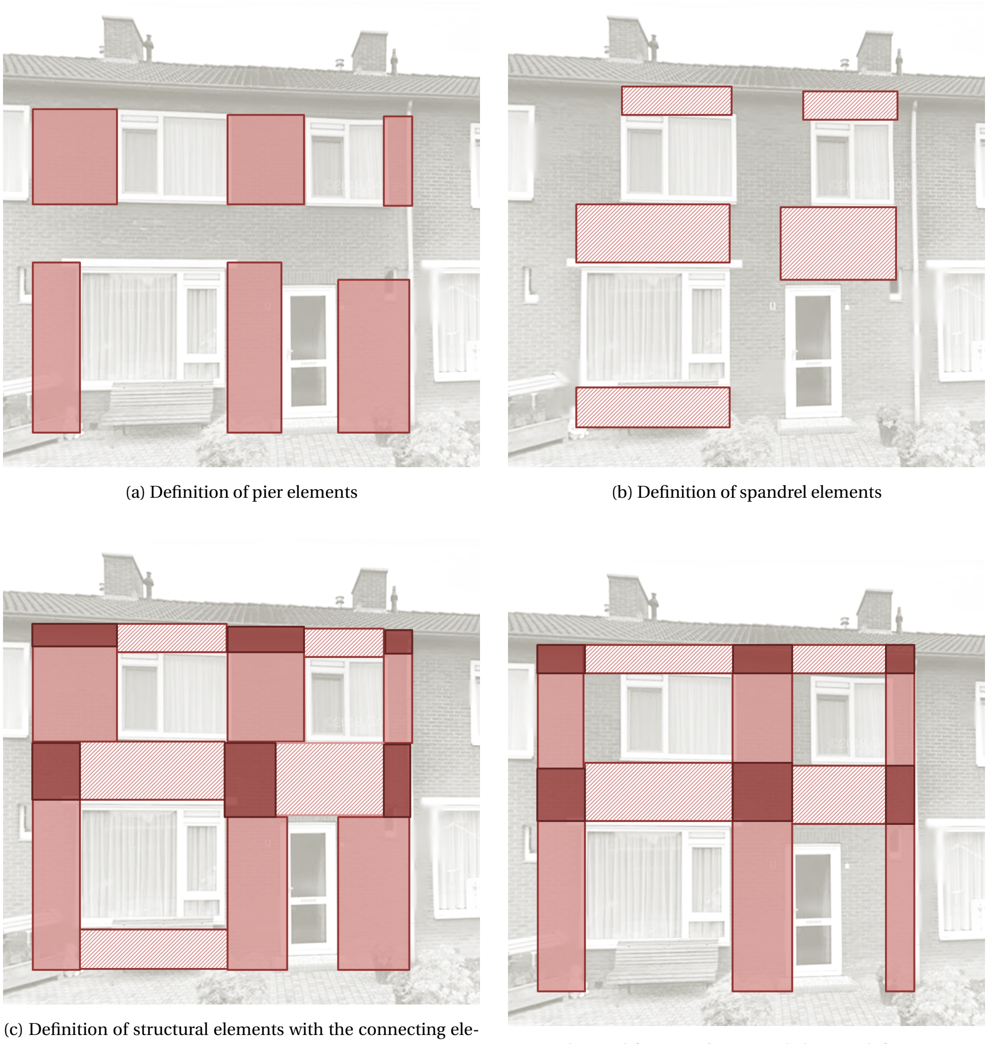

(a) Definition of pier elements

(b) Definition of spandrel elements

(c) Definition of structural elements with the connecting elements

(d) Simplification of structural element definition

Figure 5.3: Definition of the most essential structural elements of a typical terraced house

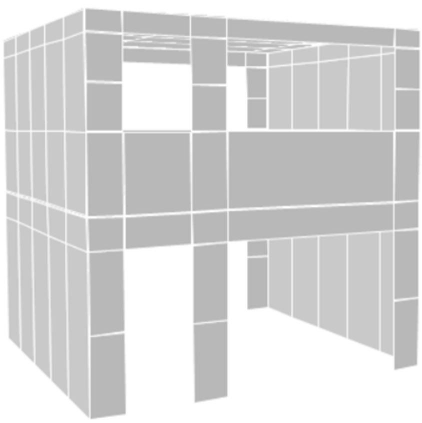

Figure 5.4: 3D representation of a terraced house in ETABS

Walls

The parts in between the pier and spandrel elements function as nodes. The longitudinal façade walls are modelled as shown in Figure 5.3d. The transversal walls of the building are considered closed walls without openings.

All elements are modelled as elastic shell elements. The non-linear behaviour of the building is modelled in the connection between the elements, which are discussed further on. The stiffness of the load bearing elements should be evaluated taking into account the effect of cracking, according to the NPR9998:2018. Since an accurate analysis of cracked elements has not been performed. The elastic flexural and shear stiffness properties of the masonry wall elements are taken to be equal to half of the stiffness of the uncracked elements, see Appendix G Figure G.2. Since the material wall properties do not change over time, it is chosen to implement the most unfavourable situation, which means that in the elastic phase the properties are reduced by fifty percent.

The focus is on the in-plane behaviour of the building. Therefore, the amount of load carried by the elements in the out-of-plane direction is reduced by applying a stiffness multiplier to the relevant wall elements, see Appendix G Figure G.2.

Floors

In this research, both floors are assumed to be concrete slabs. A concrete floor is modelled following a rigid diaphragm approach. For timber floors, this approach is inappropriate, since they are more flexible and therefore follow a flexible diaphragm approach. Figure 5.5 shows the diaphragm extent as modelled in ETABS for both first and second floor.

The floors are either one-way or two-way spanning, as explained in section 2.2. In this research, the first floor is spanning in one direction, from one transversal wall to the other, and the second floor is being carried by both the transversal walls and the longitudinal façade walls. However, the transversal walls take the majority of the vertical loads. The distribution of the loads is done by ETABS and depending on the dimensions of the building, around 75% of the loads are taken by the transversal walls and 25% by the longitudinal walls. Furthermore, wider façade piers bear a larger part of the loads.

The floor-to-wall connection details are based on building specimens representing typical URM cavity-wall terraced houses, used for shake table tests in [36, 17]. In ETABS, the floors are modelled as membrane slab elements, which transfer 100% of the loads that are applied directly to the supporting structural elements. Whereas shell elements have bending stiffness and consequently resist part of the load through flexural deformation. When performing a pushover analysis it is preferred that the floors do not take a portion of the vertical load, so the loads only transfer in the in-plane direction of the slab.

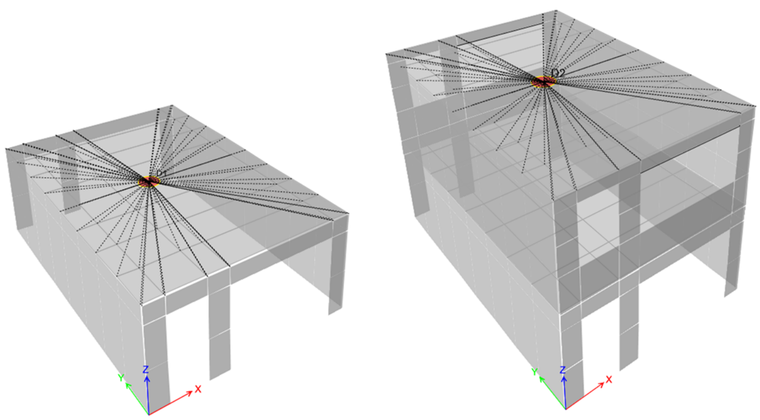

Figure 5.5: Diaphragm extent of the first and second floor

The thickness of a concrete floor in the analysis is assumed to be according to Table 7.4N of Eurocode 2. It proposes a basic span/effective depth ratios for different structural systems of reinforced concrete members. One-way or two-way slabs have a basic span/effective depth ratio of 26 for slightly stressed concrete see Figure 5.6. This value is generally on the conservative side but its a good estimate.

Table 7.4N: Basic ratios of span/effective depth for reinforced concrete members without axial compression

Structural System	K	Concrete highly stressed ρ = 1,5%	Concrete lightly stressed ρ = 0,5%
Simply supported beam, one- or two-way spanning simply supported slab	1,0	14	20
End span of continuous beam or one-way continuous slab or two-way spanning slab continuous over one long side	1,3	18	26
Interior span of beam or one-way or two-way spanning slab	1,5	20	30
Slab supported on columns without beams (flat slab) (based on longer span)	1,2	17	24
Cantilever	0,4	6	8

Note 1: The values given have been chosen to be generally conservative and calculation may frequently show that thinner members are possible.
Note 2: For 2-way spanning slabs, the check should be carried out on the basis of the shorter span. For flat slabs the longer span should be taken.
Note 3: The limits given for flat slabs correspond to a less severe limitation than a mid-span deflection of span/250 relative to the columns. Experience has shown this to be satisfactory.

Figure 5.6: Table 7.4N from Eurocode 2

Connections between elements

The non-linear behaviour of the piers and the spandrel elements is modelled by links between the elements described above. The analysis is mechanism based and considers the most prominent failure mechanisms for either piers and spandrels based on the NPR 9998:2018.

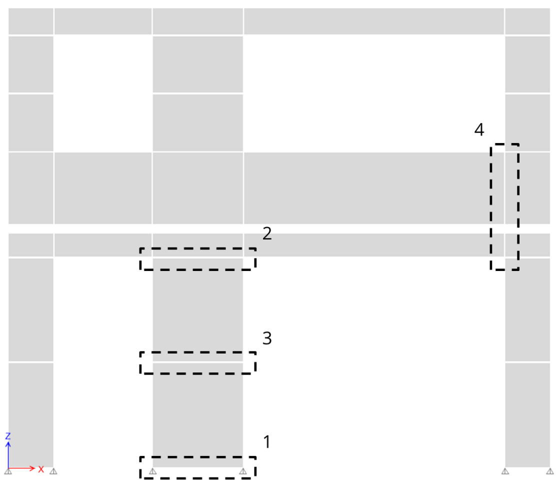

Figure 5.7: Connections between the elements in the façade wall in the ETABS model to account for the failure mechanisms

Piers

The seismic behaviour considered for the masonry piers are shear sliding behaviour, shear tension behaviour and rocking or flexural behaviour. The rotation of a pier that collapses by reaching the moment resistance is limited by the crushing of masonry in the most compressed area, caused by toe crushing. This limit is included in the rocking drift limit, which is based on the compressive strength of the masonry, according to the NPR 9998:2018, see equation E.5. This equation is the result of calibration of relevant test results of masonry piers applied in Groningen [45, 46]. When the numerical model passes this limit, the capacity curve is stopped. The pier has failed due to either toe crushing or rocking or a combination of the two.

Rocking of the piers is explicitly included in the ETABS model by compression only 'gap' links. In the model these links provide the connection between the piers and foundation (shown in Figure 5.8a) and between the piers and rigid elements (Figure 5.8b). The compression only 'gap' link does not take any tension forces. The links allow uplift to occur when the uplift force exceeds the gravity force, causing the pier to rock. When this happens before the pier exhibits shear behaviour, the pier starts rocking.

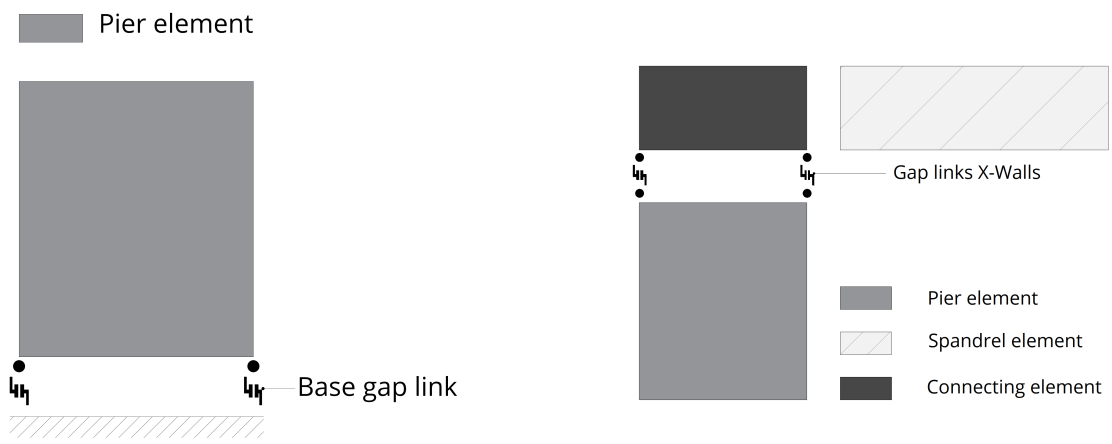

(a) Gap link at the base of the structure, connecting the foundation with pier elements

(b) Links used to model the connection between pier and rigid elements

Figure 5.8: Gap links used to incorporate rocking mechanism.

The shear behaviour is concentrated at non-linear links, MultiLinear Plastic links in ETABS, located at mid height of the piers for convenience. Backbone curves are used to represent the force-displacement relationship of each pier. Both shear sliding and shear tension failure have been considered for the derivation of the backbone curve, which are determined according to the formulas in the NPR9998:2018, Annex G. Appendix E gives an overview of the used formulas according to the NPR9998:2018.

The multi linear force displacement relationship is a function of the wall geometry, material properties and tributary gravity loads, which differs for each wall in the model. Piers connected to the transversal walls, experience active flange effect when pushed. Due to this effect, the compressive stress is considered higher, leading to a higher shear resistance in one direction, as presented in Figure 5.9b (A pier on the other side presents opposite behaviou)r. The passive flange effect is not taken into account. The magnitude of the flange effect is discussed further on. For the central piers, the flange effect is not present. Therefore, the shear capacity is equal in both direction as indicated in Figure 5.9a.

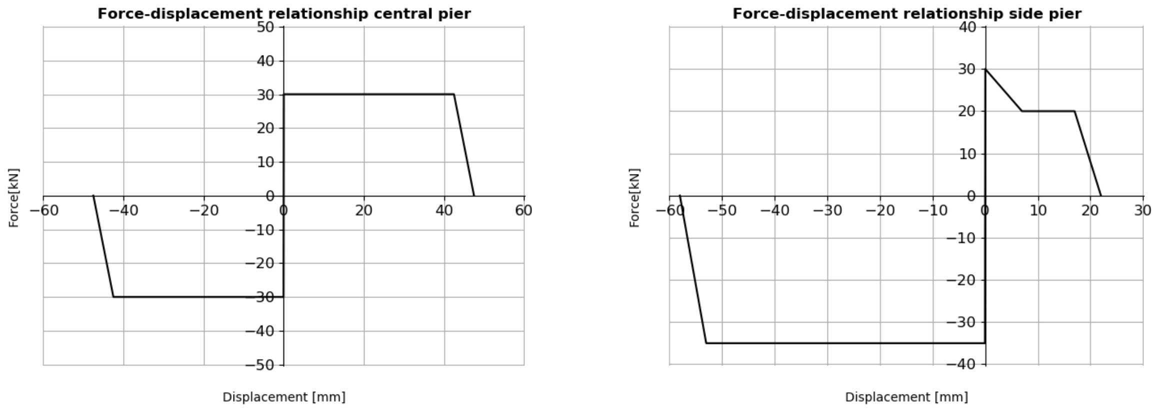

(a) Backbone curve for a central pier

(b) Backbone curve for a side pier with flange effect load taken into account

Figure 5.9: Force-displacement relationships for various pier elements

Figure 5.10 presents that, next to the MultiLinear Plastic link, two different link types are used to model the shear failure mechanism of the pier in ETABS. The linear 'shear free' links provided at the wall ends transfer the overturning forces. The linear 'connector' links modelled along the length of the pier above and below the split ensure an even distribution of shear forces to the MultiLinear Plastic links.

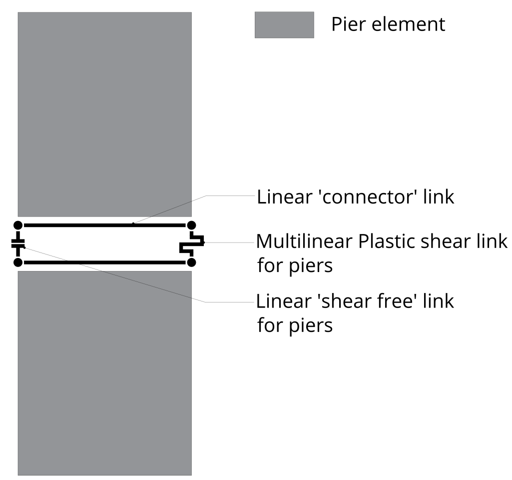

Figure 5.10: Links used to model non-linear shear deformation of the pier walls

Spandrels

The unreinforced masonry spandrels are modelled in a similar way as the masonry piers described above. Shear deformation is modelled with MultiLinear Plastic links at the bottom of the spandrels to transfer shear and chord forces. The input parameters for the force-displacement relationship are determined following the NPR9998:2018 Annex G. The failure mechanisms considered for the spandrels are flexural and shear failure, depending on which one is governing. Formulas used to calculate the capacity can be found in Appendix F. Figure 5.11 shows an example of a backbone curve of the shear links for spandrels.

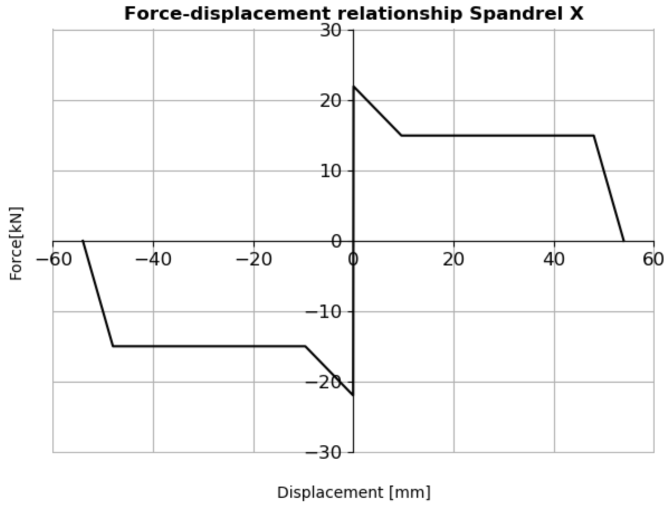

Figure 5.11: Example of the non-linear input of shear links for spandrels

Figure 5.12 shows the various links used to model the spandrel behaviour. The linear 'shear free' link transfers chord forces similar to the 'shear free' links used for the pier behaviour. Linear 'connector' links ensure an even distribution of shear forces to the non linear links. Since the model is constructed per storey, some spandrels are modelled with two separate elements as shown in Figure 5.12 on the right. In that case, three links are modelled as 'shear free' links and only one, at the bottom of the spandrel, is modelled as a non-linear link representing the shear deformation.

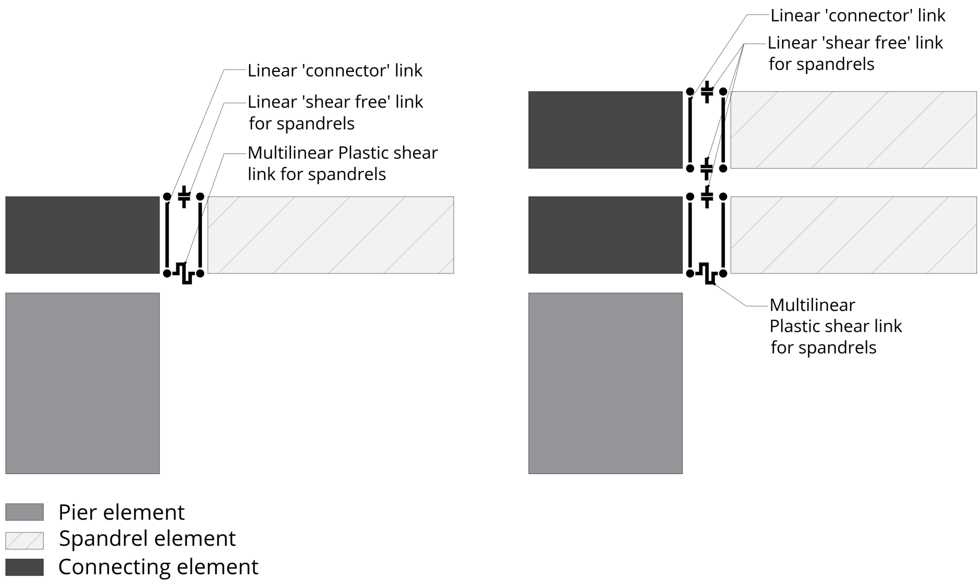

Figure 5.12: Links used to model the connection between spandrel and rigid elements

Floor connections

The connections between the floors and the walls depend on the way the details are designed within the researched typology. In Section 2.2 the most common details of this building typology are described. The first floor is carried by the transversal walls only. The second floor is carried by both the transversal walls as the longitudinal walls. The connection between the floors and the walls is realised by linear rigid links, see Figure 5.13, which assume a perfect rigid connection at each stage of the pushover analysis. When piers at second floor start rocking, the vertical load distribution of the gravity analysis is maintained, assuming that the transversal loads keep contact with the floors. In reality this not the case. During a seismic event the connection between floor and wall could detach, either completely or partly. This can have significant influence on the load path and therefore the capacity of certain elements. Although this can have an influence, it is not taken into account into the model. Figure G.18 shows the link properties within ETABS.

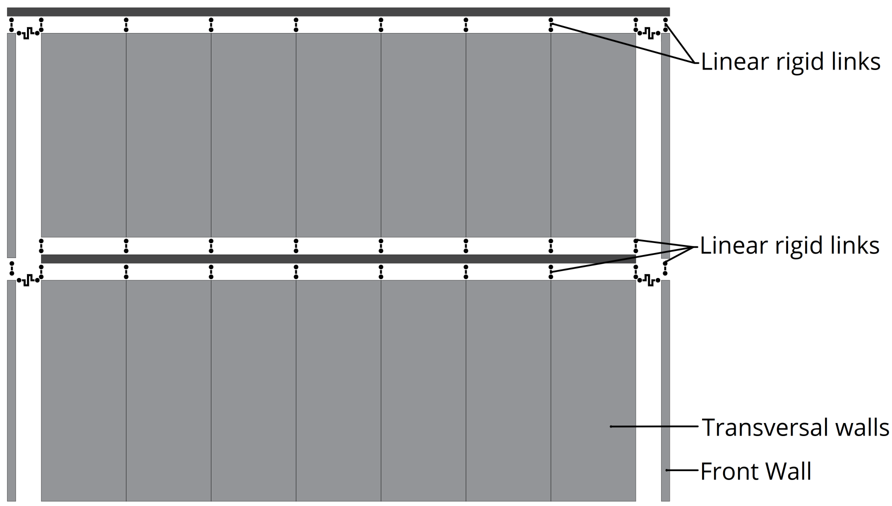

Figure 5.13: Links used to model the connection between floors and transversal side walls and longitudinal front walls

Flange effect

Since the transversal walls and the longitudinal façade walls are connected, they can be considered as flanged walls. For the piers to be able to move during a seismic event, they have to overcome part of the weight of the transversal walls and part of the load that is carried by the transversal walls from the floors. This effect is called the flange effect. This can have beneficial effect on the performance of the piers and the overall performance of the structure, since this creates an extra axial force, which has to be overcome. Flanged walls can have considerably higher strength and stiffness than those without flanges [47].

Instead of connecting both wall elements, it is chosen to model the flange effect as links between the side walls and the front walls, resembling the connection between the two, see Figure 5.14. The is done to get a get better insight in the amount of force that is taken by the piers due to the flange effect. When side and front wall would have been directly connected, it would have not been possible to get insight in the force distribution related to this flange effect, since it is determined by the program (ETABS). The links provide an extra axial force to the connected pier elements, pushing the piers back, which results in more resistance to rocking behaviour.

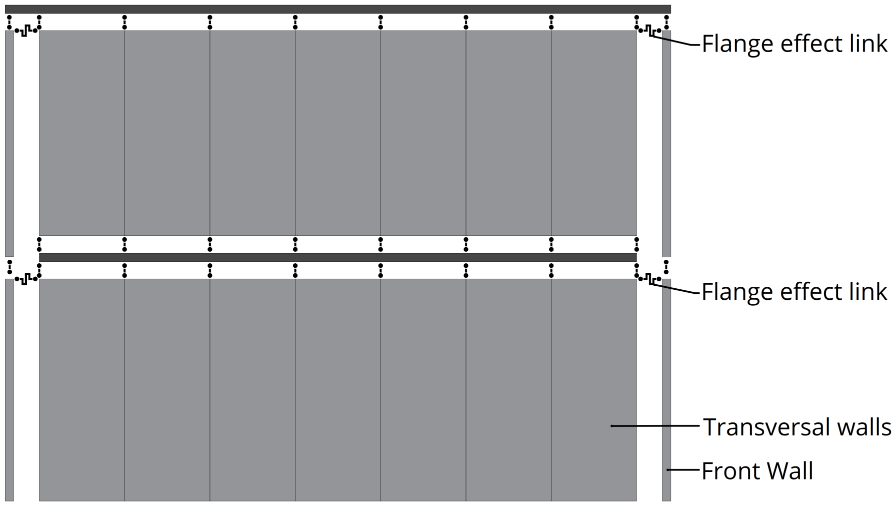

Figure 5.14: Schematisation of the flange links in the ETABS model

The load transfer from adjacent flanges is pre-estimated. The magnitude of force that the link can transfer is limited to this estimation. The contribution of the flanges is only considered when the in-plane mechanism determines the rotation of the pier and the following uplift of the transversal wall, which happens for flexural and shear splitting failure modes.

Five different strategies can be used to estimate the flange effect, according background articles of the NPR 9998:2018 [16, 46]:

- No flange contribution
- Recommendations according to Eurocode 6 (EN 1996-1 5.5.3
- Recommendations according to NPR 9096-1-1 - Masonry structures - Simple design rules, based on NEN-EN 1996-1-1+C1
- Procedure described in Moon et al [47], excluding the possible contribution from uplifted floors;
- Procedure described in Moon et al [47], including the possible contribution from uplifted floors;

The study compares numerical predictions to experimentally recorded values for the peak base shear for seven experimental tests performed on large scale structures, from lab tests carried out by several institutions such as EUCENTRE, TU Delft, Arup and NAM. The predictions are carried out by four different analysis methods, namely a mechanism based analysis, equivalent frame based analysis by 3Muri software, equivalent frame based analysis by DIANA software and a full finite element based analysis.

The results for the sensitivity of the flange contribution assumptions, are presented in Figure 5.15. It shows for every case study that the flange contribution is most accurately modelled when the procedure described in Moon et al. [47] is used, including the possible contribution from uplifted floors. The results are on average closer to the experimental results and therefore this procedure is used in this research.

Case study	Mechanism based analyses (SLaMA)					EF / macroelements (3Muri)	EF / fibre elements (Diana)	Full fem / NLPO (Diana)	Full fem / NLTH (Diana)
	No flange	EN 1996	NPR 9096	Moon et al (no floors)	Moon et al (with floors)				
TUD_BUILD-1	1.68	1.56	1.45	1.36	1.30	1.07[1]	0.88[2]	0.83[3]	0.80
TUD_BUILD-2	1.70	1.62	1.54	1.40	1.23	1.28[1]	0.91[2]	0.99	N/A
EUC_BUILD-1	3.49	3.34	3.08	3.01	2.95	3.15[5]	1.35	1.44	0.98
EUC_BUILD-2	2.34	2.03	2.03	2.03	2.03	2.62[5]	1.15	N/A	1.10
EUC_BUILD-6	2.90	2.83	2.75	2.54	2.34	N/A	N/A	0.88	1.26
LNEC_BUILD-1	4.47	4.30	4.16	4.09	4.09	N/A	N/A	N/A	0.97
LNEC_BUILD-3	2.70	2.42	2.30	2.19	2.17	N/A	N/A	N/A	1.42
No. Analyses	**7**	**7**	**7**	**7**	**7**	**4**	**4**	**4**	**6**
Average	**2.76**	**2.59**	**2.47**	**2.38**	**2.30**	**2.03**	**1.07**	**1.03**	**1.09**
St. deviation	**1.00**	**0.99**	**0.95**	**0.96**	**0.99**	**1.01**	**0.22**	**0.28**	**0.22**

Figure 5.15: Ratio between experimental and predicted peak base shear forces for seven experimental tests performed on large scale URM structures at the laboratories of TU Delft, EUCENTRE and LNEC (Source:[16])

The procedure proposed by Moon et al.[47] is based on likely crack patterns relating to uplift in flange walls. The crack pattern of the transversal walls, which act as flanges to the adjacent piers of the front façade, is assumed to be at an angle of 45 degrees with respect to the base. The tensile crack initiates from the corner of the pier and propagates diagonally upward, as shown in Figure 5.16. It is assumed that the trapezoid area or triangular area above the 45 degrees crack moves together with the in-plane wall [47], act as a flange. Therefore, this area is considered as the effective flange area. The corresponding width is not larger than half of the length of the transversal wall, as shown in Figure 5.16, thus depending on the length of the transversal wall. The possible contribution to the flange effect of the floors that lay on top of the side walls is considered. The slab on the first floor is considered to be spanning in one-way. Therefore the loads are taken by the side walls. The load from the floor that is taken into account is half of the load that is carried by one side wall, see Figure 5.16. Since the concrete slab on the second floor is considered to be a two-way spanning slab, the loads that are taken into account are different. The magnitude of the considered load from the floor is based on the load distribution of a two-way spanning slab, as this is likely carried by the side wall that acts as a flange, see Figure 5.16. The floor loads consists of its self weight and the superimposed dead load. The live load is not taken into account.

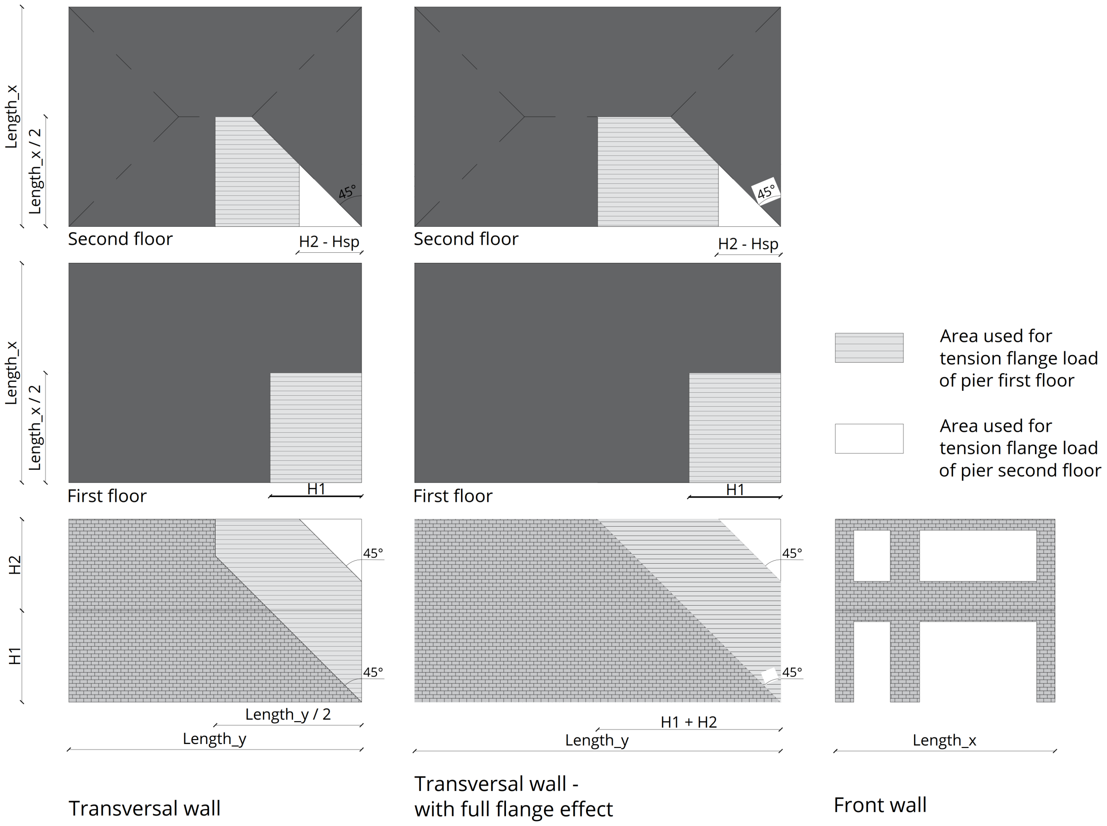

Figure 5.16: Loads taken into account for the flange effect; left: partial flange effect and right: full flange effect.

5.3 Loads

The loads that are taken into account by the model, are a combination of vertical loads (self weight, super dead load and live loads) and lateral loads, representing the seismic action. The magnitude and the implementation into ETABS is discussed in this section.

Vertical Loads

For a seismic design situation, first the vertical actions have to be taken into account. These vertical loads consist of the permanent loads "G" and the variable live loads "Q". The permanent loads include the self weight of all structural elements and additional permanent loads from non-structural elements.

The self weight of the structural elements, the walls and floors, are based on the unit weight of concrete and masonry units and on the geometry of the structure. The self weight of the structural elements, such as the floor slabs and the walls is automatically generated in ETABS. The concrete floor slabs are considered to have a weight of 25 kN/m^3, whereas the walls are considered to have a weight of 20 kN/m^3.

The additional permanent loads (or super imposed dead load) on the floors account for loads from inner walls, ceilings, installations and floor finish. This load is assumed to be 1,65 kN/m^2, see Table B.1 of Appendix B for the calculation.

The variable live load considered is according to Table NB.1-6.2 of NEN-EN 1991-1-1 for floors of houses and has a value of 1,75 kN/m^2. Table 5.1 shows an overview of the loads considered on the first floor slab.

Type of load	Unit	Value	Reference
Self weight concrete floor	kN/m^3	25	
Additional permanent load	kN/m^2	1,65	See Table B.1 Appendix B
Variable live load	kN/m^2	1,75	NEN-EN 1991-1-1 / Table NB.1 - 6.2

Table 5.1: Loads on the first floor slab

The roof structure has not been modelled. Its weight and mass have been added to the weight and mass of the second floor of the model, by increasing the weight and mass modification factor of the second floor slab in ETABS. The gable roof structure is assumed to consist of a ride beam, rafters and purlins, covered with roof tiles. According to the geometry of the building, weight and mass of the roof can be determined. Table B.2 of Appendix B shows an example of the calculation of the weight of the roof structure.

The outer leaf of the cavity wall is not modelled. To account for the mass of the clay brick veneer, the mass of inner leaf (thick shell elements in ETABS) is modified by a factor of 2.

Lateral loads

For the pushover analysis lateral forces are distributed over the height of the structure. These loads are increased in order to push the building until the ultimate capacity of the structure is reached. The load patterns used are described in section 4.2. The lateral loads are applied at the location of the masses in the model, which in ETABS is at diaphragm level, where the masses of the model are lumped. The model is pushed in both directions with both load patterns. So, four pushover analyses are performed.

Load cases

The design value E_d of the effects of actions in the seismic design situation are determined in accordance with 6.4.3.4 of NEN-EN 1990. The inertial effects of the design seismic action is evaluated by taking into account the presence of the masses associated with all gravity loads appearing in the following combination of actions:

$$\sum G_{k;j}{}'+{}'\sum \psi_{E;i} \times Q_{k;i} \tag{5.2}$$

Where:
- $G_{k;j}$: is the characteristic value of the permanent action;
- $\psi_{E;i}$: is the combination factor for variable action, for use in combination with seismic action;
- $Q_{k;i}$: is the variable action.

The combination coefficients $\psi_{E;i}$ for the calculation of the effects of the seismic actions are computed with the following formula:

$$\psi_{E;i} = \phi \times \psi_{2;i} \tag{5.3}$$

Where:
- ϕ: is a coefficient that takes into account that not all mass of the structure moves along;
- $\psi_{2;i}$: is the combination coefficient for the quasi-permanent value of the variable action q_i;

According to the NPR 9998:2018, for classes of surface loads A to C, the value of ϕ for the roof is 1,0 and for the other storeys the value of ϕ is 0,6. The combination coefficient for the quasi-permanent value of the variable action, $\psi_{2;i}$, has a value of 0,3 (EN 1990/Table A.1.1). The combination factor, $\psi_{E;i}$, for the roof is therefore 0,3. For the other storeys the value of $\psi_{E;i}$ = 0,18.

Analysis

After all loads and masses are assigned correctly, a gravity analysis is performed within ETABS. This provides the force distribution within the structure. With these forces the backbone curves for piers and spandrels are determined according to the NPR 9998:2018. After determining the correct non-linear properties, all links in ETABS are updated. Furthermore, the masses per diaphragm are determined to establish the magnitude of the lateral load patterns. Then for each load pattern, in both negative and positive direction of the model, the load cases are set up, as shown in Appendix G Figure G.22. After that, the non-linear load cases are run with ETABS and the output consists of four capacity curves (for uniform and triangular load patterns in both directions).

In addition to strength and deformation capacities of local members, as described the previous sections, global limit state criteria, such as inter storey and effective height drift limits are applied to determine the global capacity of the building. If one of these capacities is exceeded, the capacity curve is stopped, since the global capacity is reached.

5.4 Validation of numerical model

To check the accuracy of the representation of the actual structural behaviour, the model is validated. The outcome is compared to tests done on similar kind of structures in the Stevin Lab at the TU Delft on behalf of the NAM [28, 29].

Description of the tests

Due to induced seismicity in Groningen, an extensive experimental campaign was carried out at TU Delft from 2015 onwards, to provide benchmarks for the validation procedures. As case study, a terraced house typology was part of the campaign. This typology of housing especially, is not designed to withstand seismic loading, due to their very slender walls, limited cooperation between building elements and the use of cavity walls. Cyclic pushover tests have been performed on full-scale assembled structures resembling a typical Dutch terraced house.

Two specimens have been tested: a CaSi brick and a CaSi element masonry assemblage. The dimensions of both specimens are basically the same and can be found in respectively Figure H.1 and H.2 of Appendix H. In both tests the inner leaf of a single housing unit was constructed by calcium silicate masonry, representing only the load bearing part of the structure. The south and north façades are represented by the slender piers connected to the transversal walls. The transversal walls are not perforated. The piers have two sizes, one larger than the other. Each floor consists of concrete slabs spanning between the load bearing transversal walls. The second floor was laid on both the load bearing transversal walls and the piers [29].

The CS brick masonry assemblage is representative of terraced houses built around 1960-1980. The masonry units have dimensions of 210x71x100-mm. The CS element masonry assemblage on the other hand is representative of terraced houses built around 1980-2000. Figure H.3 shows the mean material properties for the used calcium silicate brick and elements.

On both structures a quasi-static cyclic pushover test is performed. The specimen was loaded by four actuators, two per each floor, as can be seen in Figure 5.17. A displacement was imposed at the second floor. A load with the same magnitude was imposed on first floor level, therefore resulting in $F1 + F3 = F2 + F4$. The load was applied by means of reversed cycles composed by 3 identical runs. A run is defined as the time needed to apply the maximum positive and negative target displacement starting and ending at zero [29].

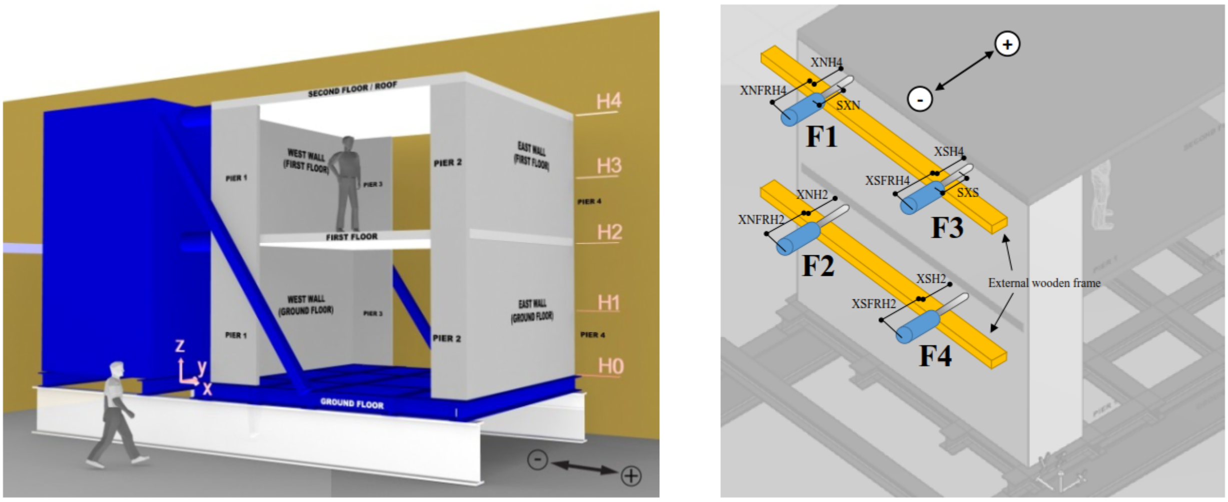

Figure 5.17: Test set up of the masonry structures tested at the TU Delft (Source: [17]).

ETABS model

Both ETABS models, representing the test specimens, were created according to the given dimensions. The loads acting on the model are only the self weight of the structural elements. The weight of a roof structure is not taken into account. Live load and additional permanent loads are neglected, as in the tests. The non-linear properties for the shear links of the piers are computed according to the NPR 9998:2018 using the given material properties of the test specimens. The rest of of the connections is modelled, as explained in the previous section. The flange effect is considered in both representative models, according to the procedure described by Moon et al. [47], including the possible contribution from uplifted floors. Figure 5.18 shows a 3D view of the model of one of the tests in ETABS.

A static non-linear pushover analysis is performed with a uniform load pattern, as is done in the tests at the TU Delft, pushing the first and second floor with the same magnitude. In contrast to the experiment, the pushover is not cyclic. Therefore not taking into account the strength reduction that can occur due to moving in both directions for various times.

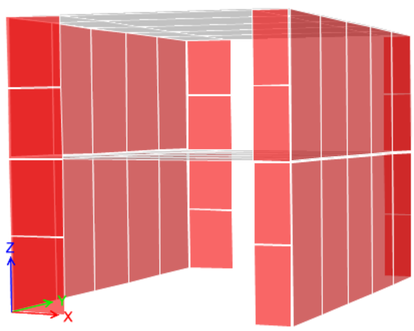

Figure 5.18: A 3D view of the ETABS model of one of the pushover tests

Results

The experimental results of both tests show that the seismic behaviour was mainly governed by the in-plane failure of the piers at the ground floor. The primary failure mechanism being the rocking of the piers. First, cracks occurred at the joint between the concrete floor and the masonry walls. Subsequently, diagonal and vertical cracks appeared in the wide piers at ground floor level, while the rest of the structure was only slightly damaged. The structural response was mainly governed by cracking of the wide piers. The deformation of the piers in both cases was accommodated by the transversal walls acting as flanges. Both experimental tests and the outcome of the numerical models is described in more detail.

CS brick masonry
The capacity curve of experimental test of the CaSi brick masonry assemblage is shown in Figure5.19a. The loading history can be divided in three phases, according to [17]:

1. Initial phase: the structures shows a linear elastic behaviour with an initial stiffness of the structure equal to 15,6 kN/mm. In this phase small horizontal cracks occur, due to which a reduction of stiffness is observed.

2. Pre peak phase: all piers show visible horizontal cracks at both the bottom and top side. Also in the transversal walls, extensive horizontal cracks developed also in the transversal walls. Furthermore, the first diagonal cracks occurred on the transversal walls, mainly located at ground floor.

3. Post peak phase: in this phase a maximum displacement of 82 mm is reached. The specimen showed asymmetrical behaviour for loading in both positive and negative direction. A maximum base shear force of 47.3 kN was reached for positive displacement. The previously observed horizontal and diagonal crack on the transversal walls further extended. After reaching the peak, the capacity and stiffness substantially decreased. Mainly caused by diagonal and vertical cracks in the larger piers. Next to that, the out-of-plane cracks on the transversal walls further developed, by forming the typical yield line envelope.

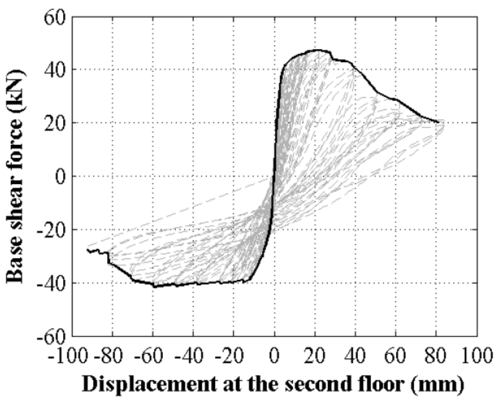

(a) Capacity curve of the experimental test of the CS brick masonry structure (Source:[17])

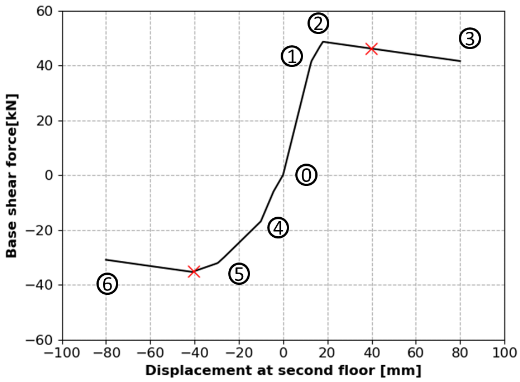

(b) Capacity curve derived by the ETABS model of the CS brick masonry structure

Figure 5.19b shows the outcome of the ETABS model for the CS brick masonry assemblage. It presents the capacity of the structure in both negative and positive direction. Appendix I shows the forces within the structural elements of the model for the different phases. The behaviour can be roughly divided in three phases:

1. Initial phase: for the positive direction (from 0 to 1) the structure shows linear elastic behaviour with an initial stiffness of 4 kN/mm. For the negative direction (from 0 to 4) linear elastic behaviour is observed as well, although with lower initial stiffness of 2 kN/mm.

2. Pre peak phase: In both positive (from 1 to 2) and negative (from 4 to 6) direction the piers on ground floor start rocking. In the positive direction first the smaller piers start rocking, while in the negative direction the larger piers start rocking. At point 5 in the negative direction the smaller piers start rocking as well. The maximum base shear force is reached at 48 kN for the positive direction. For the negative direction the maximum base shear has not yet reached its maximum.

3. Post peak phase: the peak is reached when the rocking mechanism of the piers of both storeys is active. After the peak is reached the capacity and stiffness decreases. In this case, in both directions the drift

limit at effective height is reached before the drift limit of the piers. Resulting in a maximum displacement of 41 mm (depicted in red in Figure 5.19b). Beyond this limit, the model keeps rocking and the capacity is decreased further. The behaviour after this limit is considered less reliable.

As can be seen in the Figures, there are some differences between the capacity curves. The initial stiffness of the structure in the ETABS model is lower than the stiffness found in the tests. The stiffness in positive direction is higher than in negative direction, which is in contrast with the experimental test. However, after the initial phase the test model shows lower stiffness in the negative direction, as is indicated in the ETABS model. Furthermore, the maximum base shear force is similar to the test. The seismic behaviour in the ETABS model is governed by rocking (as shown in Figure 5.20), which is similar to the test. The observed cracks in the test in the transversal walls, are not observed in the ETABS model, since the model is only used to study the in-plane behaviour of the façade walls. The ETABS model can be pushed as far the test, however, for this modelling approach the displacement capacity depends on prescribed limits of local members and global limit state criteria. Results beyond these limits are therefore considered unreliable. In this case, the drift limit at effective height is reached at 41 mm, as presented with the red crosses in Figure 5.19b).

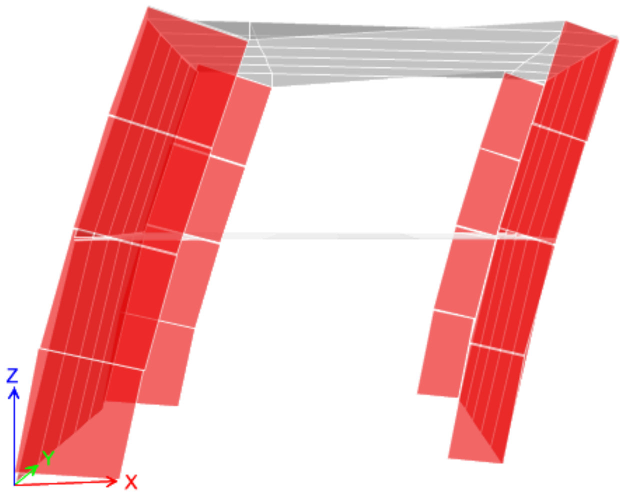

Figure 5.20: A 3D view, showing the failure mechanism presented by the ETABS model

CS element masonry
The capacity curve of the cyclic pushover test of the CS element masonry assemblage is shown in Figure 5.21a. For the test the loading history can be divided in four phases, according to [28]:

1. Elastic phase: linear elastic behaviour of the specimen with initial stiffness of the structure equal to 27 kN/mm. It ends when first cracks appear at the floor-to-wall connections.

2. Pre peak phase: the cracks start being visible. The piers of both storeys start rocking and a gradual reduction of stiffness is observed.

3. Peak phase: the peak resistance of the building is achieved. With a base shear of 68.5 kN at a displacement of the top floor equal to 8.6 mm in the negative direction. The peak is reached when the rocking mechanism of the piers of both storeys is fully active. Also in the transversal walls some cracks appear.

4. Post peak phase: the rocking of the piers localises at ground floor level. Extensive cracks are visible on the transversal walls. The test is continued until failure of the larger piers at ground floor in both façade walls.

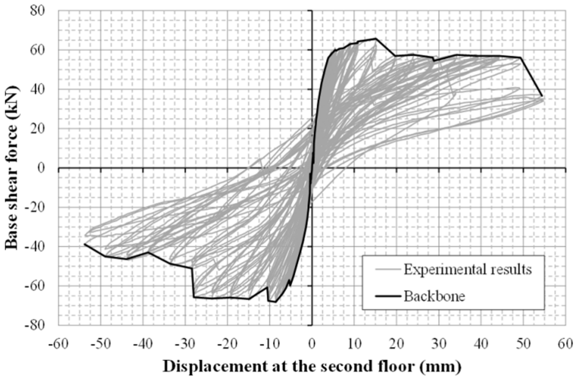

(a) Capacity curve of the experimental test of the CS elements masonry structure (Source:[28]

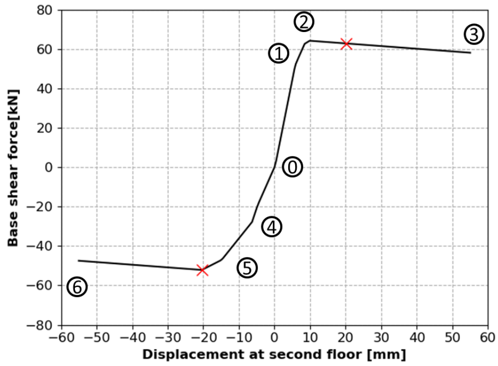

(b) Capacity curve derived by the ETABS model of the CS elements masonry structure

Figure 5.21b shows the outcome of the ETABS model for the CS element masonry assemblage. It presents the capacity of the structure in both negative and positive direction. The behaviour of the structure can be roughly divided in three phases:

1. Initial phase: for the positive direction (from 0 to 1) the structure shows linear elastic behaviour with an initial stiffness of 9 kN/mm. For the negative direction (from 0 to 4) also linear elastic behaviour is observed, although with lower initial stiffness of 4.5 kN/mm.

2. Pre peak phase: In both the positive (from 1 to 2) and negative (from 4 to 5) direction the piers on ground floor start rocking. In the negative direction the larger piers start rocking, followed by the rocking of the smaller piers. The maximum base shear force is reached at 53 kN for the positive direction. For the negative direction the maximum base shear force is reached at 41 kN.

3. Post peak phase: the peak is reached when the rocking mechanism of the piers of both storeys is active. After the peak is reached the capacity and stiffness decreases. The global capacity of the ETABS model is reached when the drift limit at effective for the NC limit state according to the NPR 9998:2018 is exceeded. In this case in both directions a maximum displacement is reached at 21 mm, due to the fact that CS elements with glue mortar are considered to have brittle failure and therefore a lower drift limit.

The initial stiffness of the ETABS model differs from test results, 9 kN/mm instead of 27 kN/mm. The peak capacity is underestimated especially in the negative direction. However, the seismic behaviour is similar. The rocking mechanism of the piers is present, especially the piers on ground floor level. The ETABS model can be pushed as far as the test speciemen, however, the global state criteria are governing.

Conclusion

There are several differences between the ETABS models and the tests. The initial stiffness both tests is underestimated. This difference can be explained by the assumption of cracked elements from the start of the ETABS analysis, underestimating the material properties in the elastic phase. Furthermore, the displacement capacity is underestimated. This modelling approach depends on prescribed capacity values, corresponding drift limits for structural elements and global drift limits. Beyond these prescribed values the outcome is less reliable. This results in a rather conservative outcome when it comes to the displacement capacity of the model with respect to the experimental tests.

The strength capacity form the ETABS models is similar to the tests. However, in some cases it is underestimated, which is preferred to an overestimation of strength. In this way the final outcome of the analysis is on the safe side. The ETABS models do not capture the behaviour of the transversal walls, whereas these walls show extensive cracks in the tests. Although the loads from the transversal walls are taken into account by the flange effect.

Furthermore, the specimens are subjected to cyclic pushover tests, which differ from the pushover analyses done with ETABS. A monotonic displacement-controlled lateral load pattern is used, which is continuously increased until an ultimate condition is reached. This is done separately in both directions, not taking into account the reduction of strength and stiffness due to the displacement in the opposite direction, as done in cyclic tests. This explains differences in capacity curves.

The mechanism based macro-element approach is not expected to predict the structural behaviour in a detailed way. Nonetheless, the overall global behaviour of the structure, which was mostly governed by the rocking of the piers, was predicted for both test in an accurate way up until the global drift limit is reached. Beyond these limits the behaviour is less reliable and shows to be less accurate.

6. Sensitivity analysis

In this chapter, the numerical model described in Chapter 5 is used to asses the structural safety of variants of the earlier defined typology of terraced houses in order to study which parameters influence the seismic behaviour. The parameters analysed are described and the results of the sensitivity analysis are presented and discussed.

6.1 Automation of analysis

The focus is on a two storey URM terraced house with large openings in the ground floor façade. Several variations are present within this typology, mainly geometric. The geometry of a building, can have a large influence on the seismic behaviour. To create a wider range of results and therefore a better insight of the behaviour, a parametric tool is created to study more variations.

The built-in Application Programming Interface (API) of ETABS allows to programmatically use it with multiple programming languages. The programming language Python is used to communicate with ETABS. In this way a lot of processes could be automated. The non-linear properties of the connections and the loads on the structure are related to the geometry of the building. For each change in geometry, loads change and all non- linear properties have to be updated. By programming these operations beforehand, change in geometry leads to a correct numerical model, according to the work flow of Figure 6.1. The work flow shows that structural properties and values for live and super dead loads are changeable as well.

The geometry, structural properties and loads are input for the Python script. Based on the input, it creates the model in ETABS. Walls, piers, spandrels, floors, connections and loads are defined. After, a gravity analysis is performed within ETABS. This provides the force distributions due to the vertical loading. The forces within the structural elements are then extracted from ETABS. Backbone curves for pier and spandrel elements are determined with these internal loads according to the NPR 9998:2018. Properties of the flange links are determined according to the forces within the structure. After determining the correct non-linear properties, all links in the model are updated. Furthermore, masses per diaphragm are extracted from the model to determine the magnitude of the lateral load patterns.

After all link connections are updated and lateral load patterns are established, various pushover analyses are performed according to Section 5.3. The outcome of the pushover analyses, the capacity curves, are extracted from ETABS and transformed into an equivalent single-degree-of-freedom system. Furthermore, the force-displacement curve is converted into an acceleration-displacement curve, according to Appendix D, to compare to the ADRS-curve of the seismic demand.

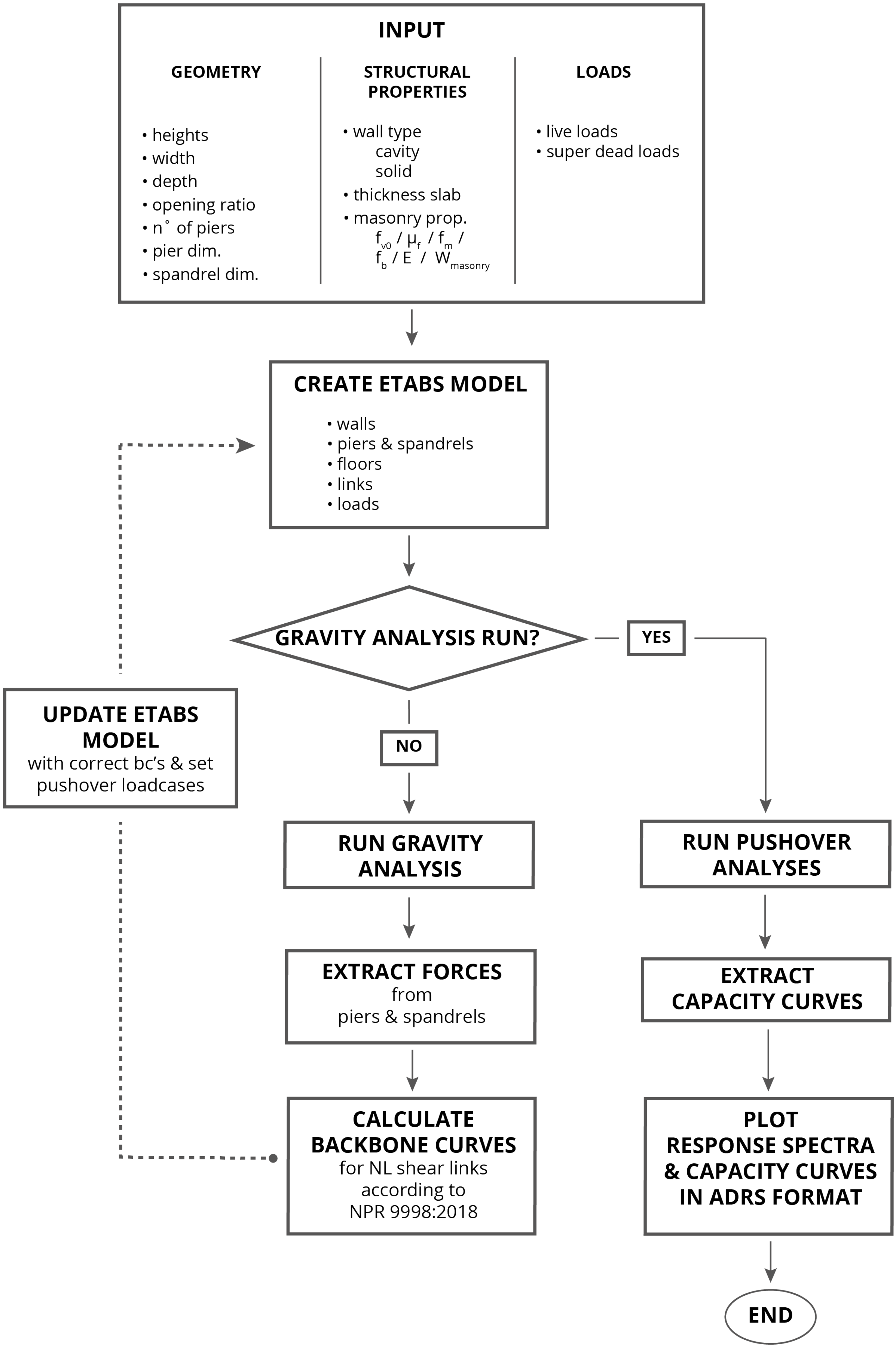

Figure 6.1: Workflow of the script made to automate the analysis in ETABS

Seismic demand

For the seismic action in Groningen, the design value of the peak ground acceleration follows from the NPR 9998 web-tool. The web-tool presents the predicted elastic response spectrum for a chosen return period on a specific location in Groningen. The seismic action is predicted for three different periods, t1, t2 and t2, which correspond with time periods 2018-2020, 2020-2023 and 2023-2027. Figure 6.2a shows an overview of the peak ground acceleration values for a return period of 2475 years for period t1 (2018-2020). Figure 6.2b shows an overview of the corresponding peak ground displacements. As can be seen, a higher peak ground acceleration does not necessarily mean a higher ground displacement.

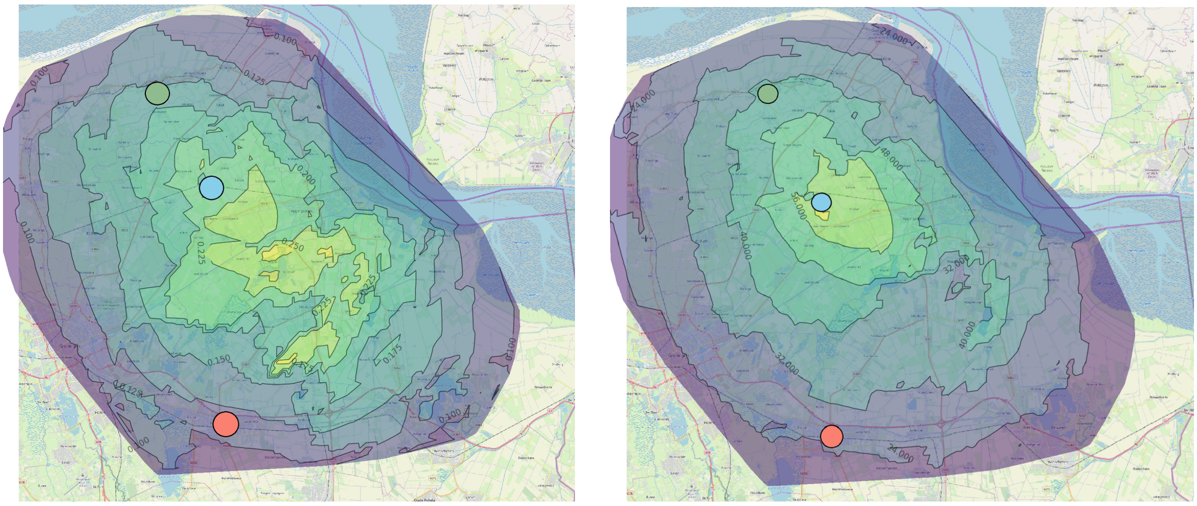

(a) Overview of the peak ground acceleration values for a 2475 years return period for T1 according to the NPR webtool

(b) Overview of the corresponding peak ground displacement values for a 2475 years return period for T1 according to the NPR webtool

After the pushover analysis is performed, the capacity curve of the structure is compared to a seismic demand spectrum. A building is considered to sustain a possible earthquake event with a return period of 2475 years, if the capacity spectrum crosses the demand spectrum. This intersection is known as the performance point of the structure.

Since this research is not bound to a single location in Groningen, three locations are chosen to compare the structural behaviour of the typology to various seismic demand spectra. Figures 6.2a and 6.2b show the locations considered, in blue, green and red, corresponding respectively with Loppersum, Uithuizen and Hoogezand. Loppersum shows the highest seismic action, followed by Uithuizen and Hoogezand shows the lowest seismic action.

The seismic demand is represented by inelastic acceleration-displacement response spectra, modified to account for energy dissipation, ductility and damping of the non linear system, by applying the spectral reduction factor, which is based on the viscous damping ratio of the system, see Appendix C. In this case the capacity curves are plotted against two different response spectrum curves for each location, one with 5% of damping ($\xi_0 = 0,05$) and one with 20% of damping ($\xi_0 = 0,05$ and $\xi_{hys} = 0,15$). In that way a lower and an upper bound for the seismic demand are established.

6.2 Input

The parameters that can be changed for each model with the help of the parametric tool are the geometry, the structural properties and the loads.

Geometry

The parameters that can be changed, to create variations within the building's geometry are the following:

- the global depth of the building
- the global width of the building

- the inter storey heights
- the opening ratio of the longitudinal front walls
- the amount of piers in each front wall
- the dimension of the piers

In order to reduce the amount of variants, the parameters are within a range of reasonable values for two storey terraced houses. Table 6.1 shows the applied values.

Inter storey height (m)	Width	Depth	Opening ratio (%)	Number of piers
2,25	$2h_1$	$2h_1$	50	2
2,5	$2,5h_1$	$3h_1$	60	3
2,75	$3h_1$	$4h_1$	70	4
3	$3,5h_1$			
3,25	$4h_1$			

Table 6.1: Variables within geometry of building typology

The inter storey height of a terraced house is considered to be between 2.25 and 3.25 meter. The width and depth of the building are related to the inter storey height. The opening ratio of the ground floor façade lies between 50 and 70%, since this typology is known for the large openings in the ground floor façade. The opening ratio of the façade wall at the second floor is 25% less than the ratio of the ground floor façade wall. The number of piers is between two and four for one façade wall. Usually a façade wall within this typology has three piers.

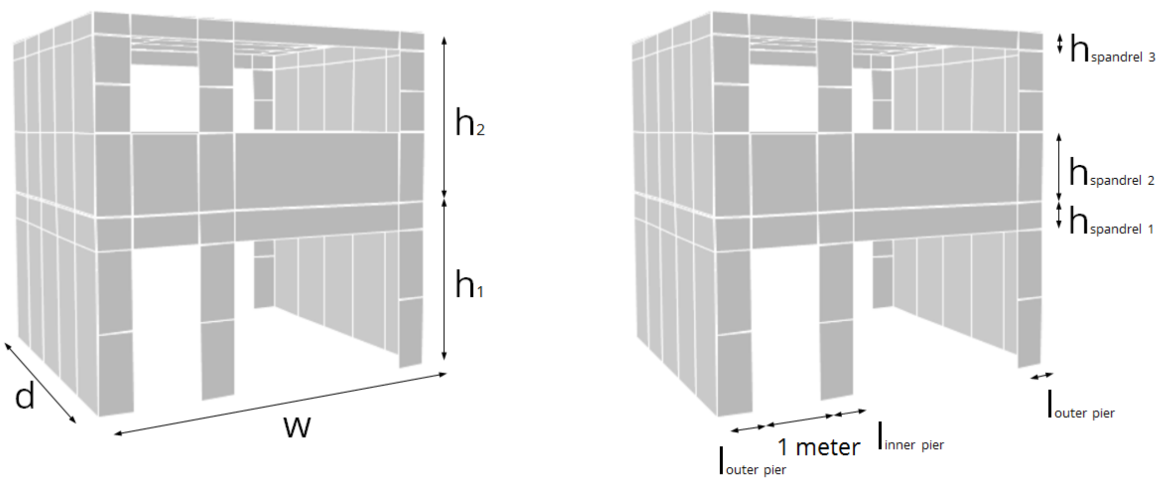

(a) Global dimensions of the model; inter storey height, depth and width

(b) Length of piers and height of spandrels

The length of the piers is considered to be related to the opening ratio. For 50%, 60% and 70% opening ratio, outer piers have a length of respectively 0,6m, 0,5m and 0,3m. The length of the outer piers are considered to be equal. The length of the inner pier in the ground floor façade is then calculated according to the opening ratio and the height of spandrel at first floor ($h_{spandrel1}$ in Figure 6.3b). In Figure 6.3b it can be seen that the space between the inner pier and the outer pier is assumed to be one meter. This is done to resemble the front door, which is always modelled on the left side of the front façade wall. The lengths of the piers can also be adjusted separately for each pier.

The height of the spandrel at first floor is related to the height of the first floor and the door height, resulting in values as given in Table 6.2. The height of the top spandrels of the second floor is kept at a height of 0,3m. The height of the lower spandrel at the second floor is calculated with respect to the opening ratio.

Height 1 (m)	Height door (m)	Height spandrel 1 (m)
2,25	2,1	0,15
2,5	2,3	0,2
2,75	2,3	0,45
3	2,5	0,5
3,25	2,7	0,55

Table 6.2: Height of spandrel at first floor related to door height and inter storey height

Symbol	Material property	Masonry (strength and stiffness values in N/mm²)			
		Clay brick (before 1945)	Clay brick (after 1945)	CaSi brick (1960-present)	CaSi elements with glue mortar (1985-present)
$f_{ma;m}$	Compressive strength	8,5	10	7	10
E_m	Young's modulus	5000	6000	4000	7500
$f_{ma;v;0}$	Initial bed joint shear strength	0,3	0,4	0,25	0,8
$\mu_{ma;m}$	Bed joint shear friction coefficient	0,75	0,75	0,6	0,8

Table 6.3: Mean values if material properties for the different types of masonry studied (Source: NPR 9998:2018, Table F.2).

Furthermore, the back façade is considered to be equal to the front façade, making it symmetric. The openings are vertically aligned, therefore the length of the piers at the first floor are equal to the piers at second floor.

Structural properties

The non-linear properties of the pier and spandrel elements are calculated according to the NPR 9998:2018, and are determined with the help of several masonry properties. The properties of masonry vary for different masonry types. Table F.2 of the NPR 9998:2018 gives the mean values of material properties of the four most common types of masonry. Table 6.3 presents the mean values for the properties that are used in the calculation.
Next to the masonry properties, the type of wall is chosen. Usually, this typology has cavity walls, consisting of two layers of masonry with a thickness of 100 mm. It would also be possible to have a solid wall present. In that case the thickness of the wall is 200 mm.

Loads

The loads on the structure are related to its geometry. The magnitude of the self weight, super dead load and the live load can be adjusted, but for this research they are equal to the values presented in Section 5.3.
The loads due to the flange effect are calculated according to [47], see Section 5.2. To see what the effect of the flange effect load is, the value for the load can be adjusted to a percentage of the total flange effect load.

6.3 Output

The output of the script is a plot of the capacity curve a model against the acceleration displacement response spectra of three different locations with damping ratios of 5 and 20%. In post processing of the ETABS response, NC drift limits from the NPR9998: 2018 have been applied. During each step of the pushover analysis the capacity curve is checked to see if one of the following limits are not exceeded:

- the drift limit at effective height
- the inter storey drift limit
- the shear or rocking drift limit for each pier element

- the flexural or shear limit for each spandrel element

The global drift limits for Near Collapse limit state are given by Table G.2 of the NPR 9998:2018. The drift limit at the effective height for unreinforced masonry with a ductile response is considered to be 0,8%. For a more brittle response, the drift limit is 0,4%. The inter storey drift limit, when having a ductile response is 1.5%. When a more brittle behaviour is assumed, the inter storey drift limit is considered to be 0,6%.

For each pier the rocking drift limit is calculated according to the NPR 9998:2018, see formula (E.5). Every pier has a different drift limit, and therefore, each pier is checked. Furthermore, the exceedance of the drift limit for shear failure is checked, which is determined according to the NPR 9998:2018, see Appendix E.

Capacity curve vs ADRS-plot

The model is pushed in two directions, here called the positive and negative direction. Figure 6.5a shows the model pushed in positive direction and Figure 6.5b shows the model pushed negative direction. The outcome of the script gives four capacity curves, two for the positive and two for the negative direction.

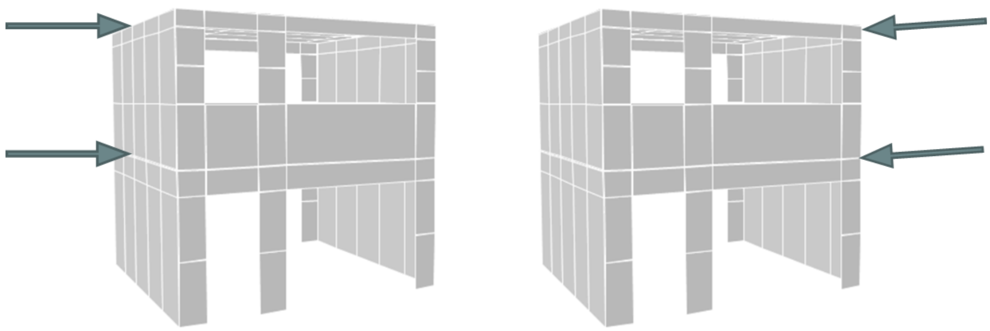

(a) The model pushed in its positive direction

(b) The model pushed in its negative direction

The output of each model shows a box at the top left of the Figure, presenting dimensions: width, depth, inter storey height, opening ratio of the ground floor, wall type, number of piers per façade wall and the length of the piers. A box on the right hand side of the Figure is the legend. Black lines show the capacity curve of the equivalent single degree of system structure due to a uniform load pattern. Dotted black lines show the capacity curve due to a triangular load pattern, as defined in Section 5.3. The coloured lines show ADRS curves of the considered locations in Groningen. Where the dotted line resembles an ADRS curve with 20% of damping ($\xi_{hys} = 0,15$ and $\xi_0 = 0,05$) and solid line resembles an ADRS curve with 5% of damping ($\xi_0 = 0,05$). When the capacity curves intersect with the seismic demand, the model satisfies the NC limit state. If not strengthening of the building is needed for that specific location.

6.4 Results

About 80 variants are assessed, with the help of the script. The influence of certain changes in geometry and structural properties on the seismic behaviour of the structure is analysed by altering the values of the discussed parameters. Most relevant outcomes and trends within the seismic behaviour are discussed. The results for all researched models are presented in the Appendices J to P, but not all are discussed.

Change in height

Changing inter storey height does not have a significant impact on the strength capacity of the building, as can be seen in Figure J.2-J.6 of Appendix J. However, the displacement capacity increases when the inter storey height is increased. This is due to the fact that the drift limit at effective height is governing, which is related to the height. All models satisfy the NC limit state for all locations considered when 15% of hysteretic damping can be taken into account.

The seismic behaviour of the models is governed by rocking of the piers, as presented in Figure 6.5. When a triangular load pattern is applied, piers at second floor start rocking, since the lateral force applied at second floor is relatively higher. Although the rocking mechanism is activated, the rocking drift limit is not exceeded before the drift limit at effective height. The same result holds for models with different opening ratios at ground floor level.

Different storey heights within one structure show similar seismic behaviour as models with equal storey heights. All models with various heights satisfy the NC limit state for all considered locations.

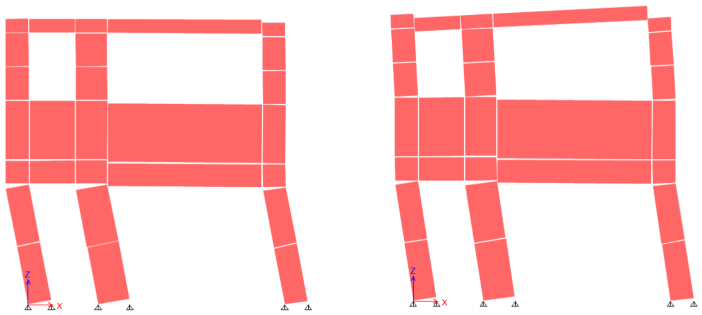

(a) The model pushed in its negative direction with a uniform lateral load pattern.

(b) The model pushed in its negative direction with a triangular lateral load pattern.

Figure 6.5: Seismic behaviour of a model with equal heights (3m) and an opening ratio of 60%

To get insight in the forces of the structural elements during the analyses, the forces of some of the analysed models are presented in Appendix R. Since more than 80 models are analysed, it is not presented for all tested models.

Change in depth and width

Increasing the depth of the structure results in an increase of weight. Furthermore, the loads due to the flange effect increase, since they are related to the depth. Although an increase of the flange effect is likely to benefit the strength capacity, the spectral acceleration capacity decreases with increasing depth, as can be seen in Appendix K. This result holds for different opening ratios at ground floor level. Since the acceleration of the system is related to the effective mass, an increase results in a decrease of the acceleration capacity since the base shear is not increased proportionately.

The seismic behaviour is governed by the rocking of piers, as presented for the various load patterns in Figure 6.6. The behaviour is similar for the other models presented in Appendix K. All these models satisfy the NC limit state when 15 % of hysteretic damping can be taken into account.

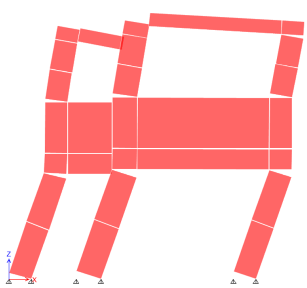

(a) Seismic behaviour due to uniform load pattern in positive direction

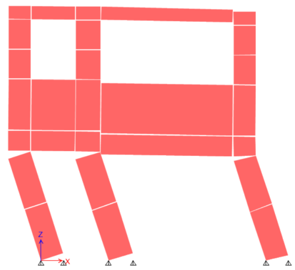

(b) Seismic behaviour due to triangular load pattern in positive direction

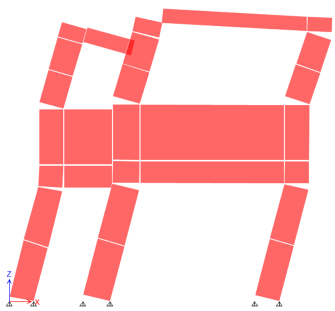

(c) Seismic behaviour due to uniform load pattern in negative direction

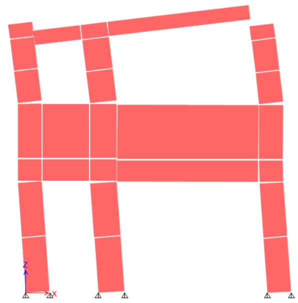

(d) Seismic behaviour due to triangular load pattern in negative direction

Figure 6.6: Seismic behaviour of model with a depth of 8,25m and 60% opening ratio, see Figure K.6.

Changes in width do not have a significant influence on the strength capacity of a structure. Only models with an opening ratio of 50% shows an increase in strength with increasing width. This is mainly due to the larger dimension of the inner piers, as the model gets wider. The seismic behaviour of all models is still governed by rocking of piers. The capacity curves of the various models tested, are shown in Appendix K. All satisfy the NC limit state.

Change in opening ratio at ground floor level

Changes in width, depth and height, are also tested for different opening ratios, as shown in Appendices J-K. Results present that a larger opening ratio of the ground floor wall has significant impact on the strength of the structure. It decreases when the opening ratio increases. Even though the strength is decreasing, models with large opening ratios up until 60% at ground floor level satisfy the NC limit state for all considered locations. The seismic behaviour is primarily governed by rocking of the piers, especially with opening ratios of more than 50%. With an opening ratio of 50% or less, shear failure is more likely to occur.

For models with opening ratios equal to or higher than 70% opening ratio, second order effects, described in Section 5.1, play an important role. The model shows soft storey behaviour, the first floor is relatively less resistant than the second floor. The P-delta effects significantly reduce the displacement capacity. Figure 6.7 presents the capacity curve obtained by ETABS. The red crosses indicate the limit for which the building can be pushed, without collapse due to the second order effects. It can be seen that, due to the low strength and limited displacement, the NC limit state is not satisfied for any location. This is also due to the fact that the seismic demand is increased by a factor of 1.25, to account for the fact that the coefficient for the sensitivity to the relative displacement of the floors is between 0,1 and 0,2. Models with an opening ratio of 70% or more need seismic strengthening in all locations considered.

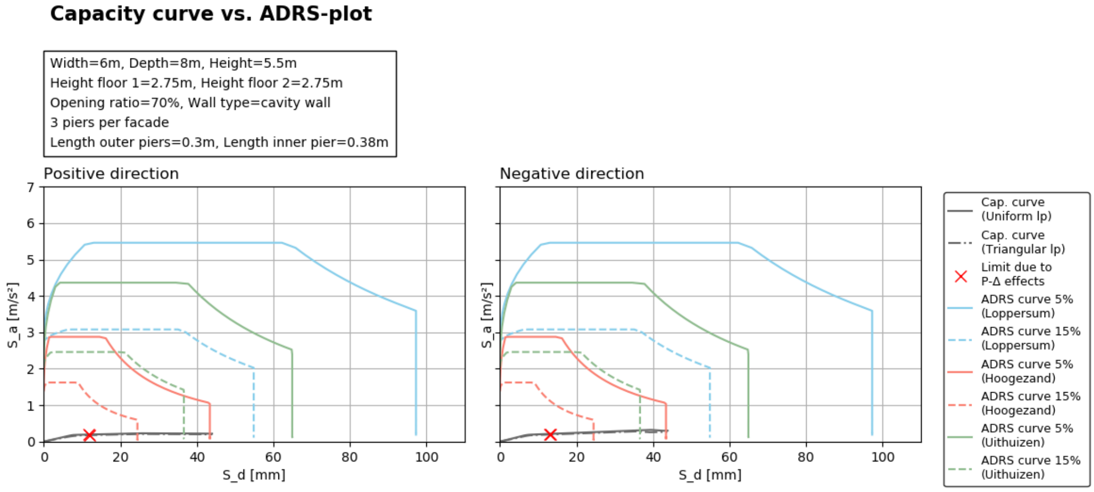

Figure 6.7: Capacity curve of a model tested with an opening ratio of the ground floor façade walls of 70%.

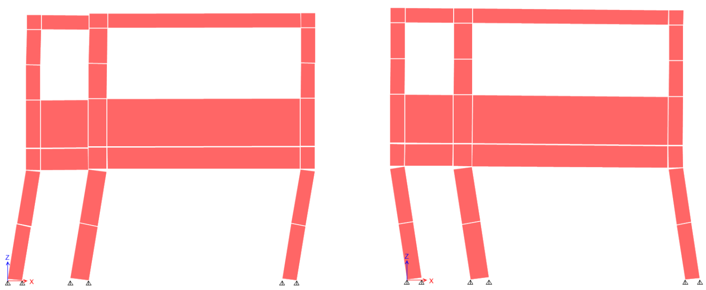

(a) Seismic behaviour of model with 70% opening ratio at ground floor level in positive direction due to uniform load pattern

(b) Seismic behaviour of model with 70% opening ratio at ground floor level in negative direction due to uniform load pattern

Figure 6.8: Seismic behaviour of model with opening ratio of 70% opening ratio.

Change in masonry

The main masonry type tested in this research is the calcium silicate brick masonry used from 1960 onwards, since this is most commonly used as the inner leaf of terraced houses. Three other masonry types, as discussed in Section 6.2, are analysed to investigate the difference in seismic behaviour.

The results show that there is a significant influence on the strength capacity and also the seismic behaviour of the elements is different. Figure Q.3a shows the behaviour of a model with CaSi brick masonry, which is governed by the rocking of piers. The same model with clay brick masonry from before 1945, shows similar behaviour, namely the rocking of piers (Figure Q.3c). The model with clay brick masonry from after 1945, presents, next to rocking behaviour, shear sliding of the right lower piers. The model with CaSi element masonry demonstrates shear sliding behaviour of the middle piers at ground floor level.

Models with CaSi element masonry used since 1985 show less displacement capacity than structures with other masonry, see Figure M.4 M.8 of Appendix M. This is due to the use of the lower drift limit at effective height, which is assumed when brittle response of the structure is expected (drift limit of 0,4% instead of 0,8%). Masonry buildings with calcium silicate elements are more likely to present brittle seismic behaviour. Because of this lower drift limit, the NC limit state is not satisfied for Loppersum. To guarantee safety for similar buildings in the Loppersum area, the building needs seismic strengthening. For the other types of masonry the higher drift limit at effective height can be applied. These models satisfy the NC limit state for all considered locations when 15% of hysteretic damping can be taken into account and therefore do not need any seismic reinforcement.

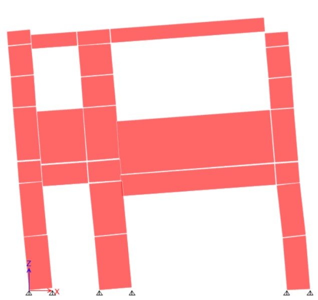

(a) Seismic behaviour of model with CaSi brick masonry used since 1960, see Figure M.5 for capacity curve

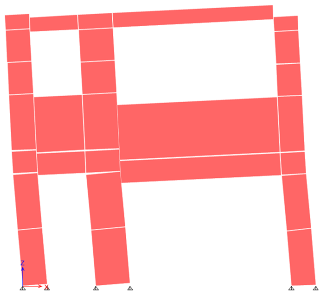

(b) Seismic behaviour of model with clay brick masonry used before 1945, see Figure M.6 for capacity curve

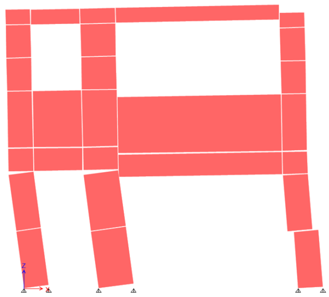

(c) Seismic behaviour of model with clay brick masonry used after 1945, see Figure M.7 for capacity curve

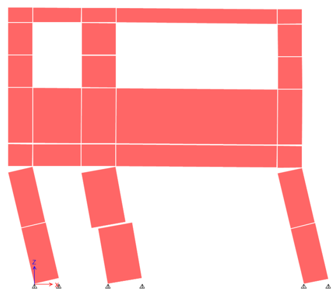

(d) Seismic behaviour of model with CaSi element masonry used since 1985, see Figure M.8 for capacity curve

Figure 6.9: Seismic behaviour of model with opening ratio of 60% tested with different types of masonry. Seismic behaviour of uniform load pattern in negative direction shown

Change in wall type

The behaviour of buildings with solid walls is compared to cavity walls. Solid walls are considered to have a thickness of 200 mm. Appendix N shows the capacity curves of the tested models. The results indicate that the strength capacity is significantly increased when solid walls are used. Models with different opening ratios show the same result.

The seismic behaviour is again governed by rocking of the piers, as is presented in Figure 6.10. No seismic strengthening is needed, since the models satisfy the NC limit state for all locations considered when 15 % of hysteretic damping can be taken into account.

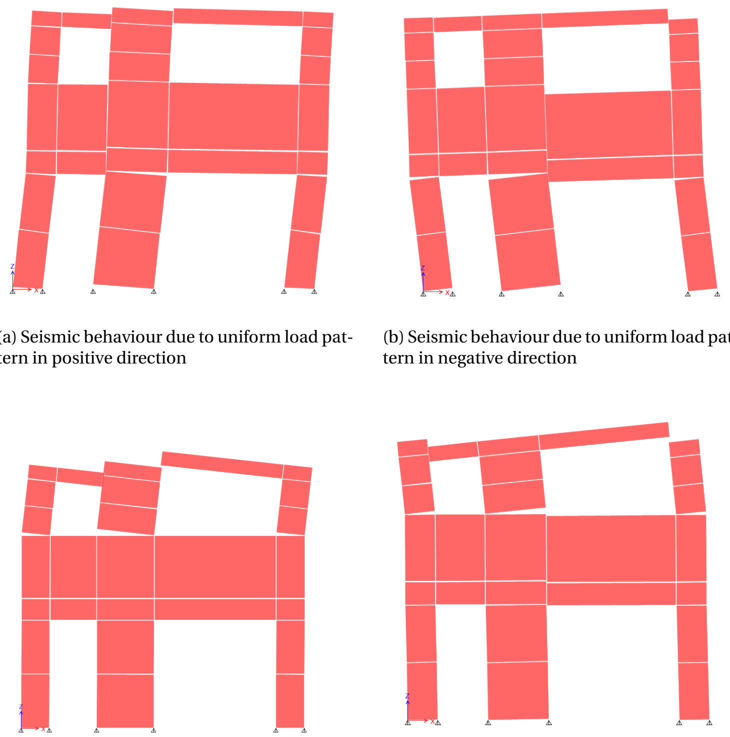

(a) Seismic behaviour due to uniform load pattern in positive direction

(b) Seismic behaviour due to uniform load pattern in negative direction

(c) Seismic behaviour due to triangular load pattern in positive direction

(d) Seismic behaviour due to triangular load pattern in negative direction

Figure 6.10: Seismic behaviour of model with solid walls of CaSi brick masonry after 1960 and an opening ratio of 50%

Change in flange effect

The flange effect is calculated according to [47], with the assumption that the connection between the transversal and longitudinal wall is strong enough to introduce the flange load to the piers. When the connections are as not as strong as expected, less flange load is introduced and the piers experience less resistance to move. To investigate the influence of the calculated flange effect, different percentages of the calculated flange effect, namely 100, 75, 50 , 25 and 0% of loads due to flange effect are tested. The capacity curves of the models tested can be found in Figures O.1 - O.5 of Appendix O. The outcomes show that higher flange effect loads result in higher strength capacity. However, the seismic behaviour is similar and still governed by the rocking of the piers. Although the piers rock, the ultimate capacity is governed by the drift limit at effective height and in this case the models satisfy the NC limit state for all locations considered.

Wider piers

The presence of slender piers due to the large openings leads primarily to rocking behaviour of the piers. The effect of wider piers on the seismic behaviour on the structure is analysed. Both enlargement of the outer piers as of the middle piers is tested. To keep an opening ratio of 50% for the ground floor façade walls, the length of the other piers is reduced accordingly.

The outcome of a structure with wider outer piers (1,8 m) on the left side of the structure, demonstrates both rocking and shear behaviour of the larger piers, as in Figure P.4. The rocking of the top larger piers is governing. However, the structure has sufficient displacement capacity to satisfy the NC limit state for all locations and therefore strengthening is not needed (Figure P.3. The same holds for a structure with wider piers (1,8 m) on the right side of the building, as shown in Figure P.4.This model shows primarily rocking behaviour. However, the drift limit at effective height is governing. The NC limit state is therefore satisfied for all locations considered.

Figure 6.11 shows the capacity curves of a model with 1,8 meter wide middle piers and 0.3 meter wide outer piers. It indicates that this model does not satisfy the NC limit state when the structure would be situated in

Loppersum, see Figure 6.11. The seismic behaviour of the model is governed by shear sliding failure of the lower middle piers, shown in Figure 6.12. Due to shear failure, the structure has less displacement capacity. The loads of the structural elements during the analyses are presented in Appendix R. It shows that after the piers fail in shear, the shear forces in the piers reduce to zero. A similar building situated in Loppersum needs to be seismically strengthened in order to satisfy the NC limit state.

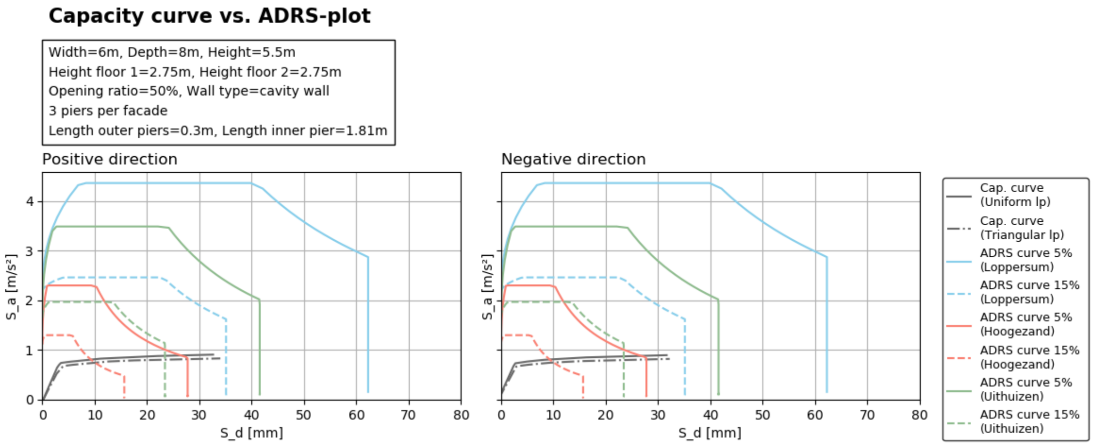

Figure 6.11

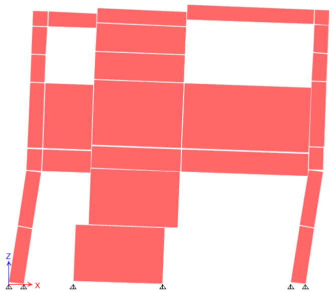

(a) Seismic behaviour due to uniform load pattern in positive direction

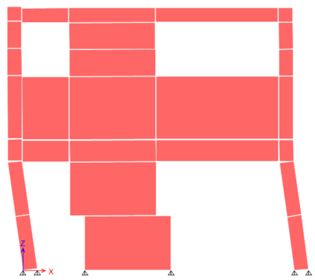

(b) Seismic behaviour due to uniform load pattern in negative direction

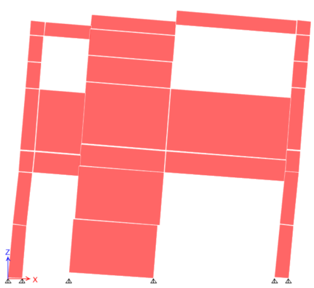

(c) Seismic behaviour due to triangular load pattern in positive direction

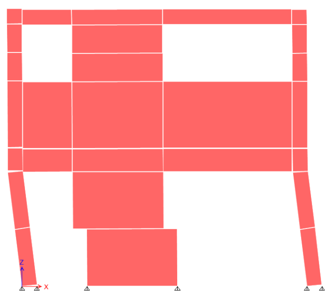

(d) Seismic behaviour due to triangular load pattern in negative direction

Figure 6.12: Seismic behaviour of model with CaSi brick masonry after 1960 and large middle piers (1,8m)

Four piers per wall

All previous analysed models consist of three piers per façade wall, which is most likely to occur in terraced houses. More piers is less expected for this building typology. To analyse the influence on the behaviour of the structure when more piers per wall are present, a model is tested with 4 piers per façade wall. The seismic behaviour and the capacity curve of the analysed model is presented in Appendix Q. The model shows rocking behaviour of all piers. The strength capacity is similar to a model with three piers, which is fairly limited. The drift limit at effective height is governing, resulting in sufficient displacement capacity. The NC limit state is satisfied for all locations in Groningen. Retrofitting is not required.

6.5 Conclusions

Seismic behaviour

It can be concluded that the seismic behaviour of buildings with slender piers is primarily governed by the rocking of the piers. This is in line with experimental tests done on a similar full-scale URM terraced house with concrete floors [36]. The response of the slender piers of the structure was mainly governed by rocking. No significant shear damage occurred in the masonry piers and due to the presence of the rigid concrete slabs the structure exhibited a box-like global response, preventing local out-of-plane failure mechanisms in the transverse walls. The full in-plane capacity of the longitudinal walls was therefore exploited.

The change in height does not have much influence on the strength capacity. The displacement capacity, however, is increased with increasing height, as the drift limit at effective height is related to the total building height and is often governing. Different storey heights within one model do not affect the capacity significantly.

The depth of a building has influence on the in-plane strength capacity. Deeper buildings have lower strength capacity, due to their increased weight. The displacement capacity however is not altered.

Larger openings at ground floor level, cause lower strength capacity. The seismic behaviour of models with an opening ratio of 60% is mainly governed by the rocking of the masonry piers. Models with opening ratios of 50% are more likely to have shear sliding failure, next to the rocking of the piers. Most analysed models with an opening ratio of 60% or less, have sufficient displacement capacity and therefore satisfy the Near Collapse limit state in most cases. For models with a 70% opening ratio at ground floor level, second order effects are governing. Displacement capacity is largely reduced and for that reason need seismic strengthening.

Different masonry types provide diverse capacity curves. Especially the use of CaSi element masonry (used since 1985) shows a way lower displacement capacity than the other masonry types, since element masonry is expected to behave in a brittle way. Therefore lower drift limits are applied.

Structures with solid walls result in a higher strength capacity than when cavity walls are present. Next to that, the load due to the flange effect has a significant influence on the strength capacity. An adequate corner connection is beneficial to the strength of this building typology, since it ensures more load due to the flange effect and a higher strength capacity accordingly. On the other hand, the flange effect can cause reduced rocking drift limits. The flange load causes a higher compressive stress on the piers, which results in a lower drift limit for rocking of the piers, according to equation E.5. In the models tested, the drift limit at effective height is still governing. But in some cases a higher flange load can cause lower displacement capacity.

Furthermore, results show that wider middle masonry piers can cause the model to exhibit shear sliding failure, which can result in less displacement capacity, hence the need of seismic strengthening in some locations in Groningen. The analysis indicates that piers from a length of 1,8 meter (H/B = 1,27) govern the global capacity. Up until a certain length, piers are likely to show shear failure. A lower aspect ratio eventually results in walls that are stiff enough to resist in-plane forces. Research by Messali et al. [48] on full-scale unreinforced masonry (URM) walls with low aspect ratios (H/B=0.6), shows that when low vertical pressure is applied, the walls still fail in shear sliding failure. However, due to the large opening ratios, low aspect ratios are often not present within the analysed building typology.

Drift capacity

The most interesting conclusion of the sensitivity analysis, is that the majority of the models, with an opening ratio of 60% or lower, satisfy the Near Collapse limit state and therefore do not need any strengthening according. Due to the large openings of the building typology, most models are governed by rocking of the piers. However, the ultimate capacity is often defined by the drift limit at effective height rather than the rocking drift limit, since this limit is not yet reached.

The rocking drift limit according to NPR 9998:2018 is tailored for the Groningen situation based on experimental tests done on rocking masonry piers[45]. Several international standards and guidelines include equations based on other empirical and physical tests to estimate the displacement capacity of rocking unreinforced masonry piers. In order to compare the drift capacity given by the NPR 9998:2018, models have been subjected to drift limits for rocking behaviour of other standards. In this case prescribed by Eurocode 8 [49] and The New Zealand 2017 NZSEE guidelines [50].

Eurocode 8 provides a rocking drift capacity at the NC limit state based on the shear ratio, (H_0/L). H_0 is the distance between the point of zero moment and the base of the wall and L is the pier length. Equation 6.1 is used to estimate the ultimate drift of a masonry wall/pier when its capacity is controlled by flexure/rocking.

$$\theta_{R;NC;EC8} = \frac{4}{3} \cdot \left[0.008\left(\frac{H_0}{L_{pier}}\right)\right] \tag{6.1}$$

The rocking drift limit according to the NZSEE guidelines estimates the drift capacity for the Life Safety limit state, which is the equivalent of the Significant Damage of the NPR. To compare to the NC limit state, a factor of 4/3 is applied. The drift limit is proportional to the aspect ratio (H_{pier}/L_{pier}), as given in equation 6.2. The NZSEE gives a maximum drift limit, since the lateral performance of a rocking wall is considered to be less reliable and it does not provide the level of resilience considered appropriate when deflections exceed this value [50].

$$\theta_{R;NC;NZSEE} = \frac{4}{3} \cdot min\left(0.003\left(\frac{H_{pier}}{L_{pier}}\right); 0.011\right) \tag{6.2}$$

The rocking drift limit according to the NPR 9998:2018 is based on relevant test results of masonry piers used in Groningen [45, 46] and is calculated with the following formula (see also E.5 of Appendix E):

$$\theta_{R;NC;f} = 0,0135\left(1 - 2,6 \times \frac{\sigma_y}{f_{ma;m}}\right) \times \left(\frac{h_{ref}}{h_{pier}}\right) \times \sqrt{\frac{h_{pier}}{l_{pier}}} \tag{6.3}$$

Table 6.4 shows the various rocking drift limits for all piers in a model with an opening ratio of 60% at ground floor level. A typical axial load ratio $(\sigma_y/f_{ma;m})$ for low rise buildings is less than 10%. Which means that for the rocking drift limit of each pier, with the same dimensions, is higher when calculated according to the NPR 9998:2018 compared to the EC8 or the NZSEE guidelines. Two times higher drift limits can be realised, as shown in Table 6.4. Furthermore, the drift limits according to the NPR exceed 0,011, which is considered to be the maximum drift limit according to the NZSEE guidelines. Apparently the NPR 9998:2018 allows rocking drift limits of three times the maximum value of the NZSEE guidelines. The drift limits according to EC8 for longer piers are similar to the NPR. However, shorter piers less high drift limits, more similar to the NZSEE guidelines.

Pier ID	Height pier (mm)	Length pier (mm)	Rocking drift limit NPR9998:2018	Rocking drift limit Eurocode 8	Rocking drift limit NZSEE Code
P1	2280	500	0,0239	0,0243	0,01467
P2	2280	700	0,0186	0,0174	0,01303
P3	2280	500	0,0234	0,0243	0,01467
P4	1320	500	0,0362	0,0141	0,01056
P5	1320	700	0,0250	0,0101	0,00754
P6	1320	500	0,0338	0,0141	0,01056
P7	2280	500	0,0239	0,0243	0,01467
P8	2280	700	0,0186	0,0174	0,01303
P9	2280	500	0,0234	0,0243	0,01467
P10	1320	500	0,0362	0,0141	0,01056
P11	1320	700	0,0250	0,0101	0,00754
P12	1320	500	0,0338	0,0141	0,01056

Table 6.4: Rocking drift limits for a model with 60% of opening ratio at the ground floor level according to various standards

Figure 6.13 shows the capacity curve of a model with the rocking drift limits calculated according to the NPR 9998:2018. Figure 6.14 presents the same model subjected to rocking drift limits according to EC 8 and NZSEE guidelines. The results demonstrate that a difference in rocking drift limit can mean the difference between strengthening and no strengthening. Both models show the same behaviour, but in the model according to NZSEE, the rocking drift limit is governing and therefore the displacement capacity is believed to be less. The majority of the models in this research, strengthening is needed if rocking drift limits similar to the NZSEE guidelines are applied. Although it must be said that the NZSEE codes are prepared for tectonic earthquakes, while in Groningen induced earthquakes are present. Tectonic earthquakes have a duration of several minutes, while the induced earthquakes occur for a small amount of time, having less impact on the behaviour of a structure.

The drift limits according to Eurocode 8 are less strict than the limits according to the NZSEE guidelines. However, when these limits are applied, the model needs to be retrofitted when a similar structure is situated in Loppersum, see Figure 6.14.

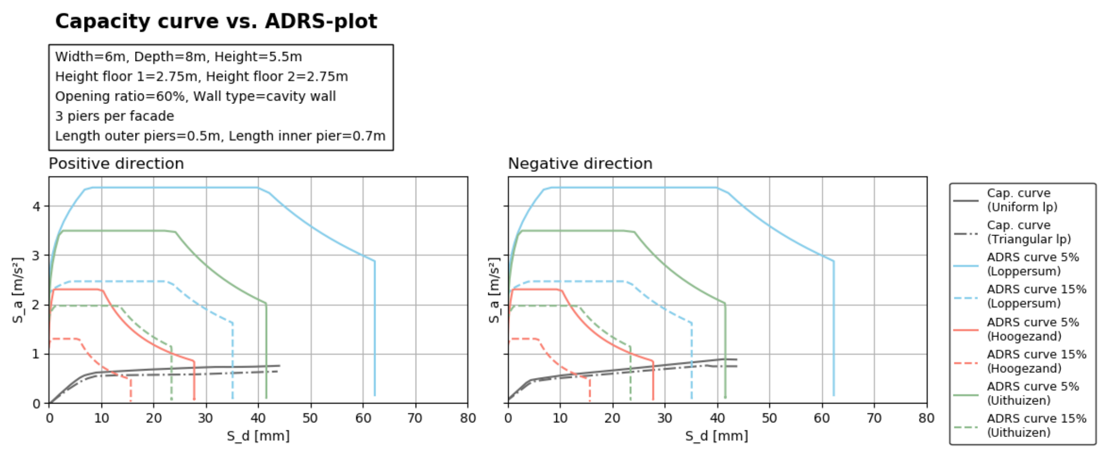

Figure 6.13: Capacity curves of a model with a 60% opening ratio. Assessed with the rocking drift limits according to the NPR 9998:2018

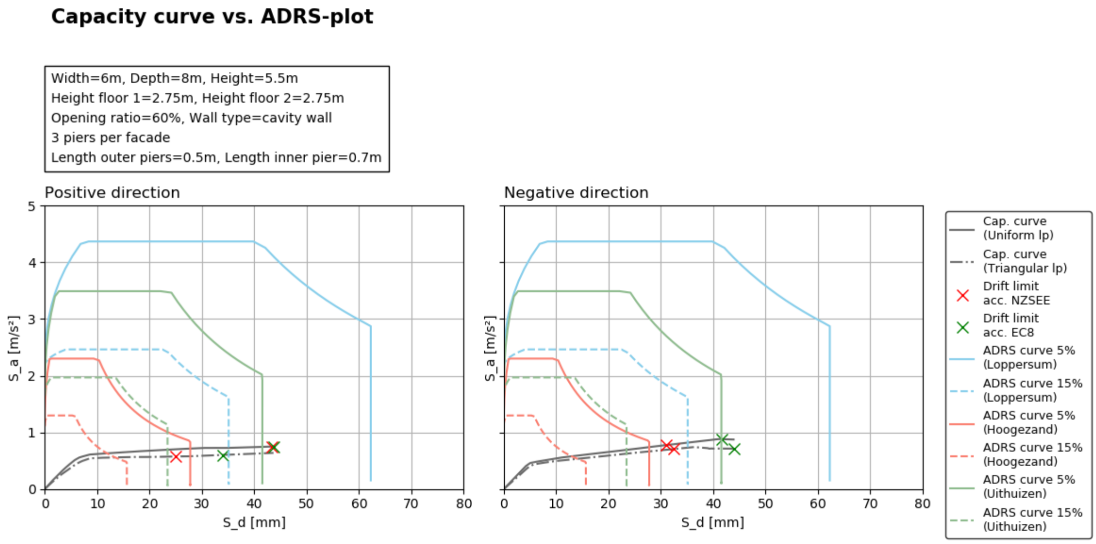

Figure 6.14: Capacity curves of the same model with the rocking drift limits according to Eurocode 8 (green) and NZSEE guidelines (red)

Other research, based on various in-plane tests, shows that walls characterized by flexural/rocking mechanisms provide much higher values of drift, on average larger than 1,10% [51]. It is evident that the differences between drift limits demonstrate the need for further investigation on the main seismic parameters that influence the in-plane response of unreinforced masonry walls.

However, global behaviour and global drift limit of the analysed models, are in line with experimental tests. A similar URM terraced house, with an opening ratio of 50% at ground floor level and two concrete floors, is tested at the EUCENTRE [36]. The ultimate global drift of the structure was 0,7%, which corresponds with a ultimate displacement of 38 mm at second floor. The behaviour was mainly governed by rocking of the slender piers. With the predicted seismic demand for 2018-2020, this building satisfies the NC limit state in all locations considered, if an additional hysteretic damping of 15% could be applied. The predicted decrease in seismic demand, due to the stop of gas extraction, is likely the cause of the satisfaction of the Near Collapse limit state of a large amount of structures.

Part III

Design and assessment of strengthening measures

7. Timber retrofit

This chapter discusses the seismic behaviour of timber and proposes timber retrofit designs for the terraced houses which are analysed in the sensitivity analysis in Chapter 6.

7.1 Seismic behaviour of timber

Timber structures generally perform well under seismic events, according to [52]. The main benefits of timber are low weight to strength ratio and ductile joints. Seismic load on a structure is proportional to its mass. Keeping the weight low reduces the seismic load on a structure. Due to these advantages of timber, engineers in high-seismic regions have significant interest in using timber in seismic engineering. Timber structures allow energy to dissipate before the load bearing capacity is reached, due to plastic deformations of the connections. Therefore, it is able to withstand higher earthquake loads.

The main construction methods used in timber engineering are: timber framed structures, cross laminated timber structures and moment resisting frames, see Figure 7.1. The main focus in this research is on timber frame shear walls and CLT wall structures.

(a) Timber frame structure in construction (Source:[53]).

(b) CLT structure in construction (Image Credit: D.R. Johnson).

(c) Timber moment frame structure in construction (Source:[54]).

Figure 7.1: Main timber construction methods

7.2 Timber frame structures

The walls of timber frame structures are composite elements, consisting of vertical timber studs, top and bottom joists, wood-based sheathing and dowel type fasteners, such as nails, screws or staples. The sheathing can be present at one or both sides. The studs are usually anchored to the foundation to prevent vertical uplift of the wall. Figure 7.2 shows a example of a timber frame shear wall with several segments.

Timber frame walls are often used for single- and multi-storey houses. Structurally, such walls can be considered as vertical diaphragms or shear walls, being able to resist lateral forces, such as wind and seismic loads. The sheathing transfers the loads effectively to the foundation, acting as bracing to the timber frame elements. The frame usually consist of solid timber elements. Next to the ability to resist to horizontal forces, they can be produced to protect against fire and provide heat and sound insulation.

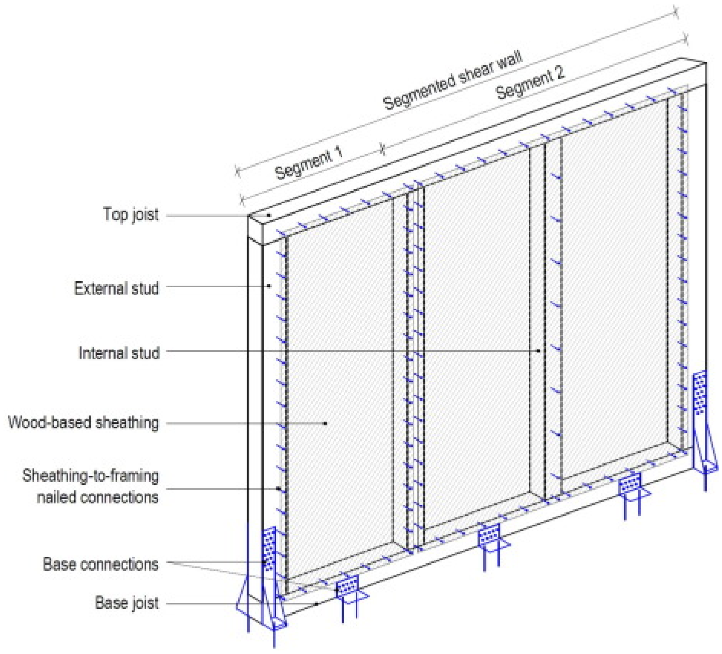

Figure 7.2: Example of a segmented timber frame shear wall (Source:[18]).

Connections

The deformation and the strength of a timber frame wall primarily depend on sheathing-to-framing connections. The performance of a wall can be calculated by evaluating the load-bearing capacity of the individual elements.

Ductile behaviour of laterally loaded timber joints with dowel-type fasteners such as nails, is realised due to the interaction of plastic deformation of the fasteners and the embedment of the timber elements to which the fasteners are connected. The characteristic load-bearing capacities can be determined using the Johansen theory as adopted in Eurocode 5 [31]. The capacity is limited to the point where the embedment strength is reached in at least one of the timber members. Figure 7.3 shows the various failure mechanism that can occur for single- and double-sided timber-to-timber connections. Which failure mechanism occurs, depends on the geometry of the joint and the material properties of the timber and the sheathing.

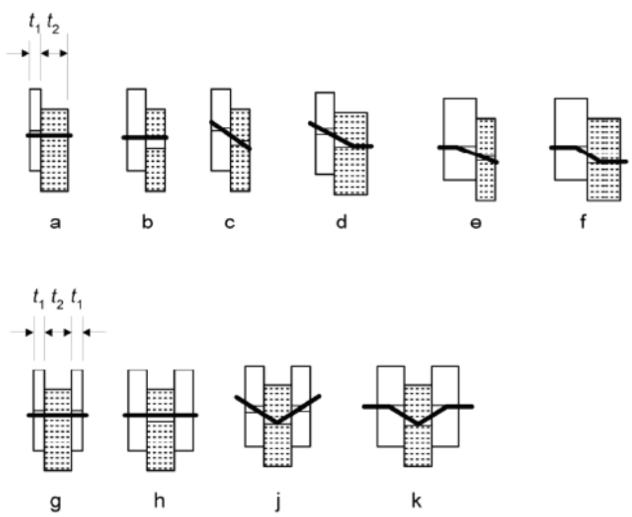

Figure 7.3: Failure mechanisms for single- and double-sided timber-to-timber connections (Source: NEN-EN 1995-1-1).

To enhance joint ductility, failure mechanism f or k in Figure7.3 is preferred, since the plastic embedment deformations of the wood and the plastic bending deformations of the fasteners contribute to the ductile behaviour. Due to adequate selection and design of the connection, brittle failure mechanisms can be avoided. Such behaviour is more likely to take place when the nail diameter d does not exceed 3.1 mm and the wood-based sheathing is at least 4d thick, according to Eurocode 8.

As a result of the distortion of the fastener connections, the shear wall displaces laterally. When there is no vertical force present, uplift of the wall occurs. This is usually prevented by application of hold-down anchors, which are positioned at the corners of the shear wall and connected to the outer studs with nails and connected to the foundation with the help of anchor bolts. The hold-down should be assessed for the tension and compression forces it endures.

7.3 Cross laminated timber structures

Cross Laminated Timber (CLT) is a relatively new construction material known as massive or ”mass” timber. It originated some 20 years ago in Austria and Germany and is gaining a significant popularity as a sustainable alternative to steel and concrete [55]. It is considered to be a heavy construction system which is used typically for residential construction in Europe and is comparable to known wood products, such as plywood, core-board or solid-wood board. The difference comes with the essential advantage of high dimensional stability in-plane due to minimized swelling and shrinkage rate caused by the cross-wise layering [56].

CLT panels consist of multiple layers of timber boards stacked crosswise (often at 90 degrees) and glued together. It consists of at least three glued layers of boards with opposite orientation between them. In special configurations, two consecutive layers can be orientated the same way to obtain specific structural capacities. Usually it is produced with an odd number of layers. Thickness and width of the timber layers vary depending on the manufacturer. Figure 7.4 shows an example.

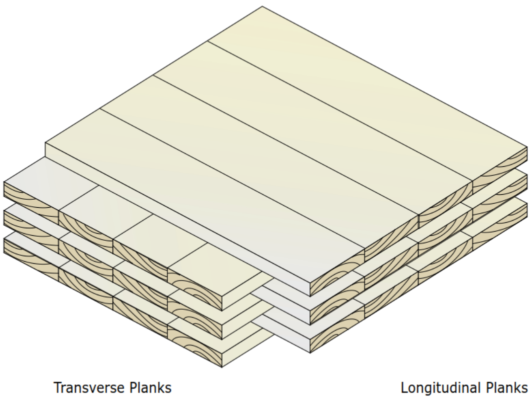

Figure 7.4: Example of CLT panel configuration (Source:[19])

CLT provides relatively high in-plane and out-of-plane strength and stiffness properties, which allow two-way action that is similar to reinforced concrete slabs. Due to the prefabricated nature, it allows a faster construction process, with more precision, increased safety and less waste.

Internationally, several full scale tests on CLT buildings have shown good results when subjected to seismic forces [57, 58, 59]. Compared to other light frame structures, a higher in-plane stiffness and a greater load-carrying capacity can be reached [60]. Although recent research shows that it is a promising building material when used for seismic engineering, still a lot of research is needed.

The seismic behaviour of CLT structures depends mostly on the performance of the connections [60], as with the light weight timber frame structures, according to several experimental studies [58, 21, 61, 62]. When energy dissipation is required, connections become significant, since they provide deformations in the elastic range. Usually steel brackets and tie-downs are used to connect the CLT walls to the foundation. Figure 7.5

shows different configurations of CLT shear walls with the connections to the foundation.

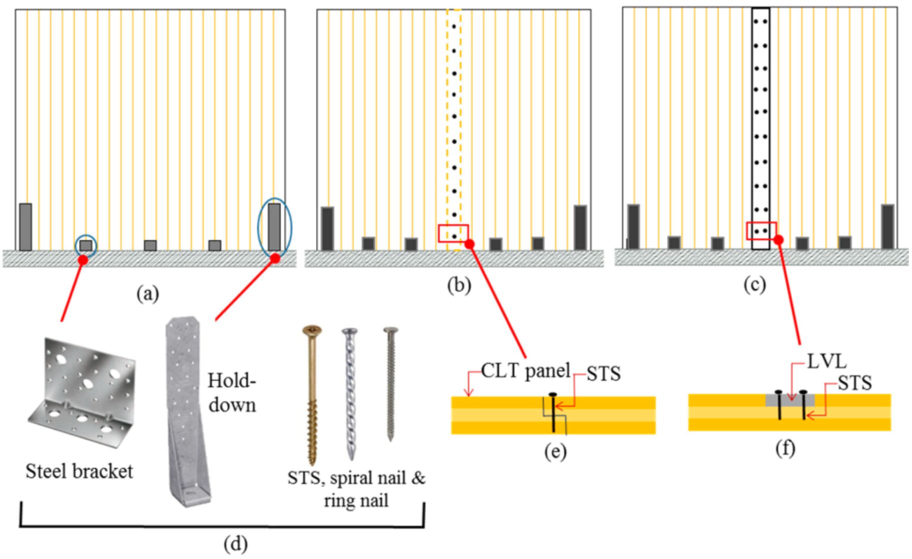

Figure 7.5: CLT shear walls: (a) single, (b) coupled wall with lap joint, (c) coupled wall with spline joint, (d) connectors and fasteners, (e) half-lap joint, (f) spline joint (Source:[20])

Comparison with timber frame shear wall

CLT shear walls experience less deformation when subjected to seismic loads compared to timber frame walls. Sheathing of timber frame walls is connected by a large number of fasteners which can all deform, whereas this is not the case for CLT walls. Figure 7.6 shows a comparison between several timber frame and CLT shear walls for three different lengths. The timber frame wall demonstrates more displacement capacity.

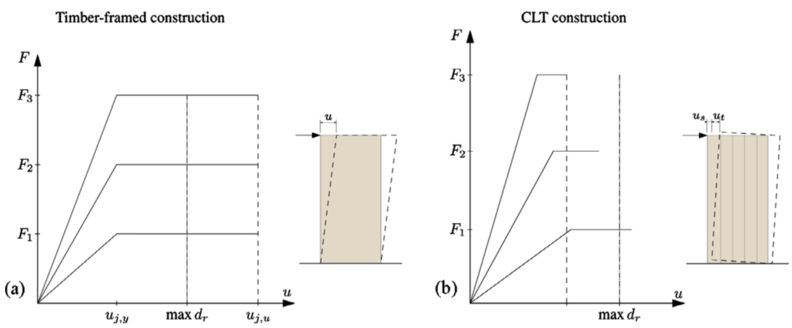

Figure 7.6: Simplified bilinear load–deflection for timber-frame (a) and CLT walls (b).(Source:[21]).

However, the CLT wall shows higher load-bearing capacity. The advantage of less deformation is that there is less permanent damage after an earthquake, because of the stiffer structure and due the fact that most of the rocking deformation can be restored.

7.4 Combined masonry-timber behaviour

Timber structures perform well during seismic events. The combined behaviour of timber and masonry under seismic loads however is less known. Several studies on the composite behaviour of timber and unreinforced masonry are discussed in this section. The use of timber frames and CLT panels as retrofit material for masonry is discussed.

Strengthening with timber frame

Research by Dizhur et al. [22] studied a timber retrofit measure for URM structures to prevent out-of-plane failures. Similar to Groningen, URM structures with cavity walls are fairly prominent in the New Zealand building stock. The retrofit measure consists of connecting a number of vertical timber members, termed as strong-backs, to the interior wall, so the wall is capable of resisting out-of-plane forces due to seismic action, see Figure 7.7. The strong-back elements act in flexure in order to transfer loads on the walls to the adjacent floor diaphragms. The timber elements are connected to the URM wall with the help of either adhesive anchors or through-plate anchors. In that way the retrofit measure are easily removable if needed. The tested retrofitted walls showed promising results. All tests sustained increased PGA values with a reduction of the out-of-plane displacements [22].

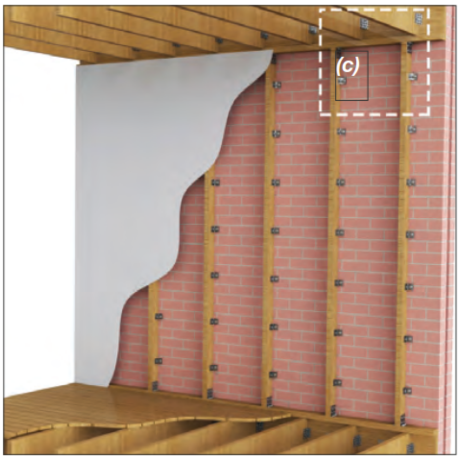

Figure 7.7: Installation of strong-backs on URM cavity wall (Source:[22]).

As part of an experimental campaign, investigating the vulnerability of terraced houses in Groningen, a strengthening measure based on research of Dizhur et al.[22] is tested. The strengthening consists of the connection between a timber frame with OSB panels and the existing unreinforced masonry. In this research, horizontal timber elements are added to the vertical members to create a timber frame, see Figure 7.8. OSB panels are nailed to the frame to increase the in-plane capacity, resembling a timber frame shear wall. During this campaign, several tests have been carried out on a URM cavity-wall terraced house end-unit with large openings on the front and back façades, especially at the ground floor. In June 2018, a shake-table test on a two-storey full-scale unreinforced masonry building was carried out at the EUCENTRE laboratory in Pavia, Italy. In November 2018, an identical building prototype was built again, but now seismically strengthened [23].

Figure 7.8: Strong-backs on URM cavity wall (Source:[23]).

The timber frame is connected to the existing masonry, so that they work together as a composite material. Both components have significantly different seismic behaviour. To get a better understanding of the composite behaviour, two in-plane cyclic tests on calcium silicate components, representing piers of the full-scale prototype, have been performed as part of the experimental campaign [23]. One specimen without and one with strengthening. The geometry of the specimen is presented in Figure 7.9. The experimental test set-up was the same for both specimens, in order to compare the results. A horizontal shear force was applied by a servo-hydraulic actuator at the top of the specimen equal to its maximum shear strength and a maximum displacement higher than 2% of the height of the specimen. The horizontal loading history was applied in a force-controlled procedure for the firsts two cycles and continued in a displacement-controlled procedure. Two vertical servo-hydraulic actuators applied a vertical load (a constant overburden stress of 0.5 MPa) and a moment, which corresponds with the maximum resisting moment at the top section. Furthermore, the out-of-plane deflection is prevented by a retaining system.

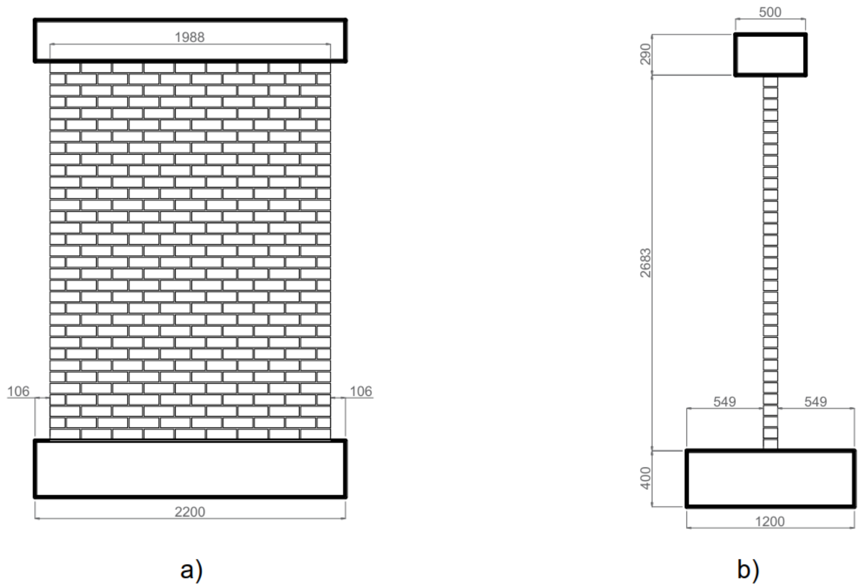

Figure 7.9: Geometry of the un-retrofitted pier component. With a) being the front view and b) the side view. Measures are in millimetres

Figure 7.10 shows the experimental shear-displacement behaviour and the backbone curve of the specimen. The behaviour of the specimen can be explained by various stages. Up until 1 in Figure 7.10 the specimen behaves elastic. After that, the specimen begins to rock (see 1 in Figure 7.11) until a top displacement of 5,4 mm is reached, during which also the maximum base shear was obtained. Then a sliding crack starts to develop (2 in Figure 7.11), due to which the specimen behaves asymmetrical: rocking behaviour when pushed in one direction, shear sliding when pushed in the other. At a top displacement of 13,5 mm (3 in Figure 7.10) toe crushing occurred at the bottom of the specimen, see 3 in Figure 7.11. Due to a combination of intensive toe crushing and the development of the sliding crack, the wall moved out of plane. The test was stopped at an ultimate displacement of 20.3 mm in the positive loading direction, since the specimen was not able any more to carry the vertical loads (4 in Figure 7.10). Failure of the specimen was mostly governed by the shear sliding behaviour at the top.

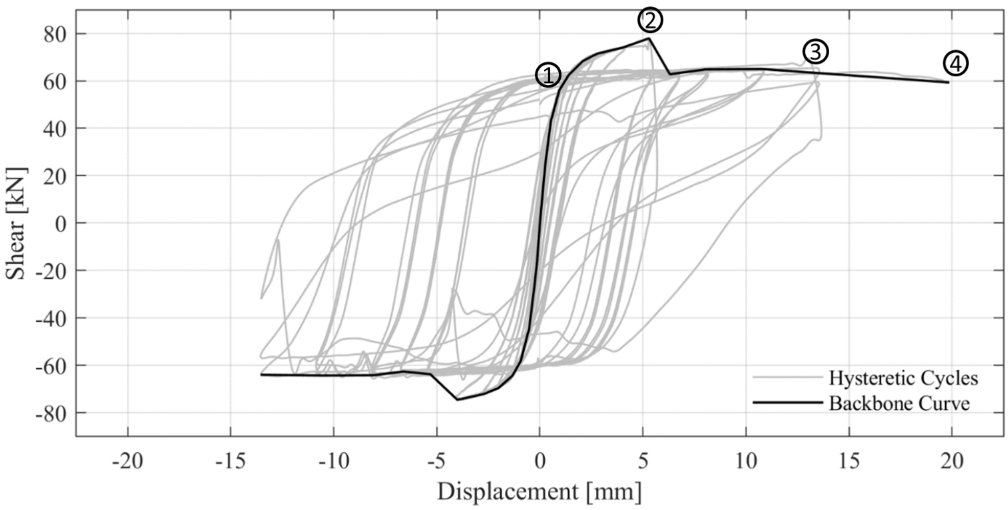

Figure 7.10: Experimental shear-displacement behaviour and the corresponding backbone curve (Source: [23]).

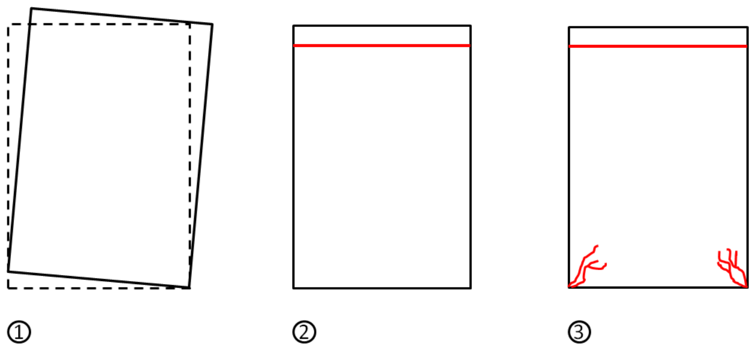

Figure 7.11: Specimen's behaviour of the various stages of the test (Source:[23]).

The other specimen was strengthened, as presented in Figure 7.12. The same test was then performed. The timber elements of the strengthening measure have a section of 80x60 mm. The thickness of the OSB panels is 18 mm. Nails are used to connect the panels to the timber frame. The connection of the angles and anchorages is done with screws. The properties of the nails, screws and steel angles are given in Appendix S.

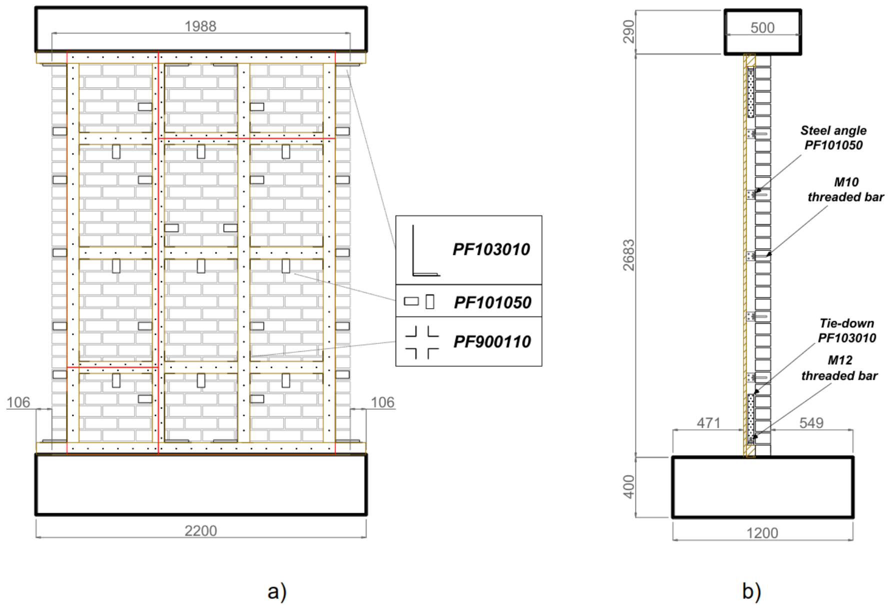

Figure 7.12: Geometry and components of the retrofitted pier component. With a) being the front view and b) the side view. Measures are in millimetres. Source: [23].

The results of this test are presented in Figure 7.13, which shows the experimental shear-displacement behaviour and the backbone curve of the retrofitted specimen. As with the other test, the behaviour of the specimen can be explained by several stages, according to [23]. Up until 1 in Figure 7.13 the specimen behaves elastic. After, the specimen starts rocking (see 1 in Figure 7.14) up until a displacement of 4 mm (2 in Figure 7.13). At that point a toe crushing mechanism is activated, see 2 in Figure 7.14, which develops until intensive toe crushing in both corners of the specimen is observed (3 in Figure 7.14 and 7.14). At a top displacement of 16,2 mm (4 in Figure 7.13) damage at a retrofit element was observed. One of the steel tie downs, in the top corner of the specimen, buckled in compression. After reaching the maximum base shear(5 in Figure 7.13), also the tie-downs at the bottom corners buckled in compression. At a top displacement of 40,4 mm a diagonal shear crack with slope of 45° was formed at the top half of the specimen, see 6 in Figure 7.14 and 7.14. The test was stopped at an ultimate displacement of 54 mm in positive loading direction, since the specimen was no longer able to carry the vertical loads, due to deep damage caused by diagonal, vertical and horizontal cracks. The failure of the specimen was mainly due to the masonry, which failed in flexure and shear. The timber retrofit still had deformation capacity.

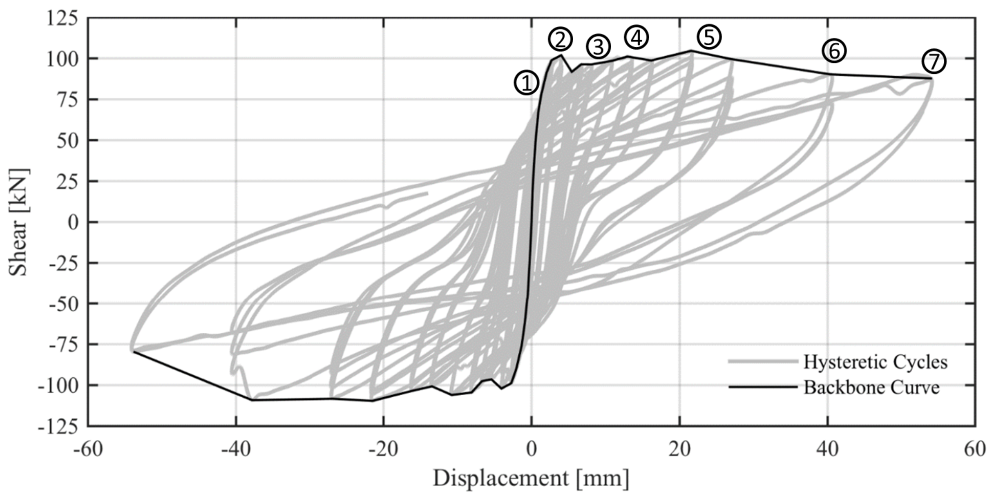

Figure 7.13: Experimental shear-displacement behaviour and the corresponding backbone curve of the retrofitted specimen (Source: [23]).

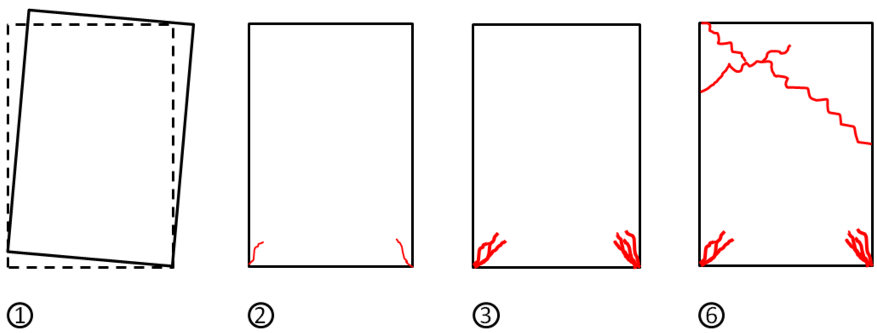

Figure 7.14: Retrofitted specimen's behaviour of the various stages of the cyclic test (Source: [23]).

Figure 7.15 shows the experimental backbone curves of both tested specimens. The strengthening measure caused an increase in stiffness, strength and most significantly in displacement. The ultimate displacement increased by 170%. Furthermore, the timber retrofit changed the behaviour of the masonry, preventing the onset of a sliding mechanism and therefore resisting higher lateral forces, with an increase of 40% of the strength capacity.

The ultimate drift limit of the un-strengthened specimen was found to be 0,75%. Drift limit at effective height according to the NPR, is 0,8%. The rocking drift limit is calculated to be 1,22% (using equation E.5). Therefore it is expected that the pier would not fail due to rocking or toe crushing. The strengthened specimen showed an ultimate drift limit of 2%. An increase of 166%, a result of the more stable rocking behaviour. When the rocking drift limit is calculated according to the NPR 9998:2018 for the un-strengthened specimen, the drift limit would be 1,22%. The application of the timber strengthening resulted in a more stable pier, which can be pushed further.

The retrofitted specimen did not experience a sudden degradation of strength or stiffness due to local damage. In the end, the behaviour of the masonry was still governing, due to diagonal cracking of the masonry. However, the timber frame was still able to take more force and displacement.

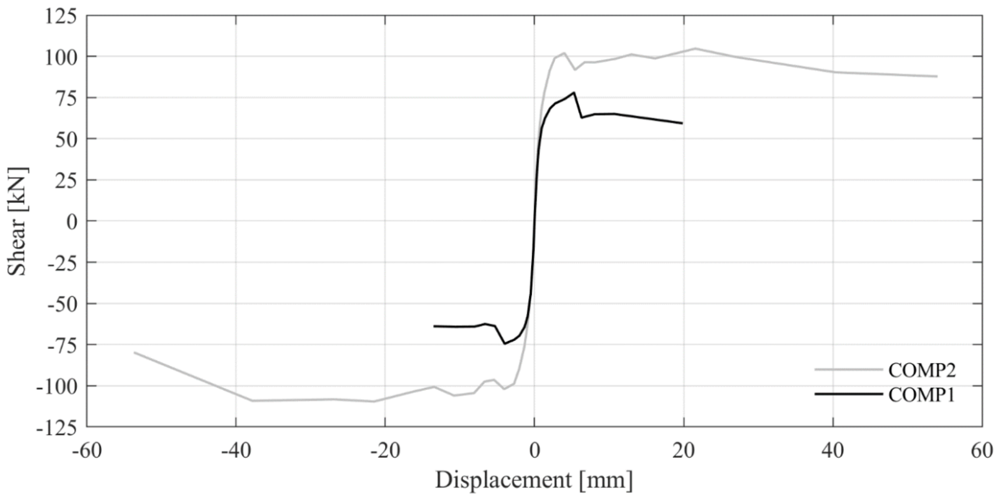

Figure 7.15: Overlap of the experimental backbone curves of both specimens (Source:[23]).

CLT strengthening

Although CLT is becoming more popular as a building material, also in earthquake prone areas, it is not often applied as strengthening for URM structures. However, due to the high stiffness, strength and in-plane stability it could be a promising retrofit material. Two studies have been found that tested URM walls strengthened with CLT panels.

Research by Sustersic et al. [24] tested URM walls strengthened with CLT panels attached in various ways. One is connected with epoxy glue and another with the help of specially developed steel connections at the bottom and top of the wall, as demonstrated in Figure 7.16. Results show that both ductility and resistance of the wall can be increased. By using the epoxy glue, the peak resistance is increased by 34% and the displacement capacity by 25%, while the initial stiffness is only slightly increased. However, no detailed information of the tests on the behaviour of this presented. The CLT panel connected with steel connections increased the shear resistance by 34% and the displacement capacity by 100%, see Figure 7.17 for the hysteresis response.

Figure 7.16: Experimental testing of URM wall (left) and URM strengthened walls with CLT panels with a glued (middle) and a bolted connection (Source:[24]).

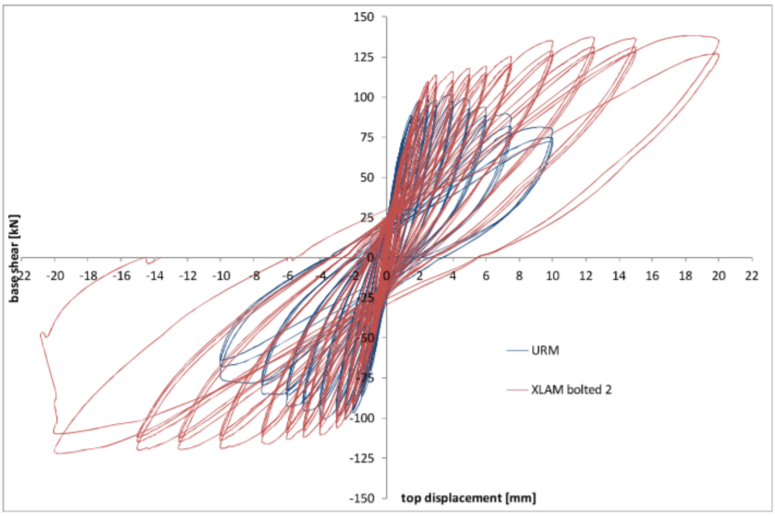

Figure 7.17: The hysteresis response of an un-strengthened URM wall and strengthened with CLT and steel connections (Source:[24]).

Another study by Pozza et al [63], tested similar wall specimens but with a slightly different connection between CLT and URM. A metallic L-shape curb is rigidly connected to the floor and then the CLT panel is screwed to the curb. The tests were done on 1,4m high masonry walls and the CLT panels were fixed on their lower and upper side to aluminium beams. The lower aluminium beam is fixed to the laboratory pavement.

Results present a reduced rocking behaviour and instead compression failure at the masonry base. Furthermore, a significant increase of the peak force and displacement capacity is shown. However, no increase in terms of elastic stiffness and therefore a negligible variation of the yielding point was found. Again, it shows that CLT walls can be used to strengthen URM walls.

Both tests are performed on a limited amount of specimens with specific dimensions. To evaluate the benefit of CLT walls on the global seismic behaviour, full-scale tests should be performed. Next to that, more research should be done on possible connections between URM and CLT.

7.5 Timber retrofit designs

The sensitivity analysis in Chapter 6, indicated the seismic behaviour of the various un-strengthened structures. The most remarkable outcome of the analysis, is that most of the researched models satisfy the NC limit state for the different locations based on the NPR 9998:2018. The main cause of this result is due to the high rocking drift limits prescribed by the NPR 9998:2018. Since most tested models showed rocking behaviour, this resulted in high values for the displacement capacity.

However, some models did not satisfy the NC limit state and therefore need seismic strengthening. Models with wide middle piers showed shear sliding behaviour of the middle piers, which resulted in a lower displacement capacity and therefore the NC limit state was not satisfied, as shown in Figure 7.18. There are mainly two ways to ensure the satisfaction of the NC limit state for a strengthened building. Either by increasing the load bearing capacity (arrows in Figure 7.18 show the increase of load bearing capacity that needs to be realised depending on the damping of the system) or by increasing the displacement capacity of the structure (red circle indicated on the right of Figure 7.18).

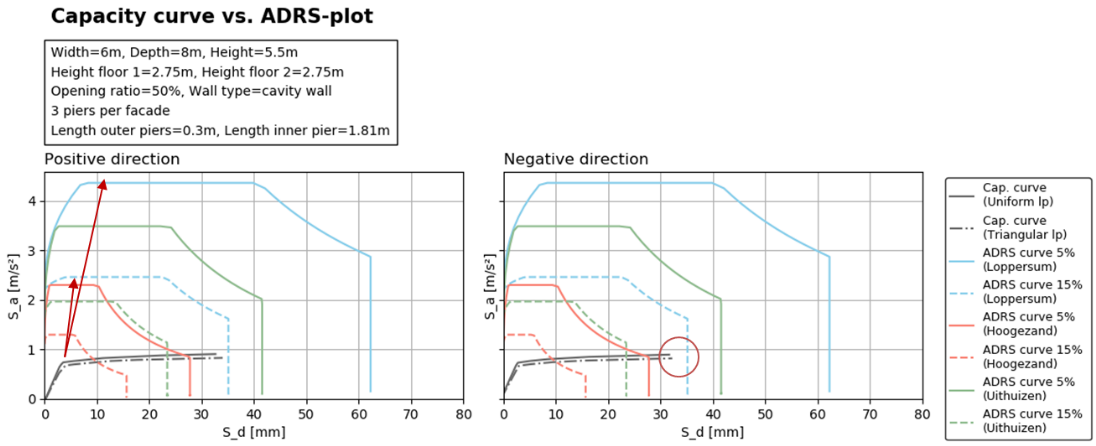

Figure 7.18: Capacity curve of model with large middle piers. In red possible ways to satisfy the NC limit state.

For the presented model, it seems more beneficial to design a retrofit measure in order to achieve a higher displacement capacity, as indicated on the right of Figure 7.18. Especially when the seismic behaviour of the masonry could be changed into rocking behaviour, the drift limit according to the NPR 9998:2018 ensure satisfaction of the NC limit state, as was observed during the sensitivity analysis for the majority of the models.

Buildings with CaSi element masonry used since 1985 did not satisfy the NC limit state in all locations, due to the assumed brittle behaviour. The drift limit at effective height is lower compared to other masonry types and therefore the displacement capacity is reduced. The application of a timber frame could create a more stable and less brittle behaviour, increasing the displacement capacity. In that way, higher drift limits could be realised.

Furthermore, models with an opening ratio of 70% at ground floor level, do need seismic strengthening, mainly due to the second order effects. Application of the tension anchors should prevent the uplift of the masonry piers, providing more lateral resistance. This is needed to effectively strengthen the model.

Implementation

For the implementation of the strengthening design a trade off needs to be made between the level of strengthening and the preparation and implementation time needed, as discussed in Section 1.2. To keep the strengthening design simple and less intrusive for the residents, it is chosen that the retrofit design primarily provides resistance to the lateral forces. The gravity loading of the structure is still mainly carried by the masonry elements. Sustaining the load bearing capacity of the masonry, results in a more slender retrofit design. The lesser the impact on residents, the better. The purpose of the retrofit design is therefore to keep the masonry intact, while contributing to the seismic resistance. Furthermore, a slender, more simple retrofit design takes less time to install and is more likely to be reversible.

Timber frame design

The strengthening measure design proposed, is based on the out-of-plane strengthening proposed by Dizhur et al. [22]. Experiments done on URM wall specimens with a variation of the out-of-plane strengthening by Dizhur et al. in Pavia, showed excellent results for strengthening in-plane [23]. Both an increase in strength and displacement was reached. Furthermore, the behaviour of the strengthened wall was different from the un-strengthened wall. Instead of shear sliding failure, the main behaviour was governed by rocking until diagonal cracks started forming. Next to increasing the seismic capacity, the strengthening measure is a cost-effective, sustainable and reversible solution.

The first proposed retrofit design consist of a timber frame connected to the masonry by anchors and wood-based panels nailed to the frame, which provides shear strength. Moreover, the frame is connected to the foundation by hold down anchors. Figure 7.19 shows a front view of the proposed framework. Single or multiple panels are connected to the framework, see Figure 7.20. To keep the dimensions of the retrofit measure limited, vertical forces are expected to be mainly transferred by the masonry piers. Degradation of the masonry during an seismic event causes some of the vertical loads to be carried by the timber elements. However, this should be limited, since the goal of the strengthening is to keep the masonry piers intact as long as possible, so they carry the vertical loads.

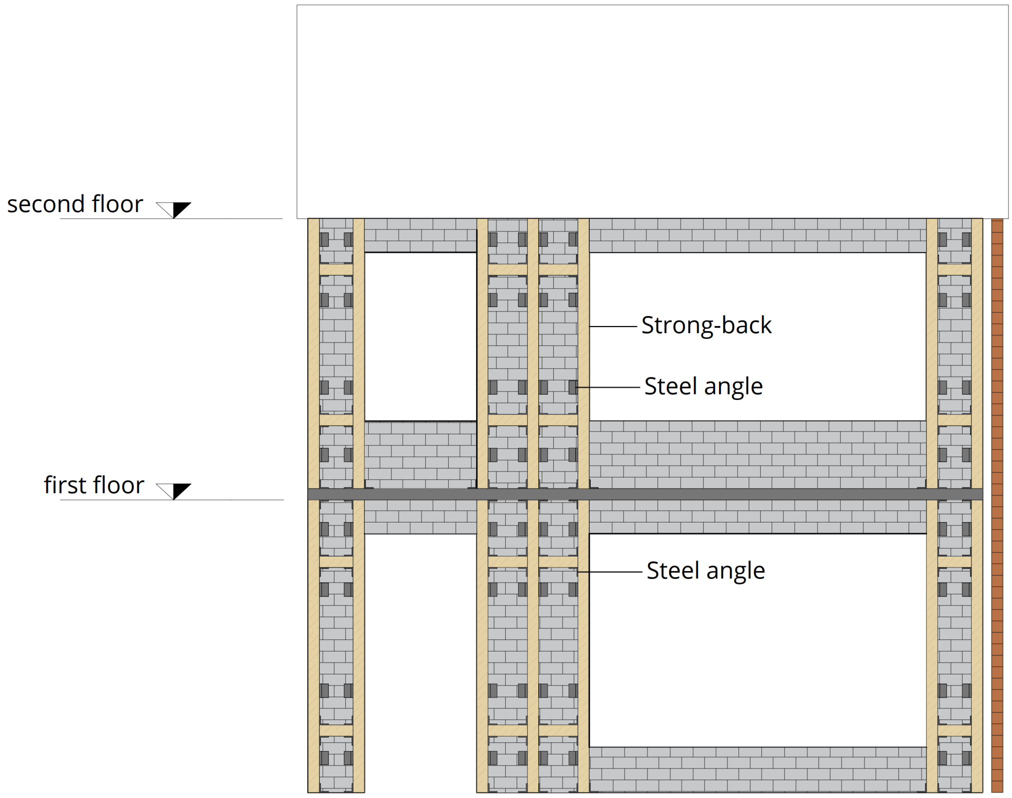

Figure 7.19: Front view of the proposed design for in-plane strengthening of URM structure using timber frame shear walls.

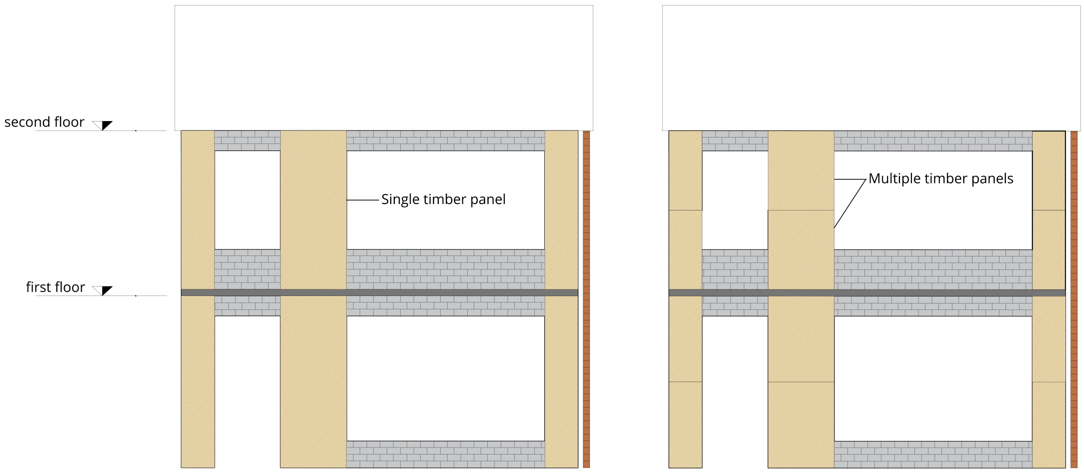

Figure 7.20: Front view of the proposed design for in-plane strengthening. Placement of the wood-based panels on top of the framework.

Figure 7.21a shows a top view of the retrofit measure and Figure 7.21b presents a side view. The dimensions given are indicative, the appropriate dimensions and other details are discussed and determined in Chapter 8.

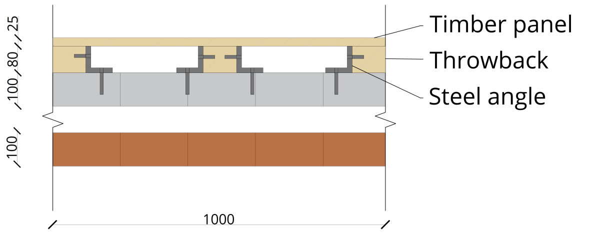

(a) Top view of the proposed strengthening measure

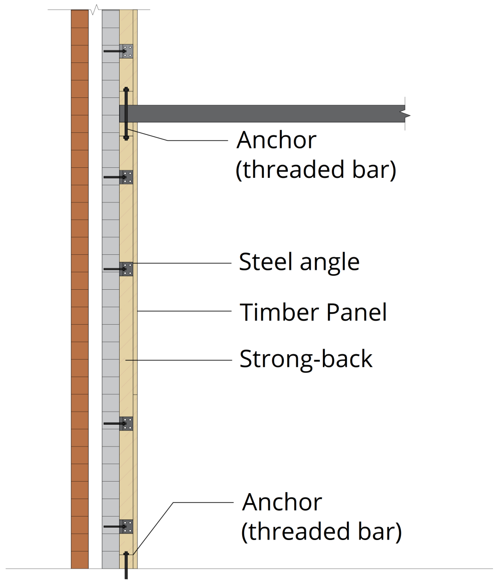

(b) Side view of the proposed strengthening measure

Figure 7.21: Top (a) and side view (b) of the proposed in-plane strengthening measure

The placement of the retrofit design is analysed in Section 8.3. Applying the retrofit measure on only a part of the structure, as indicated in Figure 7.22, could be sufficient. Less structural intervention is preferred.

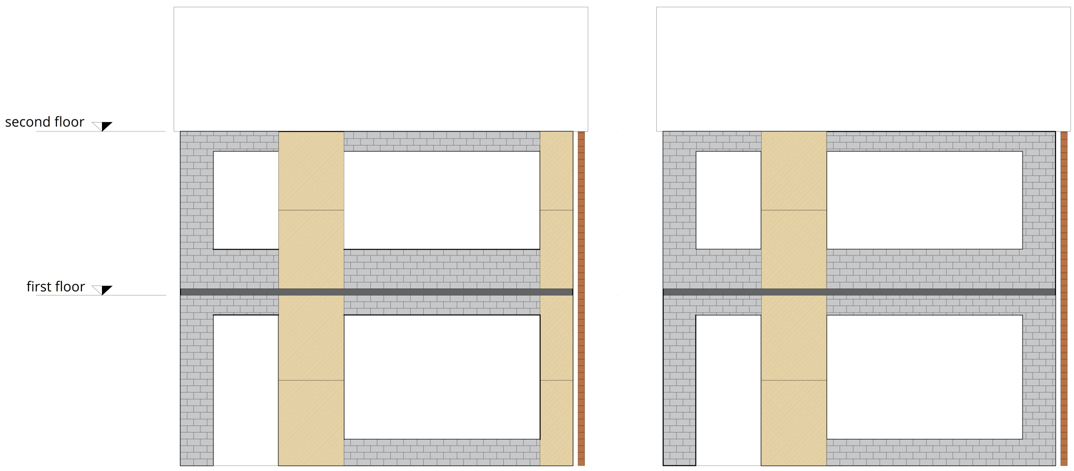

Figure 7.22: The proposed retrofit timber frame design applied on part of the masonry structure.

CLT design

Next to a retrofit measure with a timber frame shear wall, a second strengthening measure is proposed. This consists of CLT panels connected to the masonry and anchored to the foundation. The benefit of CLT is that due to the high stiffness it has a high in-plane strength. Figure 7.23, shows a front view of the proposed strengthening measure. The CLT panels are anchored to the unreinforced masonry. Ankle brackets are used to connect the walls to the foundation. Figure 7.24 shows a top and side view of the proposed retrofit measure.

The amount of anchors and brackets is indicative. Furthermore, the thickness of the CLT panel is indicative. It is preferred to keep the thickness as small as possible. Analysis should indicate from which thickness the proposed design would be beneficial. However, it is likely that the thickness is less than the timber frame shear wall, due to the benefits of CLT.

As research by [21] indicates (see Figure 7.6) timber shear walls show more displacement and therefore ductility than CLT walls, due to the large number of fasteners which can all deform. However, the resistance to lateral loads is likely to be more increased when CLT walls are applied, depending on the configuration [21]. The vertical loads are still mainly transferred by the masonry piers. However, due to high strength to thickness ratio and the complete connection to the masonry, the CLT member is likely to take more vertical loads than the timber frame.

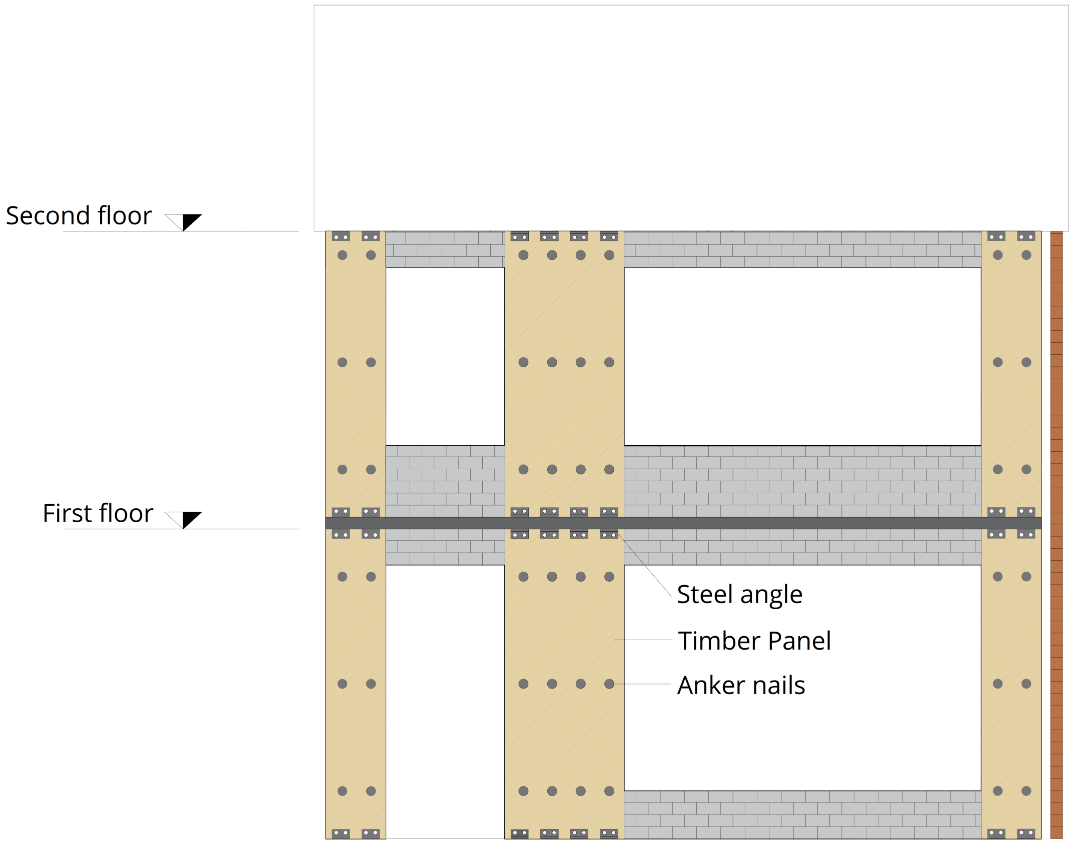

Figure 7.23: Front view of the proposed design for in-plane strengthening of URM structure using CLT panels.

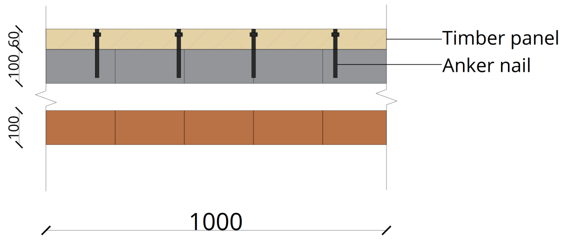

(a) Top view of proposed CLT strengthening measure; Dimensions are indicative.

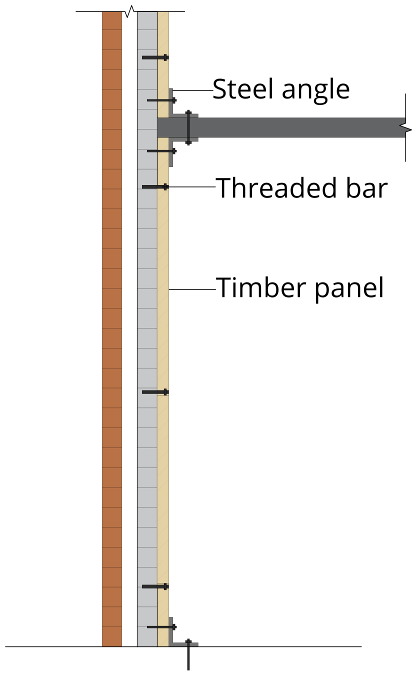

(b) Side view of proposed CLT strengthening measure

Figure 7.24: Top (a) and side view (b) of the proposed CLT strengthening measure

8. Numerical Analysis Timber Retrofit

It is chosen to analyse the timber frame shear wall strengthening measure proposed in Chapter 7. The tests done on a similar strengthening approach by [23] present useful information on the composite behaviour and the results of the test are discussed in detail. Tests performed on CLT retrofiited specimens, show promising results. However, the outcome of the tests are briefly described. Next to that, there are no full-scale tests performed on similar retrofit measures. Therefore, the retrofit design that is numerically tested in this Chapter, is the timber frame shear wall retrofit design.

The effect of the proposed retrofit measure is analysed with ETABS. Models determined to be unsafe according to the NPR 9998:2018 during the sensitivity analysis of Chapter 6, are adjusted to account for the retrofit measure. The numerical model is altered by two interventions: the shear behaviour of the masonry piers is changed and hold-down anchors are implemented. The alternations to the model are described in the next section. After that, the effect of the proposed retrofit measure for the different models is discussed.

8.1 Combined masonry-timber wall behaviour

The experimental tests done in Pavia [23], with a similar strengthening design, showed the behaviour of several wall specimens. The numerical model for the retrofit measure is based on these results (discussed in Section 7.4) and on the seismic behaviour of masonry and timber individually.

Timber frame wall displacement capacity

The test done in Pavia demonstrated that the timber retrofit still had deformation capacity after the collapse of the masonry [23]. In order to design a timber frame wall with sufficient displacement capacity, the timber behaviour is described in the following section by both exploring the elastic and plastic behaviour of timber.

Elastic behaviour

Timber frame shear walls are often used as part of the stabilising structure, being able to resist lateral forces from wind or earthquakes. The elastic horizontal behaviour, when subjected to lateral loading, consists of several different contributions of deformation. It can be obtained by several different analytical expressions, proposed in literature and standards. Different contributions to the total displacement can be considered.

Essential to estimating the deformations of a structure, is the calculation of the racking-stiffness of the shear-wall. According to research of [64], for the calculation of the stiffness and therefore the elastic displacement of a timber shear wall the following contributions have to be taken into account:

- fastener slip along the perimeter of the wall (48%)
- shear deformation of the sheathing board (12%)
- strain in the studs (8%)
- strain in the hold down anchorages (13%)
- compression perpendicular to grain in the bottom rail (15%)

Calculation of the different contributions according to [64], are given in Appendix U. With the racking stiffness of the system, the deformation can be estimated. The research shows that the slip of the fasteners has the largest contribution to the total elastic deformation, around 48%. The fastener-slip modulus K_{ser} as stated in Eurocode 5 [31], agrees very well with the slip-modulus determined from test-data and can therefore be used for calculating the timber frame shear wall stiffness, according to research of [64].

Research by [32], provides a simplified equation to describe the elastic behaviour of timber shear walls, which is based on four different contributions to the total deformation (see also Figure 8.1):

- deformation of the sheathing-to-framing connection (45%)
- deformation due to rigid-body rotation (45%)
- deformation due to rigid-body translation (6%)
- deformation of the sheathing panels (4%)

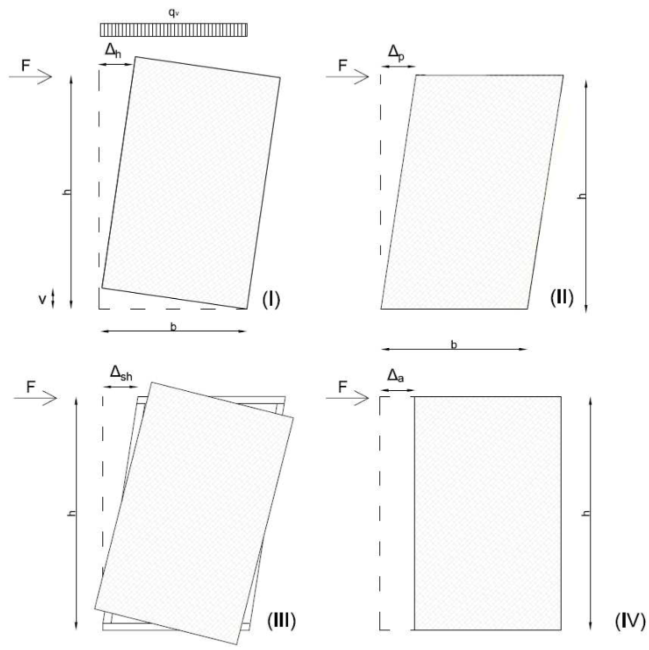

Figure 8.1: Timber frame deformation contribution: rigid-body rotation (I), Sheathing-panel shear deformation (II), Sheathing-to-framing connection (III) and Rigid body translation (IV)(Source:[25]).

The calculation of the deformation contributions according to [32], are given in Appendix T. It is evident that in both studies the deformation of the sheathing-to-fastener connection plays an important role (more than 45% of the total elastic deformation) in determining the total elastic displacement. The deformation due to rigid-body rotation, considered in [32], takes the tensile deformation of the hold down connections into account, as is done in the research of [64]. Both studies also take the shear deformation of the sheathing panel into account, which has little contribution. In this research, the formulas presented by Casagrande et al. [32] are used to predict the elastic deformation of the timber frame shear wall.

Non-linear behaviour

The timber retrofit should not fail prior to the masonry piers, since it gives the masonry a higher shear capacity, which results in higher displacements due to ensured rocking behaviour. If the timber fails earlier, the masonry is likely to fail directly in shear. To achieve sufficient lateral displacements, the non-linear timber behaviour is of significant importance.

In standards the non-linear response of a complete structure usually is taken into account by modification of the elastic seismic forces via the behaviour factor (q). The value for q, which represents the relationship between the ductility of the components and the global ductility, is often given in the standards. The behaviour factor is predominantly used for Lateral Force and Modal Response Spectrum analyses. However, the ductility of local components is not provided in standards. This ductility factor (μ) is needed, since the behaviour of local components is investigated in the analysis. Due to the lack of values for this factor in the standards, it should be based on experimental tests, which are discussed in the following section.

To predict the non-linear behaviour of a certain wall configuration, an analytical elasto-plastic mode is used, as proposed by [26]. For each of aforementioned contribution to the elastic behaviour, an idealised elasto-perfectly plastic curve is obtained. First the yield displacement Δ_y is determined based on the strength and the stiffness of each contribution. The yield displacement of sheathing-to-framing connection for example is calculated as:

$$\Delta_{y,sh} = \frac{R_{sh}}{K_{sh}} \tag{8.1}$$

The stiffness K_{sh} is determined with the stiffness of the fastener, according to Eurocode 5 [31]. The sheathing-to-panel strength is also determined according to the Eurocode 5. The ultimate displacement is obtained by multiplying the yield displacement by the ductility of the component, in this case the sheathing-to-framing connection ductility μ_{sh}, see formula (8.2).

$$\Delta_{ult,sh} = \mu_{sh} \cdot \Delta_{y,sh} \tag{8.2}$$

The non-linear behaviour of sheathing-to-framing connection is captured in an elastic perfectly plastic curve as shown in Figure 8.2.

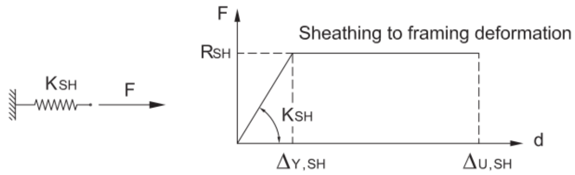

Figure 8.2: Sheathing-to-framing connection spring mechanical behaviour.(Source:[26]).

Ductility

The ductility factor (μ) used in equation 8.2, is not given in standards and therefore should be based on experimental tests. Ductility ratios of various tests of timber shear walls are analysed. An overview of analysed tests on full-scale timber frame shear wall configurations, is given in Appendix V. The tests consist of single timber shear walls subjected to horizontal loads, either monotonic or cyclic loading. Different sheathing layouts, different measurements, various fixation solutions to the base and different fastener types are analysed. The ductility ratios presented, are based on the yield displacement and the ultimate displacement of the timber shear wall specimens, which is defined as the displacement at 80% of the maximum shear force, after this maximum load is reached, according to the Equivalent Energy Elastic-Plastic (EEEP) Curve. The EEEP curve is a perfect elastic-plastic load-displacement curve, see Figure 8.3.

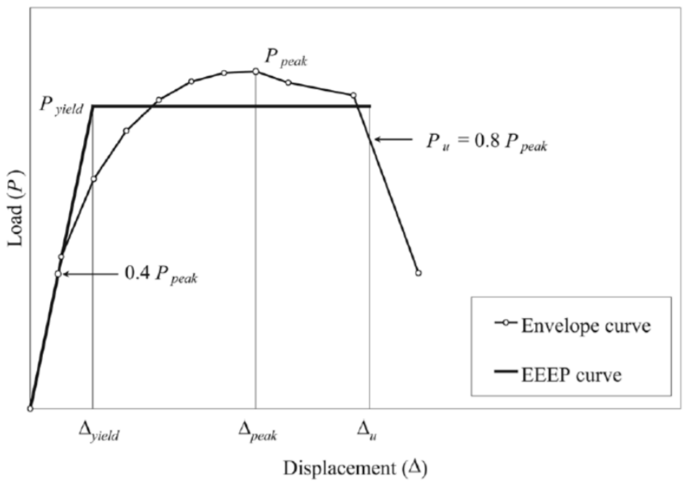

Figure 8.3: EEEP curve with relation to an envelope curve of a tested specimen(Source:[27]).

Ductility ratios range between 1,4 and 9,1, with an average ductility ratio of 4,3, according to the analysed tests. Monotonic loaded specimens show a higher ductility ratio. However, cyclic loading simulates the seismic behaviour in a better way and therefore gives more realistic ductility values. Furthermore, the fastener type applied, has influence on the ductility ratio. Specimens with nail type fasteners show on average higher ductility ratios than screws. Specimens without hold-down anchors present lower ductility ratios than with hold down anchors.

Table V.3 of Appendix V presents an overview of several experimental monotonic and cyclic tests which have been performed on solely the sheathing-to-framing connection. The nailed connections show high ductility ratios, 3 to 4 times higher then the overall ductility ratio of a shear frame wall.

Higher ductility ratios are beneficial, when the displacement capacity of the building should be improved. It that case, a timber shear wall should be designed with nail type fasteners and hold-down anchors connecting it to the base, since they provide more ductile behaviour.

For each pier of each strengthened model, wall deformation is checked to see if the ultimate displacement can be achieved. Furthermore, the configuration and the dimensions of the wall are determined in Section 8.3.

Implementation of seismic retrofit in ETABS

The combined masonry-timber behaviour is considered to work together as a composite material, assuming that the connection between the timber and the masonry is not governing. The model, therefore, does not capture the differential movement between the masonry and the timber wall system. Due to this assumption, the additional shear capacity provided by the timber retrofit are added to the capacity of the non-linear link properties previously used to represent the shear capacity of the masonry wall, considering they work in parallel. This results in pier elements with a higher shear capacity.

The non-linear shear deformation of unreinforced masonry piers is included in the model by non-linear links, as described in Chapter 5. The force-displacement relationship is presented by a backbone curve, which is calculated according to the NPR 9998:2018. Figure Z.9a shows an example of such a backbone curve, based on a 0,7 x 2,3 meter masonry pier of one of the tested models.

The non-linear behaviour of the timber wall under seismic loading, is determined by calculation of the sheathing-to-panel strength and stiffness and associated ductility, as discussed in Section 8.1, and depends on the configuration of the wall. The total displacement is determined by calculation the elastic displacement of the timber wall as proposed by [25] and multiplying that with a ductility factor. Figure Z.9b presents a proposal for the backbone curve of a timber wall with a certain configuration. The combined behaviour, which is a combination of the two as shown in Figure 8.5, is implemented in the shear links of the piers that are strengthened. The values for the updated combined backbone curve are determined in Section 8.3 for each retrofitted model.

Due to the higher shear capacity, the piers are more likely to show rocking behaviour, as was presented by the experimental test in Pavia [23]. The test showed shear sliding behaviour of the walls was prevented and that the walls demonstrated rocking behaviour up until a point that the masonry showed diagonal cracks. The timber however, still allowed more displacement.

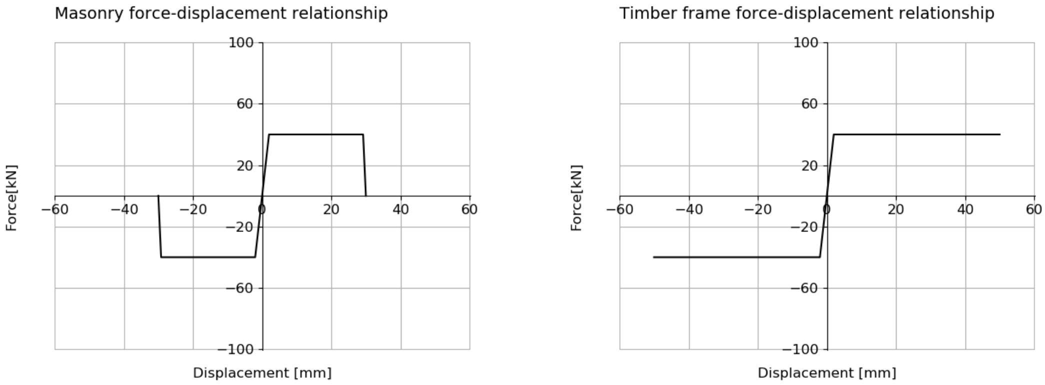

(a) Example of a force-displacement relationship for masonry piers governed by shear behaviour according to the NPR 9998:2018.

(b) Example of an idealised force-displacement relationship of a timber frame shear wall, based on Eurocode 5 [31]

Figure 8.4: Idealised force-displacement relationships of both masonry and timber walls.

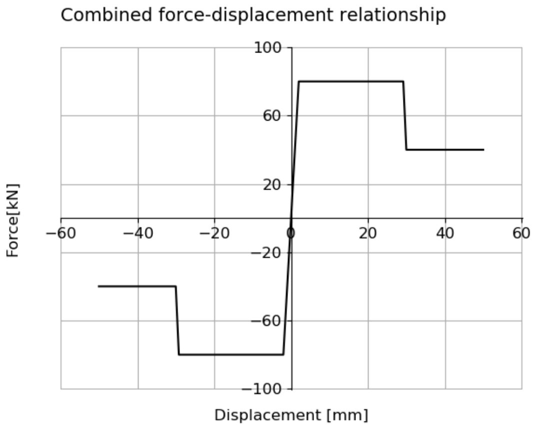

Figure 8.5: Example of proposed idealised combined masonry-timber shear behaviour, as input for ETABS.

8.2 Hold-down anchors

The timber frame is connected to the foundation by means of hold-down anchors, see Figure 8.6a and 8.6b. This anchors prevent the shear wall from lifting up. The behaviour of a single hold-down anchor is obtained from characteristic values given by the manufacturer of this type of hold-down anchors, Rothoblaas [30].

(a) Example of a hold-down anchor (WHT angle bracket by Rothoblaas) (Source:[30]).

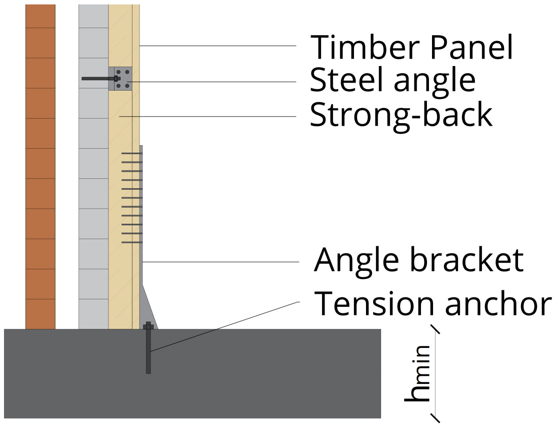

(b) Detail of the application of the angle bracket and tension anchor, as applied in the proposed retrofit design.

Figure 8.6: Application of hold-down anchor.

Various hold-down connections from Rothoblaas have been tested by Casagrande et al. [33] to determine the capacity, the stiffness and the ductility of the connections and to investigate their loss of capacity under cyclic loads. The characteristic values for the capacity of each component of the connection are presented in Appendix W. The minimum capacity value is used as the governing capacity of the hold-down connection, according to formula 8.3. Coefficients γ_m and k_{mod} are taken as 1,0 and 1,1 respectively, according to the NPR 9998:2018 and Eurocode 5. Furthermore, the capacity is related to the type of fasteners, the way of fixing and which anchor is used, as is presented in Appendix W.

$$R_d = min\Big(\frac{R_{1,ktimber} \cdot k_{mod}}{\gamma_m}; \frac{R_{1,ksteel}}{\gamma_{steel}}; \frac{R_{1,kcls}}{\gamma_{cls}}\Big) \tag{8.3}$$

The test results are shown in Table 8.1. Next to the stiffness and capacity, it shows the yield and ultimate displacement and the corresponding ductility. Experimental testing, showed that the strength values can be extended to the case where an OSB panel is placed between the WHT connection and the timber frame, provided that there is adequate sheathing-to-framing fastening. The strongest hold-down anchor (WHT 620) is also tested with partial fixing (not all nail holes are used). The partial fixing did not cause a significant reduction of strength, see Table 8.1. However, total fixing of the connection was characterized by the brittle tensile breakage of the steel plate. Instead, partial fixing showed more ductile behaviour. In seismic regions the partial fixing is therefore recommended, according to [33]. The maximum load in the tests is obtained according to the EN 12512. The tests show higher maximum loads than prescribed by the manufacturer, see Appendix W. For the analysis the lower characteristic maximum load is applied in combination with the lower stiffness derived from the experimental tests.

Test ID	**F_{max} (kN)**	**K_{ser} (N/mm)**	**v_y (mm)**	**v_u (mm)**	**μ (-)**
WHT340	60.19	5705	8.92	21.2	2.37
WHT440	78.14	6609	9.28	28.47	3.07
WHT620	107.32	13247	6.38	20.7	3.24
WHT620 P	100.089	9967	7.94	30.00	3.78

Table 8.1: Results of tested hold-down anchors (Source:[33]).

Implementation in ETABS

The hold-down anchors are represented by non-linear links, which only transfer tension forces. The links are attached to the top of the pier elements and attached to the foundation, as shown in Figure 8.7. When implemented at second floor, the links are attached to the concrete floor diaphragm.

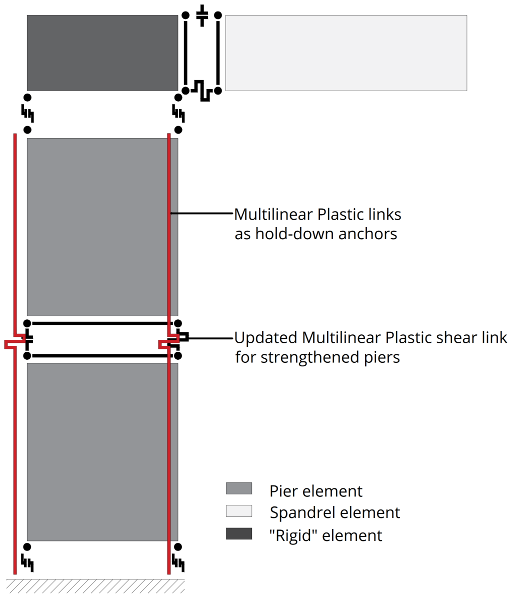

Figure 8.7: Multilinear Plastic links in red added to the numerical model, representing the hold-down anchors

As the piers start rocking, the link elongates and therefore a force is applied on top of the pier. Which is similar to pulling the pier element back to its position, see Figure 8.8. The other link shortens and does not apply any additional force. The magnitude of the force applied, is related to the force-deformation curve of the hold-down connection.

The behaviour of the anchors under compression loading is not considered in the model. The analysis is not time depended. Therefore, degradation of the anchors in time due to compression forces is not modelled. The test done in Pavia [23] demonstrated that at some point the angle brackets can buckle under compression loads, as discussed in Section 7.4. However, this did not influence the results significantly. To prevent the buckling, the thickness (3 mm on the applied brackets) of the steel should be increased.

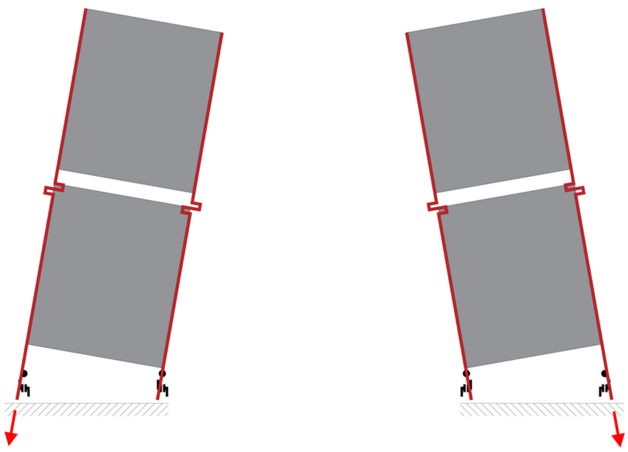

Figure 8.8: Tension force that is generated when the piers start rocking, displayed in both ways.

The link holds a backbone curve, which is based on the characteristic capacity and stiffness of the applied hold-down-connection, according to the tests [33], see Figure 8.9. It is assumed to be elastic perfectly plastic. When multiple anchors are applied, the backbone curve of the link is adjusted accordingly. Multiple anchors are considered to work in parallel, therefore the total stiffness is assumed to be the sum of the stiffnesses, resulting in a higher force, since the displacement is constant. The properties for the largest hold-down anchors (WHT 620) are used for the analysis. Figure W.4 shows the configuration that is used in red. It consists of M24 anchor and the angle bracket is nailed to the timber with 55 $\varnothing 4 \times 40$ nails.

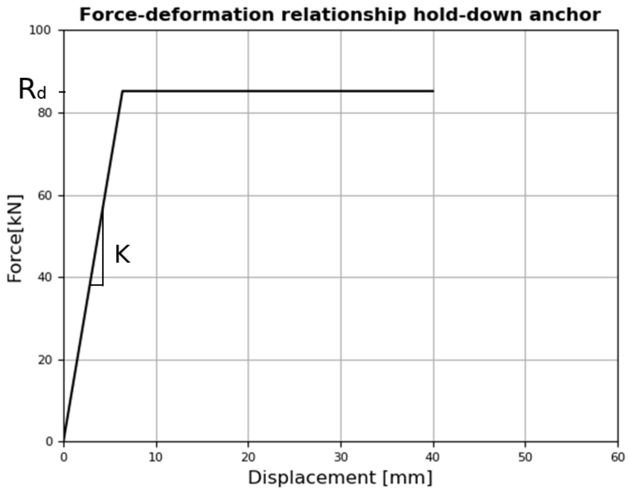

Figure 8.9: Assumed force-deformation relationship of hold-down anchor, based on the characteristic stiffness and design strength.

Foundation design

To ensure that steel failure of the anchors will be governing, the foundation needs to be of certain dimensions and properties to prevent it from failing. The foundation and concrete element can limit the capacity of the anchors significantly. However, in this research it is assumed that steel failure is governing. The concrete grade needs to be at least C20/25, according to tests done on the anchors [30]. The minimum thickness of the concrete depends on which anchors are applied and how many. The WHT620 angle bracket with a M24 anchor, which are applied in the analysis, require a minimum concrete thickness of 300 mm. The minimum spacing between anchors, depends on which anchor type is applied. The applied anchor requires a spacing of 100 mm [30]. In an anchor group, only anchors of the same type, size and length are used. According to the simplified design method the anchors of a group are loaded equally.

For the implementation of the anchors on the second floor, the placement of the anchors should not be too close to the edge. The minimum edge distance depends on which anchors are applied and is the maximum value of $(h_{ef}/2; 5d)$.

For the installation of the anchors a hole needs to be drilled. The chemical anchor is injected in the hole. After, the threaded bar is placed and the angle bracket is installed. The angle bracket is nailed to the timber elements, after which the nut is tightened on the bar. Chemical anchors are applied, since they have good performance under seismic actions, according to [65]. Figure W.7 shows the assembling of the anchors in concrete.

8.3 Effect of strengthening measures

The models that are determined to be unsafe according to the NPR 9998:2018 during the sensitivity analysis of Chapter 6, are strengthened. The configuration and the effect of the retrofit measure is discussed in this section.

During the sensitivity analysis the models are checked against drift limits for un-strengthened masonry buildings, as prescribed in the NPR 9998:2018. Seismically strengthened buildings adopt drift limits as per new supplementary lateral load resisting system, as stated in the NPR 9998:2018. However, values for strengthened masonry buildings are not prescribed. Values should be based on extensive experimental and analytical research. The tests done in Pavia [23] demonstrate an increase in displacement capacity. The ultimate drift limit increased with 166% ($\theta_u = 0,075\%$ to $\theta_u = 2\%$) with the application of the timber frame. To quantify this increase more accurately, more comparable experiments should be performed. The displacement capacity is increased, but the outcomes of only one experiment are insufficient to quantify a realistic value for the drift limit. Due to the lack of more research, drift limits for un-strengthened masonry are used to check the strengthened models. However, the presented capacity curves are pushed further than the aforementioned drift limits, to demonstrate the extra displacement that is needed to satisfy the NC limit state. Additionally, it shows the expected seismic behaviour of the structure.

Furthermore, application of the retrofit design has influence on the equivalent viscous damping of the system. For un-strengthened masonry loaded in-plane a hysteretic damping between $\xi_{hys} = 0(0\%)$ and $\xi_{hys} = 0,15(15\%)$ is applied, depending on the expected behaviour, as described in Section 4.2. To take the damping in account, the seismic demand is adjusted by a spectral reduction factor. To estimate the hysteretic damping of the retrofitted structures equation 8.4 according to (G.14) of the NPR 9998:2018 [34] is used. An estimate is given for each strengthened model.

$$\xi_{sys} = \frac{2}{\pi} \times \eta_{eff} \times \frac{(1-r)\left(1-\frac{1}{\mu_{sys}}\right)}{(1-r+\mu_{sys} \times r)} \tag{8.4}$$

Where:

ξ_{sys} is the hysteretic damping;

μ_{sys} is the global structural ductility;

r is the post yield to initial stiffness ratio;

η_{eff} s the efficiency factor, defined as the ratio of the actual area enclosed by the hysteresis loop to that of the assumed

$$\mu_{sys} = \frac{u_{cap,sys}}{u_{y,sys}} \tag{8.5}$$

Model with wide middle piers

A model with 1,8 meter wide middle piers shows, according to the sensitivity analysis, shear sliding failure of the middle lower piers, see Figure8.12a. The NC limit state is not satisfied in one of the considered locations.

First, the retrofit design is applied to only the middle piers on ground floor level, which fail in shear, and connected to the foundation with two WHT 620 anchors per pier (one anchor in each corner of the pier). The anchors have a capacity of 85 kN, as presented in Figure W.4. Figure 8.12a shows the effect on the behaviour, which is governed by rocking behaviour instead of shear sliding. Figure X.1 presents the accompanying capacity curve. The model is checked against the NPR 9998:2018 drift limits for the un-strengthened situation, since only part of the structure is strengthened. Even then the model satisfies the NC limit state in all locations considered. The forces within the structural elements and the applied tension anchors during the analyses are presented in Appendix Y.

The configuration of the timber frame shear wall that needs to be applied, is calculated and presented in Appendix Z. It consists of 70 x 80 C24 timber framework of 1,8 by 2,75 meter, with an OSB panel of 20 mm thick nailed to the framework by $\varnothing 4 \times 75$ nails with a spacing of 50 mm. Results show that, to ensure rocking behaviour, the shear capacity of the middle piers needs to be increased with at least 40 kN, from 43 kN (in the un-strengthened situation) to 80 kN. The sheathing-to-framing connection of the proposed retrofit has a shear capacity of 39 kN, see Figure Z.2. The total elastic displacement of the system is calculated according to [32], and is expected to be around 13 mm. With a ductility of 4-5, which is reasonable according to the analysed experimental tests given in Appendix V, the total displacement is considered to be 52-65 mm. Nailed connections show even higher values, according to Table V.3 of Appendix V. The backbone curve that is used for input in ETABS is presented in Figure Z.5. The timber frame wall shows more displacement capacity than the masonry piers. The capacity of the anchors is not used until its full capacity, as shown in Figure Y.23. However, this is on the assumptions that steel failure is governing and the anchors are not buckled in compression.

Application of the strengthening to all lower piers and to all piers of the structure is analysed. The results are shown in Figures X.3 and X.4 of Appendix X. It shows that this does not influence the behaviour and the capacity of the structure significantly. Therefore, in this particular case, strengthening of only the lower middle piers is sufficient.

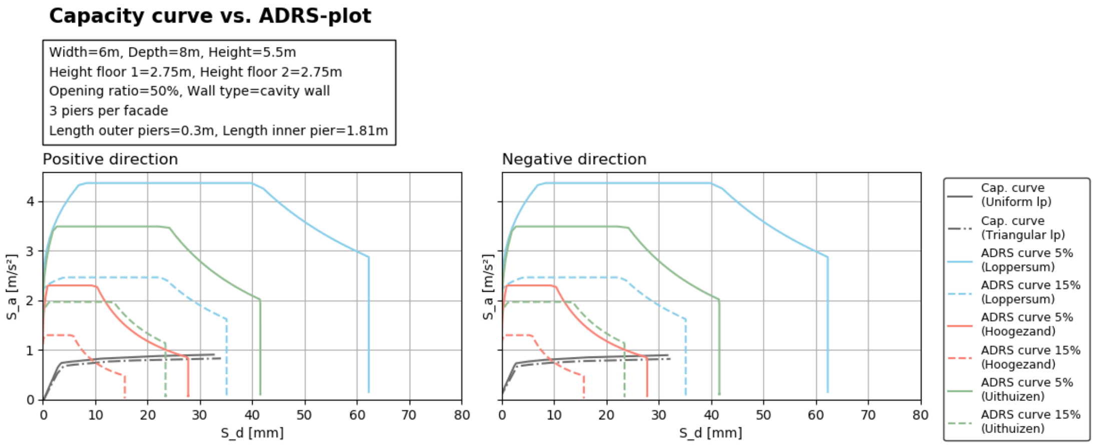

Figure 8.10: Capacity curve of a model with large middle piers, that is not strengthened.

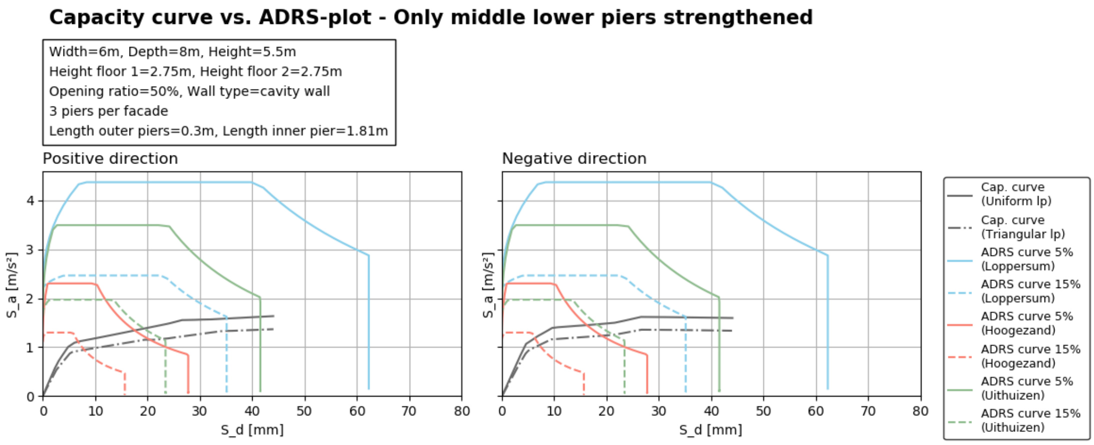

Figure 8.11: Capacity curve of a model with large middle piers, for which only the lower middle piers are strengthened with timber frame shear walls.

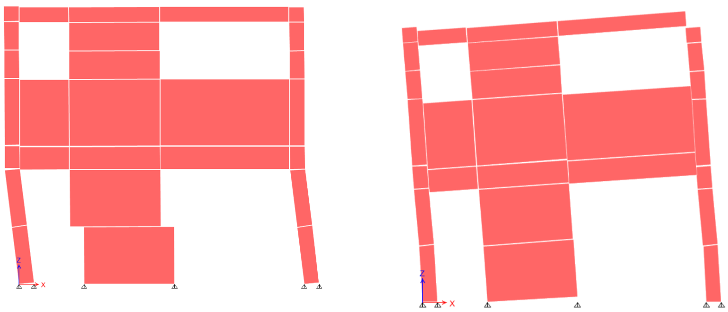

(a) Seismic behaviour of the un-strengthened situation. Shear failure occurs at the lower middle pier.

(b) Seismic behaviour of the strengthened situation. Rocking mechanism is governing.

Figure 8.12: Seismic behaviour of un-strengthened and strengthened model with large middle piers.

Estimation of the hysteretic damping when the building is strengthened is presented in Table 8.2. Both formulas G.14 and G.15 of NPR 9998:2018 [34] are used to estimate the damping. It indicates that the global ductility of the structure is 8.8, which is higher than without strengthening, caused by change of shear to rocking behaviour. The hysteretic damping is estimated to be between 0,13 and 0,17. The assumption of 15% damping is therefore acceptable.

u_y	5	mm
u_{cap}	44	mm
μ_{sys}	8,8	-
k_e	22	kN/mm
k_2	1	kN/mm
r	0,045	-
η_{eff}	0,35	-
ξ_{hys} (G.14)	0,139	-
ξ_{hys} (G.15)	0,168	-

Table 8.2: Estimation of the hysteretic damping of a model where only lower middle piers are strengthened, according to formulas (G.14 and G.15) of the NPR [34].

Model with CaSi element masonry

The structures built with CaSi element masonry, are likely to have brittle behaviour and therefore acquire lower drift limits according to the NPR. Due to this lower limits, the model does not satisfy the NC limit state for all locations considered. In order to satisfy the NC limit state the mode, the model is strengthened.

The model is analysed with strengthening by timber frame shear walls in different ways:

- one where all piers at ground floor level are strengthened with two WHT 620 anchors per pier
- one where all piers are strengthened with two WHT 620 anchors per pier
- one where all piers at ground floor level are strengthened with ten WHT 620 anchors per pier
- one where all piers are strengthened with ten WHT 620 anchors per pier.

The application of ten anchors per pier is rather unrealistic, however it is chosen to investigate if the strengthening measure would be sufficient in ideal circumstances. Table 8.3 shows the results of the strengthened models. Appendix X presents the corresponding capacity curves. The results are displayed until the drift limit at effective height is reached for un-strengthened ductile masonry behaviour, due to a lack of renewed drift limits when retrofitted, see Figure 8.13 (drift limit of 0,8%). The red crosses indicate the drift limits at effective height for brittle masonry behaviour in the un-strengthened situation.

In order to satisfy the NC limit state in all locations considered, the drift limit at effective hight should be increased to 0,64 %, which is an increase of 60%. According to experimental tests [23] and results from ETABS, this could be realised. However, the aforementioned tests are performed on CaSi brick masonry, which show more ductile behaviour. Experimental tests have to be performed on retrofitted element masonry, to examine if it would behave less brittle when strengthened with timber elements.

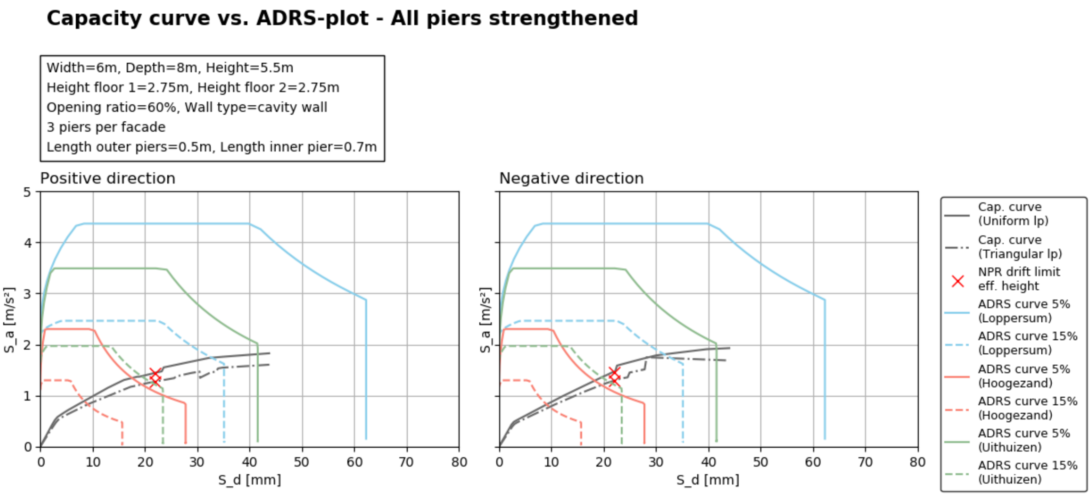

Figure 8.13: Capacity curve of a model with CaSi element masonry, for which is all piers are strengthened with timber shear walls.

The configuration of the timber frame shear wall that needs to be applied, is calculated and presented in Appendix Z. The retrofit measure consists of 70 x 80 C24 timber framework of 0,7 by 2,75 meter, with an OSB panel of 18 mm thick nailed to the framework by $\varnothing 3.1 \times 70$ nails with a spacing of 50 mm. Less spacing results in a larger displacement capacity. The seismic behaviour of the masonry piers is already governed by rocking, therefore significantly increasing the shear capacity is not needed. The retrofit measure is therefore designed upon reaching sufficient displacement. Calculation for the capacity and the displacement are given in Appendix Z. The backbone curve that is used for input in ETABS is presented in Figure Z.10.

Model	**Strength (kN)**	**Increase (%)**
Un-strengthened	121,5	-
All piers at ground floor level strengthened	128,1	5
All piers at ground floor level strengthened with multiple anchors	169	39
All piers strengthened	128	5
All piers strengthened with multiple anchors	242	99

Table 8.3: Results of a strengthened model with CaSi element masonry.

The strength of the model is significantly increased, especially when all piers are strengthened with the application of multiple anchors per pier rather than only strengthening of the lower piers, see Table 8.3. However, even if an unrealistic amount of ten anchors per pier is applied, the NC limit state is not satisfied when the drift limit for the un-strengthened situation are used. This type of strengthening is not suitable to increase the strength in a sufficient way. Therefore more research has to be done on the controlled displacement of the strengthened masonry, so drift limits can be adjusted for the strengthened situation.

Estimation of the hysteretic damping when the structure is strengthened is presented in Table 8.4. It indicates that the global ductility of the system is rather high. The hysteretic damping is estimated between 0,11 and 0,17. Retrofitting only the lower piers results in a lower value for the hysteric damping. Depending on the effect of the retrofit design on element masonry, which should be experimentally tested, the lower amount of damping can still result in satisfaction of the safety standards, as is indicated in Figure 8.13.

Strengthening	Only lower piers	All piers	
u_y	3,75	3,4	mm
u_{cap}	35	35	mm
μ_{sys}	9,3	10,3	-
k_e	19,5	20,6	kN/mm
k_2	1,5	1	kN/mm
r	0,077	0,049	-
η_{eff}	0,35	0,35	-
ξ_{hys} (G.14)	0,112	0,132	%
ξ_{hys} (G.15)	0,168	0,167	%

Table 8.4: Estimation of the hysteretic damping of a model with CaSi element masonry, according to formulas (G.14 and G.15) of the NPR [34].

Model with an opening ratio of 70%

The seismic behaviour of these models is largely affected by the second order effects. The displacement capacity of the structure is significantly reduced. To effectively strengthen this model, the resistance of the first floor should be increased. In order to do so, the proposed strengthening is applied in various configurations to evaluate the effect on the seismic behaviour:

- one where all piers at ground floor level are strengthened with two WHT 620 anchors per pier
- one where all piers are strengthened with two WHT 620 anchors per pier
- one where all piers at ground floor level are strengthened with ten WHT 620 anchors per pier

The capacity curves of the strengthened models are presented in Figure X.12 to X.14. When all lower piers of the model are strengthened with two anchors per pier, the increase in both strength and capacity is minimal. The NC limit state is not satisfied for any of the locations. When more tension anchors are applied, both strength and displacement are increased more significantly. However, the NC limit state is still not satisfied in any of the locations.

Although the first floor is the most weak, the effect of applying strengthening at the second floor is analysed. The results show there is no significant difference in strength and displacement capacity compared to only strengthening the first floor, see Table 8.5. This is expected, since the increase in strength is mainly realised by the tension anchors preventing the uplift of the masonry piers. Because almost no uplift is recorded for the piers at second floor, the strength of the structure is not increased.

The proposed retrofit design is not suited for strengthening of structures with opening ratios of 70% at ground floor level. The tension anchors should provide extra resistance to the lateral loads, by preventing uplift of the piers. However, the anchors used in the model do not provide enough resistance, not even when large amounts of tension anchors are applied. Furthermore, application of 10 anchors per pier is not reasonable, due to the lack of space and high tension forces that the foundation need to take care of.

Model	**Strength (kN)**	**Increase (%)**	**Displacement (mm)**	**Increase (%)**
Un-strengthened	11,7	-	23,4	-
All piers at ground floor level strengthened	12,13	4	23,5	0,4
All piers at ground floor level strengthened with multiple anchors	15,26	30	29,3	25
All piers strengthened	12,34	6	25,4	9

Table 8.5: Results of strength and displacement capacity of strengthened model with an opening ratio of 70%

Model subjected to other rocking drift limits

The rocking drift limit is up for discussion. Various standards apply different drift limits. Especially for the assessment of this building typology, the rocking drift limit is of crucial importance, as discussed in Section 6.5.

It can mean the difference between strengthening and no strengthening. Therefore, the effect of the retrofit design is analysed for models which are evaluated according to the NZSEE drift limits.

One model with an opening ratio of the ground floor façade of 60% is analysed. Appendix X shows the corresponding capacity curves of the model strengthened with timber frame shear walls in different ways:

- one where all piers at ground floor level are strengthened with two WHT 620 anchors per pier
- one where all piers are strengthened with two WHT 620 anchors per pier
- one where all piers at ground floor level are strengthened with ten WHT 620 anchors per pier
- one where all piers are strengthened with ten WHT 620 anchors per pier.

Table 8.6 shows the increase in strength and displacement for each of the aforementioned strengthened models. The results are remarkable, showing a decrease of the displacement capacity when only the lower piers of the model are reinforced. This can be explained by the fact the second floor shows more relatively more displacement compared to the first floor and therefore the rocking drift limit for top piers is reached earlier.

When all piers are strengthened, the structure moves more as a whole, resulting in an increase of the displacement capacity. Furthermore, the strength of the structure is significantly increased, especially when applied on all piers. The forces within the structural elements and applied anchors are presented in Appendix Y. Analysis indicates that the tension anchors are not used till their full capacity. However, the increase in strength is not sufficient to satisfy the NC limit state. Tests have shown that the behaviour of the wall is more reliable when strengthening is applied. Increasing the drift limits, is key for this strengthening measure to satisfy the NC limit states according to the NPR 9998:2018 when this type of modelling approach is applied.

Model	**Strength (kN)**	**Increase (%)**	**Displacement (mm)**	**Increase (%)**
Un-strengthened	78,5	-	26,28	-
All piers at ground floor level strengthened	79,2	1	21,7	-17
All piers at ground floor level strengthened with multiple anchors	80,7	3	21	-20
All piers strengthened	114	45	33,3	27
All piers strengthened with multiple anchors	150	91	33,6	28

Table 8.6: Results of a strengthened model with an opening ratio of 60%

The configuration of the timber frame shear wall that needs to be applied, is similar to the retrofit applied for the model with CaSi element masonry and is calculated and presented in Appendix Z. The retrofit measure consists of 70 x 80 C24 timber framework, with an OSB panel of 18 mm thick nailed to the framework by $\varnothing 3.1 \times 70$ nails with a spacing of 50 mm.

Estimation of the hysteretic damping when the building is strengthened is presented in Table 8.7. It indicates that when only the lower piers are reinforced, 15% of damping is an adequate assumptions. However, when all piers are strengthened, the hysteretic damping is likely to be less, between 0,06 and 0,016. A smaller amount of damping, requires more displacement capacity to satisfy the NC limit state. An extra displacement of 10-15 mm is needed. When higher drift limits are prescribed for the strengthened situation, it is possible to achieve this deformation without collapse of the building.

Strengthening	Only lower piers	All piers	
u_y	9	8	mm
u_{cap}	44	44	mm
μ_{sys}	4,9	5,5	-
k_e	8,3	7,5	kN/mm
k_2	0,3	1,9	kN/mm
r	0,036	0,256	-
η_{eff}	0,35	0,35	-
ξ_{hys} (G.14)	0,15	0,063	%
ξ_{hys} (G.15)	0,156	0,160	%

Table 8.7: Estimation of the hysteretic dampingof a strengthened model with an opening ratio of 60%, according to formulas (G.14 and G.15) of the NPR [34].

Part IV

Conclusions

9. Conclusions

In this chapter, the main findings with regard to the research questions are summarised and general conclusions are described.

This research aims to investigate the possibilities of enhancing the seismic in-plane performance of typical low-rise unreinforced masonry buildings in the Groningen area with the application of timber elements. The building typology most vulnerable to seismic in-plane loads is analysed, consisting of a two storey terraced house with concrete floors and large openings in the ground floor façade walls. The in-plane behaviour of these walls is considered weak, and despite reduced seismic risk, the structures are likely to be unsafe. A sensitivity analysis is carried out to indicate the governing failure mechanisms for geometric variants of the building typology. Non-linear static pushover analyses are performed to assess the in-plane behaviour according to the Dutch guidelines for the Near Collapse limit state using a macro-element modelling approach in ETABS. After, a timber retrofit design is proposed, for which the effect on the performance is evaluated.

Conclusions on the sensitivity analysis, effect of the seismic retrofit, the applied methodology and the standards and guidelines are discussed in this Chapter.

Sensitivity analysis

The sensitivity analysis indicates that the majority of the models show predominantly rocking behaviour, due to the presence of slender piers. This ductile behaviour ensures relatively large lateral displacement, resulting in high displacement capacities. As a result, most of the models satisfy the Near Collapse limit state in all considered locations in Groningen. Furthermore, results indicate that models with wide masonry piers, calcium silicate element masonry and high opening ratios of 70% at ground floor level are structurally unsafe.

Buildings with an opening ratio equal to 50%, may have wide masonry piers at ground floor level. These are more likely to exhibit shear sliding behaviour. This behaviour is governing from pier widths of 1,8 meter. In that case, the Near Collapse limit state is not satisfied and therefore reinforcement is needed.

Structures with CaSi element masonry are expected to behave in a more brittle way. Therefore, lower drift limits are applied, resulting in a reduction of displacement capacity and therefore Near Collapse limit is not satisfied for all locations. These models need to be strengthened.

Furthermore, structures with high opening ratios of 70% at ground floor level, are governed by second order effects, which largely reduces the displacement capacity. To satisfy the Near Collapse limit state, the structure needs to be seismically retrofitted.

Seismic retrofit

Based on the outcomes of the sensitivity analysis, a retrofit design is proposed, consisting of a timber framework connected to the inner masonry piers with an OSB panel nailed on top of it to increase the stiffness. The timber retrofit is attached to the foundation by tension anchors. The retrofit is designed to withstand the lateral loads and displacements, while the masonry transfers the majority of the vertical loads, in order to minimize the size of the retrofit measure.

For the model with wide middle piers, strengthening only the middle piers at ground floor level, results in sufficient displacement capacity and therefore satisfaction of the safety standards. The seismic behaviour changes from shear failure into rocking. Furthermore, the tension anchors applied provide a higher lateral resistance, increasing the strength of the structure.

When the retrofit measure is applied to the model with the CaSi element masonry, an increase in strength is recorded. However, the increase in strength is not sufficient to satisfy the NC limit state. An increase in displacement capacity of 60% is needed to satisfy the NC limit state. This is likely to happen, according to tests done on a similar strengthening measure [23]. However, more research is needed on element masonry specimens, since the tests, upon which the new drift limits are based, are performed on brick masonry instead. To ensure more ductile behaviour of the whole structure, all piers should be seismically strengthened.

Applying the proposed retrofit measure to models with an opening ratio of 70% at ground floor level, is not sufficient. The retrofit measure does not improve the resistance to the lateral forces adequately and therefore second order effects are still governing. To satisfy the Near Collapse limit state, the resistance to the lateral forces should be significantly increased. The tension anchors, which should provide this resistance, do not contribute sufficiently.

Based on the results, it can be concluded that a timber frame shear wall can significantly enhance the in-plane behaviour. Especially when applied to wider piers, which are more likely to show shear behaviour. An increase in shear capacity prevents this behaviour and results in more stable rocking behaviour due to which larger displacements can be realised. The ductile connections between panel and framework ensure that the retrofit can handle these large displacements. However, the increase of lateral resistance of the structure is limited. The tension anchors provide some resistance to the lateral forces but this is in most cases insufficient. Furthermore, the resistance of the anchors is largely depended on the design of the foundation and structural elements to which these anchors are attached.

Seismic standards/guidelines

The structure is composed of piers, spandrels and elements that connect them. The analysis is mechanism based, using the governing mechanisms for each of these structural elements, according to the recommendations of the Dutch guideline NPR 9998:2018 [34]. The strength and displacement capacities of the structural elements are based on the mean properties of the actual masonry, geometry and the loads within and on the structure. The outcomes of the numerical models, depend on prescribed drift limits from standards which are based on experimental tests. The capacity curves presented by ETABS need to be assessed afterwards. Judging the capacity curves of the numerical models by drift limits according to other standards can lead to different results when it comes to retrofitting. The sensitivity analysis showed that when models are assessed according to NSZEE guidelines, most models are likely to need seismic strengthening. Establishing the appropriate limits for each model, is therefore essential. It can mean the difference between strengthening and not strengthening.

From experimental tests done on a similar retrofit design [23], it is likely to assume that drift limits of the strengthened situation can be increased, which could result in satisfying the Near Collapse limit state, since there would be sufficient displacement capacity. In order to guarantee the increase in drift limit of the strengthened building, more tests should be performed. In this case also tests on element masonry specimens.

10. Discussion

In this chapter, interpretations of the results are discussed, together with the relevance and limitations of this thesis.

Methodology

The masonry structures are modelled using a macro-element modelling approach in ETABS. This approach in combination with the ability to automate the analysis of numerical models with help of the Application Programming Interface (API) for ETABS, results in a powerful parametric tool. A large amount of variants of the building typology are assessed, creating a better overview of the seismic behaviour of the typology as a whole. If a more advanced modelling approach would have been chosen, this approach would be too complicated and time consuming.

The non-linear static pushover method considers non-linear structural behaviour without the need to define the often complex characteristics of structural elements and therefore maintaining simplicity. The analysis gives a good insight into the propagation of damage and it accounts for second order effects. Furthermore, capacity curves of the global behaviour can easily be compared to the seismic demand of various locations, without changing the input of the numerical model. However, one of the disadvantages is the assessment of both loading directions separately, therefore not taking into account dynamic effects. Another disadvantage is the consideration of only in-plane behaviour, lacking the out-of-plane interaction.

Sensitivity analysis

This research focusses on the behaviour of geometrical variants of a certain building typology, which is assumed to be vulnerable to in-plane seismic loads. It is assumed that the façade walls partly carry the second floor. Maintaining this load-bearing function of the piers is therefore essential to the global behaviour. Houses where the transversal walls completely carry the vertical loads, are likely to behave in a different way. Collapse of the façde wall would then not necessarily lead to failure of the whole structure. Consequently, results of the analysis are not representative for this variation in the typology.

For the evaluation of the in-plane behaviour an additional hysteretic damping of 15% of the system is considered. According to the NPR 9998:2018 [34], this value is conservative when ductile behaviour is expected. However, the expected damping largely depends on the condition and material properties of each individual building. As the results indicate, models are likely to satisfy the Near Collapse limit state even if no hysteretic damping can be applied in two of the three locations investigated. For houses in areas with higher seismic risk, the additional damping is of significant importance and should be applied carefully. Nonetheless, most of the buildings showed displacement capacities beyond the 5% inherent damping.

In this research it is chosen to model the flange effect with a separate connection to the transversal walls, which gives more insight and control in the distribution of the flange forces. Furthermore, properties of the flange links can be changed and the effect could be evaluated. Results show that the flange effect has significant influence on the strength of the structure, which is expected from tests. If both wall elements are attached without a link, the effect of the flange loads could not have been studied. However, another way of modelling could result in different outcomes, but it is expected that the applied modelling approach will roughly perform similarly.

Despite the simplistic macro-modelling approach, the outcomes of the tested models, are in line with full-scale tests done on a similar URM terraced house, on both the capacity and the global seismic behaviour [36]. Additionally, validation of masonry assemblages tested at the TU Delft shows similar seismic behaviour and capacity [17] compared to the ETABS models. The relatively large displacements realised due to the rocking behaviour, are reasonable and within the safety limits when analysed according to the NPR guidelines. The reduction of seismic risk, as a result of the stop of gas extraction, ensures that most of these buildings no longer need to be retrofitted to improve the in-plane behaviour.

Seismic retrofit

Due to the simplicity of the macro-modelling approach, an advanced numerical representation of the strengthening measure cannot be implemented in ETABS. Therefore, a simplified numerical representation of the strengthening is applied, which does not take into account certain aspects of the retrofit design. Differential movement between the masonry and OSB wall systems is not captured. The additional shear capacity provided by the panels is instead added directly to the capacity of the non-linear link element previously used to represent the shear capacity of the masonry piers.

Furthermore, modelling of the hold-down connections is based on the assumption that rupture of the steel of the anchors is governing. However, the resistance of the anchors is largely depended on the design of the foundation and structural elements to which these anchors are attached. Although minimum thickness and strength are described, a detailed analysis on the foundation for each individual building is necessary before application of the anchors, since it can be a limiting factor to the performance of the design. Next to that, degradation of the tension anchors through buckling due to compression forces is not captured. A time dependent analysis should incorporate this effect.

Although the representation of the timber retrofit is based on certain assumptions and simplifications, the global behaviour is similar to what is expected based on tests done on a similar retrofit measure in Pavia [23]. Shear behaviour of the masonry piers is changed to a more stable rocking behaviour, enhancing the displacement capacities of the whole structure accordingly. Furthermore, results show that application of the retrofit design does not increase the lateral resistance significantly, which is in accordance with what was found in the experimental tests [23].

11. Recommendations

The sensitivity analysis revealed that, according to the NPR 9998:2018, structures with wide piers, element masonry and with extremely large openings at floor level do not satisfy the Near Collapse limit state for all considered locations in Groningen. Other changes in geometry do not significantly change behaviour or capacity of the structures. It is therefore recommended to focus on seismic assessment of the aforementioned variants of the building typology, when considering in-plane behaviour. Performing non-linear time history analyses on these variants should gain more detailed information on the seismic behaviour.

Dutch guidelines and other standards do not provide any drift limits for strengthened structures. The analysis of retrofitted models demonstrates that the Near collapse limit state is satisfied, when drift limits are increased. Experimental testing on the proposed retrofit measure is needed to provide the seismic standards with results, upon which new increased drift limits can be based. Overall consistent definition of capacity values and corresponding drift limits for each possible failure mechanism is essential for reliable evaluation of the in-plane response of unreinforced masonry structures. And as this research indicates, especially when buildings are assessed using non-linear analyses. It can mean the difference between strengthening and no strengthening.

The variant study, performed with the help of the API for ETABS, shows good potential when it comes to analysing large amount of buildings from the same building typology. It is recommended to use a parametric tool in combination with a macro-modelling approach, since it gives adequate insight in global seismic behaviour of a complete building typology, with relatively low computational time. It exposes the vulnerable variants, which then can be assessed in more detail.

Analysis of the retrofit shows the importance of ductile behaviour. In order to provide this ductility it is advised to use ductile sheathing-to-framing connections, consisting of nails with a small diameter and a panel thickness of at least 4d. Furthermore, it is advised to connect the retrofit to the foundation with anchors, which benefits ductile behaviour of the sheathing-to-framing connection. Tensile anchors show an important role in the increase of the lateral resistance. However, the type and capacity of the anchors depends largely on the strength of the foundation and concrete elements to which they are attached. Although minimum values for the foundation design are presented, a detailed analysis of the capacity of the surrounding components of the tensile anchors is recommended.

Future research

This research assesses the seismic behaviour of two storey terraced houses based on certain modelling and analysis assumptions. For future research various aspects that were not studied should be analysed. A number of recommendations for future research are given.

Terraced houses with concrete floors are analysed, which are represented by rigid diaphragms. Besides concrete floors, timber floors are frequently present within the studied building typology. Modelling of timber floors requires a flexible diaphragm, which will introduce different seismic behaviour and most likely torsional effects, due to the reduction of mass and the absence of box-type behaviour. The effect of the proposed strengthening design on the global behaviour is likely to be different. Research on the implementation of the design in combination with timber floors should be conducted to study this effect.

The connection between the concrete floors and the wall, upon which they rest, is considered rigid. Floors are always connected to the walls. In reality this is not the case. Future research should consider the potential non-linear effects of wall-floor connections more carefully.

To decrease the setup time of the numerical model, as well as the computational time for the variant study, the configuration of the structural elements is simplified. For a more detailed and building specific analysis, structural elements should be modelled with their actual dimensions. Future research should be conducted to analyse the effect on the seismic behaviour.

Out-of-plane behaviour is not taken into account for the assessment of the considered building typology. Mainly because the in-plane direction for this typology is seismically weak, due to the large openings in the façades. However, for a more detailed seismic assessment of the unsafe structures according to this research, the out-of-plane behaviour should be taken into account.

Pounding effects are not taken into account, since a block of terraced houses consists of units with similar structural systems. Therefore, the effect is likely to be negligible. However, for future research it would be interesting to see if this assumption is valid.

Analysis of the timber frame shear wall retrofit measure is chosen over the proposed CLT retrofit design, since more detailed research is available on masonry retrofitted with timber framework. The proposed retrofit design with CLT panels, should be analysed in more detail. To do so, more experimental testing on strengthened masonry pier specimens and full-scale specimens is required.

Furthermore, strengthening is applied to mainly the masonry pier elements. The effect of strengthening the spandrel elements in combination with the pier elements on the seismic behaviour of the structure should be investigated. The strengthening of spandrels can result in a better introduction of the forces to the piers.

Bibliography

[1] Koninklijk Nederlands Meteorologisch Instituut, "Aardbevingen (gr.)." `https://www.nam.nl/feiten-en-cijfers/aardbevingen.html`, 2019.

[2] Mijnraad, "2018-06-29 Advies Mijnraad veiligheidsrisico's en versterkingsopgave Groningen," June 2018.

[3] Arup, "Arup project title: Groningen 2013, Structural Upgrading Study," tech. rep., November 2013.

[4] J. van Elk and D. Doornhof, "Induced Seismicity in Groningen, Assesment of Hazard, Building Damage and Risk," tech. rep., November 2017.

[5] Joost de Vree, "Staal: fundering op staal." `http://www.joostdevree.nl/shtmls/staal_fundering_op_staal.shtml"`.

[6] "Types of masonry foundations, their construction and uses." `https://theconstructor.org/building/types-masonry-foundations-construction-uses/18989/`.

[7] Z. Salát, "Numerical Modelling of Out-of-Plane Behavior of Masonry Structural Members," Master's thesis, Technical University of Catalonia, July 2015.

[8] D. D'Ayala and E. Speranza, "Definition of Collapse Mechanisms and Seismic Vulnerability of Historic Masonry Buildings," *Earthquake Spectra*, vol. 19, no. 3, pp. 479–509, 2003.

[9] M. A. ElGawady, P. Lestuzzi, and M. Badoux, "Static Cyclic Response of Masonry Walls Retrofitted with Fiber-Reinforced Polymers," *Journal of Composites for Construction*, vol. 11, no. 1, pp. 50–61, 2007.

[10] W. van der Mersch, "Modelling the seismic response of an unreinforced masonry structure," Master's thesis, Delft University of Technology, June 2015.

[11] S. Lagomarsino, A. Penna, A. Galasco, and S. Cattari, "Tremuri program: An equivalent frame model for the nonlinear seismic analysis of masonry buildings," *Engineering Structures*, vol. 56, pp. 1787 – 1799, 2013.

[12] F. A. Najam, "Nonlinear static analysis procedures for seismic performance evaluation of existing buildings – evolution and issues," in *Facing the Challenges in Structural Engineering*, (Cham), pp. 180–198, Springer International Publishing, 2018.

[13] NEN. `http://seismischekrachten.nen.nl/webtool.php`, 2019.

[14] B. Pantò, E. Raka, F. Cannizzaro, G. Camata, S. Caddemi, E. Spacone, and I. Caliò, "Numerical macro-modeling of unreinforced masonry structures: A critical appraisal," in *Proceedings of the Fifteenth International Conference on Civil, Structural and Environmental Engineering Computing*, (Stirlingshire, Scotland), September 2015.

[15] G. S. view. `https://www.google.com/maps/@53.4040952,6.6661413,3a,75y,198.18h,88.01t/data=!3m6!1e1!3m4!1sjDaGv6LedCzoI4S1l_HAgQ!2e0!7i13312!8i6656"`, Oktober 2014.

[16] F. Messali, J. G. Rots, and M. Longo, "Prediction of the peak base shear capacity of seven experiments on full-scale urm structures: comparison between different methods," tech. rep., TU Delft, September 2018.

[17] R. Esposito, K. Terwel, G. Ravenshorst, R. Schipper, F. Messali, and J. G. Rots, "Cyclic pushover test on an unreinforced masonry structure reseambling a typical dutch terraced house," in *6th World Conference on Earthquake*, (Santiago, Chile), pp. 1–12, 2016.

[18] N. Gattesco and I. Boem, "Stress distribution among sheathing-to-frame nails of timber shear walls related to different base connections: Experimental tests and numerical modelling," *Construction and Building Materials*, vol. 122, pp. 149 – 162, 2016.

[19] E. Karacabeyli, B. Douglas, and F. P. Laboratory, *CLT handbook: Cross-laminated timber*. FPInnovations, 2013.

[20] M. Shahnewaz, S. Alam, and T. Tannert, "In-plane strength and stiffness of cross-laminated timber shear walls," *Buildings*, vol. 100, no. 8, 2018.

[21] W. Seim, J. Hummel, and T. Vogt, "Earthquake design of timber structures – remarks on force-based design procedures for different wall systems," *Engineering Structures*, vol. 76, pp. 124 – 137, 2014.

[22] D. Dizhur, M. Giaretton, I. Giongo, and J. M. Ingham, "Seismic retrofit of masonry walls using timber strong-backs," *Journal of the Structural Engineering Society of New Zealand Inc*, vol. 30, no. 2, pp. 30–44, 2017.

[23] M. Miglietta, N. Damiani, L. Mazzella, L. Grottoli, G. Guerrini, and F. Graziotti, "Full-scale shaking table test on a dutch urm cavity-wall terraced-house end unit a retrofit solution with strong-backs and osb boards euc-build-7," tech. rep., EUCENTRE, University of Pavia and IUSS, May 2019.

[24] I. Sustersic and B. Dujic, "Seismic strengthening of existing concrete and masonry buildings with cross-lam timber panels," *Materials and Joints in Timber Structures: Recent Developments of Technology*, vol. 9, pp. 713–723, 2014.

[25] D. Casagrande, "STUDY OF TIMBER-FRAME BUILDING SEISMIC BEHAVIOUR BY MEANS OF NUMERICAL MODELLING AND FULL-SCALE SHAKE TABLE TESTING," Master's thesis, University of Trento, April 2014.

[26] D. Casagrande, S. Rossi, T. Sartori, and R. Tomasi, "A predictive analytical model for the elasto-plastic behaviour of a light timber-frame shear-wall," *Construction and Building Materials*, July 2015.

[27] M. He, H. Huang, and N. Zhou, "Racking performance of wood shear walls fabricated using chinese wood-based panels," in *World Conference on Timber Engineering*, (Trentino, Italy), 2010.

[28] F. Messali and Manimaran, "Structural behaviour of a calcium silicate element masonry assemblage: comparison of blind predictions," tech. rep., May 2017.

[29] R. Esposito, S. Jafari, G. Ravenshorst, R. Schipper, and J. G. Rots, "Influence of the behaviour of calcium silicate brick and element masonry of the lateral capacity of structures," in *10th Australian Masonry Conference*, (Sydney, Australia), February 2018.

[30] Rothoblaas, *Wood connectors and timber plates*, 2015.

[31] CEN, European Committee for Standardisation, *Eurocode 5: Design of timber structures - Part 1-1: General - Common rules and rules for buildings*. 2005.

[32] D. Casagrande, S. Rossi, T. Sartori, and R. Tomasi, "Proposal of an analytical procedure and a simplified numerical model for elastic response of single-storey timber shear-walls," *Construction and Building Materials*, February 2015.

[33] D. Casagrande, A. Polastri, T. Sartori, C. Loss, and M. Chiodega, "Experimental campaign for the mechanical characterization of connection systems in the seismic design of timber buildings," in *World Conference on Timber Engineering*, (Vienna, Austria), 2016.

[34] NEN, Koninklijk Nederlands Normalisatie-instituut, *NPR 9998 - Assessment of structural safety of buildings in case of erection, reconstruction and disapproval - Induced earthquakes - Basis of design, actions and resistances*. 2018.

[35] Arup, "Data Documentation Exposure Database Version 5," tech. rep., January 2018.

[36] F. Graziotti, U. Tomassetti, A. Rossi, S. Kallioras, A. Penna, and G. Magenes, "Shaking table test on a full-scale URM cavity wall building," *Bulletin of Earthquake Engineering*, 2017.

[37] S. Jafari, J. G. Rots, R. Esposito, and F. Messali, "Characterizing the material properties of dutch unreinforced masonry," *Procedia Engineering*, vol. 193, pp. 250 – 257, 2017. International Conference on Analytical Models and New Concepts in Concrete and Masonry Structures.

[38] F. Messali, R. Esposito, S. Jafari, G. Ravenshorst, P. Korswagen, and J. G. Rots, "A multiscale experimental characterisation of dutch unreinforced masonry buildings," in *Proceedings of the 16th European Conference on Earthquake Engineering*, (Thessaloniki, Greece), June 2018.

[39] G. Magenes and A. Menon, "A review of the current status of seismic design and assessment of masonrybuildings in europe," *Journal of Structural Engineering*, vol. 35, no. 6, pp. 247 – 256, 2009.

[40] I. Idrizi and Z. Idrizi, "Numerical modeling and analysis of unreinforced masonry walls," *Journal of Civil Engineering and Architecture*, vol. 11, pp. 870–878, 2017.

[41] P. B. Lourenço, J. G. Rots, and J. Blaauwendraad, "Two approaches for the analysis of masonry structures: micro and macro-modeling," *HERON*, vol. 40, no. 4, 1995.

[42] MBIE, SESOC, NZSEE, and NZGS, "The Seismic Assessment of Existing Buildings (the Guidelines); Part C2: Assessment Procedures and Analysis Techniques," tech. rep., July 2017.

[43] Computers and Structures, Inc. `https://wiki.csiamerica.com/display/kb/Pushover`, 2019.

[44] Y. Nakamura, G. Magenes, and M. Griffith, "Comparison of pushover methods for simple building systems with flexible diaphragms," (Lorne, Victoria), pp. 1–11, Australian Earthquake Engineering Society, November 2014.

[45] F. Messali and J. G. Rots, "In-plane drift capacity at near collapse of rocking unreinforced calcium silicate and clay masonry piers," *Engineering Structures*, vol. 164, pp. 183–194, 2018.

[46] NEN, "Achtergrondartikelen bij annex g van npr 9998:2018," tech. rep., NEN, 2018.

[47] T. Yi, F. Moon, R. Leon, and L. Kahn, "Flange effects on the nonlinear behaviour of urm piers," *TMS Journal*, vol. 26, November 2008.

[48] F. Messali, G. Ravenshorst, R. Esposito, and J. Rots, "Large-scale testing program for the seismic characterization of dutch masonry walls," in *16th World Conference on Earthquake*, (Santiago, Chile), 2017.

[49] CEN, European Committee for Standardisation, *Eurocode 8: Design of structures for earthquake resistance – Part 3: general rules, seismic actions and rules for buildings, Design Code EN 1998-3.* 2005.

[50] N. Z. S. f. E. E. NZSEE, *The seismic assessment of existing buildings, Part C8: Seismic assessment of unreinforced masonry buildings.* 2017.

[51] P. Morandi, L. Albanesi, F. Graziotti, T. L. Piani, A. Penna, and G. Magenes, "Development of a dataset on the in-plane experimental response of urm piers with bricks and blocks," *Construction and Building Materials*, vol. 190, pp. 593–611, 2018.

[52] H. J. Blass and C. Sandhaas, *Timber Engineering - Principles for design.* 2017.

[53] "Timber frame beginner's guide." `https://www.homebuilding.co.uk/timber-frame-guide/"`.

[54] "Retallack resort and spae." `https://www.djr-roof-trusses.co.uk/photo-gallery/17-retallack-resort-spa`.

[55] M. Izzi, A. Polastri, and M. Fragiacomo, "Advanced modelling of CLT wall systems for earthquake resistant timber structures," in *3rd International Network on Timber Engineering Research (INTER) Meeting*, vol. Paper INTER/49-1-6, (Graz, Austria), August 2016.

[56] R. Brandner, G. Flatscher, A. Ringhofer, G. Schickhofer, and A. Thiel, "Cross laminated timber (CLT): overview and development," *European journal of wood and wood products*, vol. 74, 3 2016.

[57] M. Popovski and I. Gavric, "Performance of a 2-story CLT House Subjected to Lateral Forces," *ASCE Journal of Structural Engineering*, vol. 142, no. 4, 2016.

[58] A. Ceccotti, C. Sandhaas, M. Okabe, M. Yasumura, C. Minowa, and N. Kawai, "Sofie project – 3d shaking table test on a seven-storey full-scale cross-laminated timber building," *Earthquake Engineering & Structural Dynamics*, vol. 42, no. 13, 2013.

[59] V. Hristovski, B. Dujic, M. Stojmanovska, and V. Mircevska, “Full-Scale Shaking-Table Tests of XLam Panel Systems and Numerical Verification: Specimen 1,” *Journal of Structural Engineering*, vol. 139, no. 11, pp. 2010–2018, 2013.

[60] M. Izzi, D. Casagrande, S. Bezzi, D. Pasca, M. Follesa, and R. Tomasi, “Seismic behaviour of Cross-Laminated Timber structures: A state-of-the-art review,” *Engineering Structures*, vol. 170, pp. 42 – 52, 2018.

[61] M. Popovski, J. Schneider, and M. Schweinsteiger, “Lateral load resistance of cross-laminated wood panels,” in *Proceedings of 11th World Conference on Timber Engineerig (WCTE2010)*, (Riva del Garda), 2010.

[62] R. Tomasi and I. Smith, “Experimental characterization of monotonic and cyclic loading responses of clt panel-to-foundation angle bracket connections,” *Journal of Materials in Civil Engineering*, vol. 27, no. 6, 2015.

[63] L. Pozza, F. Evangelista, and R. Scotta, “Clt used as seismic strengthener for existing masonry walls.,” in *Atti del XVII Convegno ANIDIS L’ingegneria Sismica*, (Pistoia, Italy), 2017.

[64] T. Hoekstra, “‘Multi-storey timber frame building’ – Modelling the racking stiffness of timber-frame shear-walls ,” Master’s thesis, TU Delft, April 2012.

[65] HILTI, “Anchor Fastening Technology Manual,” tech. rep., September 2014.

[66] K. Beyer and A. Dazio, “Quasi-static monotonic and cyclic tests on composite spandrels,” *Earthquake Spectra*, vol. 28, no. 3, pp. 885–906, 2012.

[67] K. Beyer and A. Dazio, “Quasi-static cyclic tests on masonry spandrels,” *Earthquake Spectra*, vol. 28, no. 3, pp. 907–929, 2012.

[68] F. Graziotti, G. Magenes, and A. Penna, “Experimental behaviour of stone masonry spandrels,” in *Proceedings of the 15th World Conference for Earthquake Engineering*, (Lissabon, Portugal), 2012.

[69] F. Graziotti, A. Penna, and G. Magenes, “Influence of timber lintels on the cyclic behaviour of stone masonry spandrels,” in *stone masonry spandrels*, (Guimaraes, Portugal), 2014.

[70] K. Beyer, “Peak and residual strengths of brick masonry spandrels,” *Engineering Structures*, vol. 41, pp. 533–547, August 2012.

[71] D. W. Dinehart and H. W. S. III, “Comparison of static and dynamic response of timber shear walls,” *Journal of Structural Engineering*, vol. 124, no. 6, pp. 686–695, 1998.

[72] A. Sinha and R. Gupta, “Strain distribution in osb and gwb in wood-frame shear walls,” *Journal of Structural Engineering*, vol. 135, no. 6, 2009.

[73] J. M. Branco, F. T. Matos, and P. B. Lourenço, “Experimental in-plane evaluation of light timber walls panels.,” *Buildings*, vol. 7, no. 3, 2017.

[74] T. Sartori, M. Piazza, R. Tomasi, and P. Grossi, “Characterization of the mechanical behaviour of light-frame timber shear walls through full-scale tests,” in *World Conference on Timber Engineering*, (Auckland, New Zealand), pp. 180–188, 2012.

[75] F. Germano, G. Metelli, and E. Giuriani, “Experimental results on the role of sheathing-to-frame and base connections of a european timber framed shear wall,” *Construction and Building Materials*, vol. 80, pp. 315 – 328, 2015.

[76] S. Schwendner, W. Seim, and J. Hummel, “Light-frame walls with osb and gfb sheathing under earthquake impact - a comparative study,” in *World Conference on Timber Engineering*, (Seoul, Republic of Korea), 2018.

[77] E. Liao, “Modelling flexible timber diaphragms in masonry buildings subjected to seismic excitations,” Master’s thesis, Delft University of Technology, March 2019.

Part V

Appendices

A. GEM taxonomy codes

GEM Taxonomy Code	Short code	Short Description
CR+PC/LPB/CR+PC/LPB/EWN/FN/HBET:1,2	PC1L	Precast RC post and beam low-rise
CR+PC/LPB/CR+PC/LPB/EWN/FN/HBET:3,20	PC1M	Precast RC post and beam mid to high-rise
CR+PC/LWAL/CR+PC/LN/EWN/FC/HBET:1,2	PC2L	Precast RC wall-slab-wall low-rise no cladding
CR+PC/LWAL/CR+PC/LN/EW/FC/HBET:1,2	PC3L	Precast RC wall-slab-wall low-rise with cladding
CR+PC/LWAL/CR+PC/LN/EW/FC/HBET:3,20	PC3M	Precast RC wall-slab-wall mid to high-rise with cladding
CR+PC/LWAL/CR+PC/LWAL/EWN/FC/HBET:1,2	PC4L	Precast RC wall-wall low-rise no cladding
CR+PC/LWAL/CR+PC/LWAL/EWN/FC/HBET:3,20	PC4M	Precast RC wall-wall mid to high-rise no cladding
CR+PC/LWAL/CR+PC/LWAL/EW/FC/HBET:1,2	PC5L	Precast RC wall-wall low-rise with cladding
CR+CIP/LPB/CR+CIP/LPB/EWN/FN/HBET:1,2	RC1L	Cast-in-place RC post and beam low-rise
CR+CIP/LPB/CR+CIP/LPB/EWN/FN/HBET:3,20	RC1M	Cast-in-place RC post and beam mid to high-rise
CR+CIP/LFM/CR+CIP/LFM/EWN/FC/HBET:1,2	RC2L	Cast-in-place RC frame low-rise
CR+CIP/LFM/CR+CIP/LFM/EWN/FC/HBET:3,20	RC2M	Cast-in-place RC frame mid to high-rise
CR+CIP/LWAL/CR+CIP/LN/EW/FC/HBET:1,2	RC3L	Cast-in-place RC wall-slab-wall low-rise with cladding
CR+CIP/LWAL/CR+CIP/LN/EW/FC/HBET:3,20	RC3M	Cast-in-place RC wall-slab-wall mid to high-rise with cladding
CR+CIP/LWAL/CR+CIP/LWAL/EWN/FC/HBET:1,2	RC4L	Cast-in-place RC wall-wall low-rise no cladding
CR+CIP/LWAL/CR+CIP/LWAL/EWN/FC/HBET:3,20	RC4M	Cast-in-place RC wall-wall mid to high-rise no cladding
MUR/LH/MUR/LH/EWN/FW/HBET:1,2	URM1L	URM house and timber post and beam low-rise
MUR/LH/MUR/LH/EWN/FW/HBET:3,20	URM1M	URM house and timber post and beam mid to high-rise
MUR/LWAL/MUR/LN/EWN/FW/HBET:1,2	URM2L	URM wall-slab-wall with solid walls and timber floors low-rise
MUR/LWAL/MUR/LN/EWN/FW/HBET:3,20	URM2M	URM wall-slab-wall with solid walls and timber floors mid to high-rise
MUR/LWAL/MUR/LN/EW/FC/HBET:1,2	URM3L	URM wall-slab-wall with cavity walls and concrete floors low-rise
MUR/LWAL/MUR/LN/EW/FC/HBET:1,2/IRIR+IRVP:CHV	URM4L	URM wall-slab-wall with cavity walls and concrete floors low-rise and large openings on ground floor walls
MUR/LWAL/MUR/LN/EW/FC/HBET:3,20	URM3M	URM wall-slab-wall with cavity walls and concrete floors mid to high-rise
MUR/LWAL/MUR/LN/EW/FW/HBET:1,2	URM5L	URM wall-slab-wall with cavity walls and timber floors low-rise
MUR/LWAL/MUR/LN/EW/FW/HBET:3,20	URM5M	URM wall-slab-wall with cavity walls and timber floors mid to high-rise
MUR/LWAL/MUR/LWAL/EWN/FW/HBET:1,2	URM6L	URM wall-wall with solid walls and timber floors low-rise
MUR/LWAL/MUR/LWAL/EWN/FW/HBET:3,20	URM6M	URM wall-wall with solid walls and timber floors mid to high-rise
MUR/LWAL/MUR/LWAL/EW/FC/HBET:1,2	URM7L	URM wall-wall with cavity walls and concrete floors low-rise
MUR/LWAL/MUR/LWAL/EW/FC/HBET:3,20	URM7M	URM wall-wall with cavity walls and concrete floors mid to high-rise
MUR/LWAL/MUR/LWAL/EW/FW/HBET:1,2	URM8L	URM wall-wall with cavity walls and timber floors low-rise
MUR/LWAL/MUR/LWAL/EW/FW/HBET:3,20	URM8M	URM wall-wall with cavity walls and timber floors mid to high-rise
MUR/LWAL/W/LPB/EWN/FN/HBET:1,2	W1L	Timber (glulam) post and beam with masonry infill walls low-rise
MUR/LWAL/W/LPB/EWN/FN/HBET:3,20	W1M	Timber (glulam) post and beam with masonry infill walls mid to high-rise
W/LPB/W/LPB/EW/FN/HBET:1,2	W2L	Timber post and beam low-rise
W/LPB/W/LPB/EW/FN/HBET:3,20	W2M	Timber post and beam mid to high-rise
W/LWAL/W/LN/EWN/FW/HBET:1,2	W3L	Timber wall-slab-wall without cladding low-rise
W/LWAL/W/LN/EW/FW/HBET:1,2	W4L	Timber wall-slab-wall with cladding low-rise
W/LWAL/W/LN/EW/FW/HBET:3,20	W4M	Timber wall-slab-wall with cladding mid to high-rise
W/LWAL/W/LWAL/EWN/FW/HBET:1,2	W5L	Timber wall-wall without cladding low-rise
W/LWAL/W/LWAL/EWN/FW/HBET:3,20	W5M	Timber wall-wall without cladding mid to high-rise
W/LWAL/W/LWAL/EW/FW/HBET:1,2	W6L	Timber wall-wall with cladding low-rise
W/LWAL/W/LWAL/EW/FW/HBET:3,20	W6M	Timber wall-wall with cladding mid to high-rise
S/LPB/S/LPB/EWN/FN/HBET:1,2	S1L	Steel post and beam with no floor low rise
S/LPB/S/LPB/EWN/FN/HBET:3,20	S1M	Steel post and beam with no floor mid rise
S/LFM/S/LFM/EWN/FC/HBET:1,2	S2L	Steel frame with concrete floor low-rise
S/LFM/S/LFM/EWN/FC/HBET:3,20	S2M	Steel frame with concrete floor mid to high-rise
S/LFBR/W/LPB/EWN/FN/HBET:1,2	W7L	Timber (glulam) post and beam with steel bracing low-rise
S/LFBR/W/LPB/EWN/FN/HBET:3,20	W7M	Timber (glulam) post and beam with steel bracing mid to high-rise
S/LFBR/S/LPB/EWN/FN/HBET:1,2	S3L	Steel portal frame with bracing in one direction low-rise
S/LFBR/S/LPB/EWN/FN/HBET:3,20	S3M	Steel portal frame with bracing in one direction mid to high-rise
S/LFBR/S/LFBR/EWN/FN/HBET:1,2	S4L	Steel braced frame with no floor low-rise
S/LFBR/S/LFBR/EWN/FN/HBET:3,20	S4M	Steel braced frame with no floor mid to high-rise
S/LFBR/S/LFBR/EWN/FC/HBET:1,2	S5L	Steel braced frame with concrete floor low-rise
S/LFBR/S/LFBR/EWN/FC/HBET:3,20	S5M	Steel braced frame with concrete floor mid to high-rise

Figure A.1: GEM Taxonomy Code for each structural system with a short code and a brief description for each system (Source:[4])

B. Gravity loads calculation

Additional permanent loads

Additional permanent loads floor		
Floor finish		
thickness	m	0,05
density	kN/m^3	25
force per area	kN/m^2	1,25
Pipes/ducts	kN/m^2	0,1
Ceiling and lighting	kN/m^2	0,3
Total	kN/m^2	1,65

Table B.1: Approximation of additional permanent loads per area for the floors

Weight of roof

Timber roof weight		
Total width building	m	6
Total length building	m	8
Thickness floor slab	m	0,231
Beams		
width	m	0,05
height	m	0,2
number of beams	-	14
Ridge beam		
width	m	0,07
height	m	0,25
Planks		
thickness	m	0,025
Total volume timber elements	m^3	2,0
Density timber	kg/m^3	500
Total mass timber	kg	998
Total area tiles	m^2	45
Mass roof tiles per area	kg/m^2	50
Total mass tiles	kg	2235
Total mass roof	kg	3232
Density concrete floor slab	kg/m^3	2500
Mass of roof structure related to dimensions floor slab	kg/m^3	333
Percentage of mass roof related to floor slab	%	13

Table B.2: Weight of timber roof structure related to floor slab second floor

Type of load	Unit	Value	Reference
Self weight concrete floor	kN/m³	25	
Additional permanent load	kN/m²	1,65	See Table B.1 Appendix B
Variable live load	kN/m²	1,75	NEN-EN 1991-1-1/Table NB.1 - 6.2
Load from self weight roof structure	kN/m³	3,3	Example value, depending on geometry
Weight modification factor of slab	-	1,13	

Table B.3: Weight of the second floor slab, with weight modification factor to account for the weight of the roof

Mass modification factors

Type of load	Unit	Value	Reference
Mass concrete floor	kg/m³	2500	
thickness floor	m	0,231	Example value, depending on the geometry
mass per area	kg/m²	577,5	
Mass additional permanent load	kg/m²	168	See Table B.1 Appendix B
Mass variable live load	kg/m²	178	NEN-EN 1991-1-1/ Table NB.1 - 6.2
Mass modification factor of slab	-	1,35	

Table B.4: Mass of the first floor, with mass modification factor to account for the mass of the additional dead load and live load

Type of load	Unit	Value	Reference
Mass concrete floor	kg/m³	2500	
thickness floor	m	0,231	Example value, depending on the geometry
mass per area	kg/m²	577,5	
Mass additional permanent load	kg/m²	168	See Table B.1 Appendix B
Mass variable live load	kg/m²	178	NEN-EN 1991-1-1/ Table NB.1 - 6.2
Mass of roof structure	kg/m²	332	Example value, depending on geometry
Mass modification factor of slab	-	1,52	

Table B.5: Mass of the second floor, with mass modification factor to account for the mass of the roof, the additional dead load and the live load

C. Response spectrum calculation

Horizontal elastic response spectrum

The horizontal elastic response spectrum is defined by the following formulas according to NPR 9998:2018:

$$0 \leq T \leq T_B : S_e(T) = a_{g;d} \times \left[1 + \frac{T}{T_B} \times (\eta \times p - 1)\right] \tag{C.1}$$

$$T_B \leq T \leq T_C : S_e(T) = a_{g;d} \times \eta \times p \tag{C.2}$$

$$T_B \leq T \leq T_C : S_e(T) = a_{g;d} \times \eta \times p \times \left[\frac{T_C}{T}\right] \tag{C.3}$$

$$T_D \leq T \leq 4 : S_e(T) = a_{g;d} \times \eta \times p \times \left[\frac{T_C \times T_D}{T^2}\right] \tag{C.4}$$

Where:

$S_e(T)$	elastic response spectrum, in g;
T	is the vibration period of a linear single degree of freedom system, in s;
$a_{g;d}$	is the value of the peak ground acceleration at surface level, including the soil factor, in g;
T_B	is the lower limit of the periods for which the spectral acceleration is constant, in s;
T_C	is the upper limit of the periods for which the spectral acceleration is constant, in s;
T_D	is the period that indicates the start of the constant displacement response of the spectrum, in s;
p	is the ratio between the peak ground acceleration and the platform value of the elastic response spectrum;
η	is the dimensionless damping correction factor with a reference value of $\eta = 1$ for 5 % viscous damping.

The values for the parameters given, follow from the NPR 9998-webtool.

Design spectrum for analysis of ductile constructions

The design spectrum $S_d(T)$ is defined by the following formulas according to NPR 9998:2018:

$$0 \leq T \leq T_B : S_d(T) = a_{g;d} \times \left[1 + \frac{T}{T_B} \times \left(\frac{p}{q} - 1\right)\right] \tag{C.5}$$

$$T_B \leq T \leq T_C : S_d(T) = a_{g;d} \times \frac{p}{q} \tag{C.6}$$

$$T_B \leq T \leq T_C : S_d(T) = a_{g;d} \times \frac{p}{q} \times \left[\frac{T_C}{T}\right] \tag{C.7}$$

$$T_D \leq T \leq 4 : S_d(T) = a_{g;d} \times \frac{p}{q} \times \left[\frac{T_C \times T_D}{T^2}\right] \tag{C.8}$$

Where:

$S_d(T)$	design spectrum, in m/s^2;
T	is the vibration period of a linear single degree of freedom system, in s;
$a_{g;d}$	is the value of the peak ground acceleration at surface level, including the soil factor, in g;
T_B	is the lower limit of the periods for which the spectral acceleration is constant, in s;
T_C	is the upper limit of the periods for which the spectral acceleration is constant, in s;
T_D	is the period that indicates the start of the constant displacement response of the spectrum, in s;
p	is the ratio between the peak ground acceleration and the platform value of the elastic response spectrum;
q	is the behaviour factor.

The values for the parameters given, follow from the NPR 9998-webtool. The behaviour factor q may have been determined using a push-over analysis or by using the provisions of Sections 5 to 9 of the NPR. In order to analyse the NC limit state, the values for q from Sections 5 to 9 of this NPR may have been multiplied by 1,33.

Damping correction factor

The value of the damping correction factor has a reference value of $\eta = 1$ for 5% viscous damping and can be amended for other damping values using the following expression:

$$\eta = \sqrt{\frac{7}{2+\xi}} \geq 0,55 \tag{C.9}$$

Where:

ξ is the viscous damping ratio of the load bearing structure, expressed in percent.

Effective Equivalent Viscous Damping

A generic consideration of the effective viscous damping for a system is as follows:

$$\xi_{sys} = \xi_0 + \xi_{hys} + \xi_{soil} \tag{C.10}$$

Where:

ξ_0 is the inherent damping (5%);
ξ_{hys} is the hysteretic damping;
ξ_{soil} is the soil damping.

The hysteretic damping can be expressed as follows:

$$\xi_{hys} = \frac{2}{\pi} \times n_{eff} \times \frac{(1-r) \times \left(1 - \frac{1}{\mu_{sys}}\right)}{(1 - r + \mu_{sys} \times r)} \tag{C.11}$$

Where:

n_{eff} is the efficiency factor, defined as the ratio of the actual area enclosed by the hysteresis loop to that of the as
r is the post yield to initial stiffness ratio;
μ_{sys} is the global structural ductility.

Importance factor

The importance factor for primary and secundary seismic elements and for non-seismic, constructive elements for new build, reconstruction and existing buildings:

Tabel 2.4 — Importantiefactoren voor primaire en secundaire seismische elementen en voor niet-seismische, constructieve elementen voor nieuwbouw, verbouw en bestaande bouw

Soort element	Gevolgklassen en categorieën	Importantiefactor γ_I		
		Bestaande bouw	Verbouw	Nieuwbouw
Primaire en secundaire seismische elementen	CC1a	–	–	0,5
	CC1b	1,0	1,0	1,1
	CC2	1,1	1,1	1,2
	CC3 en CC4	1,2	1,2	1,3
Niet-seismische, constructieve elementen	Alle categorieën	1 [a]	1 [a]	1 [a]

[a] Elementen in categorie 4 die van relatief grote hoogte op een aangrenzend dak vallen waaronder mensen kunnen verblijven: 1,2.

Figure C.1: Table for Importance factor (Source: NPR 9998:2018)

Transformation of elastic response spectrum to ADRS-format

The elastic displacement response spectrum, $S_{De}(T)$, shall be obtained by direct transformation of the elastic acceleration response spectrum, $S_e(T)$, using the following expression:

$$S_{De}(T) = S_e(T)\left[\frac{T}{2\pi}\right]^2 \tag{C.12}$$

Where:

$S_{De}(T)$	is the elastic displacement response spectrum;
$S_e(T)$	is the elastic acceleration response spectrum;
T	is the vibration period of a linear singel degree of freedom system.

D. Transformation to equivalent SDOF system

Transformation of nonlinear pushover capacity curve to equivalent SDOF sytem

$$S_a = V^*_{cap;base} / m_{eff} \tag{D.1}$$

$$S_d = u^*_{roof;cap} for n \leq 4 \tag{D.2}$$

Where:

S_a	is the spectral acceleration;
S_d	is thespectral displacement;
$V^*_{cap;base}$	is the base shear capacity of the SDOF system;
m_{eff}	is the effective mass of the equivalent SDOF system;
$u^*_{roof;cap}$	is the lateral displacement capacity of the centre of mass at roof level of the SDOF sytem

Effective mass

The mass of an equivalent SDOF system m_{eff} is determined according to B.2 of NEN-EN 1998-1:

$$m_{eff} = \sum m_i \phi_i = \sum F_i \tag{D.3}$$

Where:

m_i	is the mass in the i-th storey;
ϕ_i	is the normalised displacement, which depends on the chosen loadpattern (normalised so that:$\phi_n = 1$).

Base shear capacity and roof displacement of the SDOF system

The base shear capacity $V^*_{cap;base}$ and the roof displacement $u^*_{roof;cap}$ are calculated as follows:

$$V^*_{cap;base} = \frac{V_{cap;base}}{\Gamma} \tag{D.4}$$

$$u^*_{roof;cap} = \frac{u_{roof;cap}}{\Gamma} \tag{D.5}$$

Where:

$V_{cap;base}$	is the base shear capacity of the MDOF system;
$u_{roof;cap}$	is the lateral displacement of the centre of mas at roof level of the MDOF system;
Γ	is the transformation factor ;

Transformation factor

They both depend on the transformation factor of the MDOF sytem according to B.2 of NEN-EN 1998-1:

$$\Gamma = \frac{m_{eff}}{\sum m_i \Phi_i^2} = \frac{\sum F_i}{\sum \left(\frac{F_i^2}{m_i} \right)} \tag{D.6}$$

According to NPR 9998:2018 G.4.3 (3), the transformation factor Γ can be taken as 1 ($\Gamma = 1$)for buildings with up to two storeys with an attic on top of it.

E. Pier failure mechanisms

Failure mechanisms for piers or walls in-plane are defined according to Annex G of the NPR 9998:2018.

Shear sliding failure (G.9.2.2)

$$V_R = l_c \times t_{pier} \times \left(f_{ma;v0;m} + \mu_{ma;m} \times \sigma_y\right) \tag{E.1}$$

and

$$V_R \leq 0,1 \times f_b \times t_{pier} \tag{E.2}$$

Where:

V_R is the capacity of an unreinforced pier or wall, based on shear sliding mechanism;
l_c is the length of the compressed part of the pier or wall;
t_{pier} is the thickness of the pier or wall;
$f_{ma;v;0;m}$ is the initial average shear strength of the masonry;
$\mu_{ma;m}$ is the average coefficient of friction for masonry;
σ_y is the average compressive stress in the compressed part of the cross section, $(= F(l_c \times t_{pier}))$;
f_b is the normalised compressive strength of the masonry units, in the direction of the applied action effect.

The upper limit for the shear sliding, $(0,1 f_b \times l_c \times t_{pier})$, takes into account the possibility of collapse due to shear stress occurring in the pressure zone. Resulting in diagonal cracks in the masonry units.

Length compression zone

The length of the compression zone l_c for rectangular sections can be determined by the following formula:

$$l_c = 3\left[\frac{l_{pier}}{2} - \frac{M}{F}\right] \tag{E.3}$$

Where:

M is the moment in the section;
F is the axial force on the pier or wall.

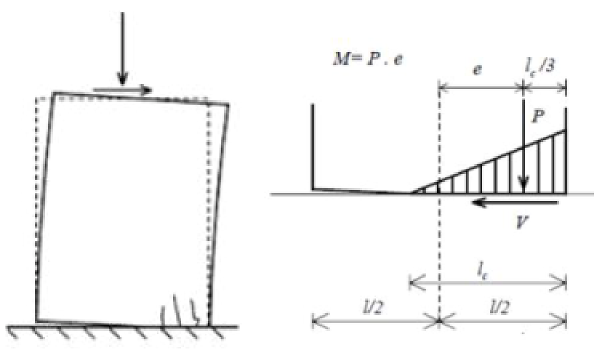

Figure E.1: Schematisation of forces acting on wall/pier for determining the length of the compression zone

Force-deformation relationship

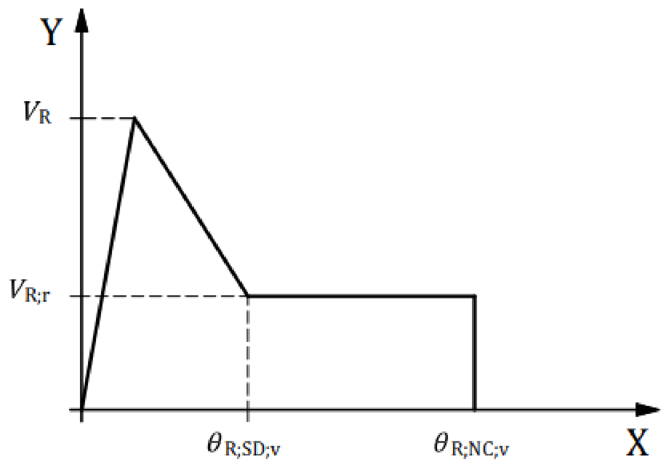

Figure E.2: Generalised force/deformation relationship for unreinforced masonry walls or piers governed by shear sliding (Source: NPR 9998:2018

Where:

- V_R is the capacity of an unreinforced pier or wall, based on shear sliding mechanism;
- $V_{R;r}$ is the residual shear sliding capacity;
- $\theta_{R;SD;v}$ is the drift limit for shear sliding of unreinforced masonry piers or walls when reaching Significant Damage limit state
- $\theta_{R;NC;v}$ is the drift limit for shear sliding of unreinforced masonry piers or walls when reaching Near Collapse limit state.

When formula (E.1) is governing, the lateral drift limit for the SD limit state $\theta_{R;SD;v}$ is equal to 0,003 and the drift limit for the NC limit state $\theta_{R;NC;v}$ is equal to 0,0075.

When formula (E.2) is governing the drift limits are based on the drift limits of the rocking failure mechanism, see formula (E.5).

The residual shear sliding capacity, $V_{R;r}$, of the pier or wall can be found by setting $f_{ma;v;0;m}$ in formula (E.1) to 0 MPa, so only the friction component remains.

Flexure failure

Flexure failure incorporates both toe crushing and rocking failure. The capacity of the pier when rocking is determined by the following formula:

$$V_{R;f} = F \times \left(\frac{l_{pier}}{2h_0}\right) \times \left(1 - 1,15\frac{\sigma_y}{f_{ma;m}}\right) \tag{E.4}$$

Where:

- $V_{R;f}$ is the rocking capacity of an unreinforced pier or wall, based on flexural strength;
- F is the imposed axial load combined with the dead load in the critical section of the pier or wall;
- l_{pier} is the horizontal in-plane dimension of the wall, or width of the pier;
- h_0 distance between the cross-section where the shear bearing capacity has been reached and the point of in
- σ_y is the average compressive stress in the full the cross section, $(= F(l_{pier} \times t_{pier})$;
- $f_{ma;m}$ is the average compressive strength of masonry, in the vertical direction.

Rocking drift limit

The rocking drift limit for the NC limit state is the result of calibration of available, relevant test results of masonry piers used in Groningen [45] and [46]. The difference in static and dynamic behaviour has been taken into account. Calibration of shaking table results has been performed and full finite element calculations were made to gain insight into the behaviour. In addition, short-term effects have been taken into consideration.

The flexural drift limit of a pier is determined by the following formula:

$$\theta_{R;NC;f} = 0,0135\left(1 - 2,6 \times \frac{\sigma_y}{f_{ma;m}}\right) \times \left(\frac{h_{ref}}{h_{pier}}\right) \times \sqrt{\frac{h_{pier}}{l_{pier}}} \tag{E.5}$$

Where:

$\theta_{R;NC;f}$	is the drift limit of the flexural strength during rocking when reaching the NC limit state;
σ_y	is the average compressive stress in the full the cross section, $(= F(l_{pier} \times t_{pier}))$;
$f_{ma;m}$	is the average compressive strength of masonry, in the vertical direction;
h_{pier}	is height of the pier or wall;
h_{ref}	is reference height of the pier or wall (=2,4 m);
l_{pier}	is the length of the pier or wall;
t_{pier}	is the thickness of the pier or wall.

F. Spandrel failure mechanisms

The in-plane failure mechanisms for spandrels are defined according to Annex G of the NPR 9998:2018.

Force-deformation relationship

The recommended generalised force-deformation relationship for URM spandrels is illustrated in Figure F.1. The relationship is based on results of experimental research from [66, 67, 68, 69]

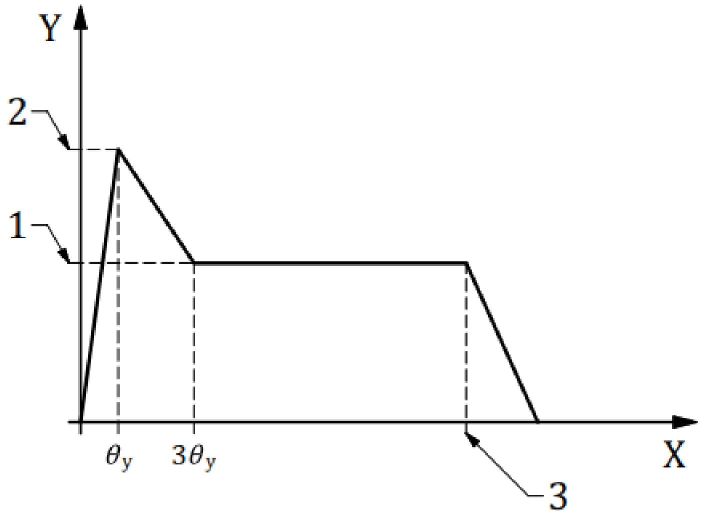

Figure F.1: Generalised force-deformation relationship for URM spandrels

Legend

1	$V_{s,fl,r}$ when $V_{s,fl} \leq V_s$
	$V_{s,r}$ when $V_{s,fl} > V_s$
2	$\min(V_{s,fl}; V_s)$
3	0,03 for rectangular spandrel
	0,0015 for curved spandrel
V_s	is the peak shear capacity of a rectangular unreinforced masonry spandrel;
$V_{s,r}$	is the residual shear capacity of a rectangular unreinforced masonry spandrel;
$V_{s,fl}$	is the peak flexural capacity of a rectangular unreinforced masonry spandrel;
$V_{s,fl,r}$	is the residual flexural capacity of a rectangular unreinforced masonry spandrel;
θ_y	is the chord rotation of the spandrel, relative to the piers.

All parameters that describe the force deformation relationship of the spandrels are discussed below.

Peak shear strength

Peak shear strength of rectangular URM spandrels can be estimated using one of the following formulas:

$$V_{s1} = \frac{2}{3}\left(f_{ma;b;per} + \mu_{ma;m} \times \sigma_{sp}\right) \times h_{sp} \times b_{sp} \tag{F.1}$$

$$V_{s2} = f_{ma;dt;m} \times \beta_{sp}\left(\sqrt{1 + \frac{\sigma_{sp}}{f_{ma;dt;m}}}\right) \times h_{sp} \times b_{sp} \tag{F.2}$$

Where:

V_s	is the peak shear capacity of a rectangular unreinforced masonry spandrel;
$f_{ma;b;per}$	is the cohesion of the bed-joint of the masonry;
$\mu_{ma;m}$	is the friction coefficient of masonry;
σ_{sp}	is the axial stress in the spandrel;
h_{sp}	is the height of the spandrel;
b_{sp}	is the width of the spandrel;
$f_{ma;dt;m}$	is the average diagonal tension strength of masonry;
β_{sp}	is the spandrel aspect ratio, see Table F.1.

Spandrel aspact ratio

The value for the spandrel aspect ratio, β_{sp}, are taken from Table F.1.

Criteria	β_{sp}
Slender spandrel where $l_{sp}/h_{sp} > 1,5$	0,67
Compact spandrel where $l_{sp}/h_{sp} < 1,0$	1,00
Linear interpolation is allowed for intermediate values of l_{sp}/h_{sp}	

Table F.1: Shear stress factor, β_{sp}, for diagonal tensile capacity

Residual shear strength

According to the NZSEE 2015 based on research of [70], the residual shear strength of cracked rectangular URM spandrels with timber lintels can be estimated with formula (F.3). When no timber lintel is present the residual shear capacity of spandrels is negligible.

$$V_{s,r} = \frac{11}{16}\sigma_{sp}\frac{{h_{sp}}^2 b_{sp}}{l_s p} \tag{F.3}$$

Where:

$V_{s,r}$	is the residual shear capacity of a rectangular unreinforced masonry spandrel;
l_{sp}	is the clear length of spandrel between adjacent wall piers.

Peak flexural strength

The peak flexural capacity of rectangular spandrels can be approximated by the following formula:

$$V_{s,fl} = \left(f_t + \sigma_{sp}\right)\frac{{h_{sp}}^2 \times b_{sp}}{3 \times l_s p} \tag{F.4}$$

Where:

$V_{s,fl}$	is the peak flexural capacity of a rectangular unreinforced masonry spandrel;
f_t	is the equivalent tensile strength of masonry spandrel.

The equivalent tensile strength of a URM spandrel, can be approximated by the following formula:

$$f_t = 1,3\left(f_{ma;b;per} + 0,5 \times \mu_{ma;m} \times \sigma_{v;m}\right) + \frac{f_{m;b;per}}{2\mu_{ma;m}} \tag{F.5}$$

Where:

$\sigma_{v;m}$ is the mean axial stress due to superimposed and dead load in the adjacent wall piers.

Residual flexural strength

The residual flexural strength of rectangular URM spandrels can be determined with the following formula:

$$V_{s,fl,r} = \frac{\sigma_{sp} \times {h_{sp}}^2 \times b_{sp}}{l_s p}\left(1 - \frac{\sigma_{sp}}{0,85 \times f_{h;m}}\right) \leq V_s \tag{F.6}$$

With :

$$f_{h;m} = 0,5 f'_{ma;m} \tag{F.7}$$

Where:

$V_{s,fl,r}$	is the residual flexural capacity of a rectangular unreinforced masonry spandrel;
$f_{h;m}$	is the compression strength of the masonry in the horizontal direction ;
$f'_{ma;m}$	is the masonry compression strength.

The upper limit for the axial stress in the spandrel, σ_{sp}, can be determined using the following formula:

$$\sigma_{sp} = \left(1 + \beta_{sp}\right) \times f_{ma;dt;m} \times \frac{l_{sp}}{\sqrt{{l_{sp}}^2 + {h_{sp}}^2}} \tag{F.8}$$

In most situation it can be assumed the axial confinement of typical unreinforced buildings is negligible. The residual flexural strength can in that case be assummed as zero.

G. ETABS input data

Wall properties

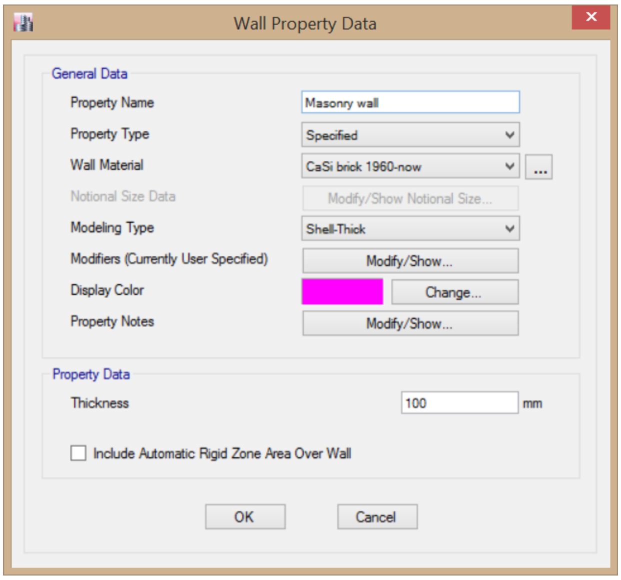

Figure G.1: Property data of a masonry wall, modelled as Shell-Thick element

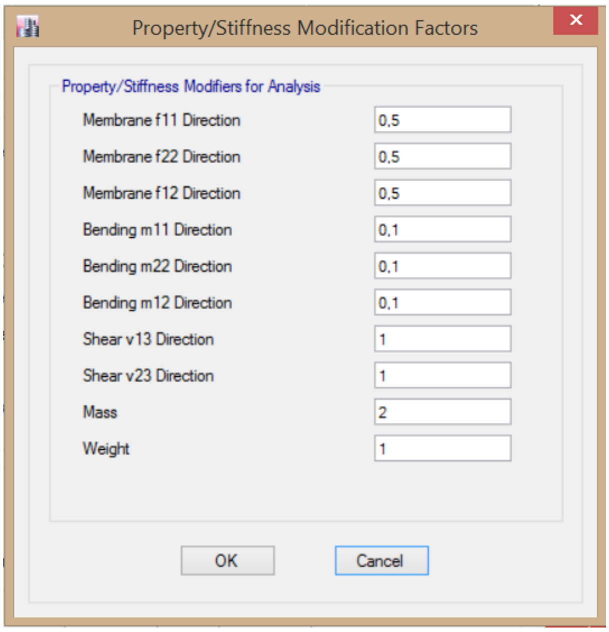

Figure G.2: Property modifiers for the masonry wall to account for cracking and the reduction of load carried in the out-of-plane direction

Floor properties

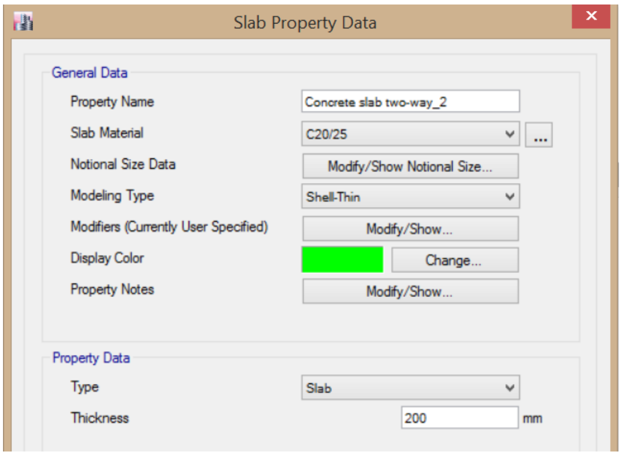

Figure G.3: Property data of a floor modelled with shell elements, to determine the load distribution of the floor onto the walls

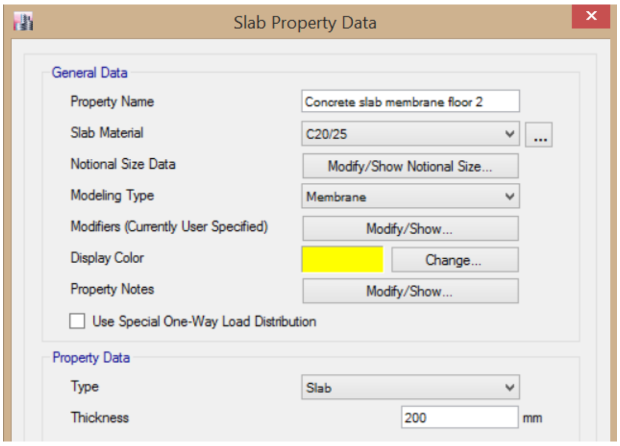

Figure G.4: Property data of a floor modelled with membrane elements, which is used to perform the pushover analysis

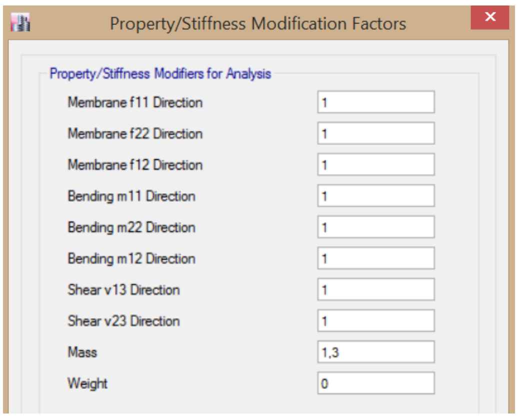

Figure G.5: Property modifiers for a floor modelled with membranes

Gap link properties

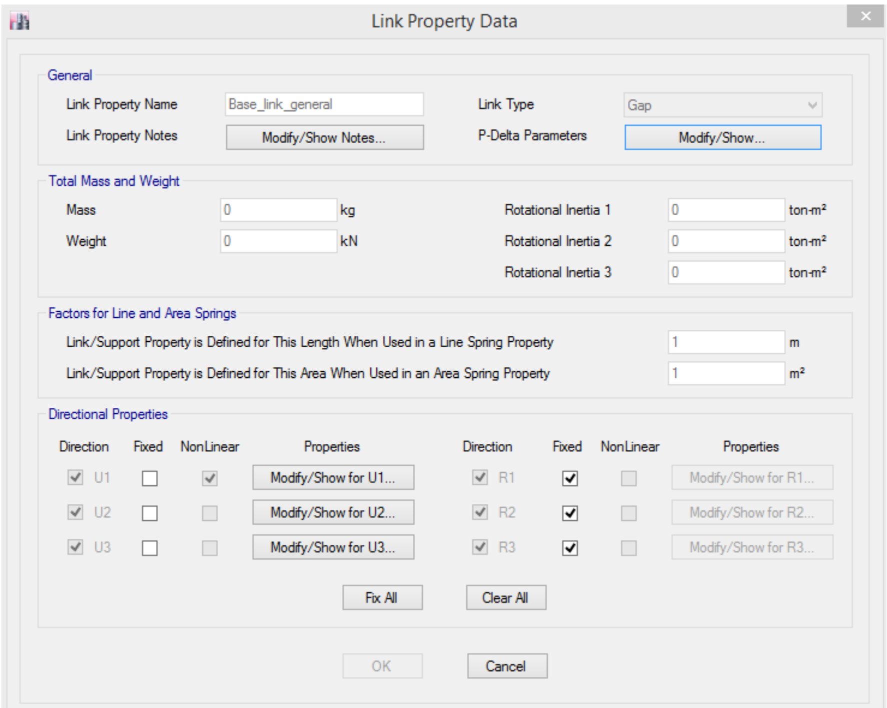

Figure G.6: Property data for a gap link element at base level

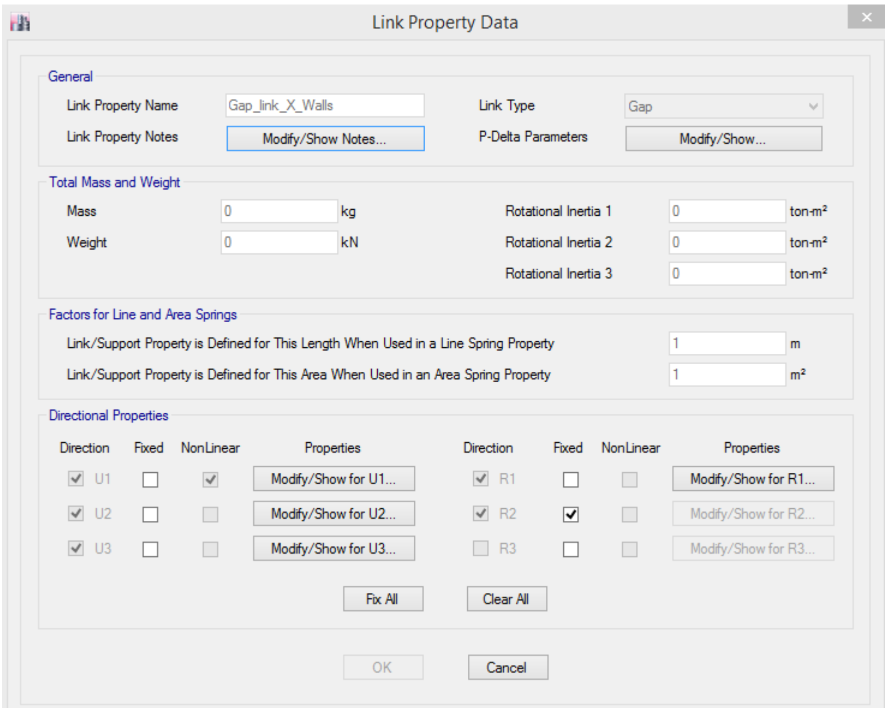

Figure G.7: Property data for a gap link element at pier ends

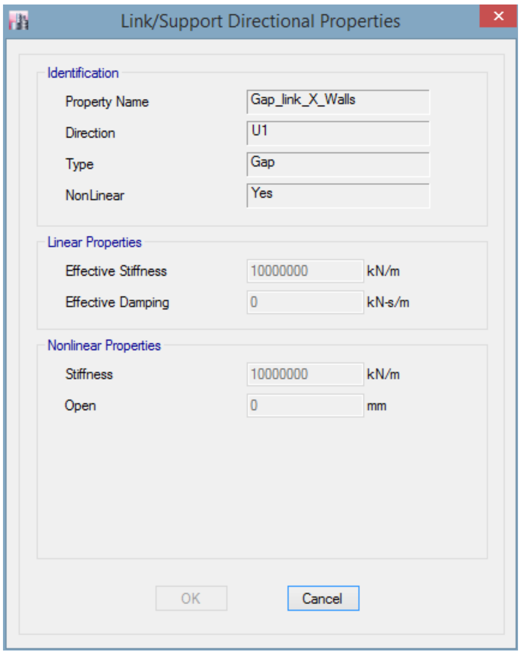

Figure G.8: Non linear property data for a gap link element at pier ends

Non-linear shear link properties piers and spandrels

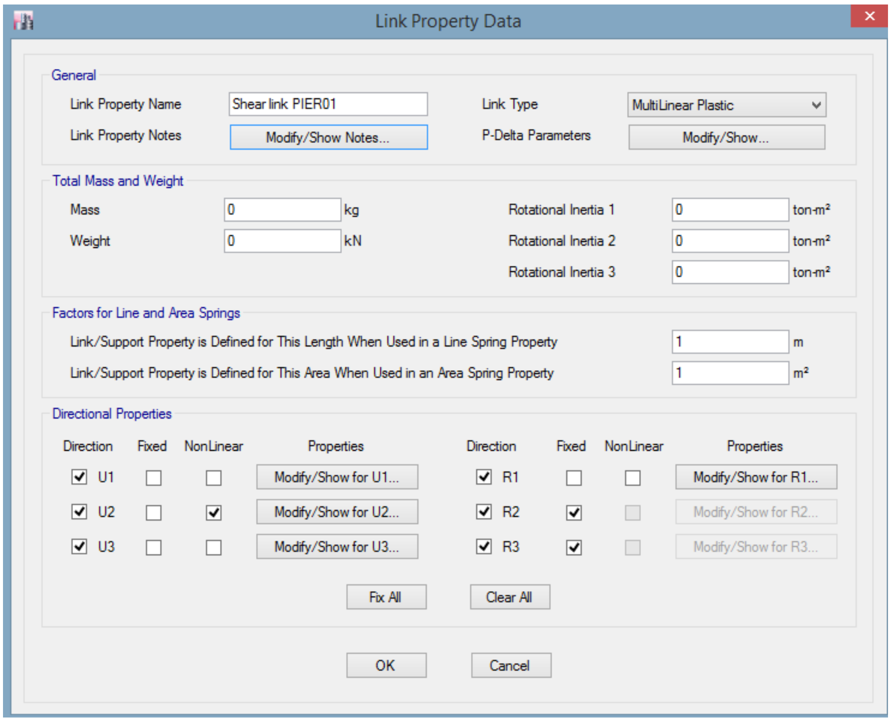

Figure G.9: Property data for MuliLinear Plastic link when used to model non-linear shear deformations in piers

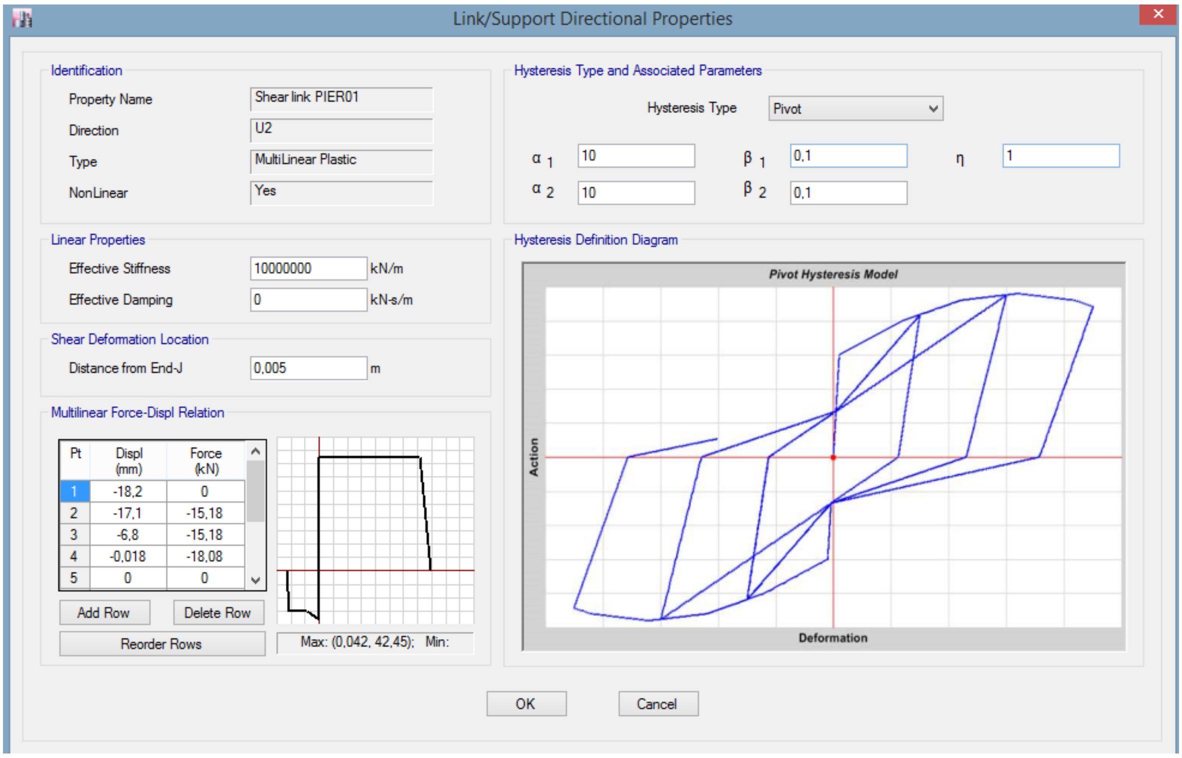

Figure G.10: Non-linear property data for MuliLinear Plastic link when used to model nonlinear shear deformations in piers

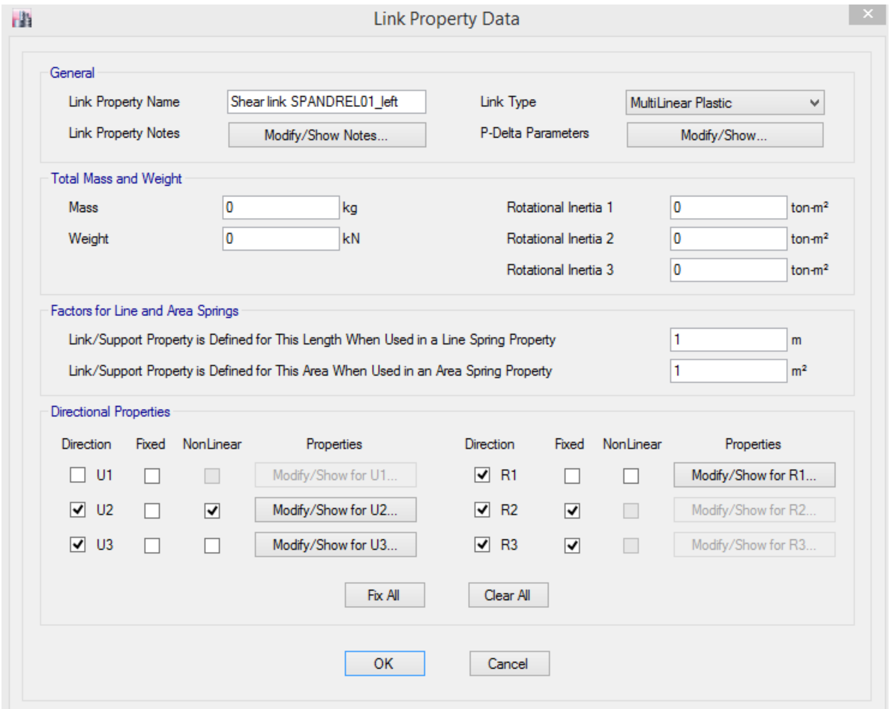

Figure G.11: Property data for MuliLinear Plastic link when used to model non-linear shear deformations in spandrels

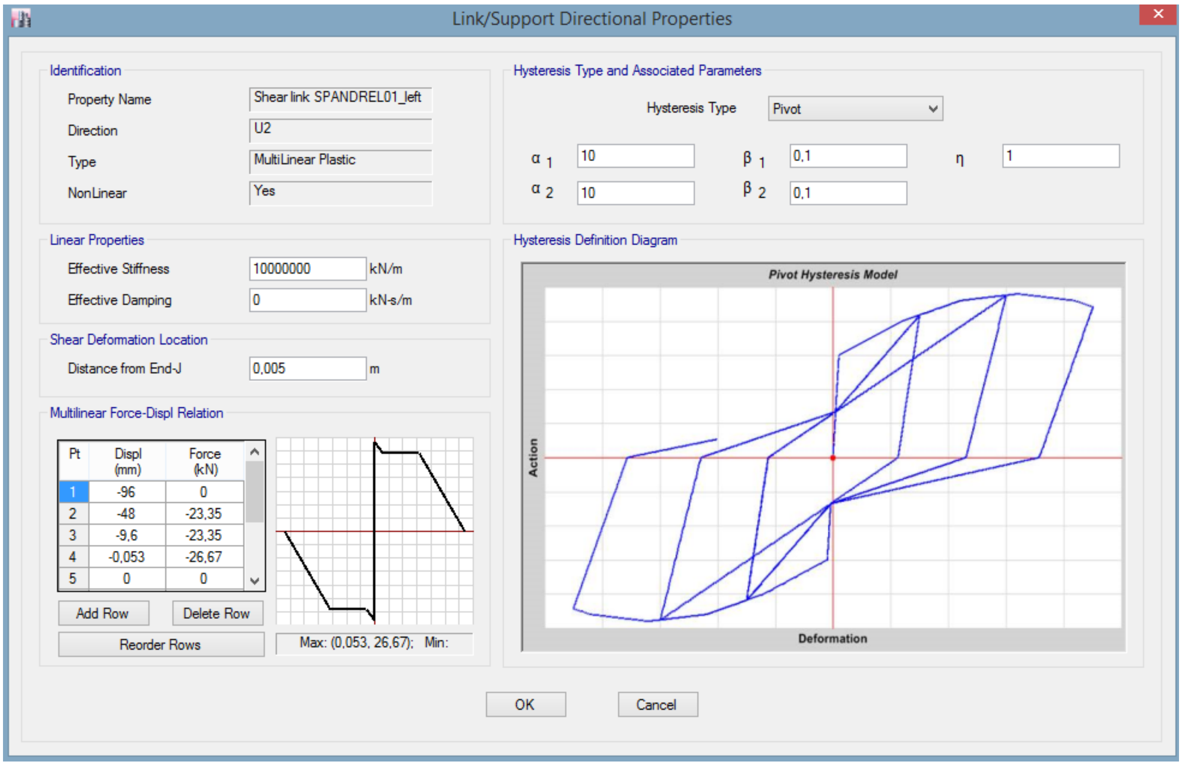

Figure G.12: Non-linear property data for MuliLinear Plastic link when used to model nonlinear shear deformations in piers

Shear free properties pier and spandrel

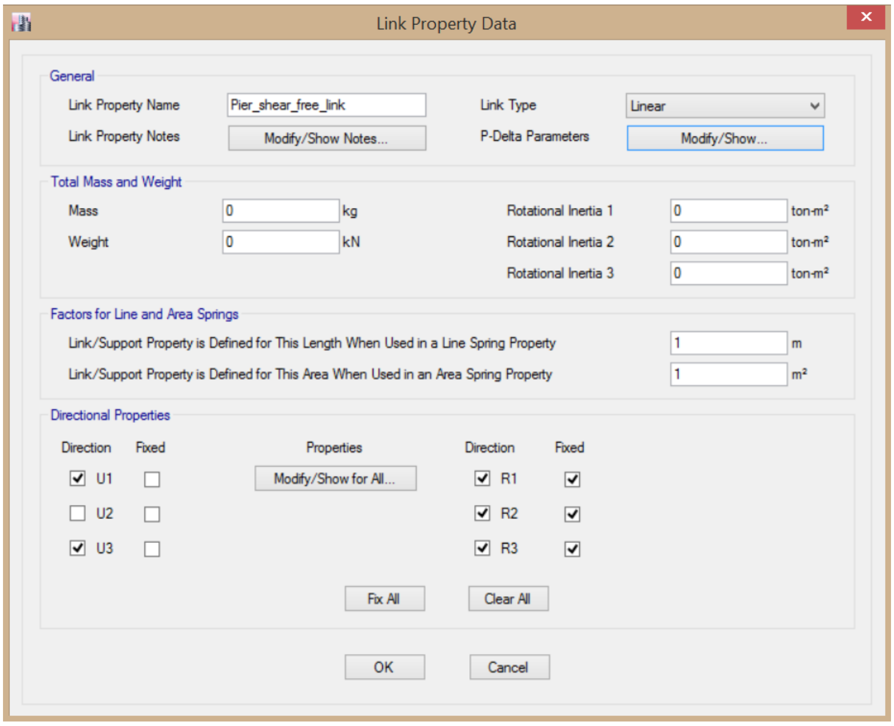

Figure G.13: Property data for Linear 'shear free' link when used to transfer wall overturning actions for pier elements

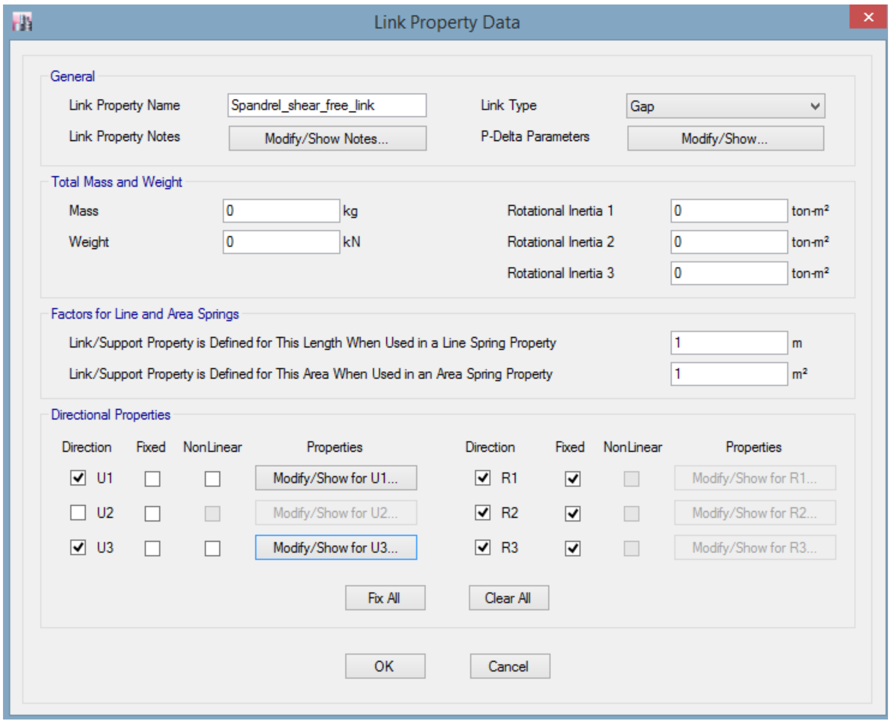

Figure G.14: Property data for Linear 'shear free' link when used to transferchord forces for spandrel elements

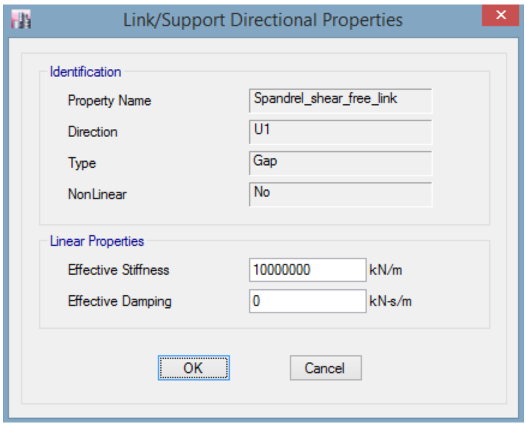

Figure G.15: Value for stiffness in U1 direction

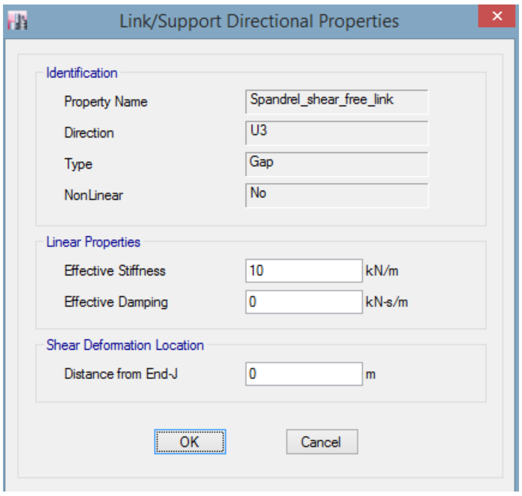

Figure G.16: Value for stiffness in U3 direction

Shear connector properties

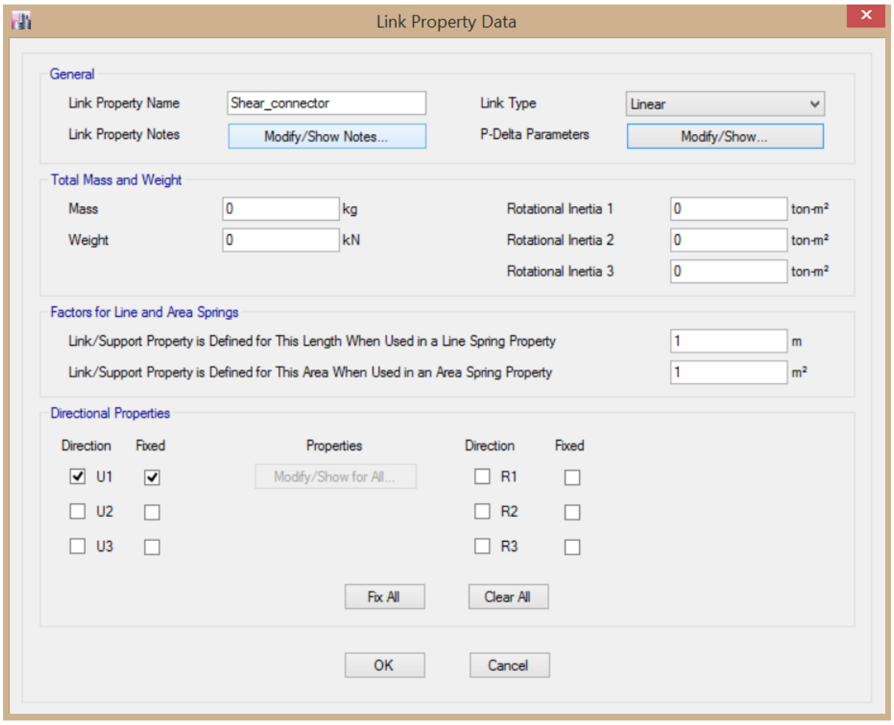

Figure G.17: Property data for Linear link when used to model connector elements in wall elements

Linear link properties

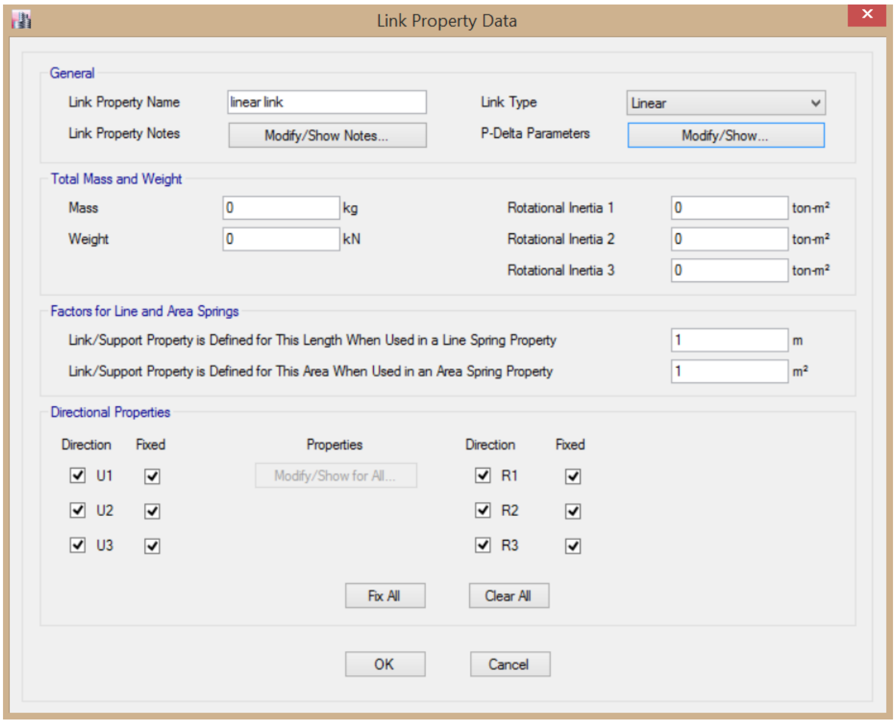

Figure G.18: Property data for Linear link when used to model a rigid connection

Flange link properties

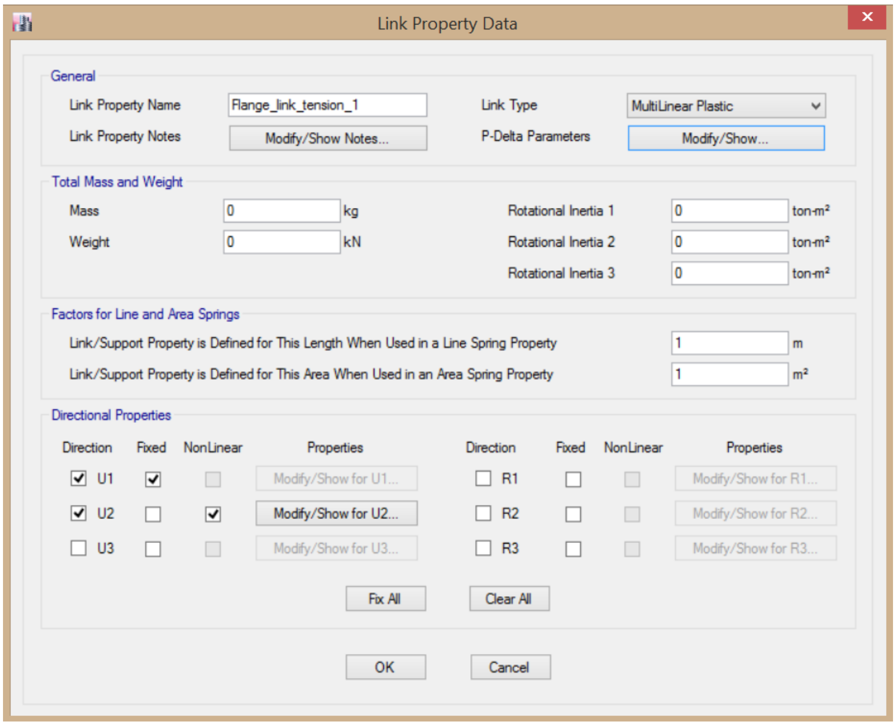

Figure G.19: Property data for MuliLinear Plastic link when used to model tension flange loads

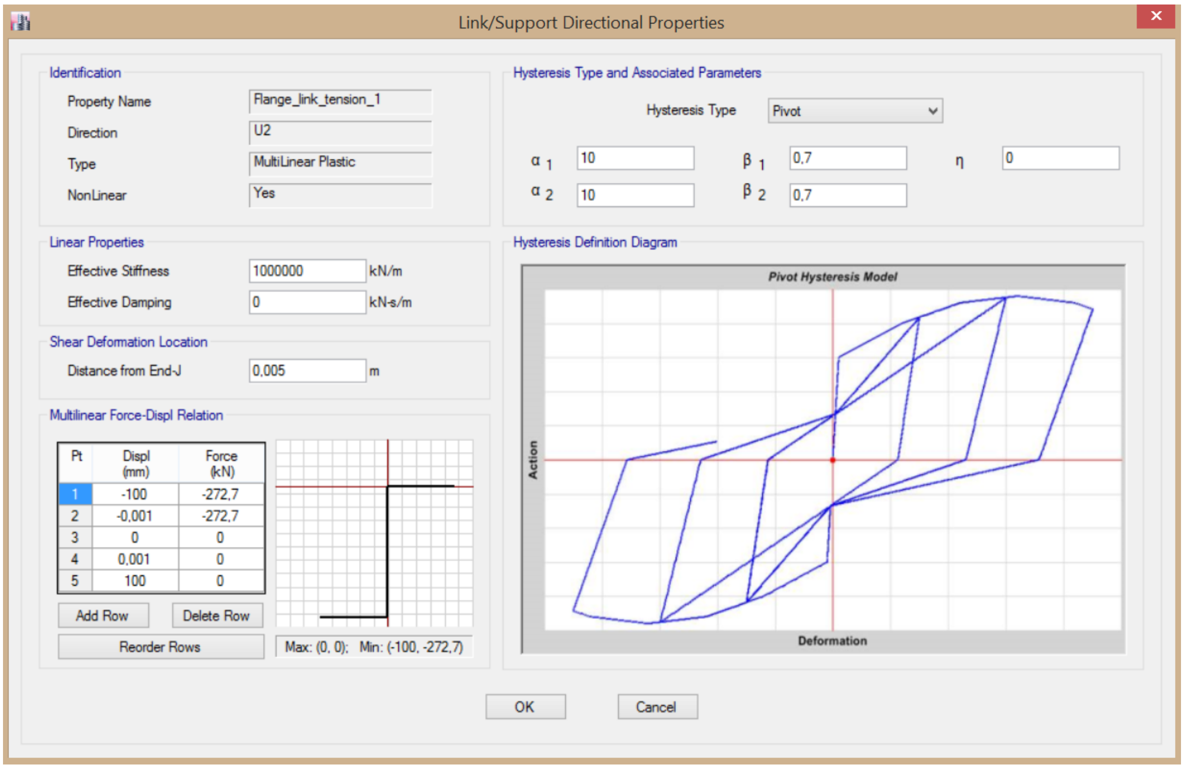

Figure G.20: Non-linear property data for MuliLinear Plastic link when used to model tension flange load on the first floor

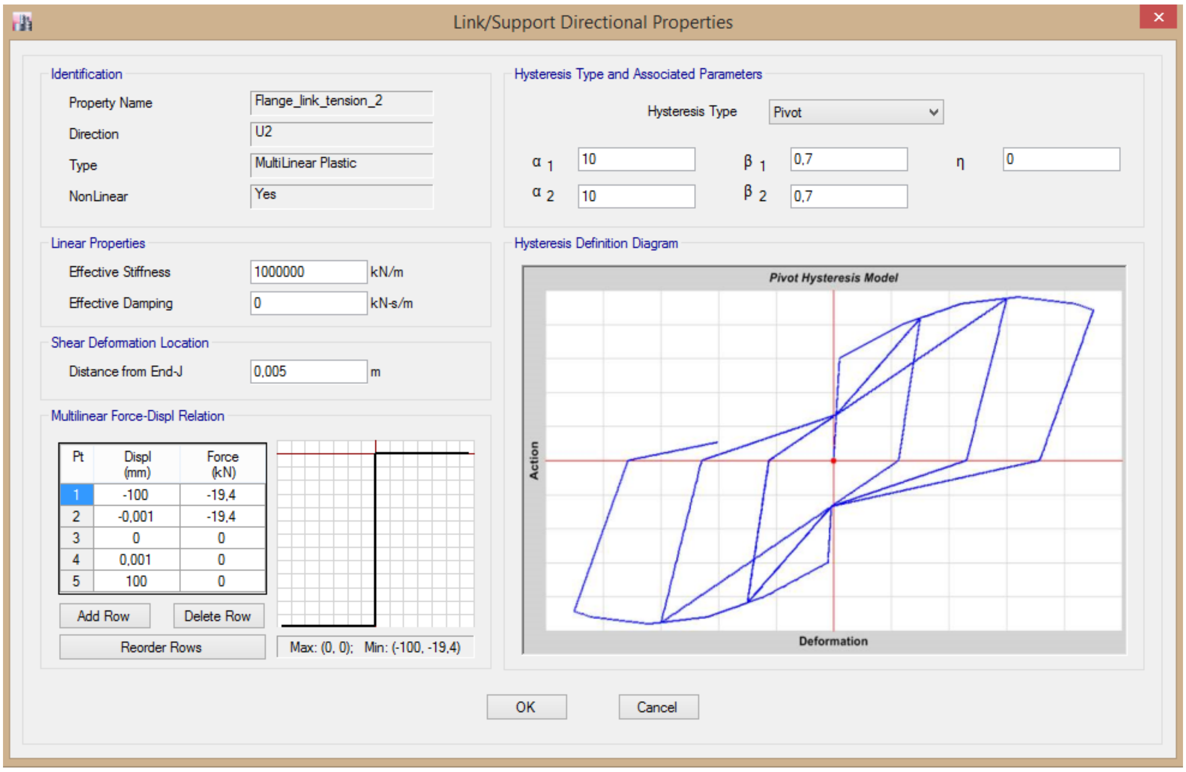

Figure G.21: Non-linear property data for MuliLinear Plastic link when used to model tension flange load on the second floor

Load case set-up

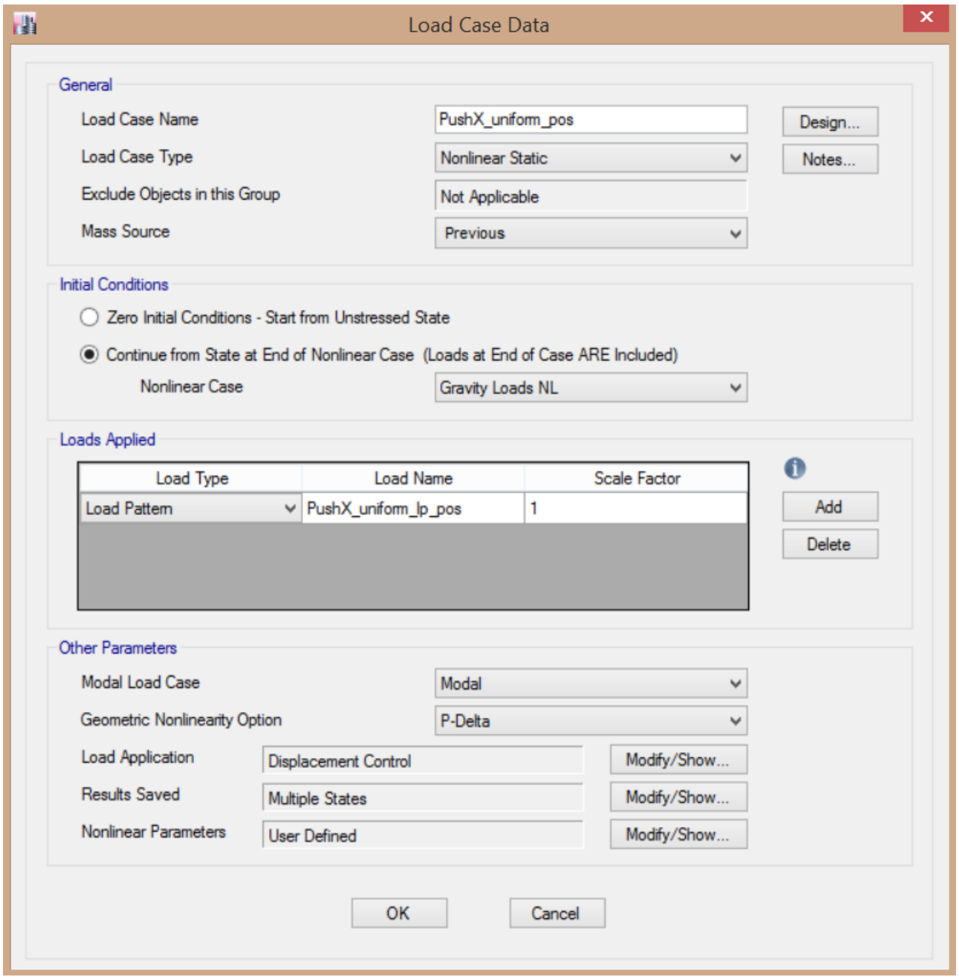

Figure G.22: Input for the data of Load Case

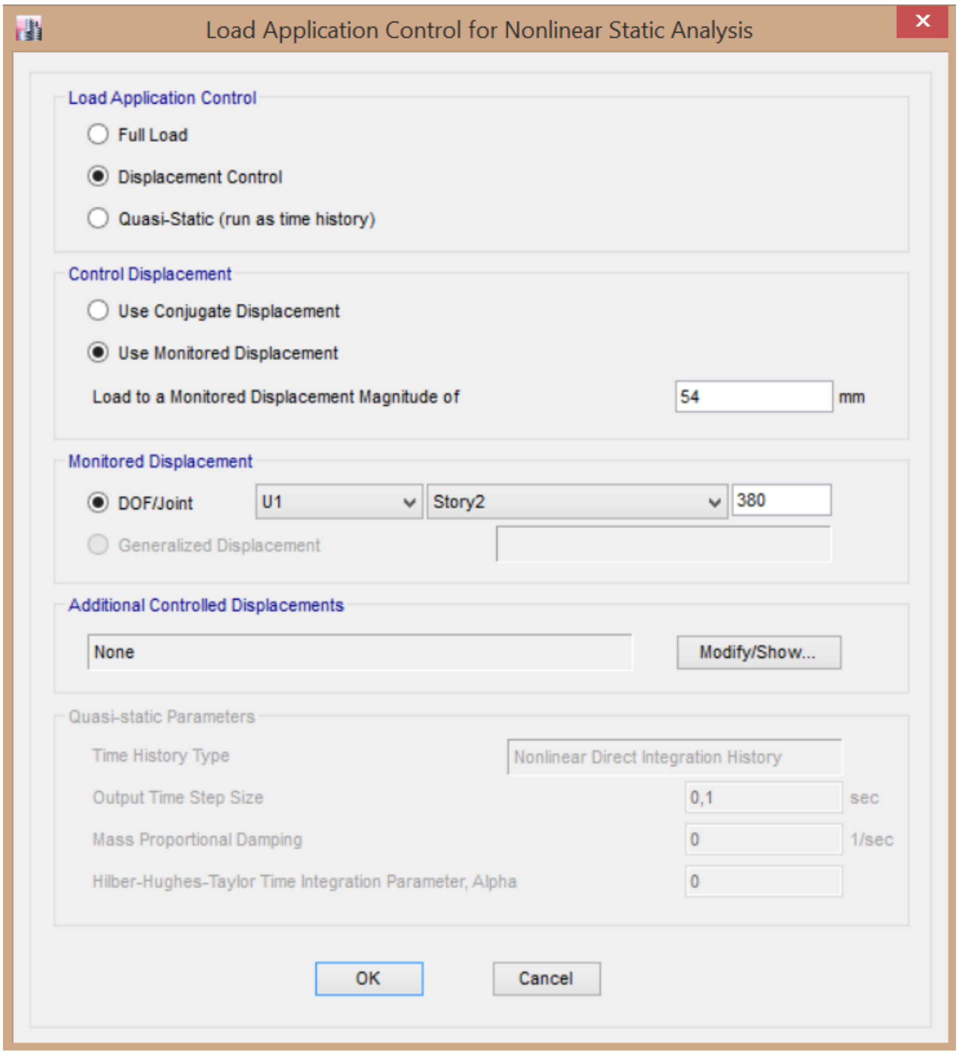

Figure G.23: Input for the Load Application Control for Nonlinear Static Analysis

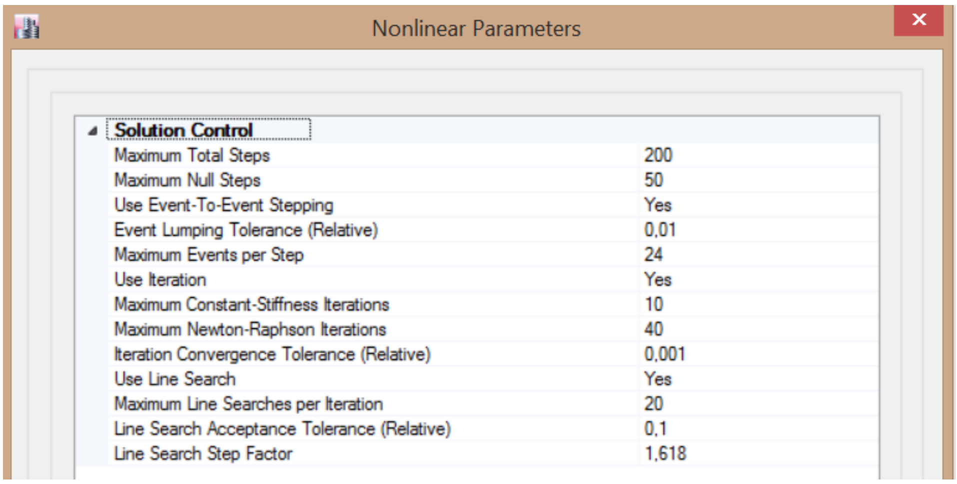

Figure G.24: Input for the non-linear parameters for the solution control

H. Validation of ETABS model

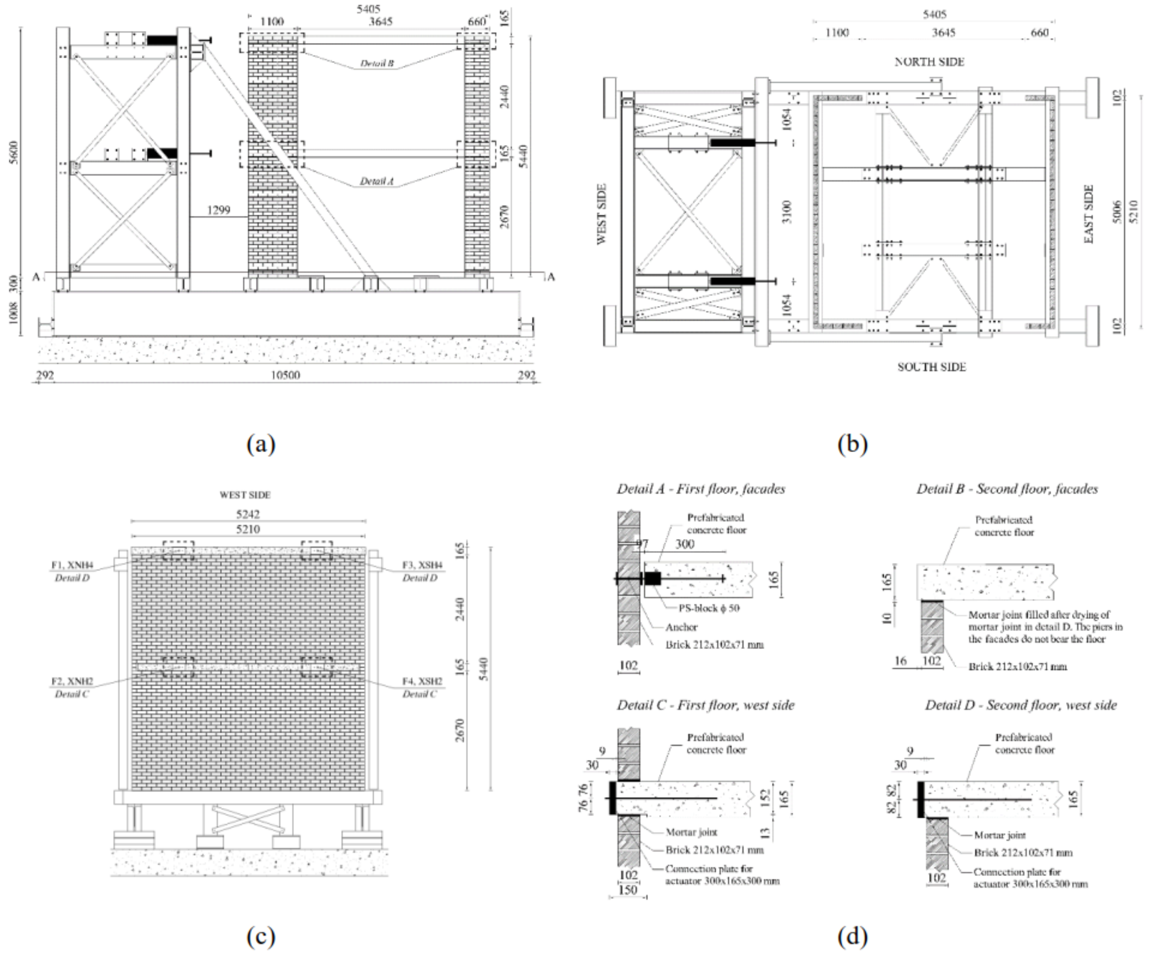

Figure H.1: Set-up and dimensions of the tested specimen of masonry bricks: (a) Front view (southern side); (b) Top view of ground floor in section A-A; (c) Side view (western side); (d) Construction details (Source:[17]

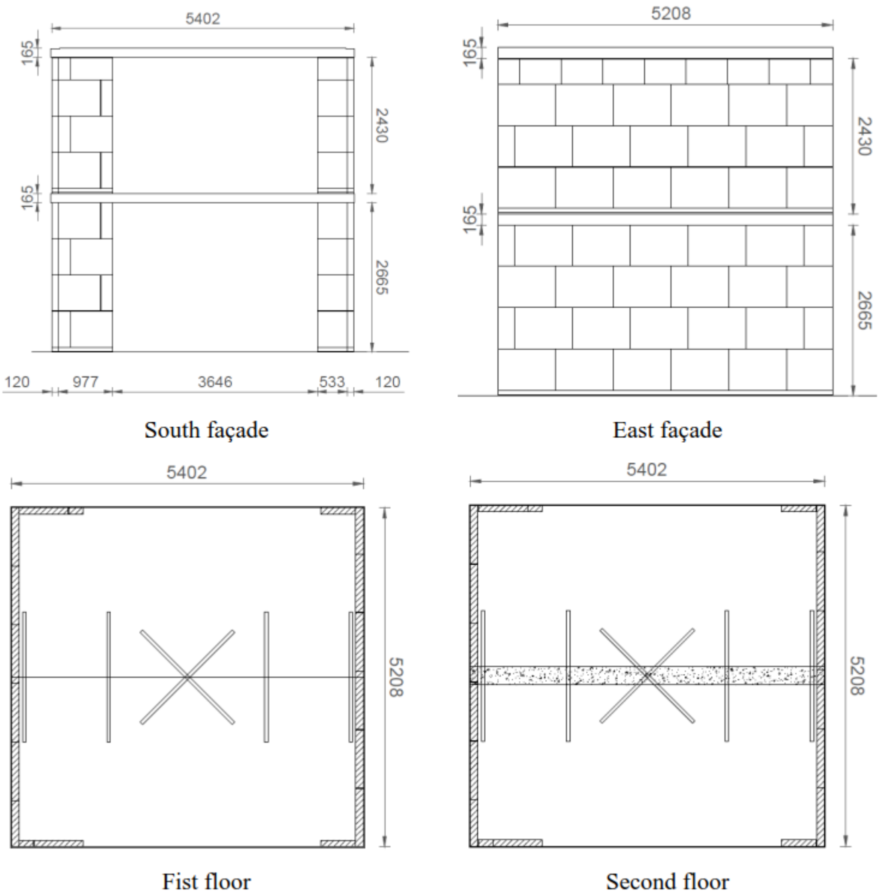

Figure H.2: Dimensions of the tested specimen of calcium silicate masonry elements (Source:[28]

Material property	Symbol	Unit	CS brick		CS element	
			Average	C.o.V.	Average	C.o.V.
Compressive strength of mortar	f_m	MPa	7.27	0.14	16.10	0.09
Compressive strength of masonry unit	f_b	MPa	13.26	0.13	19.50	0.06
Compressive strength of masonry perpendicular to the bed joints	f'_m	MPa	6.01	0.09	13.93	0.07
Compressive strength of masonry parallel to the bed joints	$f'_{m,h}$	MPa	7.55	0.02	9.42	0.17
Elastic modulus of masonry in the direction perpendicular to bed joints	E	MPa	3339	0.25	8001	0.12
Elastic modulus of masonry in the direction parallel to the bed joints	E_h	MPa	2081	0.42	7400	0.13
Out-of-plane masonry flexural strength parallel to the bed joint	$f_{x,1}$	MPa	0.21	0.25	0.58	0.14
Out-of-plane masonry flexural strength perpendicular to the bed joint	$f_{x,2}$	MPa	0.76	0.47	0.73	0.04
Masonry initial shear strength of calcium silicate masonry	f_{v0}	MPa	0.12	-	0.83	-
Masonry shear friction coefficient of calcium silicate masonry	μ	-	0.49	-	1.49	-

Figure H.3: Material properties of the replicated calcium silicate brick masonry for both the masonry elements and the bricks (Source:[29]

I. Element forces test model TU Delft

Axial loads in pier elements

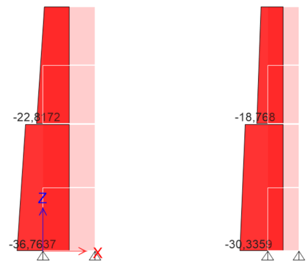

Figure I.1: Axial forces due to gravity loading of TU Delft brick model; 0 in Figure 5.19b

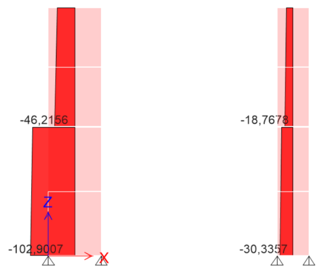

(a) Axial forces at 1 in Figure 5.19b of TU Delft brick model

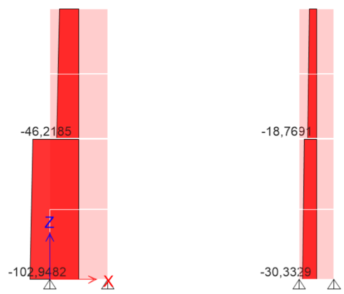

(b) Axial forces at 2 in Figure 5.19b of TU Delft brick model

Figure I.2: Axial forces of piers pushed in positive direction of TU Delft brick model

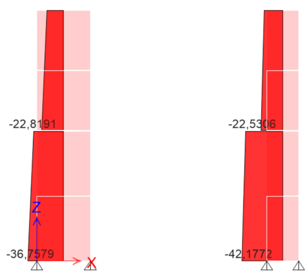

(a) Axial forces at 4 in Figure 5.19b of TU Delft brick model

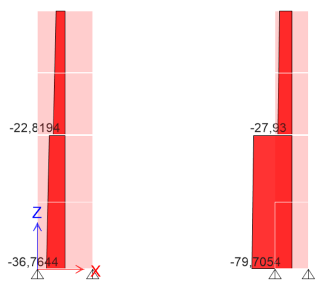

(b) Axial forces at 5 in Figure 5.19b of TU Delft brick model

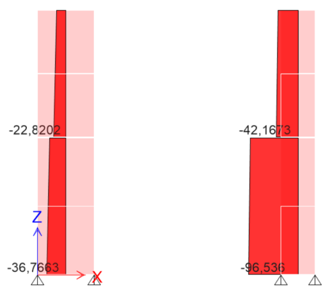

(c) Axial forces at ultimate negative capacity in Figure 5.19b of TU Delft brick model

Figure I.3: Axial forces of piers pushed in negative direction of TU Delft brick model

Reaction forces pier elements

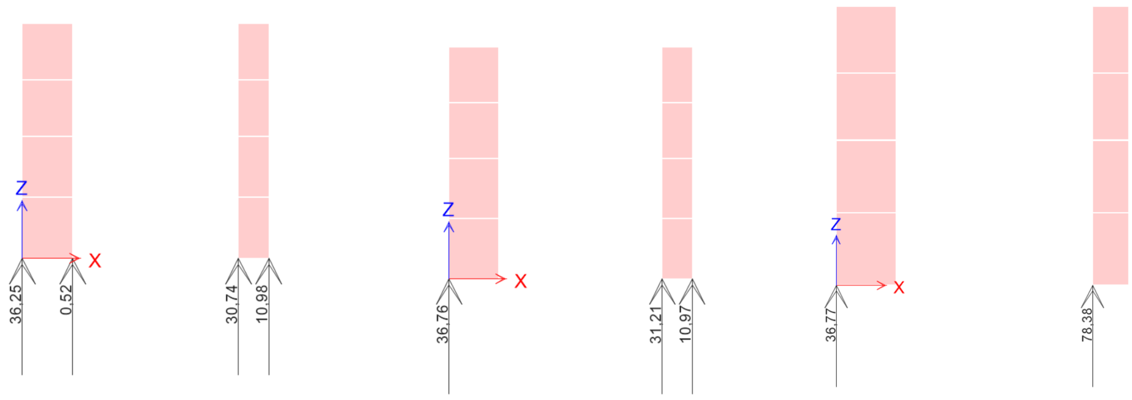

(a) Reaction forces before 4 in Figure 5.19b of TU Delft brick model; just before the larger pier starts rocking

(b) Axial forces at 4 in Figure 5.19b of TU Delft brick model; larger pier starts rocking

(c) Axial forces at 5 in Figure 5.19b of TU Delft brick model; Both piers show rocking behaviour.

Figure I.4: Axial forces of piers pushed in negative direction of TU Delft brick model

Shear forces in pier elements

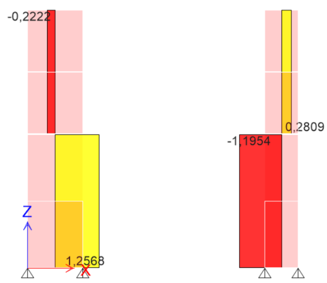

Figure I.5: Shear forces of piers due to gravity loading of TU Delft brick model

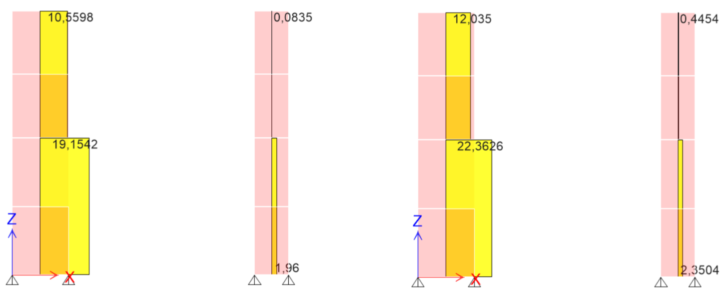

(a) Shear forces at 1 in Figure 5.19b of TU Delft brick model

(b) Shear forces at 2 in Figure 5.19b of TU Delft brick model

Figure I.6: Shear forces of piers pushed in positive direction of TU Delft brick model

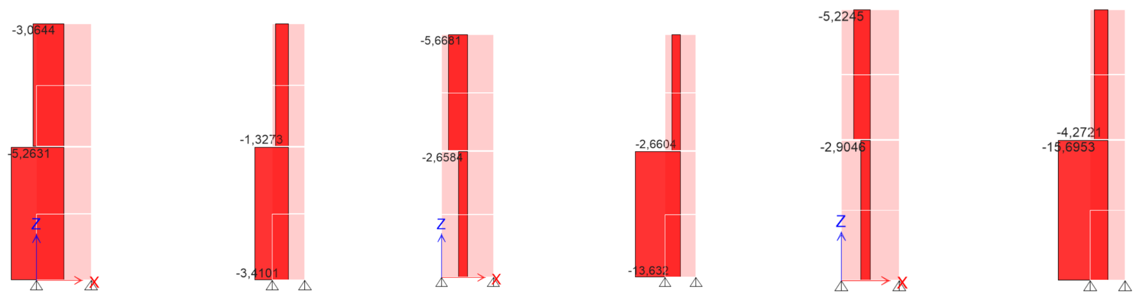

(a) Shear forces at 4 in Figure 5.19b of TU Delft brick model

(b) Shear forces at 5 in Figure 5.19b of TU Delft brick model

(c) Shear forces at ultimate negative capacity in Figure 5.19b of TU Delft brick model

Figure I.7: Shear forces of piers pushed in negative direction of TU Delft brick model

J. Results sensitivity analysis - different heights

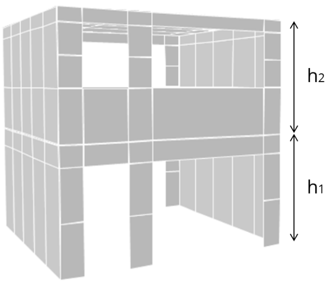

Figure J.1: Difference in storey height where h1 is equal to h2

H1 = H2 with opening ratio of 50%

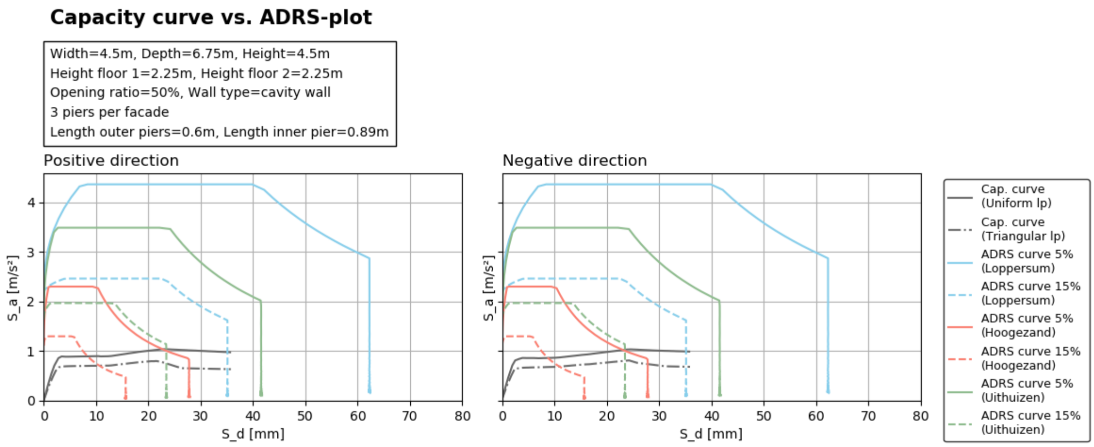

Figure J.2: Capacity curve of model with a height of 2.25 meter and a opening ratio of 50%

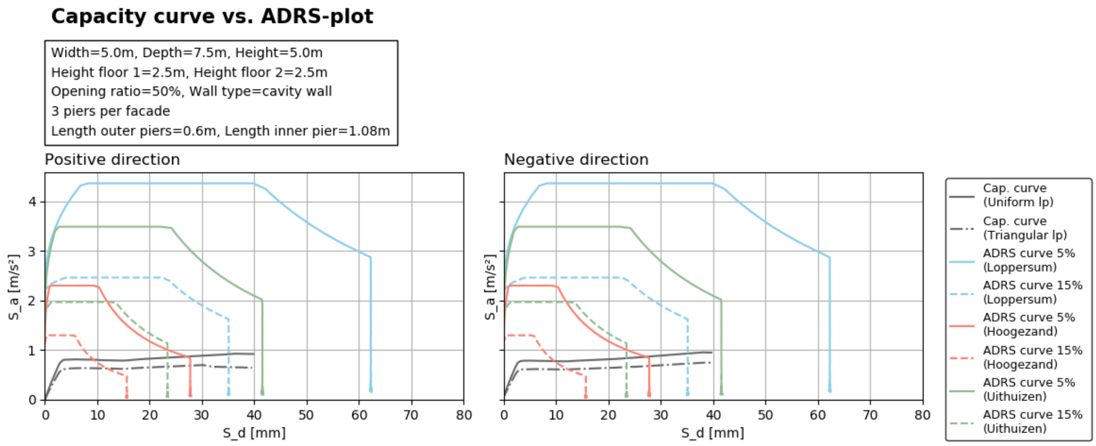

Figure J.3: Capacity curve of model with a height of 2.5 meter and a opening ratio of 50%

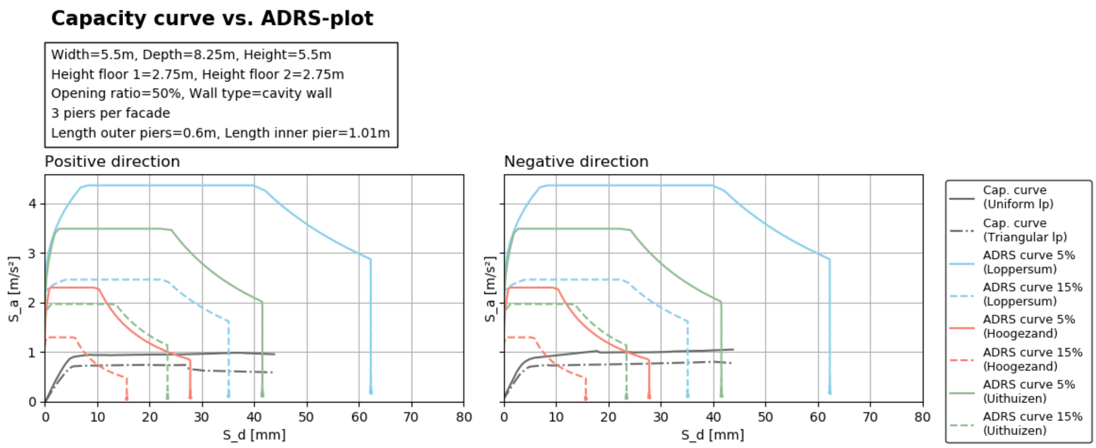

Figure J.4: Capacity curve of model with a height of 2.75 meter and a opening ratio of 50%

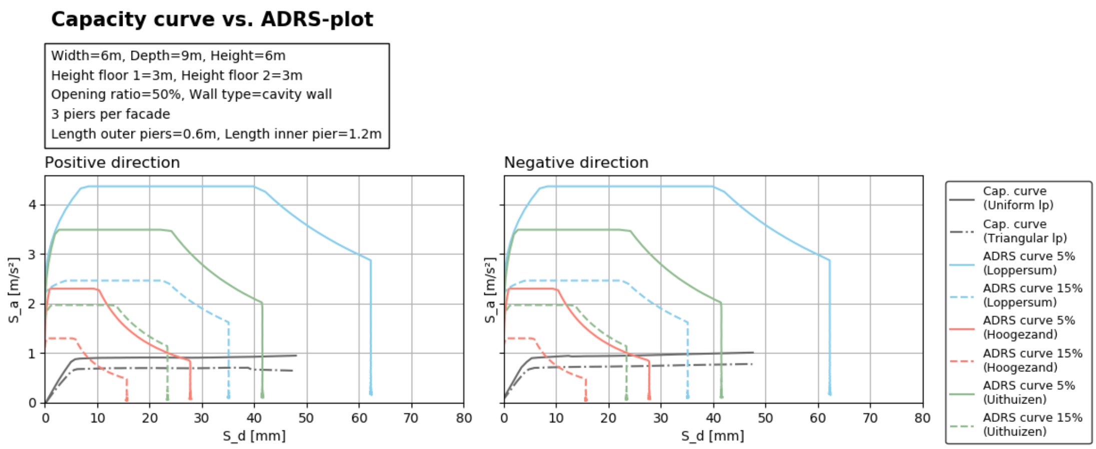

Figure J.5: Capacity curve of model with a height of 3 meter and a opening ratio of 50%

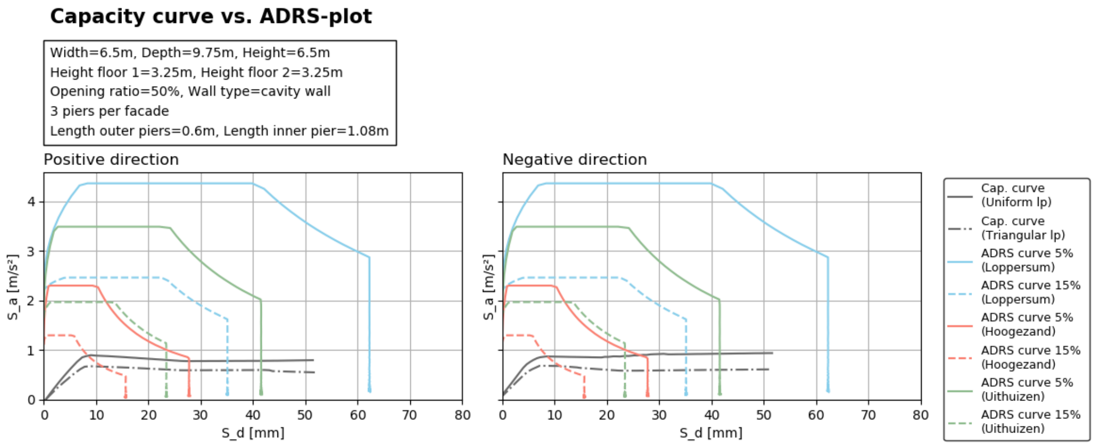

Figure J.6: Capacity curve of model with a height of 3.25 meter and a opening ratio of 50%

H1 = H2 with opening ratio of 60%

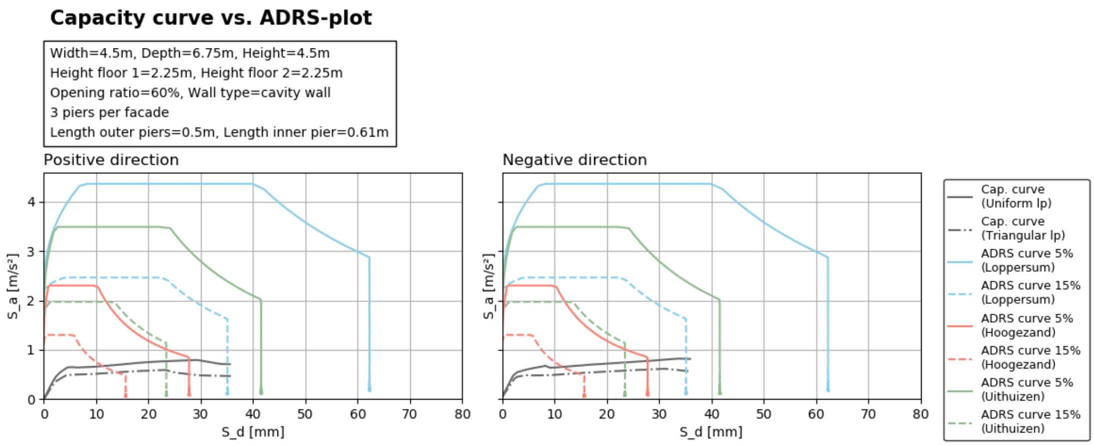

Figure J.7: Capacity curve of model with a height of 2.25 meter and a opening ratio of 60%

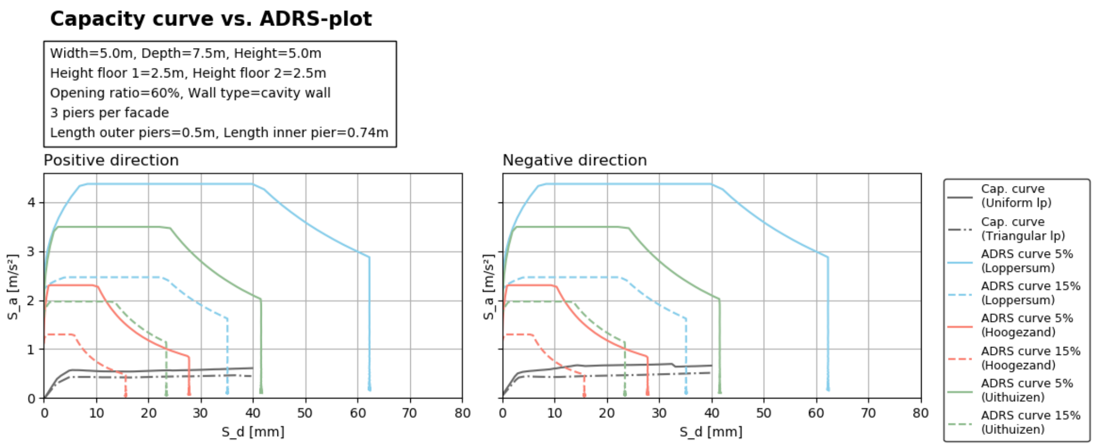

Figure J.8: Capacity curve of model with a height of 2.5 meter and a opening ratio of 60%

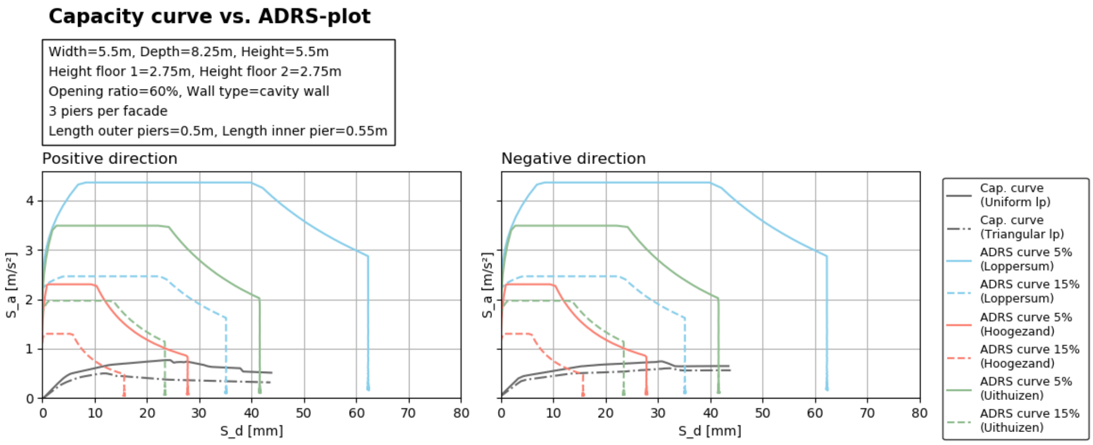

Figure J.9: Capacity curve of model with a height of 2.75 meter and a opening ratio of 60%

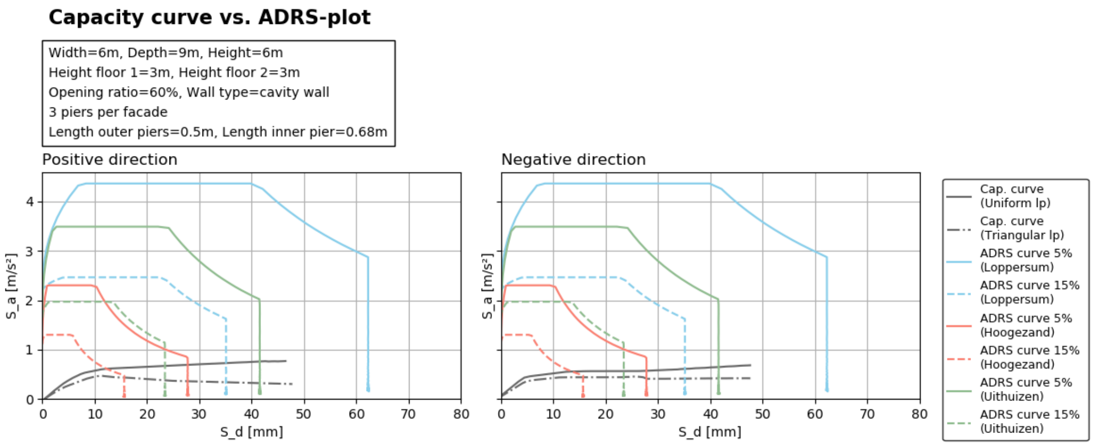

Figure J.10: Capacity curve of model with a height of 3 meter and a opening ratio of 60%

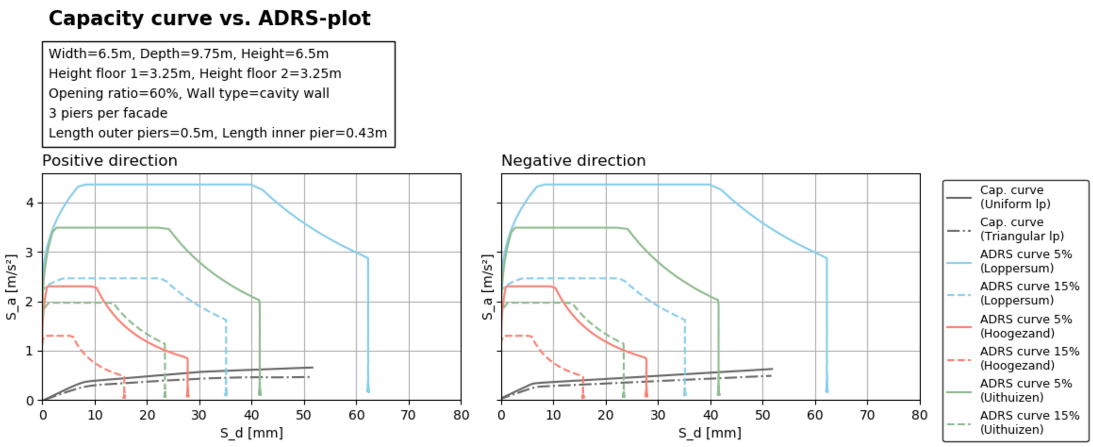

Figure J.11: Capacity curve of model with a height of 3.25 meter and a opening ratio of 60%

H1 = H2 with opening ratio of 60% and width of 6 m and depth of 8 m

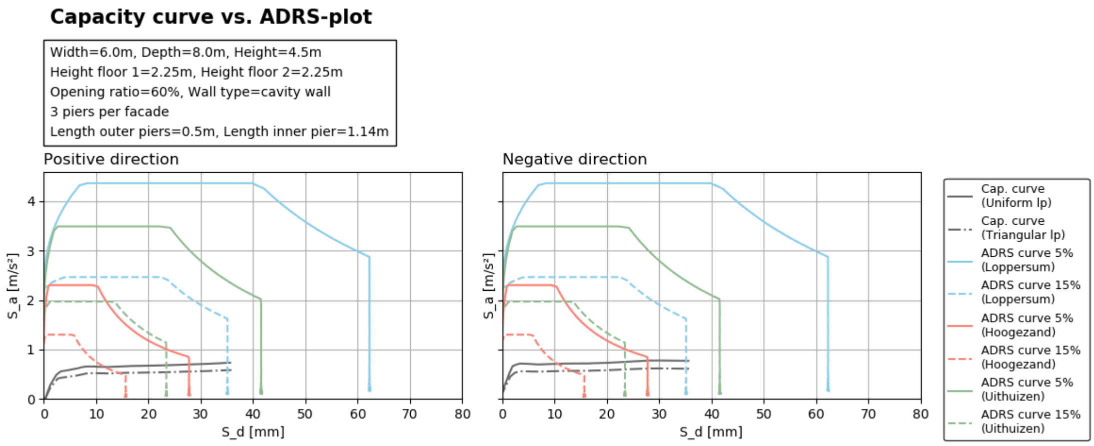

Figure J.12: Capacity curve of model with a height of 2.25 meter, a constant width and depth and a opening ratio of 60%

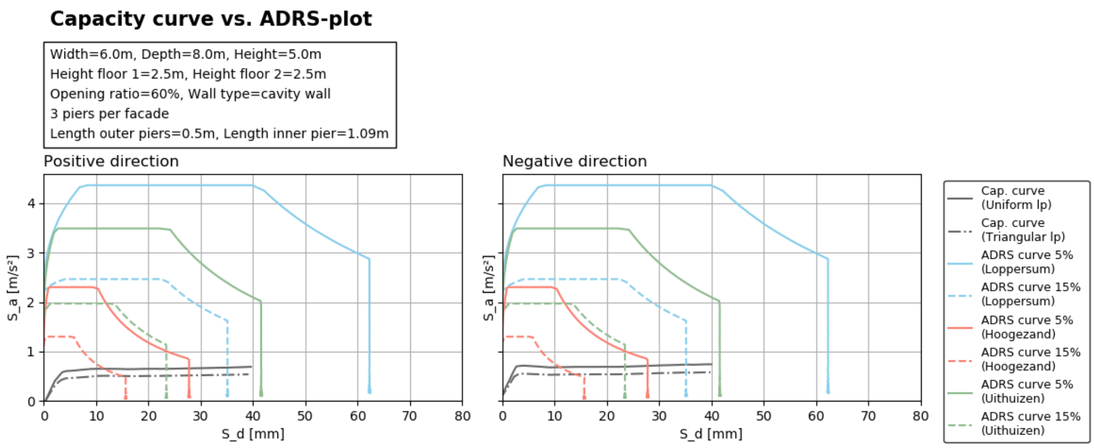

Figure J.13: Capacity curve of model with a height of 2.5 meter, a constant width and depth and a opening ratio of 60%

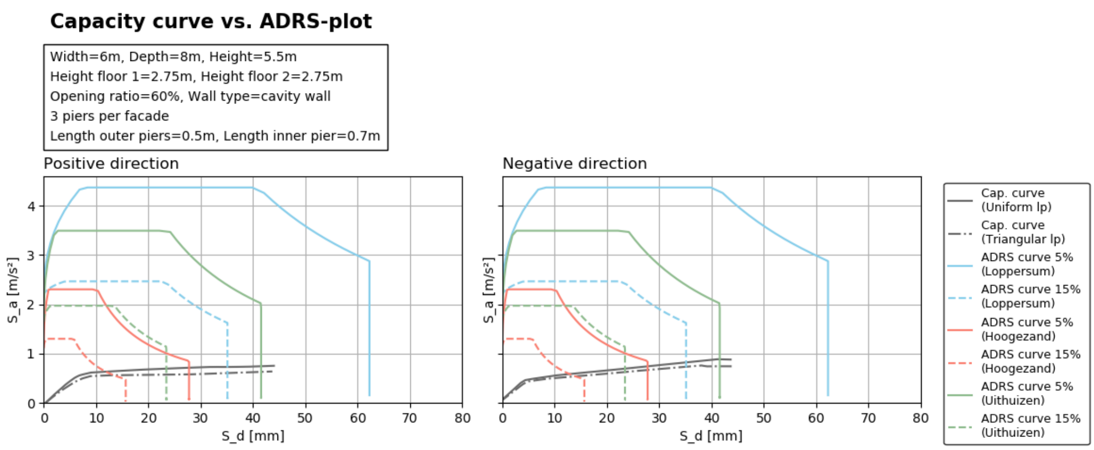

Figure J.14: Capacity curve of model with a height of 2.75 meter, a constant width and depth and a opening ratio of 60%

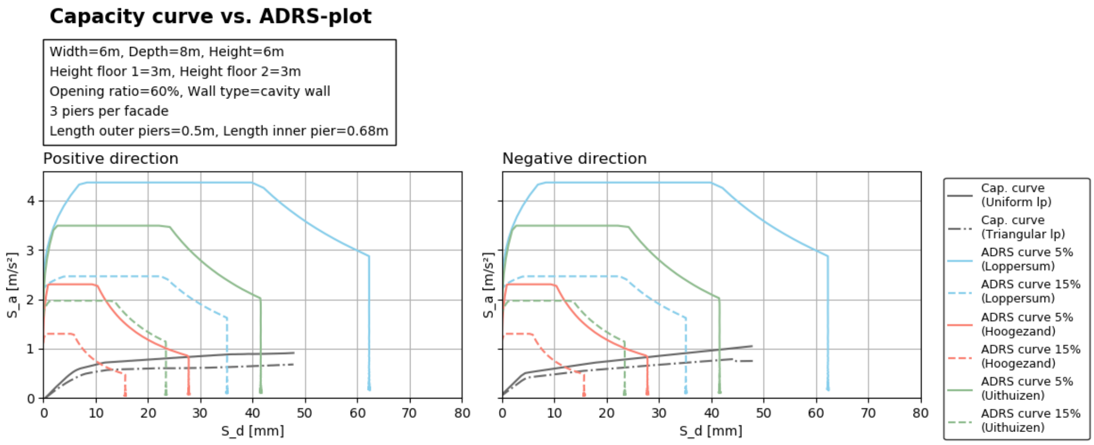

Figure J.15: Capacity curve of model with a height of 3 meter, a constant width and depth and a opening ratio of 60%

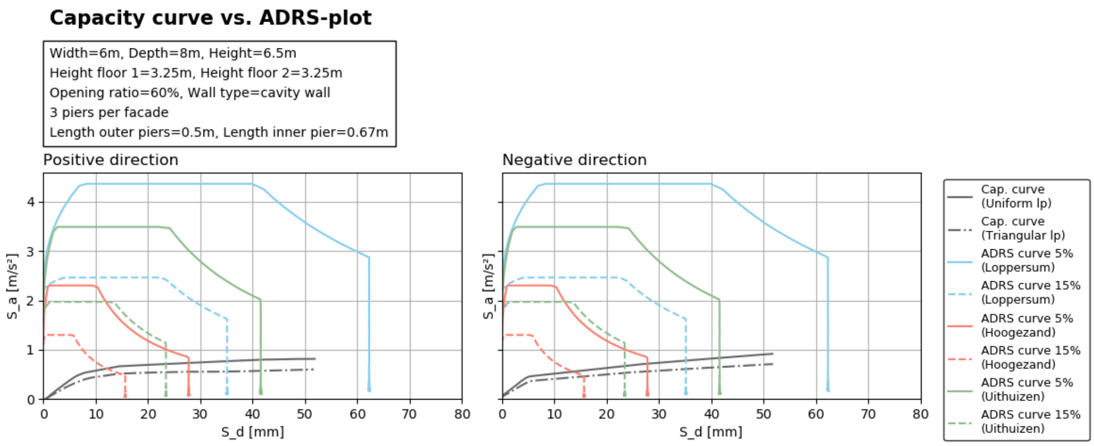

Figure J.16: Capacity curve of model with a height of 3.25 meter, a constant width and depth and a opening ratio of 60%

H1>H2, with opening ratio equal to 50%

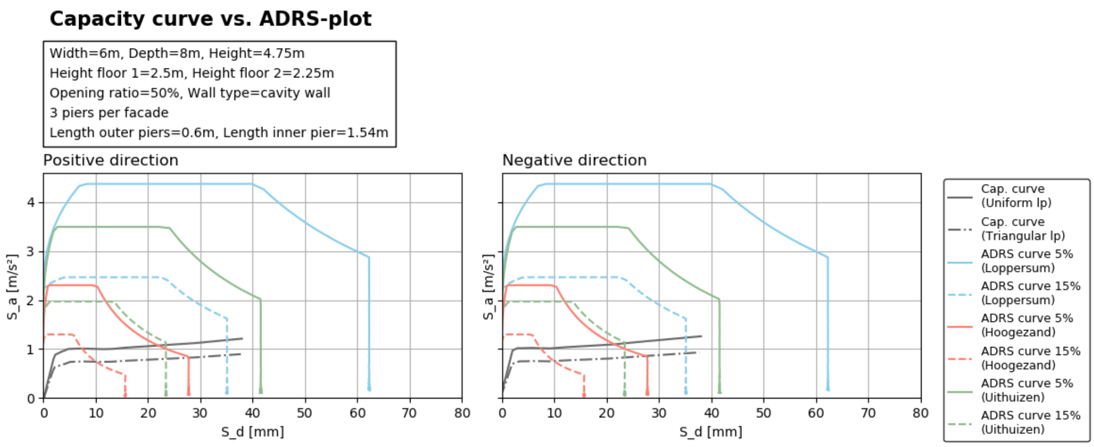

Figure J.17: Capacity curve of model with h1 = 2.5 m and h2 = 2.25 m, a constant width and depth and a opening ratio of 50%

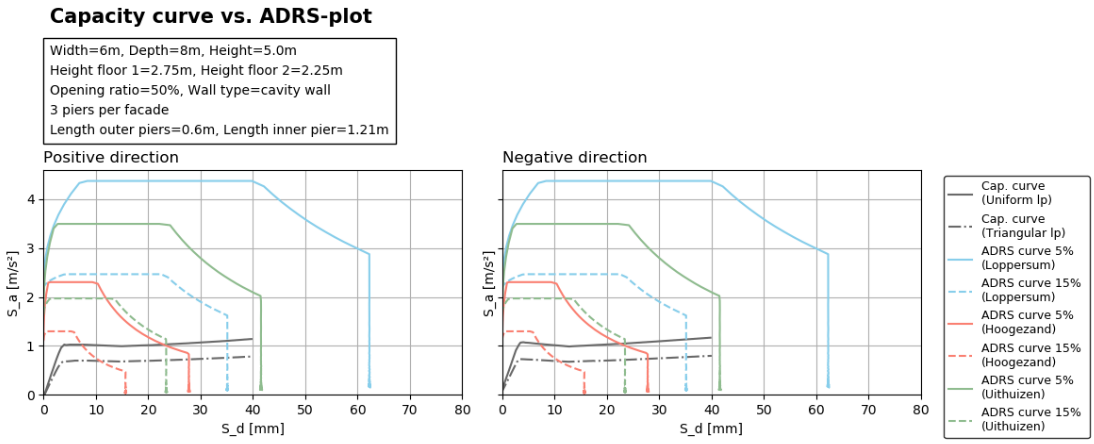

Figure J.18: Capacity curve of model with h1 = 2.75 m and h2 = 2.25 m, a constant width and depth and a opening ratio of 50%

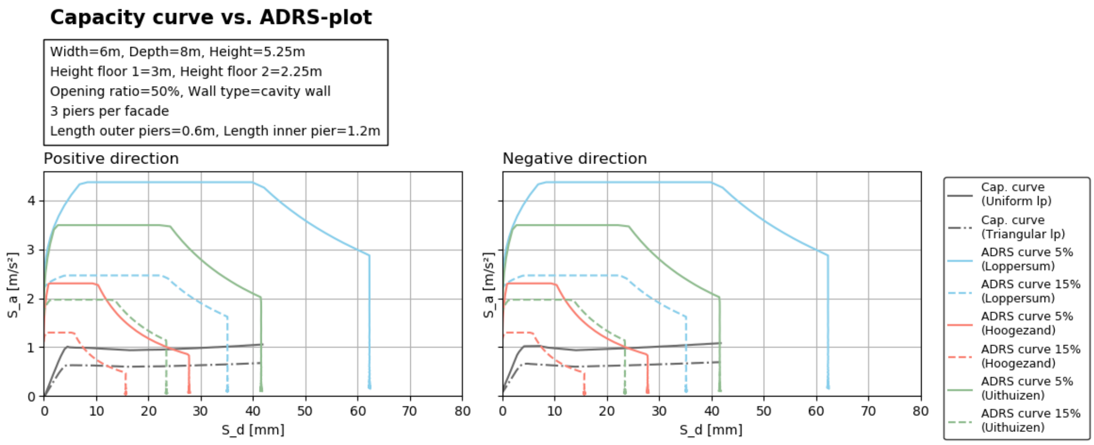

Figure J.19: Capacity curve of model with h1 = 3 m and h2 = 2.25 m, a constant width and depth and a opening ratio of 50%

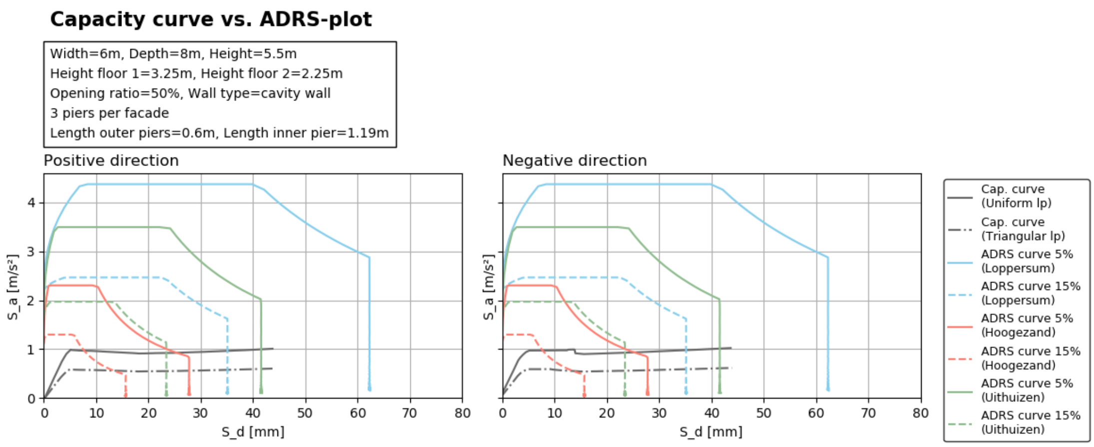

Figure J.20: Capacity curve of model with h1 = 3.25 m and h2 = 2.25 m, a constant width and depth and a opening ratio of 50%

K. Results sensitivity analysis - different depths and widths

Different depths

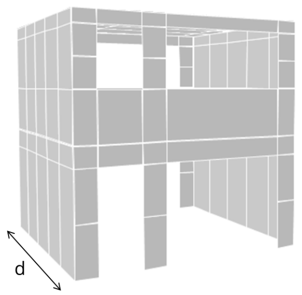

Figure K.1: Depth of the structure

Change of depth with opening ratio of 50%

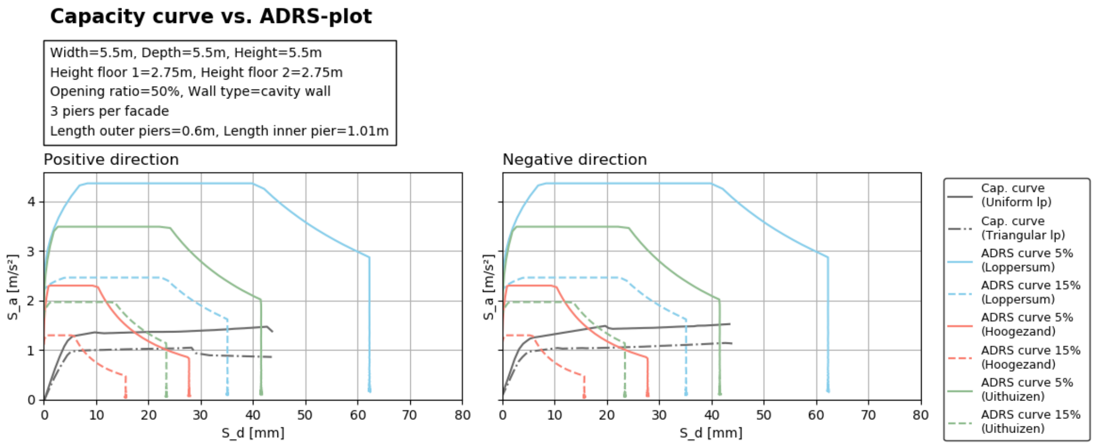

Figure K.2: Capacity curve of a model with depth of 5,5m and 50% opening ratio

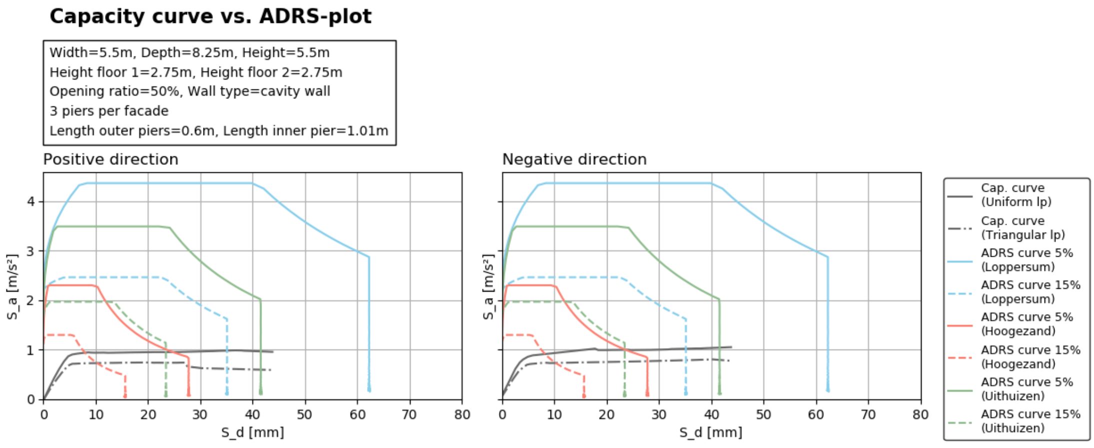

Figure K.3: Capacity curve of a model with depth of 8,25m and 50% opening ratio

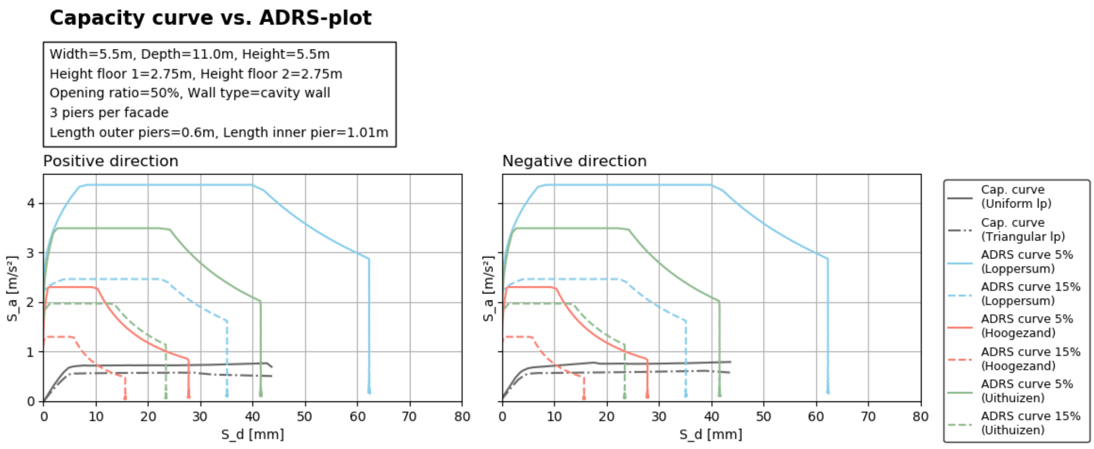

Figure K.4: Capacity curve of a model with depth of 11m and 50% opening ratio

Change of depth with opening ratio of 60%

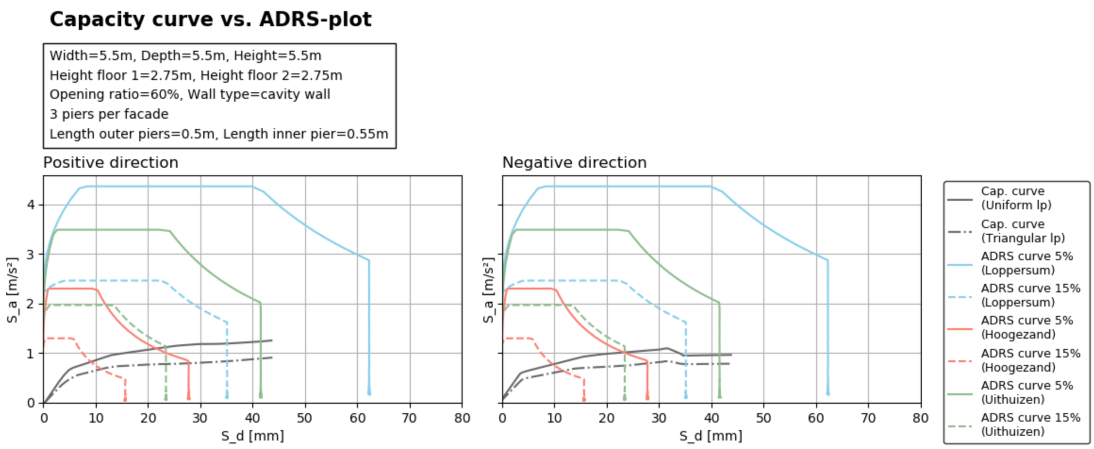

Figure K.5: Capacity curve of a model with depth of 5,5m and 60% opening ratio

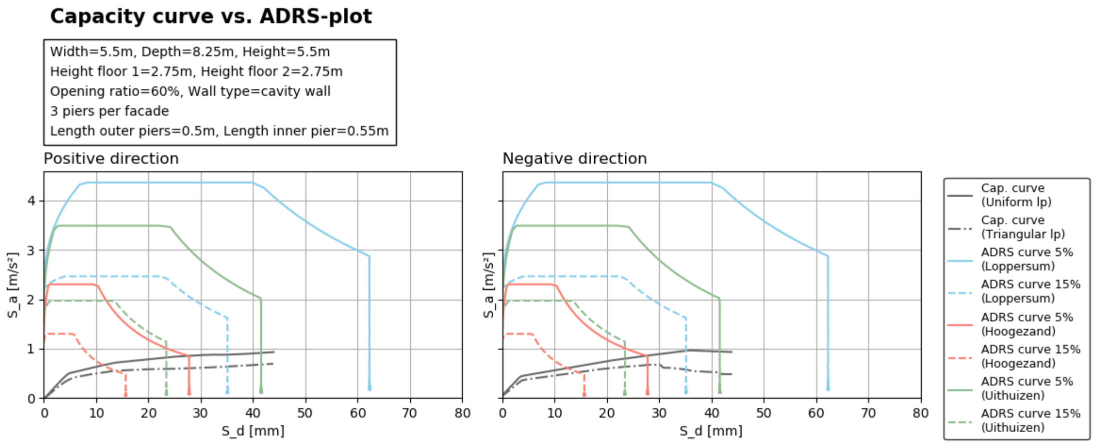

Figure K.6: Capacity curve of a model with depth of 8,25m and 60% opening ratio

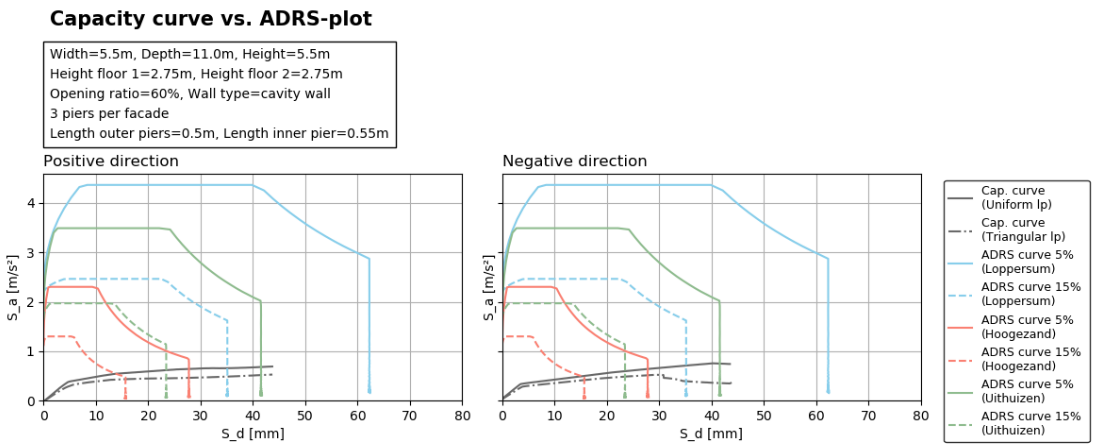

Figure K.7: Capacity curve of a model with depth of 11m and 60% opening ratio

Different widths

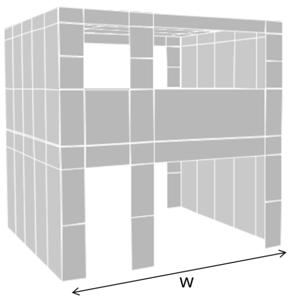

Figure K.8: Width of the structure

Change of width with opening ratio of 50%

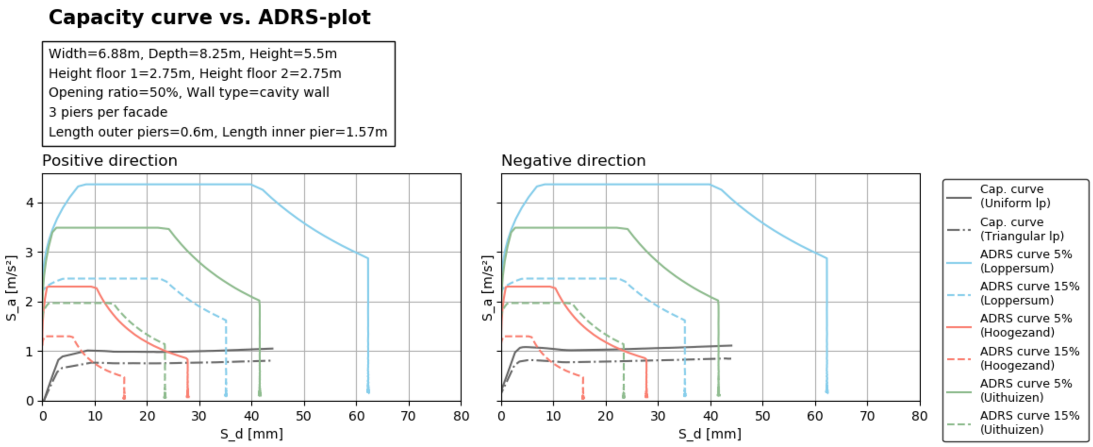

Figure K.9: Capacity curve of a model with a width of 6,88m and 50% opening ratio

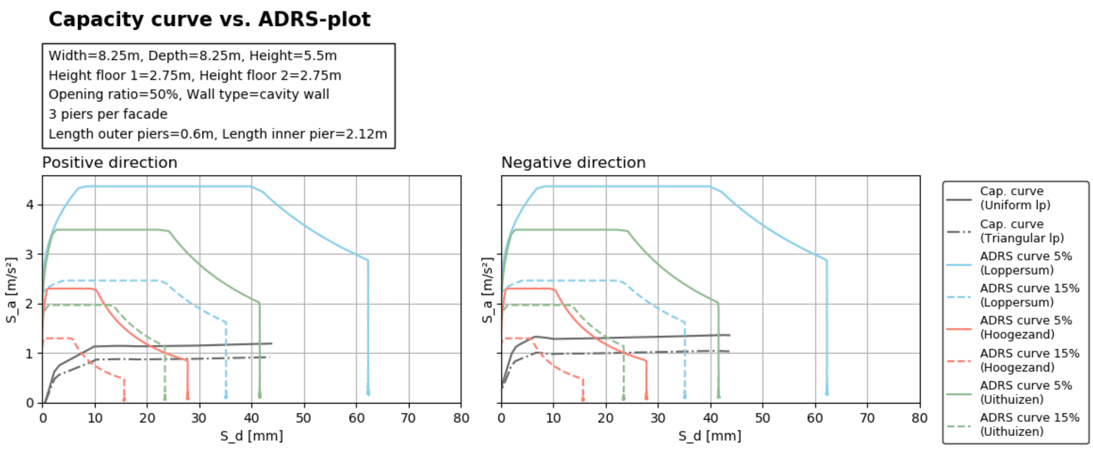

Figure K.10: Capacity curve of a model with a width of 8,25m and 50% opening ratio

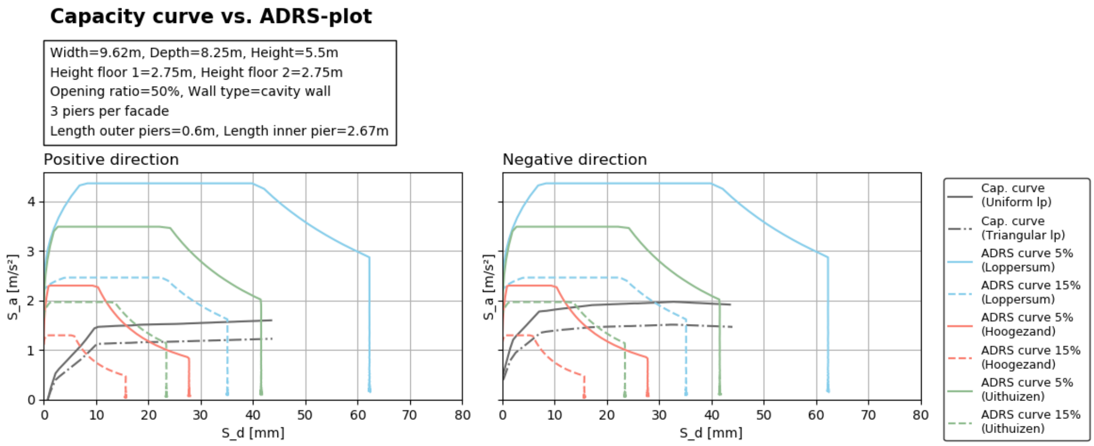

Figure K.11: Capacity curve of a model with a width of 9,62m and 50% opening ratio

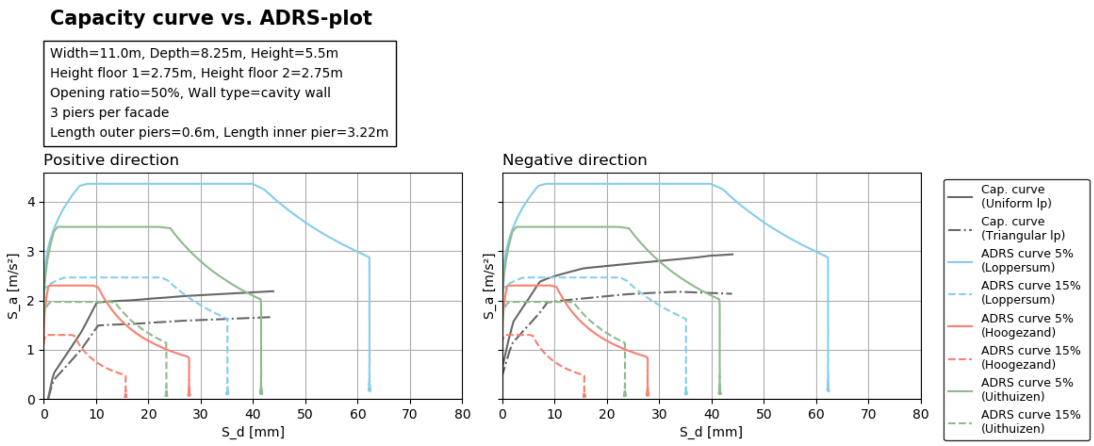

Figure K.12: Capacity curve of a model with a width of 11m and 50% opening ratio

Change of width with opening ratio of 60%

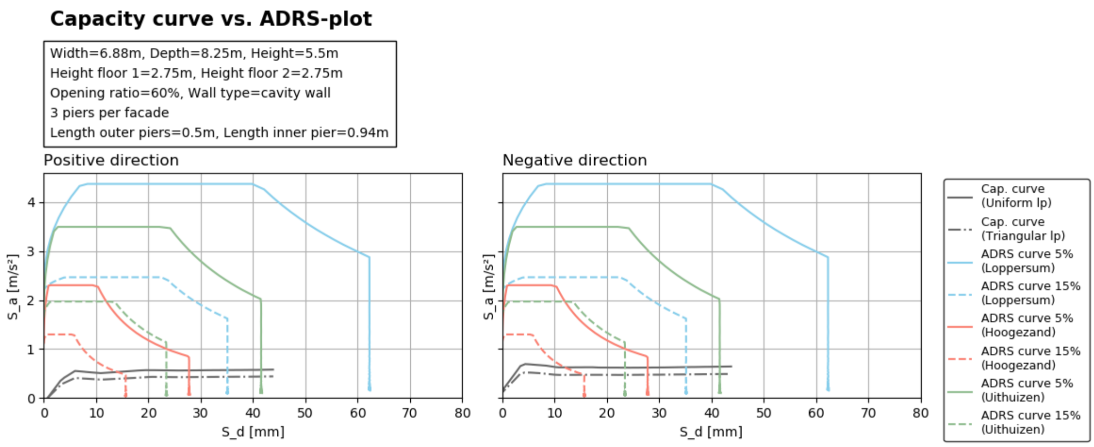

Figure K.13: Capacity curve of a model with a width of 6,88m and 60% opening ratio

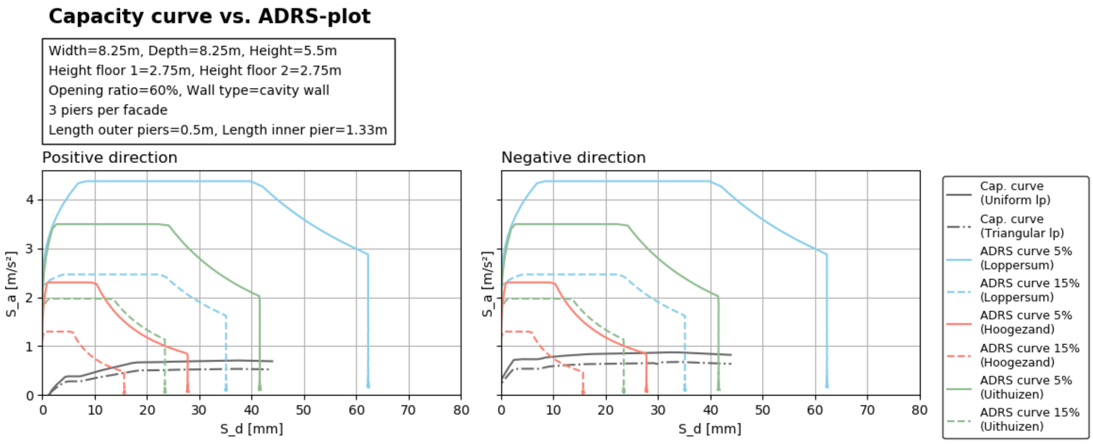

Figure K.14: Capacity curve of a model with a width of 8,25m and 60% opening ratio

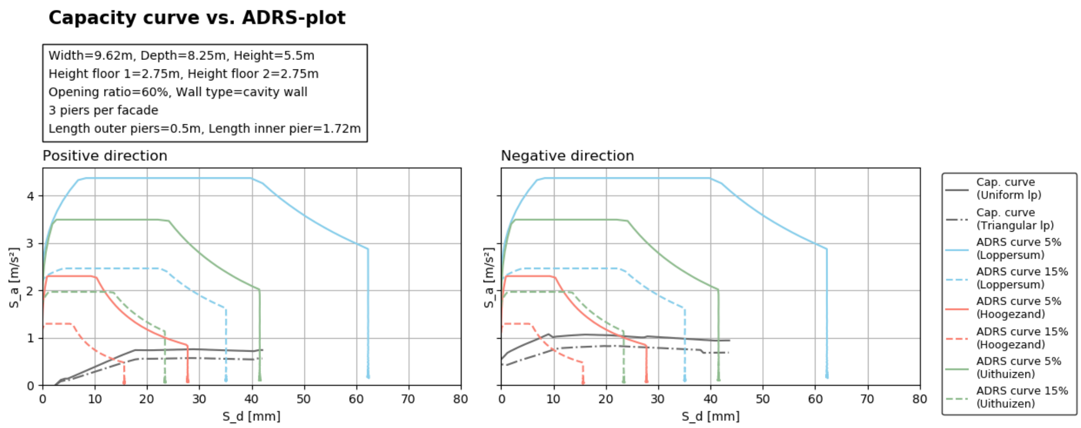

Figure K.15: Capacity curve of a model with a width of 9,62m and 60% opening ratio

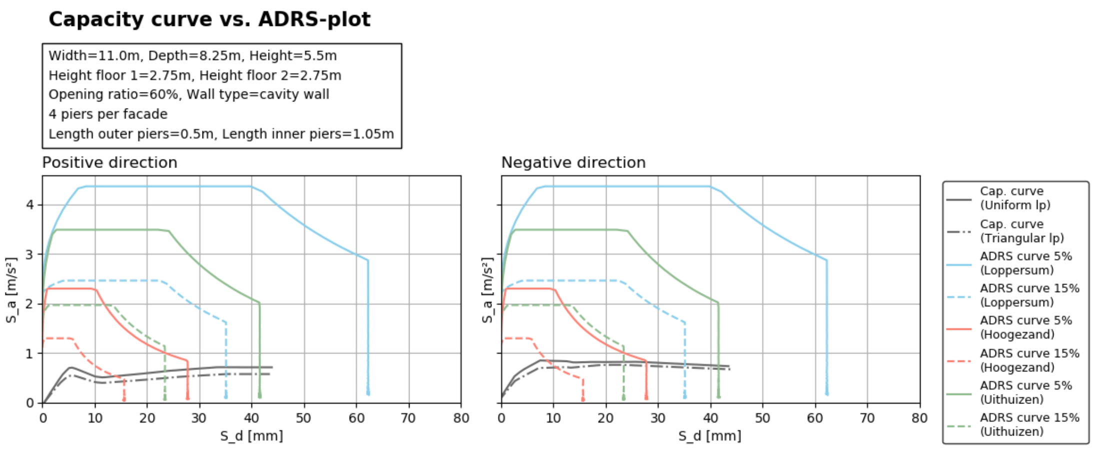

Figure K.16: Capacity curve of a model with a width of 11m and 60% opening ratio

L. Results sensitivity analysis - opening ratio 70%

Load pattern	**Uniform-**	**Triangular-**	**Uniform+**	**Triangular+**
Ptot (kg)	110028	110028	110028	110028
Ptot (kN)	1080	1080	1080	1080
u1 (mm)	12,86	13,18	11,72	11,97
Vtot (kN)	25,48	25,62	23,38	23,4
h1 (mm)	2750	2750	2750	2750
θ	0,20	0,20	0,20	0,20
Factor (1/(1-θ))	1,25	1,25	1,25	1,25

Table L.1: Calculation of P-Δ effects for a model with 70% opening ratio at ground floor level. Results show that the effects are governing the system and therefore a factor needs to be applied.

M. Results sensitivity analysis - different masonry

Change of masonry with opening ratio of 50%

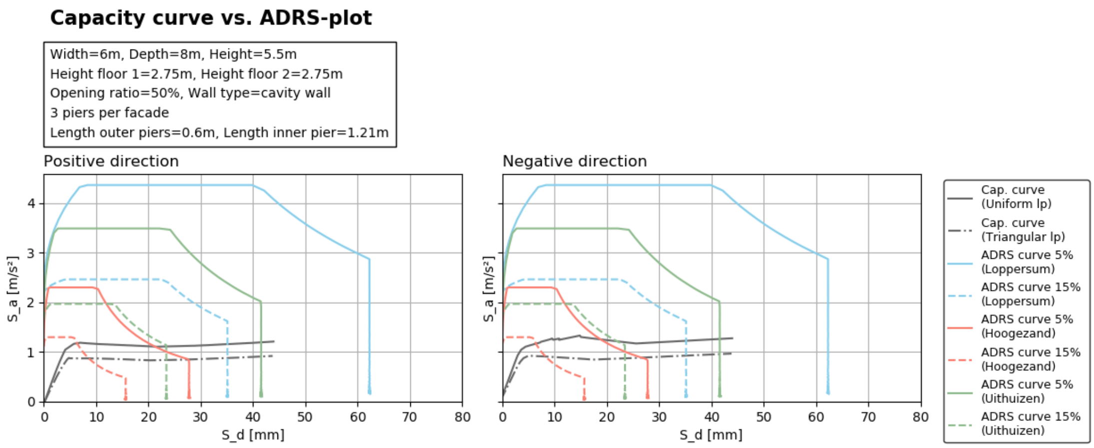

Figure M.1: Capacity curve of a model with the usual CaSi brick masonry used from 1960 onwards

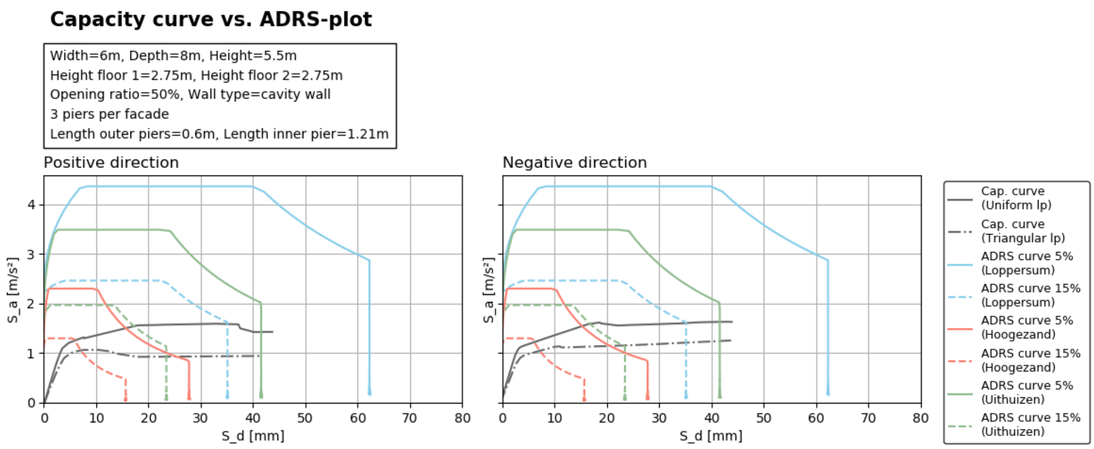

Figure M.2: Capacity curve of a model with clay brick masonry used before 1945

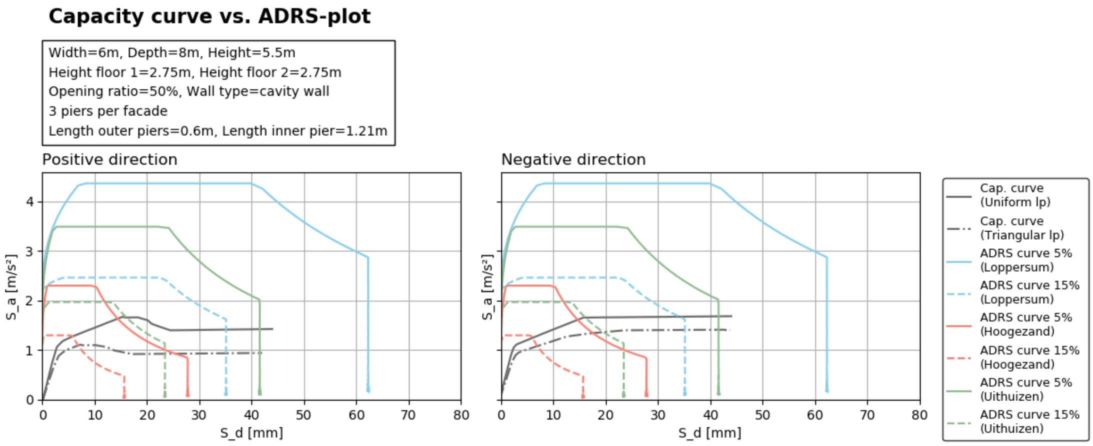

Figure M.3: Capacity curve of a model with clay brick masonry after 1945

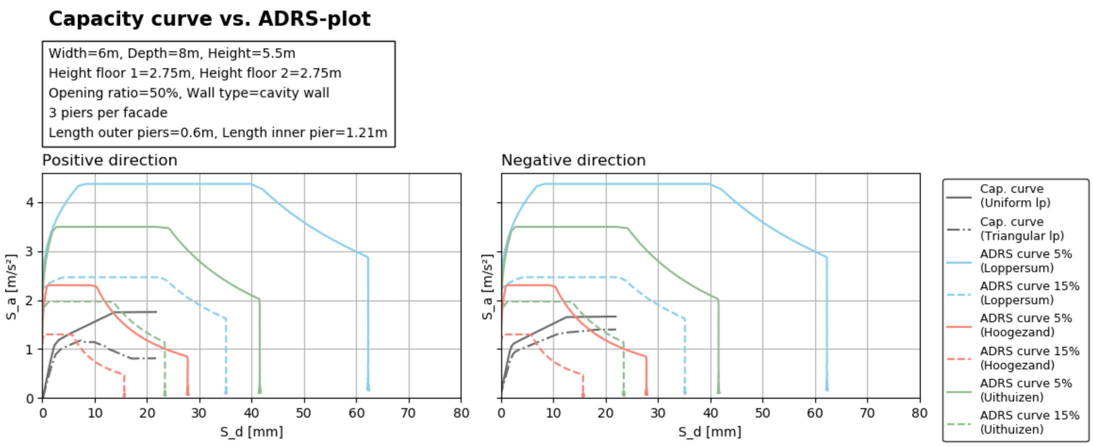

Figure M.4: Capacity curve of a model with CaSi element masonry used from 1985 onwards

Change of masonry with opening ratio of 60%

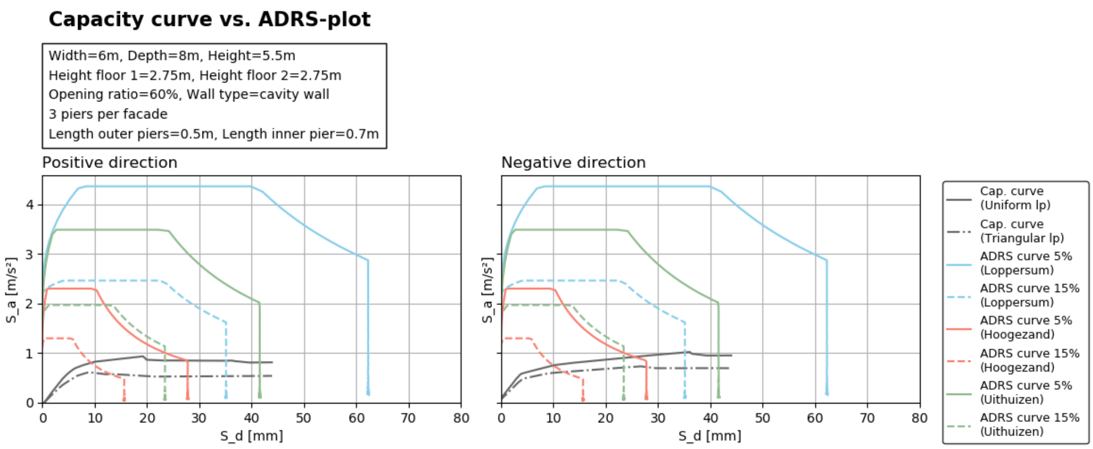

Figure M.5: Capacity curve of a model with the usual CaSi brick masonry used from 1960 onwards

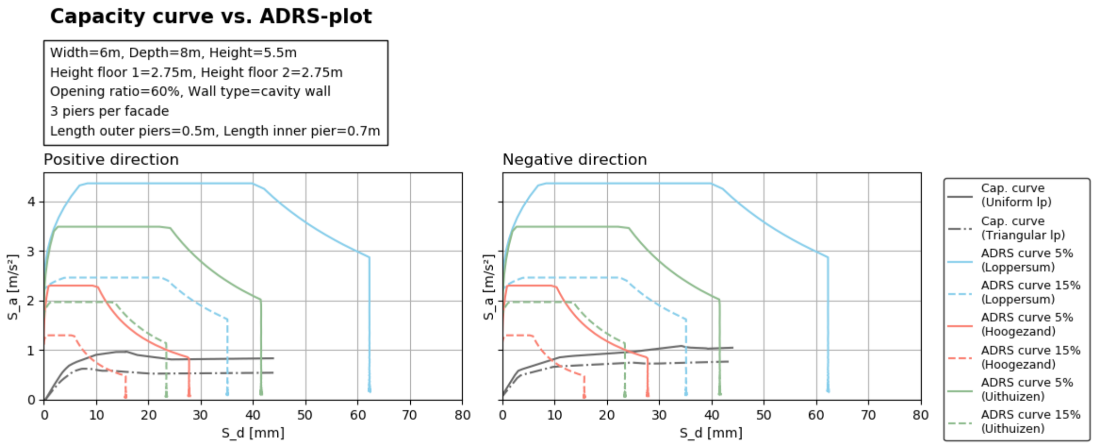

Figure M.6: Capacity curve of a model with clay brick masonry used before 1945

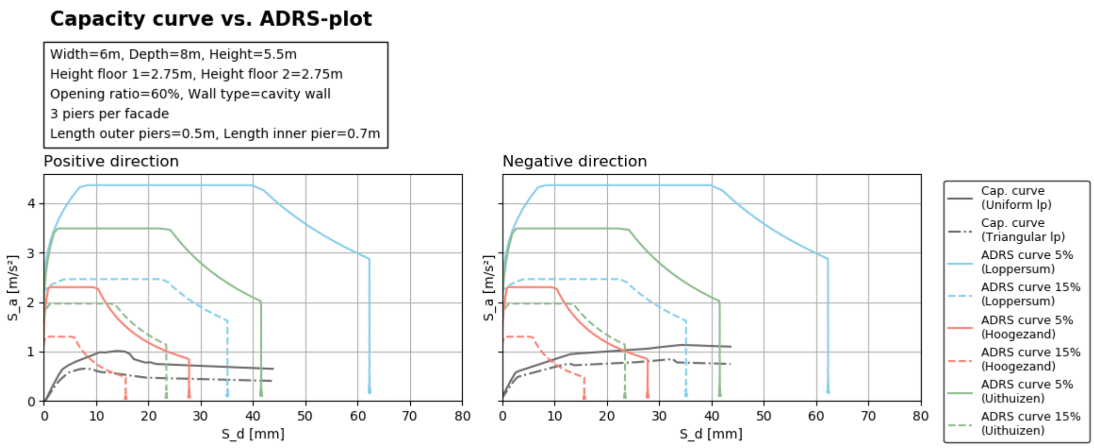

Figure M.7: Capacity curve of a model with clay brick masonry used after 1945

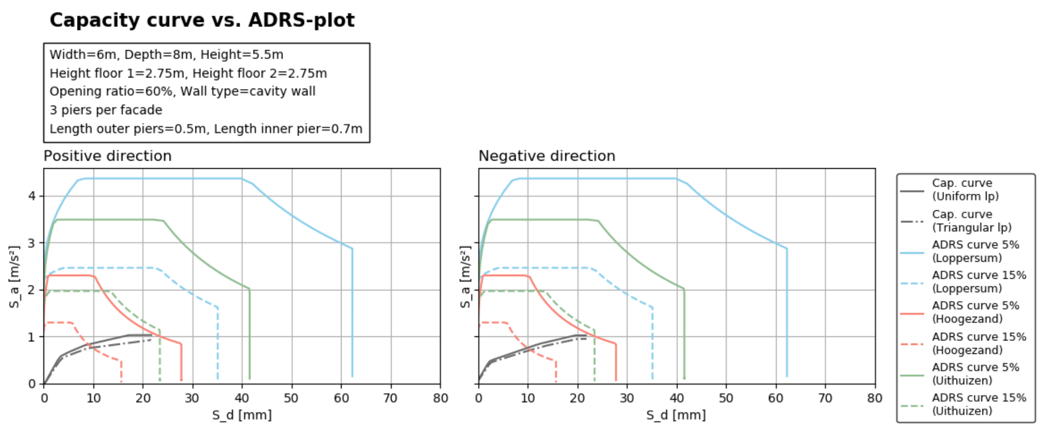

Figure M.8: Capacity curve of a model with CaSi element masonry used from 1985 onwards

N. Results sensitivity analysis - different wall type

Solid wall vs cavity wall with opening ratio of 50%

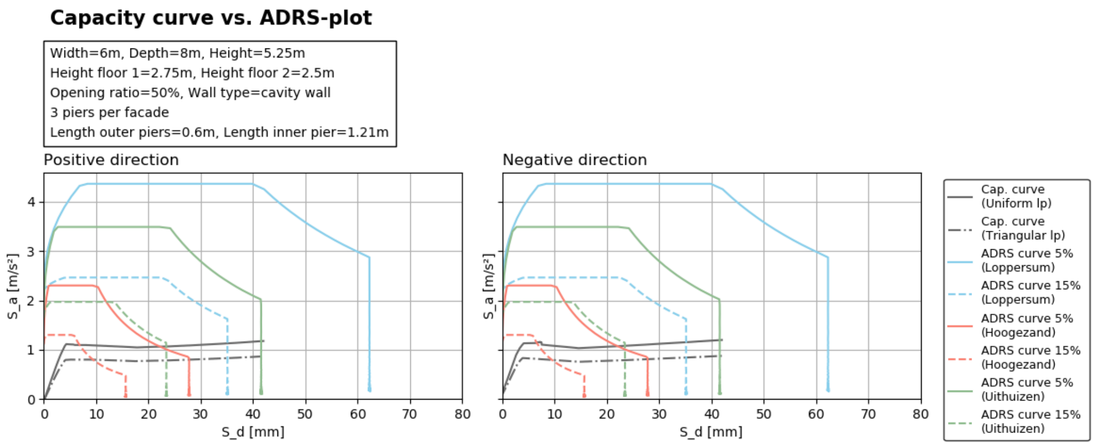

Figure N.1: Capacity curve of a model with cavity walls and opening ratio of 50%

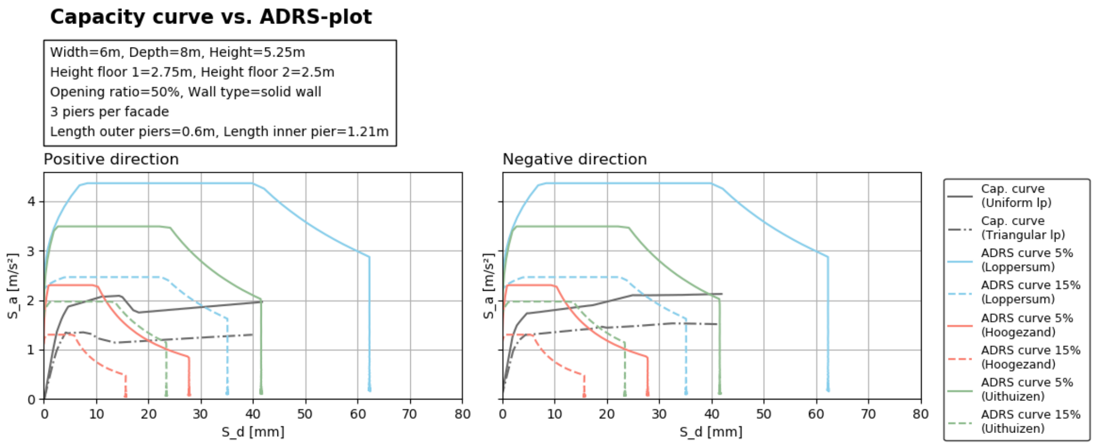

Figure N.2: Capacity curve of the same model with solid walls and opening ratio of 50%

Solid wall vs cavity wall with opening ratio of 60%

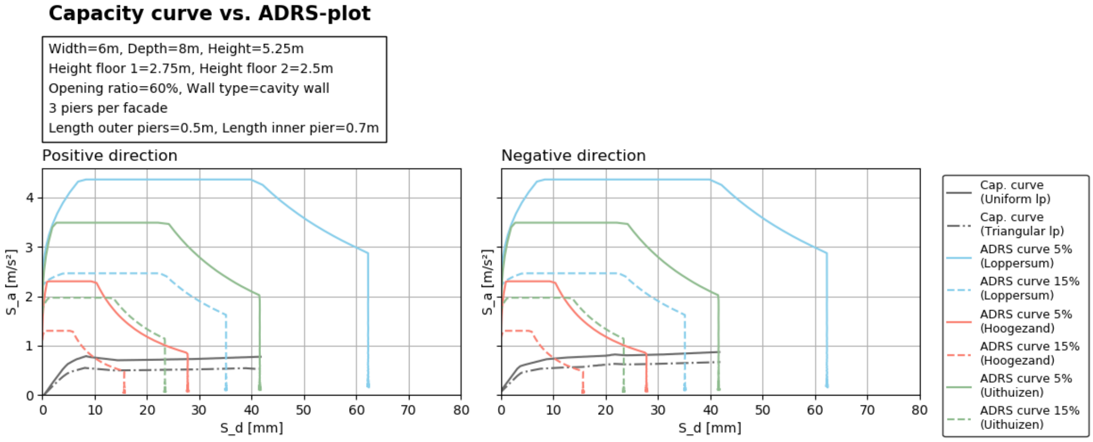

Figure N.3: Capacity curve of a model with cavity walls and opening ratio of 60%

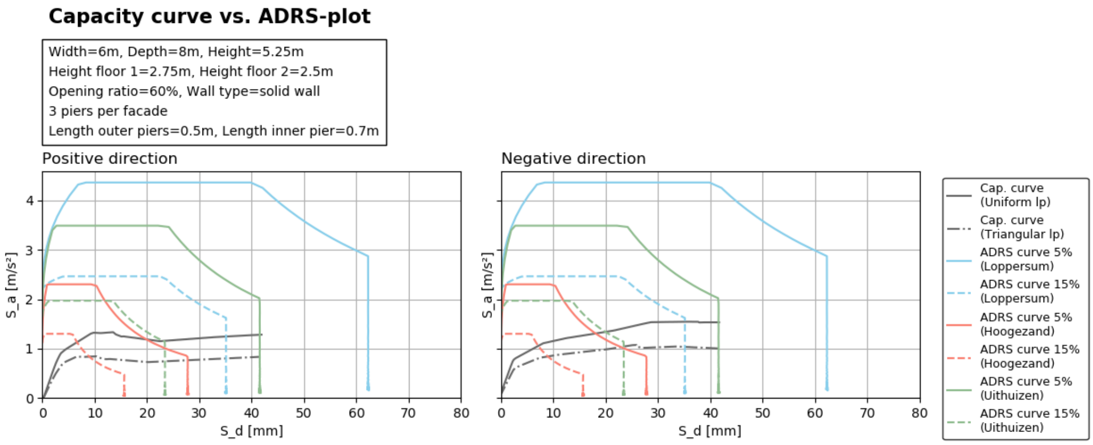

Figure N.4: Capacity curve of the same model with solid walls and opening ratio of 60%

O. Results sensitivity analysis - difference in flange effect

Change of flange effect with opening ratio of 60%

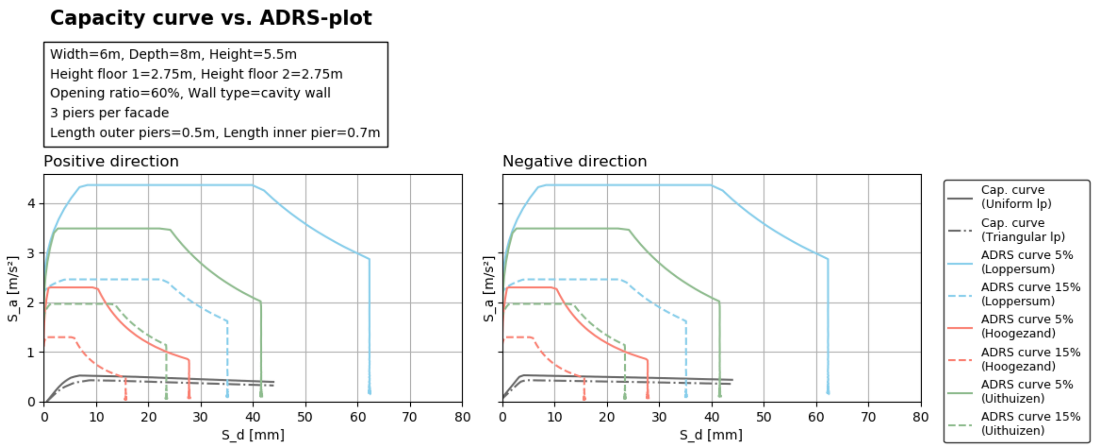

Figure O.1: Capacity curve of a model without flange effect load

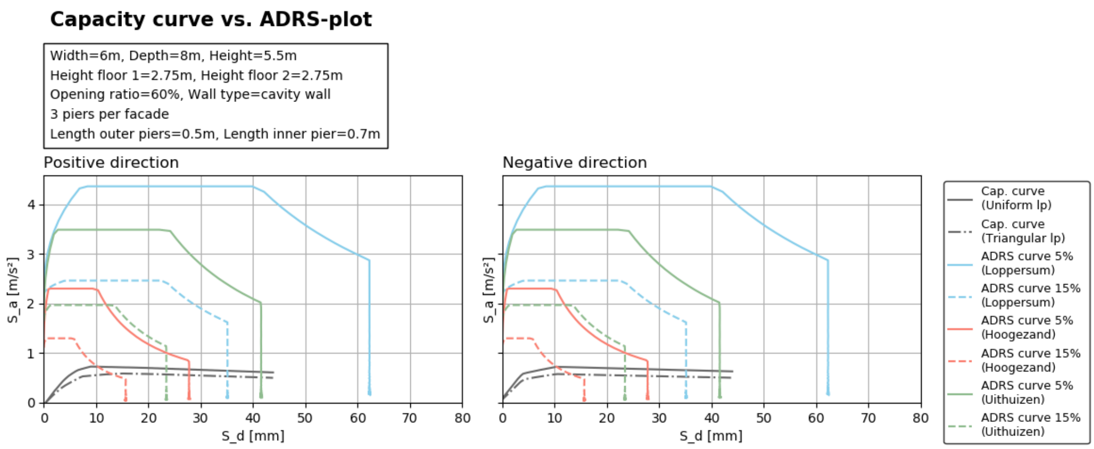

Figure O.2: Capacity curve of the same model with 25% of the calculated flange effect load

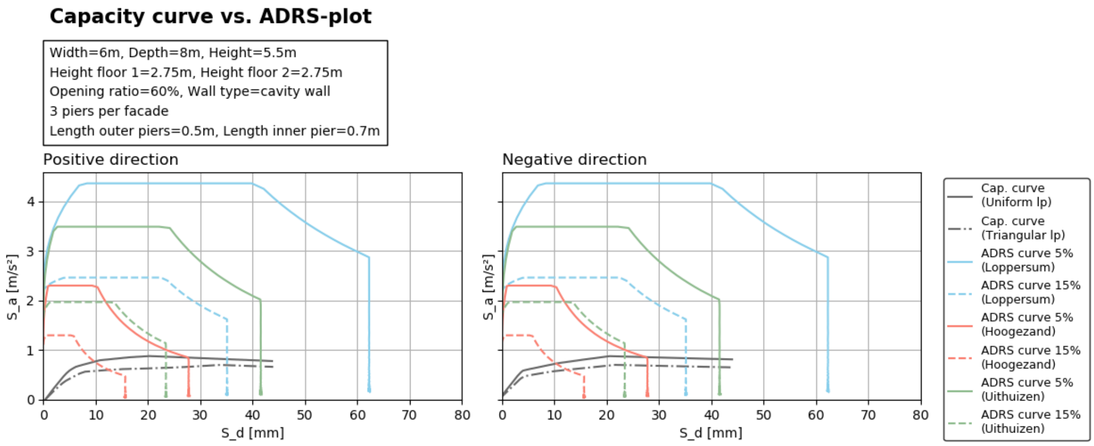

Figure O.3: Capacity curve of the same model with 50% of the calculated flange effect load

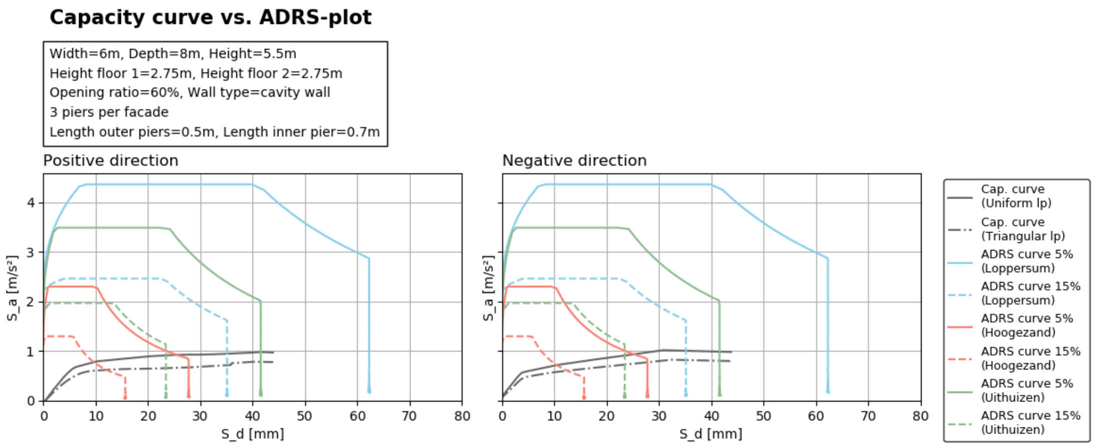

Figure O.4: Capacity curve of the same model with 75% of the calculated flange effect load

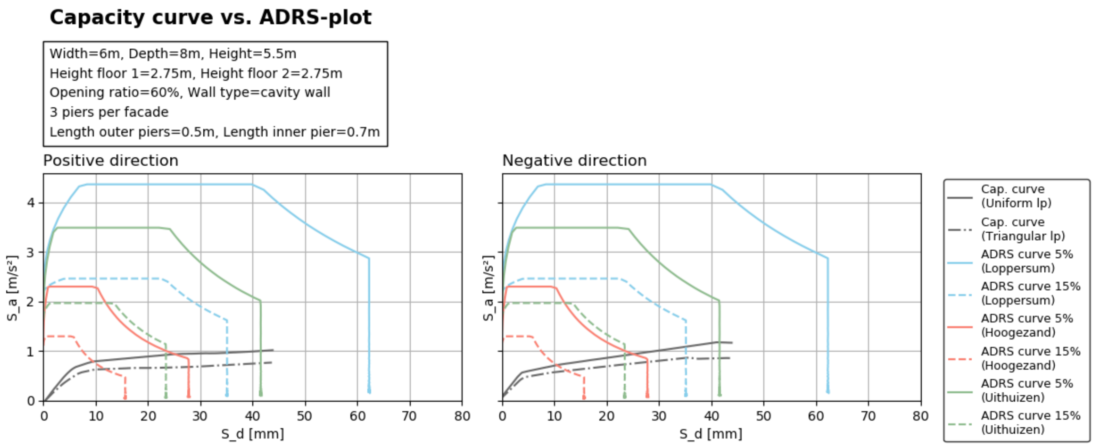

Figure O.5: Capacity curve of the same model with 100% of the calculated flange effect load

P. Results sensitivity analysis - Larger outer piers

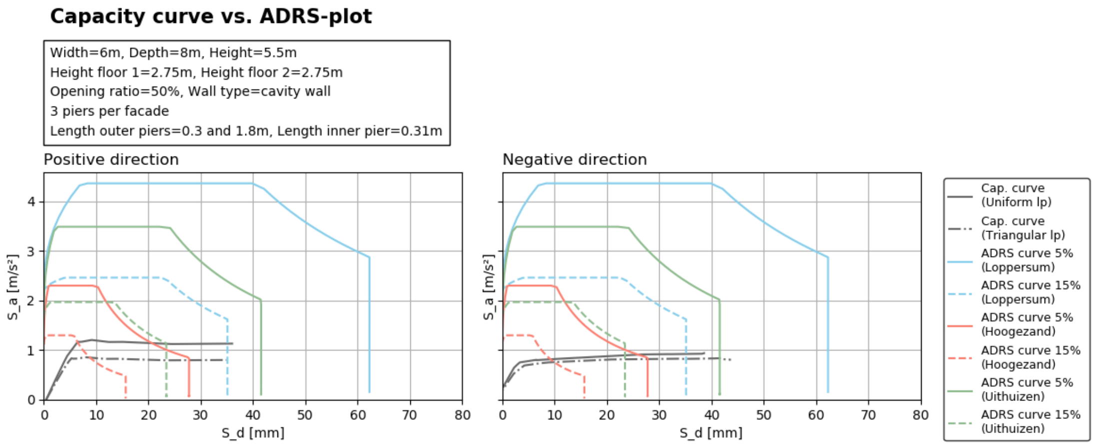

Figure P.1: Capacity curve of model with larger outer piers on the left side of the building

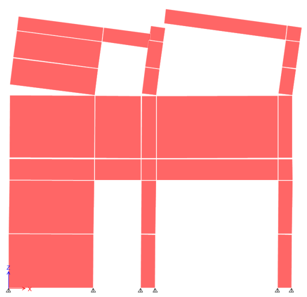

(a) Seismic behaviour due to uniform load pattern in positive direction

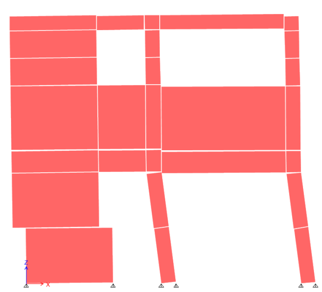

(b) Seismic behaviour due to uniform load pattern in negative direction

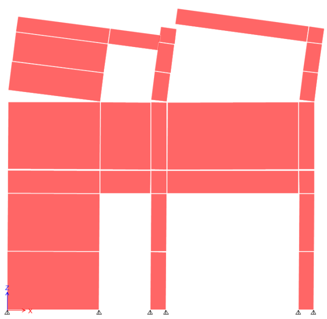

(c) Seismic behaviour due to triangular load pattern in positive direction

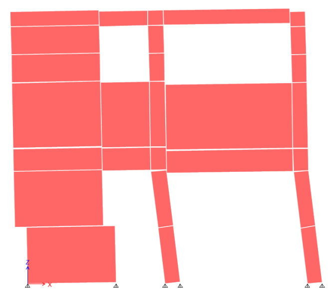

(d) Seismic behaviour due to triangular load pattern in negative direction

Figure P.2: Seismic behaviour of model with larger outer piers on the left hand side

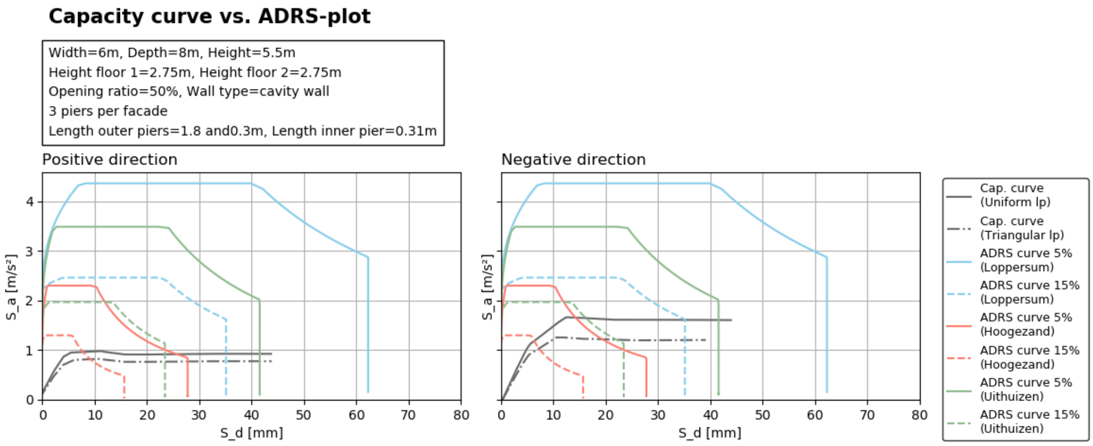

Figure P.3: Capacity curve of model with larger outer piers on the right side of the building

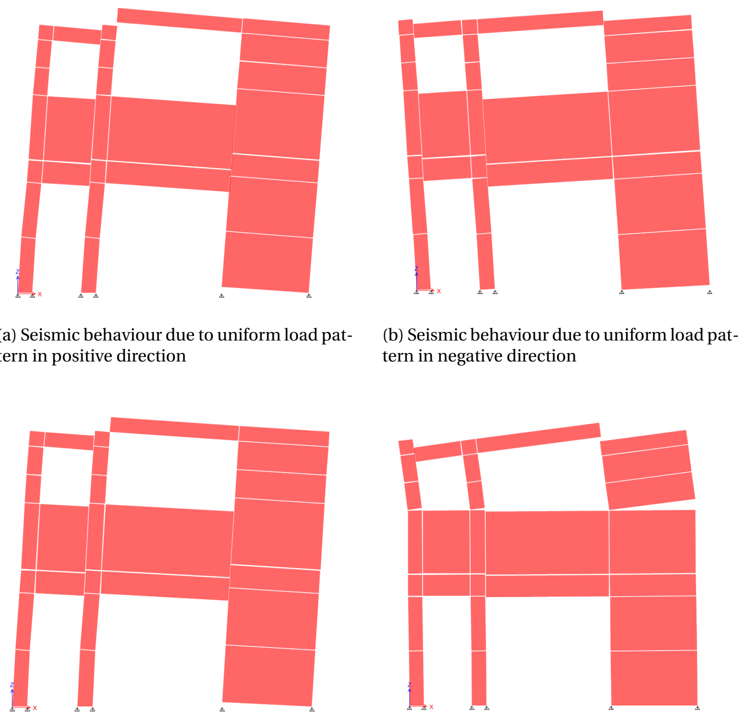

(a) Seismic behaviour due to uniform load pattern in positive direction

(b) Seismic behaviour due to uniform load pattern in negative direction

(c) Seismic behaviour due to triangular load pattern in positive direction

(d) Seismic behaviour due to triangular load pattern in negative direction

Figure P.4: Seismic behaviour of model with larger outer piers on the right hand side

Q. Results sensitivity analysis - Four piers

Four piers

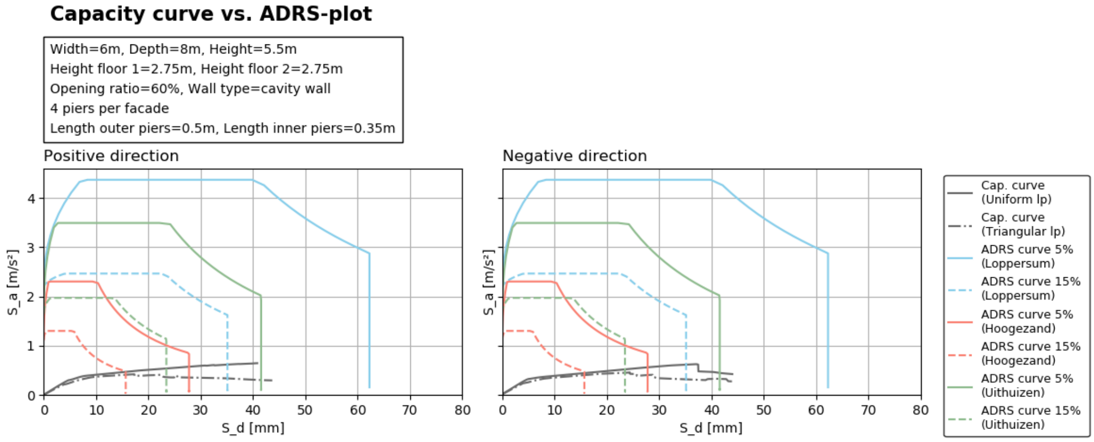

Figure Q.1: Capacity curve of model with four piers for each wall and an opening ratio of 60%

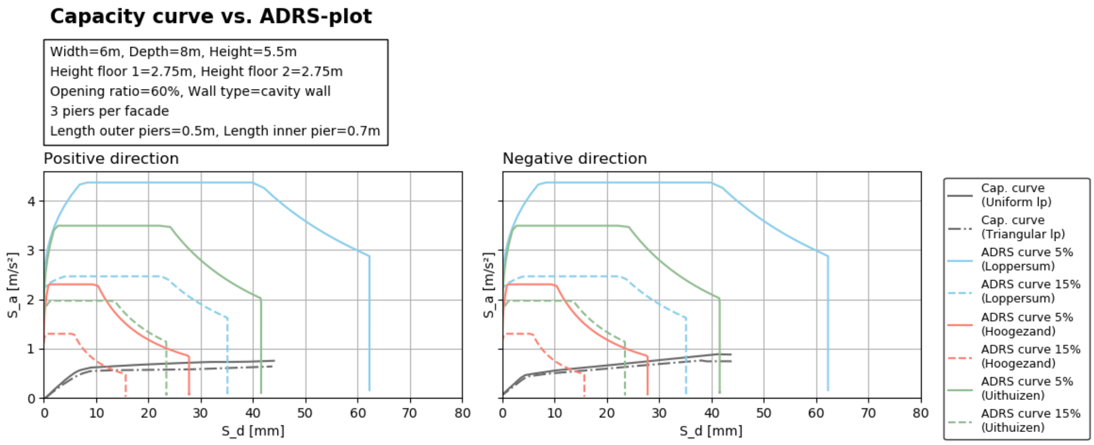

Figure Q.2: Capacity curve of the same model with three piers for each wall and an opening ratio of 60%

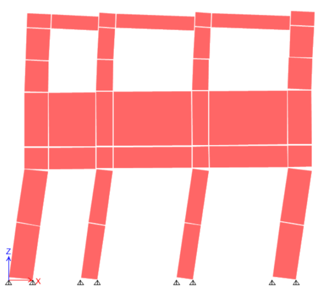

(a) Seismic behaviour due to uniform load pattern in positive direction

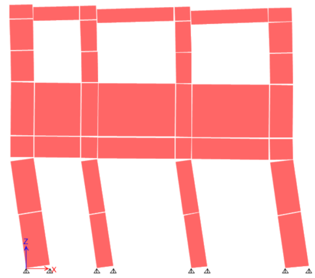

(b) Seismic behaviour due to uniform load pattern in negative direction

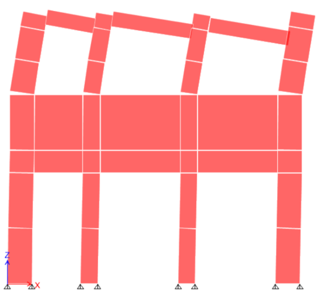

(c) Seismic behaviour due to triangular load pattern in positive direction

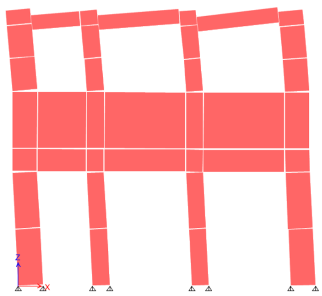

(d) Seismic behaviour due to triangular load pattern in negative direction

Figure Q.3: Seismic behaviour of model with four piers and an opening ratio of 60%

R. Element forces un-strengthened models

Model with 60% opening ratio and height of 2,75 m

Presentation of forces in the structural elements due to gravity loading and the pushover analyses in both directions of a model with an opening ratio of the ground floor façade walls of 60%, an inter storey height of 2,75m, width of 6m and a depth of 8m. The corresponding capacity curve is presented in Figure R.1.

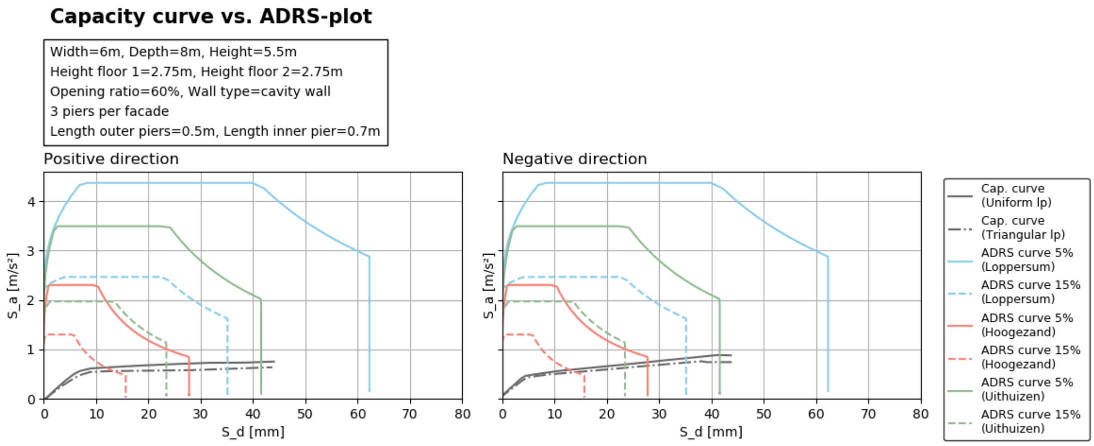

Figure R.1: Capacity curve of a model with an opening ratio of the ground floor façade walls of 60%, an inter storey height of 2,75m, width of 6m and a depth of 8m.

Axial loads piers

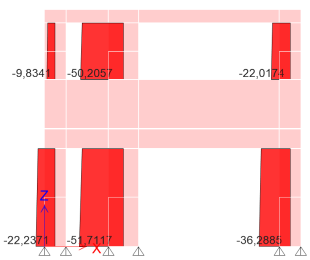

Figure R.2: Axial forces due to gravity loading

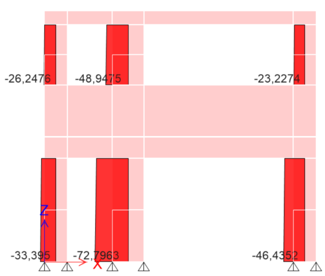

(a) Axial forces at end elastic phase

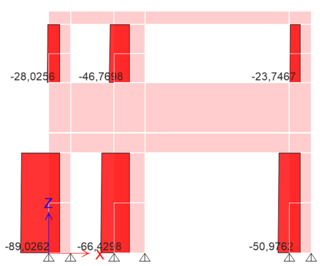

(b) Axial forces at step 80

Figure R.3: Axial forces of piers pushed in positive direction

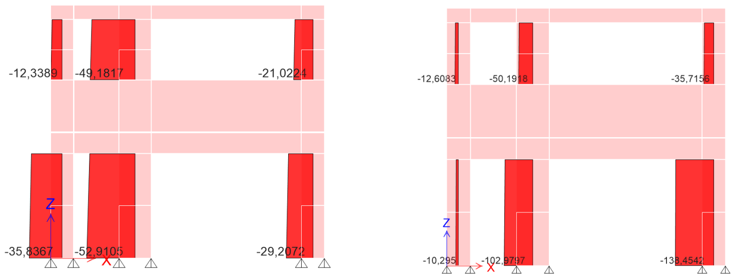

(a) Axial forces at end elastic phase

(b) Axial forces at end capacity curve

Figure R.4: Axial forces of piers pushed in negative direction

Shear forces piers

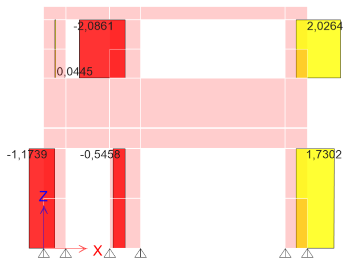

Figure R.5: Shear forces of piers due to gravity loading

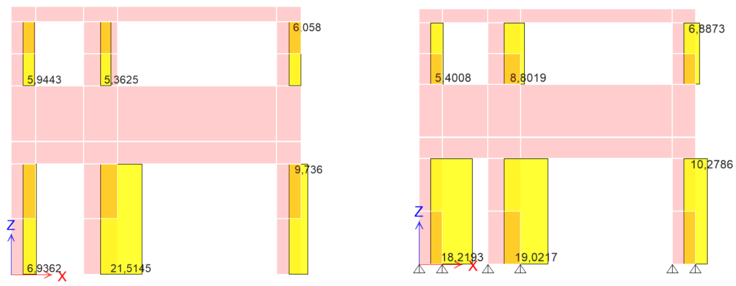

(a) Shear forces at end elastic phase

(b) Shear forces end of capacity curve

Figure R.6: Shear forces of piers pushed in positive direction

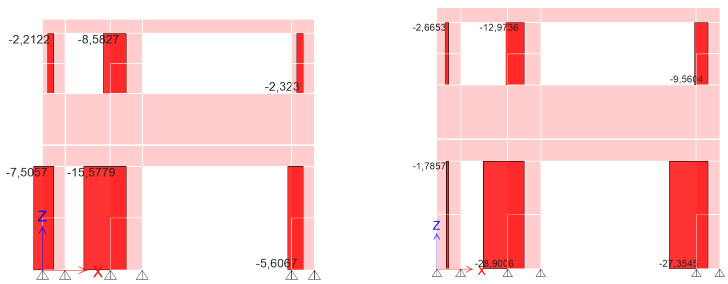

(a) Shear forces at end elastic phase

(b) Shear forces end of capacity curve

Figure R.7: Shear forces of piers pushed in negative direction

Axial loads transversal walls

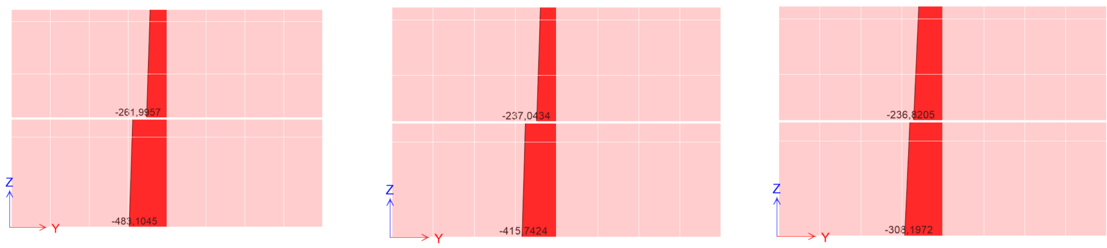

(a) Axial forces due to gravity loading (b) Axial forces at end elastic phase (c) Axial forces at end capacity curve

Figure R.8: Axial forces of left transversal walls pushed in positive direction

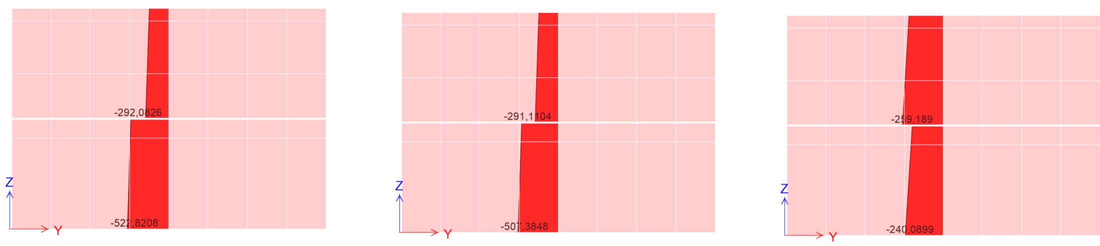

(a) Axial forces due to gravity loading (b) Axial forces at end elastic phase (c) Axial forces at end capacity curve

Figure R.9: Axial forces of right transversal walls pushed in positive direction

Shear forces spandrels

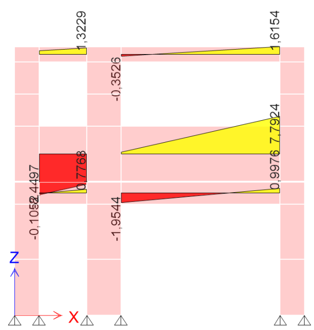

Figure R.10: Shear forces of spandrels due to gravity loading

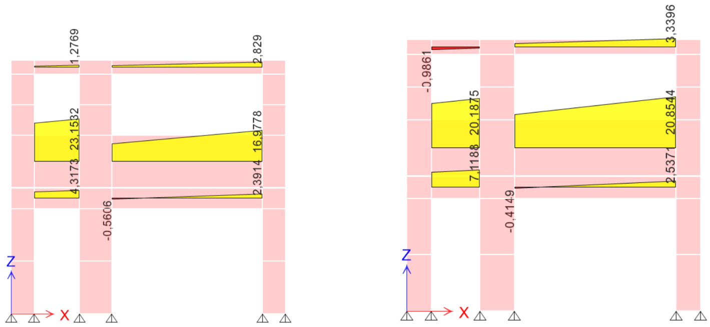

(a) Shear forces of spandrels at end elastic phase

(b) Shear forces of spandrels at end of capacity curve

Figure R.11: Shear forces of spandrels pushed in positive direction

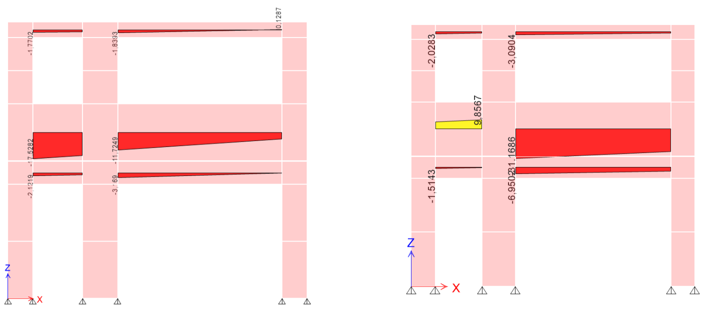

(a) Shear forces of spandrels at end elastic phase

(b) Shear forces of spandrels at end of capacity curve

Figure R.12: Shear forces of spandrels pushed in negative direction

Model with wide middle piers

Presentation of forces in the structural elements due to gravity loading and the pushover analyses in both directions of a model with wide middle piers (1,8m), an inter storey height of 2,75m, width of 6m and a depth of 8m. The corresponding capacity curve is presented in Figure R.13.

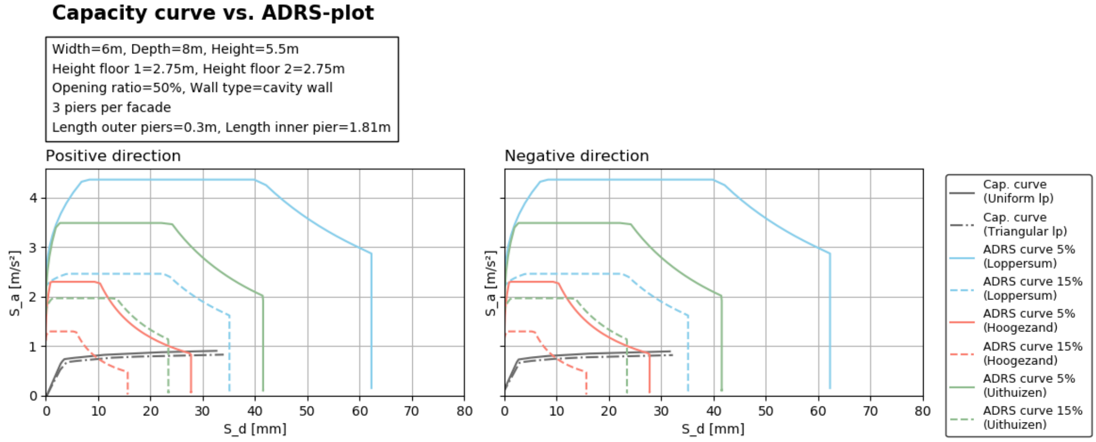

Figure R.13: Capacity curve of a model with wide middle piers, an inter storey height of 2,75m, width of 6m and a depth of 8m.

Axial loads piers

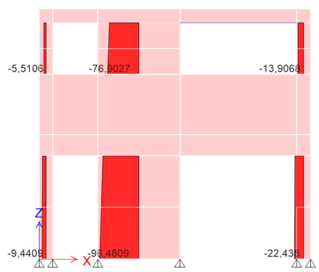

Figure R.14: Axial forces due to gravity loading

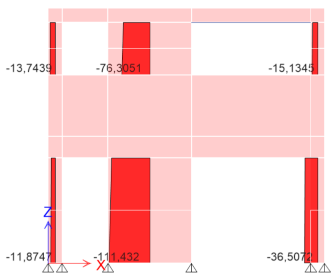

(a) Axial forces at end elastic phase

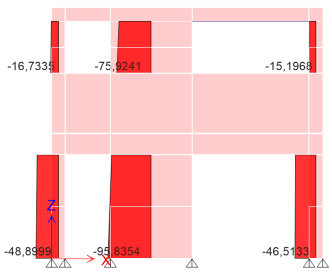

(b) Axial forces before failure middle piers

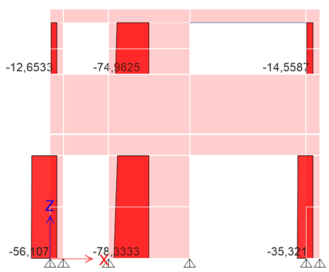

(c) Axial forces after failure of middle piers

Figure R.15: Axial forces of piers pushed in positive direction of model with large middle piers

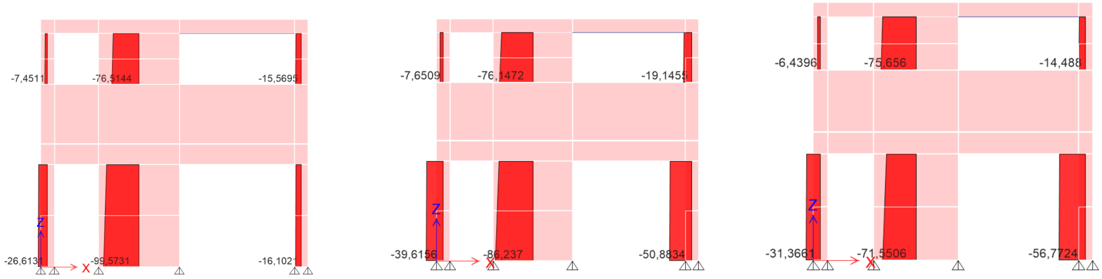

(a) Axial forces at end elastic phase

(b) Axial forces before failure middle piers

(c) Axial forces after failure middle piers

Figure R.16: Axial forces of piers pushed in negative direction of model with large middle piers

Shear forces piers

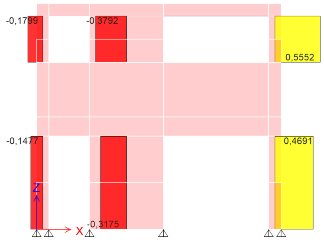

Figure R.17: Shear forces of piers due to gravity loading

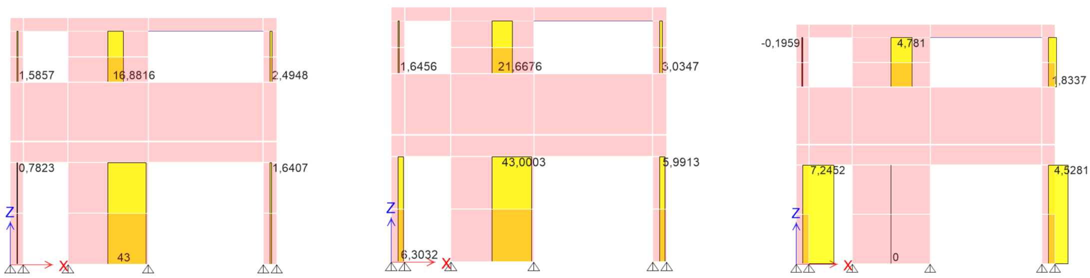

(a) Shear forces at end elastic phase

(b) Shear forces before failure middle piers

(c) Shear forces after failure middle piers

Figure R.18: Shear forces of piers pushed in positive direction

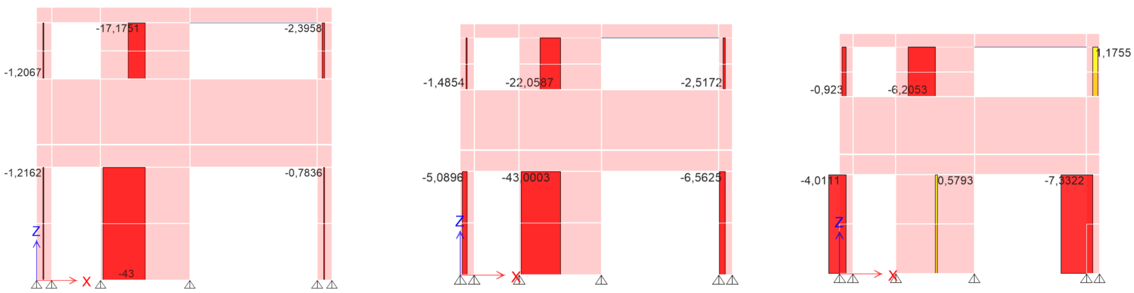

(a) Shear forces at end of elastic phase

(b) Shear forces before failure middle piers

(c) Shear forces after failure middle piers

Figure R.19: Shear forces of piers pushed in negative direction

Shear forces spandrels

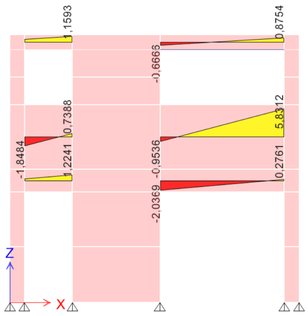

Figure R.20: Shear forces of spandrels due to gravity loading

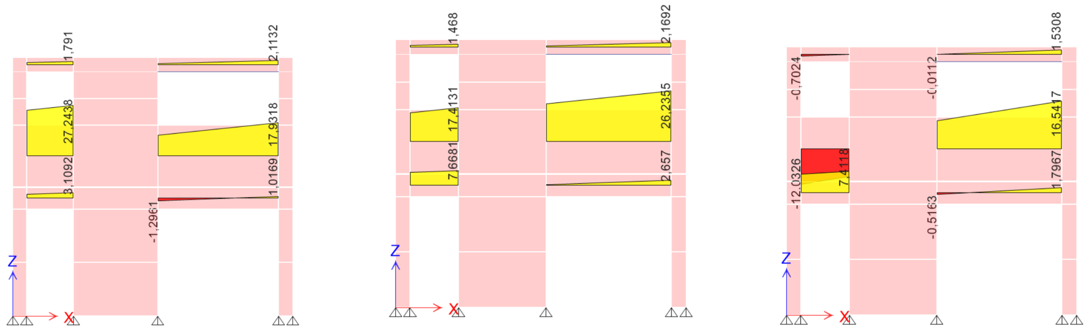

(a) Shear forces of spandrels at end elastic phase

(b) Shear forces of spandrels before failure middle piers

(c) Shear forces of spandrels after failure middle piers

Figure R.21: Shear forces of spandrels pushed in positive direction

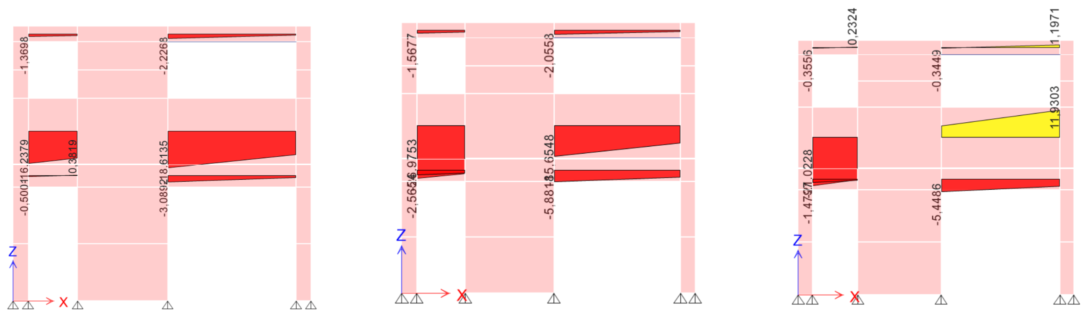

(a) Shear forces of spandrels at end elastic phase

(b) Shear forces of spandrels before failure middle piers

(c) Shear forces of spandrels after failure middle piers

Figure R.22: Shear forces of spandrels pushed in negative direction

S. Mechanical properties EUCENTRE test

Producer: Rothoblaas	Code	Typology	B [mm]	P [mm]	H [mm]	Thickness [mm]	Weight [kg]
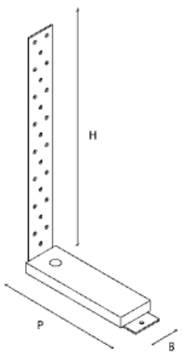	PF103010	Tie-down Concrete-to-timber	40	182	340	2	1.2
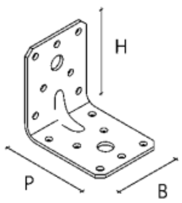	PF900110	Steel angle Timber-to-timber	55	70	70	2	0.1
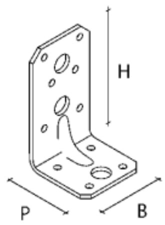	PF101050	Steel angle Strong-back-to-masonry	50	50	90	3	0.15

Figure S.1: Properties of steel angles used in the retrofitted specimen of the EUCENTRE tests

Producer: Rothoblaas	Code	Type	d_1 [mm]	L [mm]	b [mm]
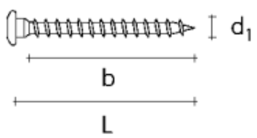	PF603570	Screws	5	70	66
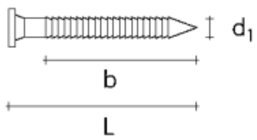	PF601475	Anker nails	4	75	60

Figure S.2: Properties of nails and screws used in the retrofitted specimen of the EUCENTRE tests

T. Deformation contributions to total elastic displacement timber frame

Sheathing-to-framing connection deformation

Calculation of the sheathing to framing connection deformation according to Casagrande et al. [32].

$$\Delta_{sh} = \frac{F \cdot \lambda(\alpha) \cdot s_c}{k_c \cdot b \cdot n_{bs}} \tag{T.1}$$

Where:
- F is the applied horizontal force;
- $\lambda(\alpha)$ is parameter depending on panel shape function;
- s_c is the fastener spacing;
- k_c is the fastener stiffness;
- b is the panel width;
- n_{bs} is the number of braced sides of the wall.

$$\lambda(\alpha) = 0.81 + 1.85 \cdot \alpha \tag{T.2}$$

Where:
- α is the panel shape function ($\frac{h}{b}$).

Rigid-body rotation

Calculation of the deformation due to rigid-body rotation, according to [32].

$$\Delta_h = \left(\frac{F \cdot h}{\tau \cdot l} - \frac{q \cdot l}{2}\right) \cdot \frac{h}{k_h \cdot \tau \cdot l} \tag{T.3}$$

Where:
- F is the applied horizontal force;
- h is the height of the panel;
- τ is parameter to determine internal lever arm (expected to be 1 for timber frames);
- q is the distributed vertical load ;
- l is the panel width;
- k_h is the stiffness of the hold down connection.

Rigid-body translation

Calculation of the deformation due to rigid-body translation, according to [32].

$$\Delta_a = \frac{F}{k_a \cdot n_a} \tag{T.4}$$

Where:
- k_a is the stiffness of the angle-bracket or screw;
- n_a is the number of the angle-brackets or screws.

Sheathing-panel shear deformation

Calculation of the shear deformation of the sheathing panel, according to [32].

$$\Delta_p = \frac{F \cdot h}{G_p \cdot t_p \cdot b \cdot n_{bs}} \tag{T.5}$$

Where:

F	is the applied horizontal force;
h	is the height of the panel;
G_p	is the panel shear modulus;
t_p	is the panel thickness;
b	is the panel width;
n_{bs}	is the number of braced sides of the wall.

U. Timber frame racking stiffness calculation method

$$R_{f,Rd} = \frac{n_{panels} \cdot n_{faces} \cdot b}{2(1 + \frac{h}{b})} \cdot \frac{K_{ser}}{s} \tag{U.1}$$

$$R_{G,Rd} = \frac{n_{panels} \cdot n_{faces} \cdot b \cdot t}{h} \cdot G_{mean} \tag{U.2}$$

$$R_{hd,Rd} = \frac{(n_{panels} \cdot b)^2}{h^2} \cdot K_{hd} \tag{U.3}$$

$$R_{c,Rd} = \frac{(n_{panels} \cdot b)^2}{h^2} \cdot K_{c,90} \tag{U.4}$$

$$R_{str,Rd} = \frac{n_{studs} \cdot b_2 \cdot h_2 \cdot (n_{panels} \cdot b)^2}{h^3} \cdot E_2 \tag{U.5}$$

Where:

- b is the panel width;
- h is the height of the panel;
- t is the panel thickness;
- s is the fastener spacing along the perimeter;
- G_{mean} is the panel shear modulus;
- K_{ser} is the fastener slip-modulus of the sheathing-to-timber fastener;
- K_{hd} is the stiffness of the hold down connector;
- b_2 is the thickness of the timber framing elements;
- h_2 is the width of the timber framing elements;
- E_2 is the timber framing elements Young's modulus;
- n_{panels} is the number of panels in an element;
- n_{faces} is the number of sides that have sheathing;
- n_{studs} is the number of studs applied on the edge of the shear wall.

V. Experimental test results on timber frame shear walls and fasteners

Wall specimens	Fasteners	Panels	Fixation to base	Loading	F_{max} (kN)	K_e (kN/mm)	Δ_{yield} (mm)	$\Delta_{ultimate}$ (mm)	μ	Number of tests	Failure	Reference
Timber structure (2,44 x 2,44); 8 studs (38 x 89 mm)	8d nails; s = 102 mm	plywood; t = 11,9 mm; (1,22 x 2,44)	Steel anchors	cyclic	32	2,36	6	54,6	9,1	4	Damage was confined to the sheathing nails, which fatigued and broke off or were pulled out from the frame.	[71]
Timber structure (2,44 x 2,44); 8 studs (38 x 89 mm)	8d nails; s = 102 mm	OSB panels; t = 12,7 mm	steel anchors	cyclic	28	2,33	6	46,6	7,8	4	Damage was confined to the sheathing nails, which fatigued and broke off or were pulled out from the frame.	[71]
2,44 x 2,44m ; frame: 38x 89 mm - spacing:610	Nails; 8d (2,87x63,5mm); spacing = 102 mm	OSB panels(2); t = 11,1 mm; on one side	hold down anchors; 16d (3,33x82,6 mm); s = 305 mm	monotonic	38,4	1,4	23,8	93,4	4	5	ductile behaviour of fasteners	[72]
Timber structure (1250 x 1950 mm) and 11 mm OSB sheathing on one side. Steel rods connected to concrete base	Screws; d =6 mm; l = 160 mm	OSB panel on one side (11 mm)	Steel rods	monotonic	10,8	0,445	23,9	80,6	3,4	1	pullout of the screws	[73]
Timber structure (1250 x 1950 mm) and 11 mm OSB sheathing on both side. Steel rods connected to concrete base	Screws; d =6 mm; l = 160 mm	OSB panel on both sides (11 mm)	Steel rods	monotonic	19	0,722	20,1	72,6	3,6	1	pullout of the screws	[73]
Timber structure (1250 x 1950 mm) and 11 mm OSB sheathing on both sides. Hold downs to timber base	Screws; d =6 mm; l = 160 mm	OSB panel on both sides(11 mm)	Hold-downs	monotonic	40,5	0,95	32,2	99,9	3,1	1	pullout of the screws	[73]
Timber structure (1250 x 1950 mm) and 11 mm OSB sheathing on both sides. Hold downs to timber base	Screws; d =6 mm; l = 160 mm	OSB panel on both sides (11 mm)	Hold-downs	cyclic	34,3	0,687	45,6	65,5	1,4	1	pullout of the screws	[73]

Table V.1: Experimental test results of timber shear walls tested under seismic loading (1/2).

Wall specimens	Fasteners	Panels	Fixation to base	Loading	F_{max} (kN)	K_e (kN/mm)	Δ_{yield} (mm)	$\Delta_{ultimate}$ (mm)	μ	Number of tests	Failure	Reference
timber frame wall (2,5 x 2,5 m); external stud:100x160mm; internal stud:60x160mm	ring nails (2,8x60mm); s = 100 mm	OSB sheating panel; t = 15 mm	hold down	monotonic	60,4	2,55	19,7	69,7	3,5	1	breaking of hold down	[74]
timber frame wall (2,5 x 2,5 m); external stud:100x160mm; internal stud:60x160mm	ring nails (2,8x60mm); s = 100 mm	OSB sheating panel; t = 15 mm	hold down	monotonic + 10 kN/m vertical loading	72,5	2,85	22,8	68,8	3,0	1	breaking of hold down	[74]
timber frame wall (2,5 x 2,5 m); external stud:100x160mm; internal stud:60x160mm	ring nails (2,8x60mm); s = 100 mm	OSB sheating panel; t = 15 mm	hold down	monotonic + 20 kN/m vertical loading	77,8	3,34	17,8	86,6	4,9	1	breaking of hold down	[74]
timber frame wall (2,5 x 2,5 m); external stud:100x160mm; internal stud:60x160mm	ring nails (2,8x60mm); s = 50 mm	OSB sheating panel; t = 15 mm	hold down	monotonic + 20 kN/m vertical loading	84,4	5,03	13,3	56	4,2	1	breaking of hold down	[74]
timber frame wall (2,5 x 2,5 m); external stud:100x160mm; internal stud:60x160mm	ring nails (2,8x60mm); s = 150 mm	OSB sheating panel; t = 15 mm	hold down	monotonic + 20 kN/m vertical loading	62,7	2,49	20,2	59,8	3,0	1	failure of sheathing to frame nails	[74]
timber frame wall (2,5 x 2,5 m); external stud:100x160mm; internal stud:60x160mm	ring nails (2,8x60mm); s = 100 mm	OSB sheating panel; t = 15 mm	without hold down	monotonic + 10 kN/m vertical loading	38,9	1,98	16,1	30,6	1,9	1	failure of sheathing to frame nails	[74]
Shear wall (2,5x2,5m); 5 studs(100x160mm)	Ring nails (2,8 x80 mm); s = 100mm	Particle board panels on both sides (1250x2500mm)	hold downs	cyclic	87,6	4,9	9,12	56	6,14			[75]
Shear wall (2,5x2,5m); 5 studs(100x160mm)	Ring nails (2,8 x80 mm); s = 100mm	Particle board panels on both sides (1250x2500mm)	hold downs	cyclic + vertical loading 40kN/m	80,5	3,8	11,1	55,9	5			[75]
Shear wall (2,5 x2,5 m); 5 studs (60x140mm)	nails (2,8 x 65mm); s =75 mm	2 X OSB; t = 18 mm							4,2			[76]
Shear wall (2,5 x2,5 m); 5 studs (60x140mm)	nails (2,8 x 65mm); s =75 mm	1 X OSB; t = 10 mm							5,8			[76]
Shear wall (2,5 x2,5 m); 5 studs (60x140mm)	nails (2,8 x 65mm); s =75 mm	1 X OSB; t = 18 mm							3,3			[76]

Table V.2: Experimental test results of timber shear walls tested under seismic loading (2/2).

Specimens	**Panel**	**Nail**	**Loading**	F_{max} **(kN)**	K_e **(kN/mm)**	Δ_{yield} **(mm)**	$\Delta_{ultimate}$ **(mm)**	μ	**Number of tests**	**failure**	**Reference**
Glulam stud G124h	particle board panel	Ring shank nail; 2,1 x 38	cyclic	0,72	1,16	0,45	6,1	14,2		fatigue failure of the nails	[75]
Glulam stud G124h	particle board panel	Ring nail a	cyclic	1,3	0,49	2,06	18,42	10,1		fatigue failure of the nails	[75]
Glulam stud G124h	particle board panel	Ring nail b	cyclic	1,3	0,89	0,95	9,63	10,2		fatigue failure of the nails	[75]
Joist (128x60mm)	Plank	nail (3x64,2)	cyclic (parallel to joist)	1,2		2	16,4	8,2		pull-out and bending failure of nails	[77]
Joist (128x60mm)	Plank	nail (3x64,2)	cyclic (perpendicular to joist)	1,1		2,5	23,0	9,2		pull-out and bending failure of nails	[77]

Table V.3: Experimental test results of timber-to-timber connections under seismic loading.

W. Hold-down anchor data

WHT340

CHARACTERISTIC VALUES													
	$R_{1,k}$ TIMBER				$R_{1,k}$ STEEL			$R_{1,k}$ UNCRACKED CONCRETE			$R_{1,k}$ CRACKED CONCRETE		
configuration	fasteners holes Ø5			$R_{1,k\ timber}$	washer	$R_{1,k\ steel}$		anchor VINYLPRO	$R_{1,k\ cls}$		anchor EPOPLUS	$R_{1,k\ cls}$	
	type	Ø x L [mm]	n_v [pcs]	[kN]		[kN]	γ_{steel}	Ø x L [mm]	[kN]	γ_{cls}	Ø x L [mm]	[kN]	γ_{cls}
• total fixing • without washer • M16 anchor	nails LBA	Ø4,0 x 40	20	**31,4**	-	**42,0**	γ_{m0}	M16 x 160	**64,84**	1,8	M16 x 160 M16 x 190	**35,66** **43,95**	1,8 1,8
		Ø4,0 x 60	20	**38,6**									
	screws LBS	Ø5,0 x 40	20	**31,4**									
		Ø5,0 x 50	20	**38,6**									
• partial fixing • without washer • M16 anchor	nails LBA	Ø4,0 x 40	14	**22,0**	-	**42,0**	γ_{m0}	M16 x 160	**64,84**	1,8	M16 x 160 M16 x 190	**35,66** **43,95**	1,8 1,8
		Ø4,0x 60	14	**27,0**									
	screws LBS	Ø5,0 x 40	14	**22,0**									
		Ø5,0 x 50	14	**27,0**									

Figure W.1: Characteristic values of WHT340 angle bracket (Source:[30]).

WHT440

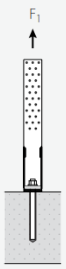

CHARACTERISTIC VALUES													
	$R_{1,k}$ TIMBER				$R_{1,k}$ STEEL			$R_{1,k}$ UNCRACKED CONCRETE			$R_{1,k}$ CRACKED CONCRETE		
configuration	fasteners holes Ø5			$R_{1,k\ timber}$	washer	$R_{1,k\ steel}$		anchor VINYLPRO	$R_{1,k\ cls}$		anchor EPOPLUS	$R_{1,k\ cls}$	
	type	Ø x L [mm]	n_v [pcs]	[kN]		[kN]	γ_{steel}	Ø x L [mm]	[kN]	γ_{cls}	Ø x L [mm]	[kN]	γ_{cls}
• total fixing • washer WHTBS50 • M16 anchor	nails LBA	Ø4,0 x 40	30	**47,1**	WHTBS50	**63,4**	γ_{m2}	M16 x 190	**74,90**	1,8	M16 x 190 M16 x 230	**41,19** **52,25**	1,8 1,8
		Ø4,0 x 60	30	**57,9**									
	screws LBS	Ø5,0 x 40	30	**47,1**									
		Ø5,0 x 50	30	**57,9**									
• partial fixing • washer WHTBS50 • M16 anchor	nails LBA	Ø4,0 x 40	20	**31,4**	WHTBS50	**63,4**	γ_{m2}	M16 x 190	**74,90**	1,8	M16 x 190 M16 x 230	**41,19** **52,25**	1,8 1,8
		Ø4,0 x 60	20	**38,6**									
	screws LBS	Ø5,0 x 40	20	**31,4**									
		Ø5,0 x 50	20	**38,6**									
• partial fixing • without washer • M16 anchor	nails LBA	Ø4,0 x 40	20	**31,4**	-	**42,0**	γ_{m0}	M16 x 160	**64,84**	1,8	M16 x 160	**35,66**	1,8
		Ø4,0x 60	20	**38,6**									
	screws LBS	Ø5,0 x 40	20	**31,4**									
		Ø5,0 x 50	20	**38,6**									

Figure W.2: Characteristic values of WHT440 angle bracket (Source:[30]).

WHT540

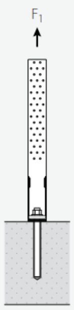

CHARACTERISTIC VALUES													
	$R_{1,k}$ TIMBER				$R_{1,k}$ STEEL			$R_{1,k}$ UNCRACKED CONCRETE			$R_{1,k}$ CRACKED CONCRETE		
configuration	fasteners holes Ø5			$R_{1,k\ timber}$	washer	$R_{1,k\ steel}$		anchor VINYLPRO	$R_{1,k\ cls}$		anchor EPOPLUS	$R_{1,k\ cls}$	
	type	Ø x L [mm]	n_v [pcs]	[kN]		[kN]	γ_{steel}	Ø x L [mm]	[kN]	γ_{cls}	Ø x L [mm]	[kN]	γ_{cls}
• total fixing • washer WHTBS50L • M20 anchor	nails LBA	Ø4,0 x 40	45	**70,7**	WHTBS50L	**63,4**	γ_{m2}	M20 x 240	**120,63**	1,8	M20 x 240 M20 x 290 (1)	**60,32** **75,39**	2,1 2,1
		Ø4,0 x 60	45	**86,9**									
	screws LBS	Ø5,0 x 40	45	**70,7**									
		Ø5,0 x 50	45	**86,9**									
• partial fixing • washer WHTBS50L • M20 anchor	nails LBA	Ø4,0 x 40	27	**42,4**	WHTBS50L	**63,4**	γ_{m2}	M20 x 240	**120,63**	1,8	M20 x 240 M20 x 290 (1)	**60,32** **75,39**	2,1 2,1
		Ø4,0 x 60	27	**52,1**									
	screws LBS	Ø5,0 x 40	27	**42,4**									
		Ø5,0 x 50	27	**52,1**									
• total fixing • washer WHTBS50 • M16 anchor	nails LBA	Ø4,0 x 40	45	**70,7**	WHTBS50	**63,4**	γ_{m2}	M16 x 190	**74,89**	1,8	M16 x 190	**41,19**	1,8
		Ø4,0 x 60	45	**86,9**									
	screws LBS	Ø5,0 x 40	45	**70,7**									
		Ø5,0 x 50	45	**86,9**									
• partial fixing • washer WHTBS50 • M16 anchor	nails LBA	Ø4,0 x 40	27	**42,4**	WHTBS50	**63,4**	γ_{m2}	M16 x 190	**74,89**	1,8	M16 x 190	**41,19**	1,8
		Ø4,0 x 60	27	**52,1**									
	screws LBS	Ø5,0 x 40	27	**42,4**									
		Ø5,0 x 50	27	**52,1**									

(1) Length obtainable from MGS threaded rods (to be cut to measure)

Figure W.3: Characteristic values of WHT540 angle bracket (Source:[30]).

WHT620

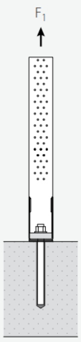

CHARACTERISTIC VALUES

configuration	$R_{1,k}$ TIMBER: type	fasteners holes Ø5: Ø x L [mm]	n_v [pcs]	$R_{1,k\,timber}$ [kN]	$R_{1,k}$ STEEL: washer	$R_{1,k\,steel}$ [kN]	γ_{steel}	$R_{1,k}$ UNCRACKED CONCRETE: anchor VINYLPRO Ø x L [mm]	$R_{1,k\,cls}$ [kN]	γ_{cls}	$R_{1,k}$ CRACKED CONCRETE: anchor EPOPLUS Ø x L [mm]	$R_{1,k\,cls}$ [kN]	γ_{cls}
• total fixing • washer WHTBS70L • M24 anchor	nails LBA	Ø4,0 x 40	55	**86,4**	WHTBS70L	**85,2**	γ_{m2}	M24 x 270	**148,98**	1,8	M24 x 270 M24 x 330 (1)	**70,57** **90,93**	2,1 2,1
		Ø4,0 x 60	55	**106,2**									
	screws LBS	Ø5,0 x 40	55	**86,4**									
		Ø5,0 x 50	55	**106,2**									
• partial fixing • washer WHTBS70L • M24 anchor	nails LBA	Ø4,0 x 40	33	**51,8**	WHTBS70L	**85,2**	γ_{m2}	M24 x 270	**148,98**	1,8	M24 x 270 M24 x 330 (1)	**70,57** **90,93**	2,1 2,1
		Ø4,0 x 60	33	**63,7**									
	screws LBS	Ø5,0 x 40	33	**51,8**									
		Ø5,0 x 50	33	**63,7**									
• total fixing • washer WHTBS70 • M20 anchor	nails LBA	Ø4,0 x 40	55	**86,4**	WHTBS70	**85,2**	γ_{m2}	M20 x 240	**114,35**	1,8	M20 x 240	**57,17**	2,1
		Ø4,0 x 60	55	**106,2**									
	screws LBS	Ø5,0 x 40	55	**86,4**									
		Ø5,0 x 50	55	**106,2**									
• partial fixing • washer WHTBS70 • M20 anchor	nails LBA	Ø4,0 x 40	33	**51,8**	WHTBS70	**85,2**	γ_{m2}	M20 x 240	**114,35**	1,8	M20 x 240	**57,17**	2,1
		Ø4,0 x 60	33	**63,7**									
	screws LBS	Ø5,0 x 40	33	**51,8**									
		Ø5,0 x 50	33	**63,7**									

(1) Length obtainable from MGS threaded bars (to be cut to measure)

Figure W.4: Characteristic values of WHT620 angle bracket (Source:[30]).

CONNECTION STIFFNESS

EVALUATION OF SLIP MODULUS K_{ser}

• K_{ser} experimental average value for WHT joints on GL24h Glulam

TYPE WHT	configuration	fastener type Ø x L [mm]	n_v [pcs]	K_{ser} [N/mm]
WHT340	• total fixing • with WHTBS50 washer	nails LBA Ø4,0 x 60	20	5705
WHT440	• total fixing • with WHTBS50 washer	nails LBA Ø4,0 x 60	30	6609
WHT540	-	-	-	-
WHT620	• partial fixing • with WHTBS70 washer	nails LBA Ø4,0 x 60	30	9967
	• partial fixing • with WHTBS70 washer	nails LBA Ø4,0 x 60	52	13247

• K_{ser} according to EN 1995:2008 for nails in a steel-to-timber (GL24h) joint

Nails (without predrill) $\frac{\rho_m^{1,5}\, d^{\,0,8}}{30}$ (EN 1995:2008 § 7.1)

TYPE WHT	fastener type Ø x L [mm]	n_v [pcs]	$K_{ser,max}$ [N/mm]
WHT340	screws LBA Ø4,0 x 60	14 20	12177 17395
WHT440	screws LBA Ø4,0 x 60	20 30	17395 26093
WHT540	screws LBA Ø4,0 x 60	27 45	23484 39139
WHT620	screws LBA Ø4,0 x 60	33 55	28702 47837

Figure W.5: Experimental average stiffness value for WHT joints on GL24h Glulam (Source:[30]).

CHEMICAL ANCHOR INSTALLATION PARAMETERS

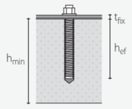

type of bar Ø x L [mm]		code	steel class	type WHT	type of washer	t_{fix} [mm]	h_{ef} [mm]	h_{min} [mm]
M16	160	FE210116 (2)	5.8	WHT340	-	9	129	240
	190	FE210118 (2)	5.8	WHT340 / WHT440	-	9	159	240
				WHT440 / WHT540	WHTBS50	19	149	240
	230	FE210121 (2)	5.8	WHT440	WHTBS50	19	189	240
M20	240	FE210117 (2)	5.8	WHT540	-	9	202	250
				WHT540	WHTBS50L	19	192	250
				WHT620	WHTBS70	29	182	250
	290	MGS M20 (3)	4.8 / 8.8	WHT540	WHTBS50L	19	240	300
M24	270	FE210122 (2)	5.8	WHT620	-	9	228	300
				WHT620	WHTBS70L	29	208	300
	330	MGS M24 (3)	4.8 / 8.8	WHT620	WHTBS70L	29	268	330

(2) Precut INA threaded rod, with nut and washer
(3) When employing threaded rods that are cut on size, the use of MUT DIN934 nut and ULS DIN 125 washer is recommended

Figure W.6: Chemical anchor installation parameters (Source:[30]).

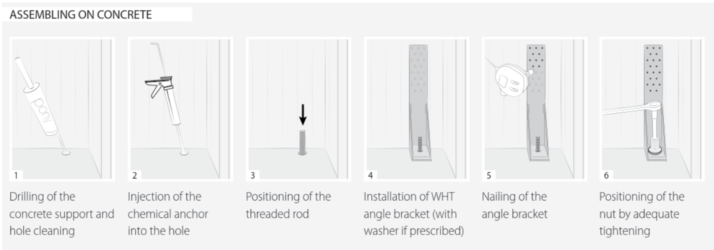

Figure W.7: Assembling of anchor (Source:[30]).

X. Results analysis - Strengthened structures

Wide middle piers

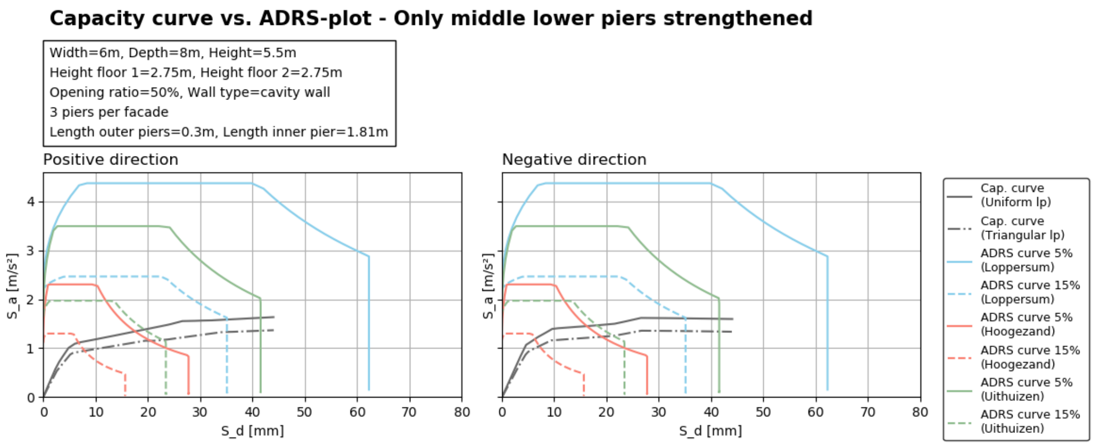

Figure X.1: Capacity curve of a model with large middle piers, for which only the lower middle piers are strengthened with timber frame shear walls.

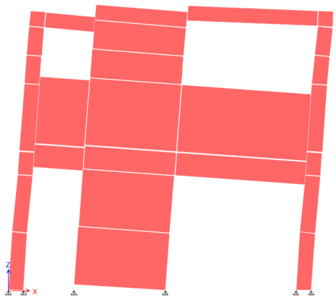

(a) Seismic behaviour due to uniform load pattern in positive direction

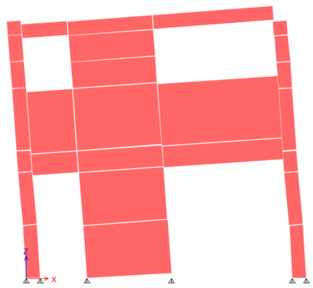

(b) Seismic behaviour due to uniform load pattern in negative direction

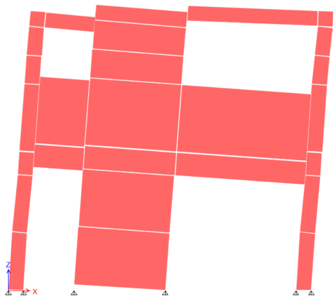

(c) Seismic behaviour due to triangular load pattern in positive direction

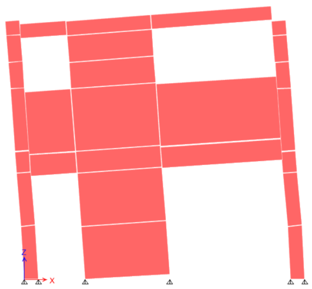

(d) Seismic behaviour due to triangular load pattern in negative direction

Figure X.2: Seismic behaviour of a model with wide middle piers (1,8m), strengthened with timber frame shear walls.

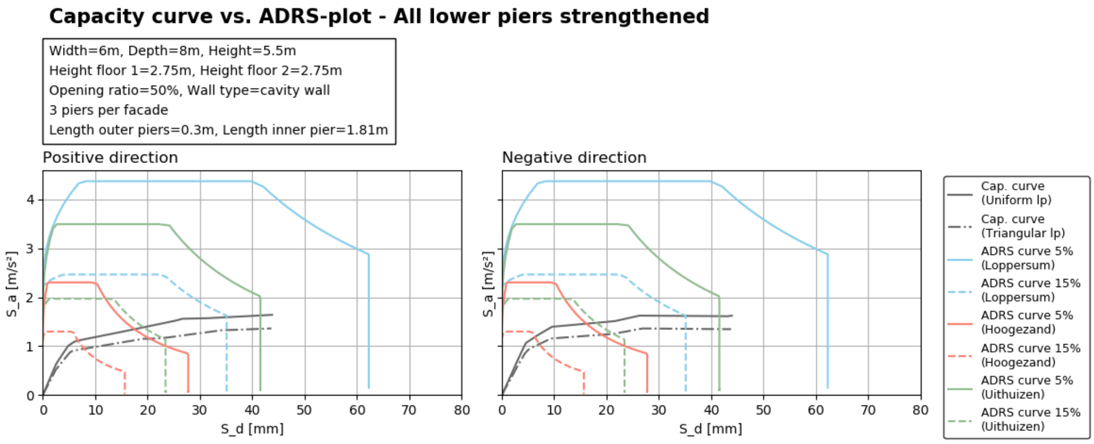

Figure X.3: Capacity curve of a model with large middle piers, for which all piers on ground floor level are strengthened with timber frame shear walls.

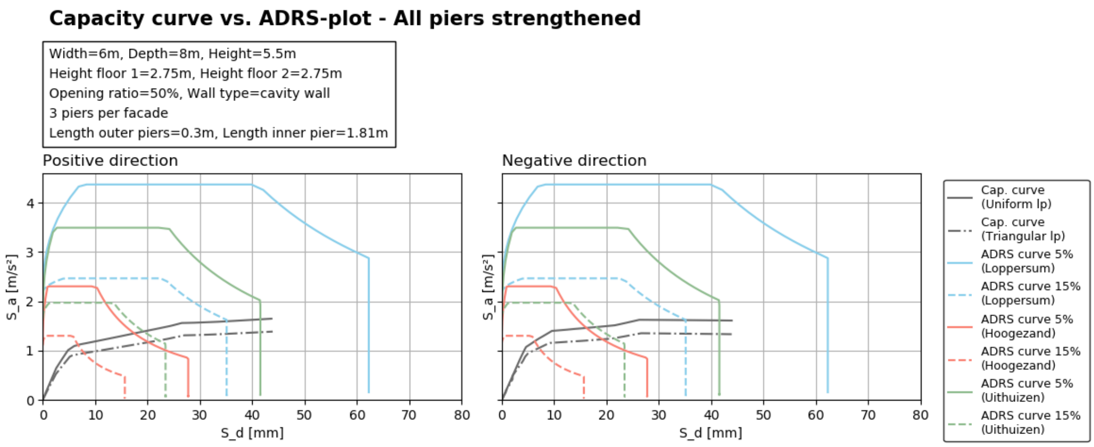

Figure X.4: Capacity curve of a model with large middle piers, for which all piers are strengthened with timber frame shear walls.

CaSi element masonry

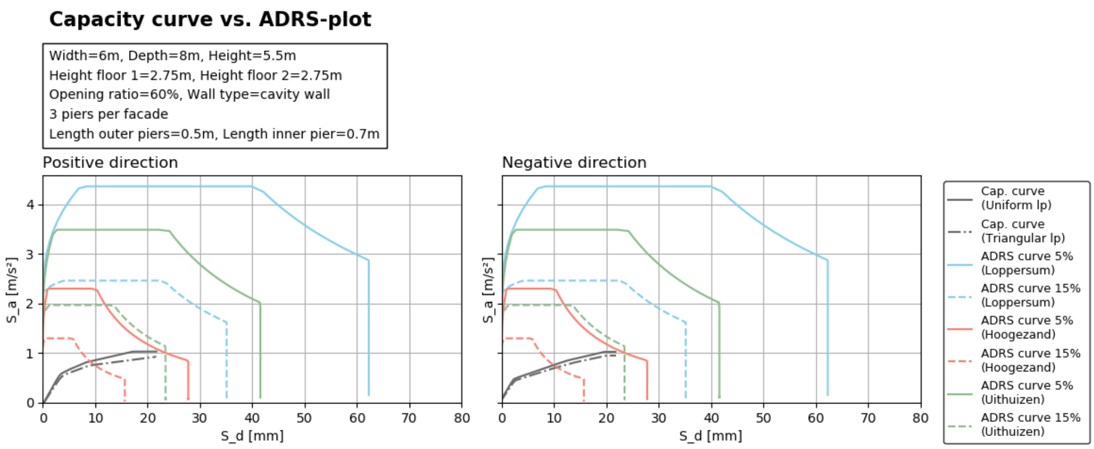

Figure X.5: Capacity curve of an un-strengthened model with CaSi element masonry used since 1985

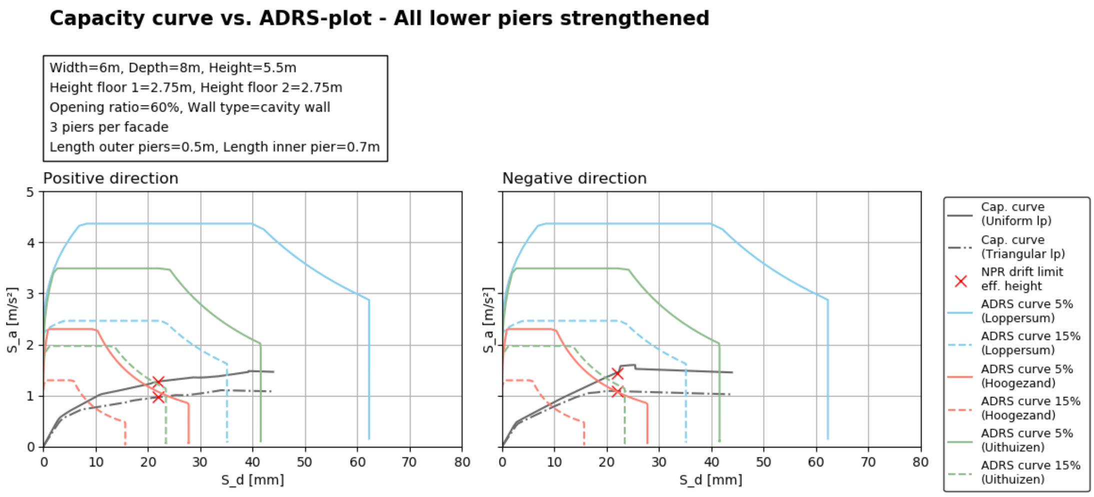

Figure X.6: Capacity curve of the same model with CaSi element masonry, for which all piers at ground floor level are strengthened with timber frame shear walls and two WHT 620 anchors per pier.

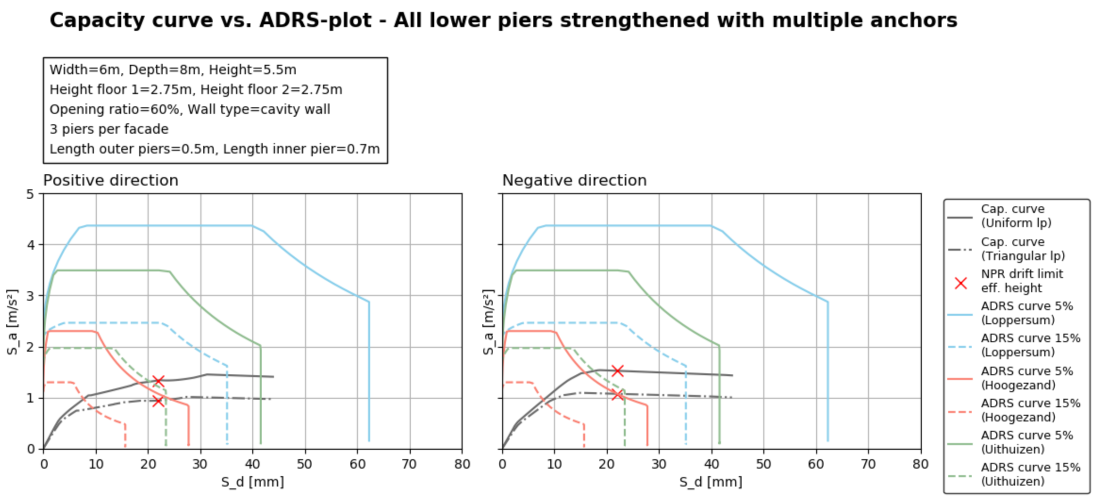

Figure X.7: Capacity curve of the same model with CaSi element masonry, for which all piers at ground floor level are strengthened with timber frame shear walls and 10 WHT 620 anchors per pier.

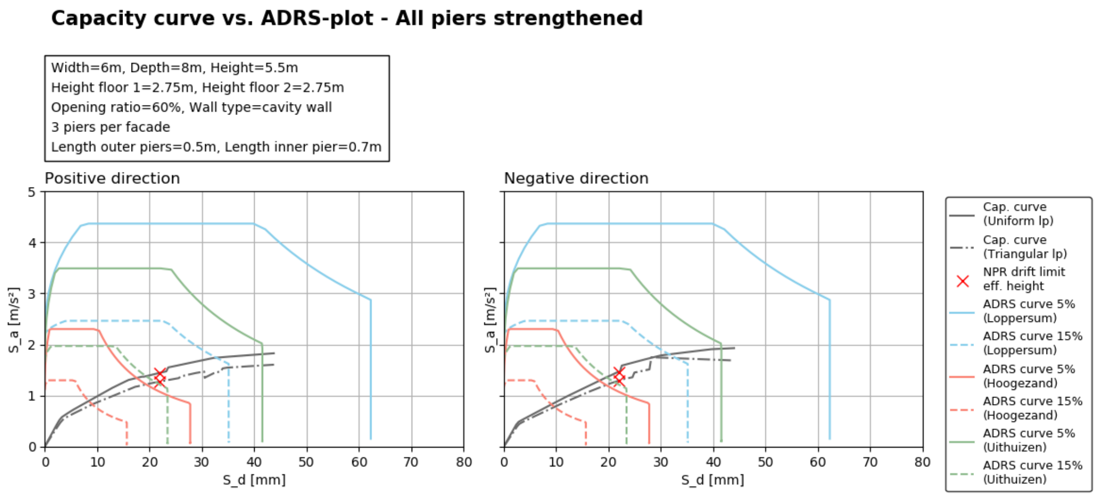

Figure X.8: Capacity curve of the same model with CaSi element masonry, for which all piers are strengthened with timber frame shear walls and two WHT 620 anchors per pier.

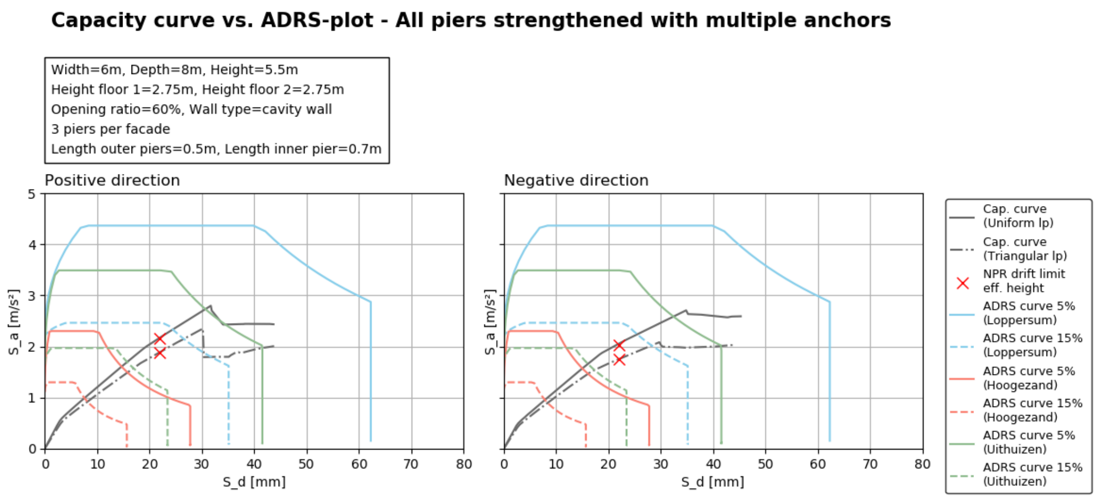

Figure X.9: Capacity curve of the same model with CaSi element masonry, for which all piers at ground floor level are strengthened with timber frame shear walls and 10 WHT 620 anchors per pier

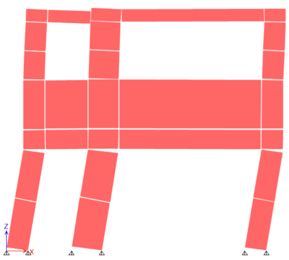

(a) Seismic behaviour due to uniform load pattern in positive direction

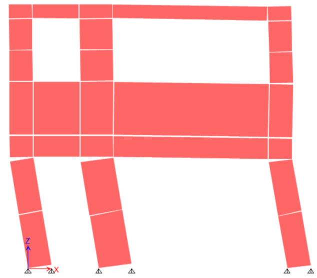

(b) Seismic behaviour due to uniform load pattern in negative direction

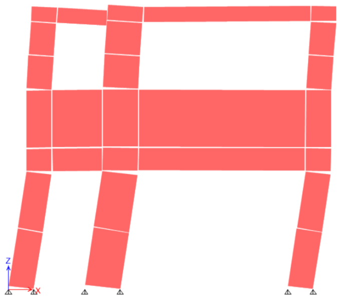

(c) Seismic behaviour due to triangular load pattern in positive direction

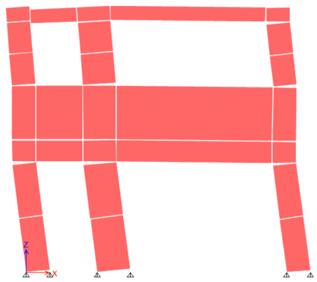

(d) Seismic behaviour due to triangular load pattern in negative direction

Figure X.10: Seismic behaviour of model with CaSi element masonry, strengthened with timber frame shear walls.

Opening ratio of 70%

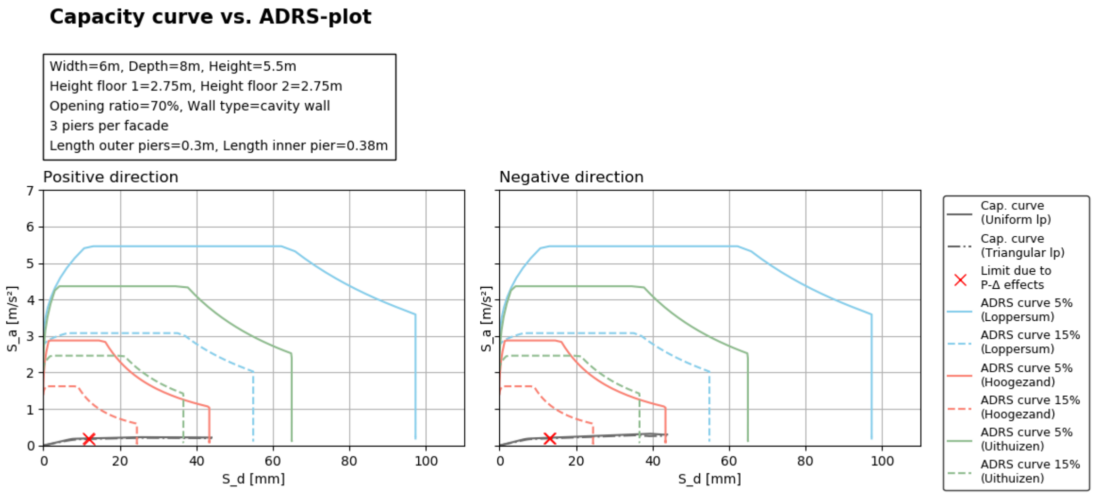

Figure X.11: Capacity curves of un-strengthened model of a terraced masonry house with an opening ratio of 70%. The limit due to the p-delta effects depicted in red

Load pattern	Uniform-	Triangular-	Uniform+	Triangular+
Ptot (kg)	110028	110028	110028	110028
Ptot (kN)	1080	1080	1080	1080
u1 (mm)	12,86	13,18	11,72	11,97
Vtot (kN)	25,48	25,62	23,38	23,4
h1 (mm)	2750	2750	2750	2750
θ	0,20	0,20	0,20	0,20
Factor	1,25	1,25	1,25	1,25

Table X.1: P-delta effect check for un-strengthened model with an opening ratio of 70%.

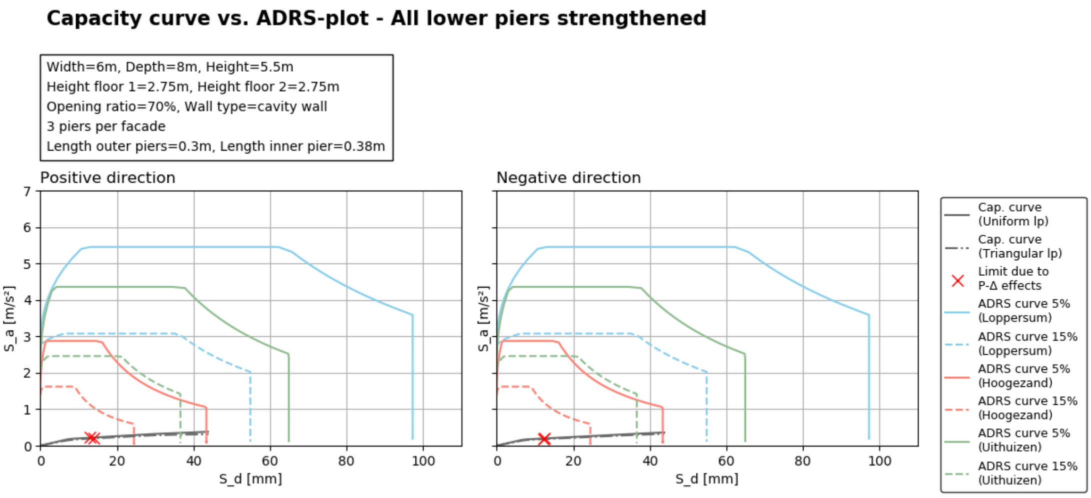

Figure X.12: Capacity curve of the same model with an opening ratio of 70% and all lower piers strengthened with timber frame shear walls and two WHT 620 anchors per pier. P-delta effects limit the displacement capacity of the structure.

Load pattern	Uniform-	Triangular-	Uniform+	Triangular+
Ptot (kg)	110028	110028	110028	110028
Ptot (kN)	1080	1080	1080	1080
u1 (mm)	12,47	12,13	14,058	13,077
Vtot (kN)	23,9	23,54	26,98	25,59
h1 (mm)	2750	2750	2750	2750
θ	0,20	0,20	0,20	0,20
Factor	1,25	1,25	1,25	1,25

Table X.2: P-delta effect check for model with all lower piers strengthened with timber frame shear walls and two WHT 620 anchors per pier.

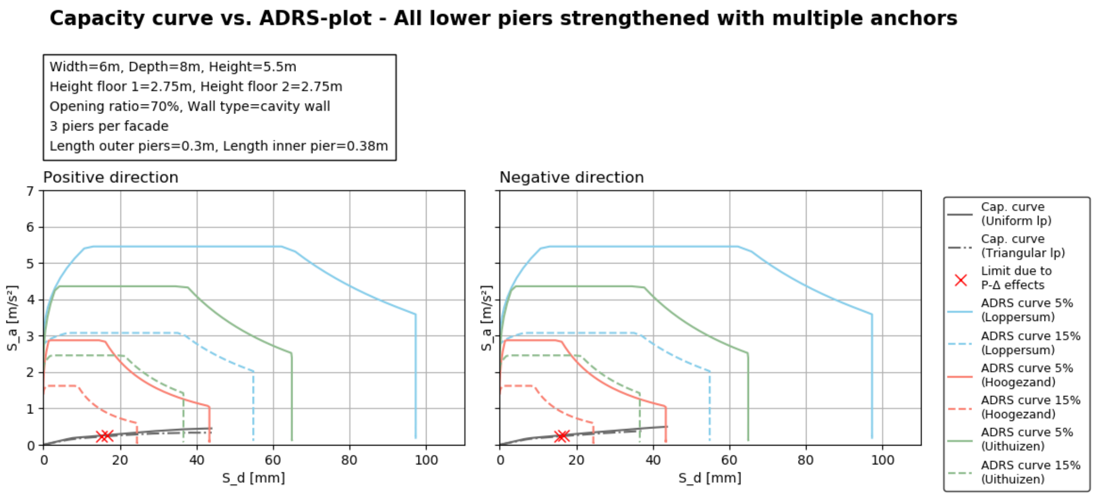

Figure X.13: Capacity curve of the same model with an opening ratio of 70% and all lower piers strengthened with timber frame shear walls and 10 WHT 620 anchors per pier. P-delta effects limit the displacement capacity of the structure, depicted in red.

Load pattern	Uniform-	Triangular-	Uniform+	Triangular+
Ptot (kg)	110028	110028	110028	110028
Ptot (kN)	1080	1080	1080	1080
u1 (mm)	16,63	15,8	16,60	15,26
Vtot (kN)	31,96	30,45	32,027	29,287
h1 (mm)	2750	2750	2750	2750
θ	0,20	0,20	0,20	0,20
Factor	1,25	1,25	1,25	1,25

Table X.3: P-delta effect check for model with all lower piers strengthened with timber frame shear walls and multiple WHT 620 anchors per pier.

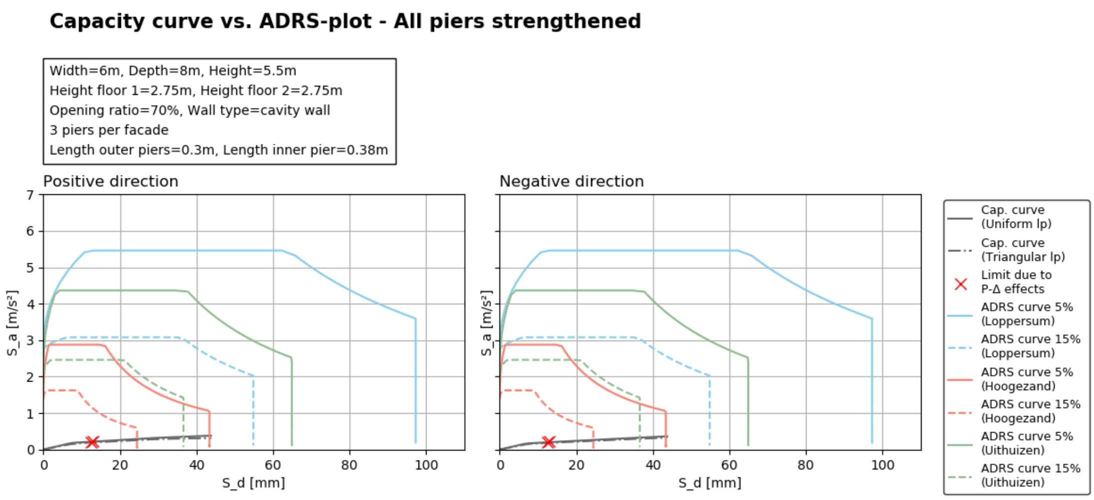

Figure X.14: Capacity curve of the same model with an opening ratio of 70% and all piers strengthened with timber frame shear walls and two WHT 620 anchors per pier. P-delta effects limit the displacement capacity of the structure.

Load pattern	Uniform-	Triangular-	Uniform+	Triangular+
Ptot (kg)	115529	115529	115529	115529
Ptot (kN)	1133	1133	1133	1133
u1 (mm)	13,028	12,49	13,04	12,43
Vtot (kN)	26,424	25,5	26,37	25,41
h1 (mm)	2750	2750	2750	2750
θ	0,20	0,20	0,20	0,20
Factor	1,25	1,25	1,25	1,25

Table X.4: P-delta effect check for model with all piers strengthened with timber frame shear walls and two WHT 620 anchors per pier.

Rocking drift limits according to NZSEE guidelines

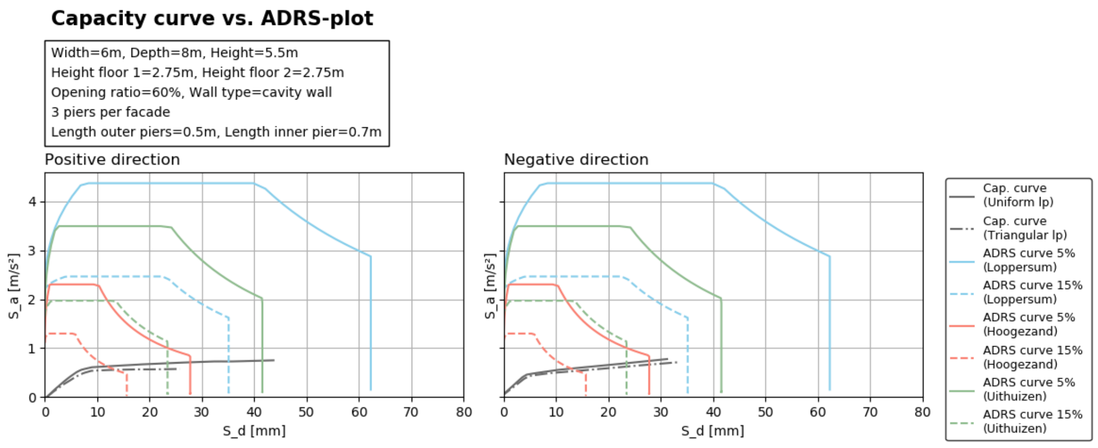

Figure X.15: Capacity curve of an un-strengthened model with an opening ratio of 60%, assessed with the NZSEE rocking drift limits

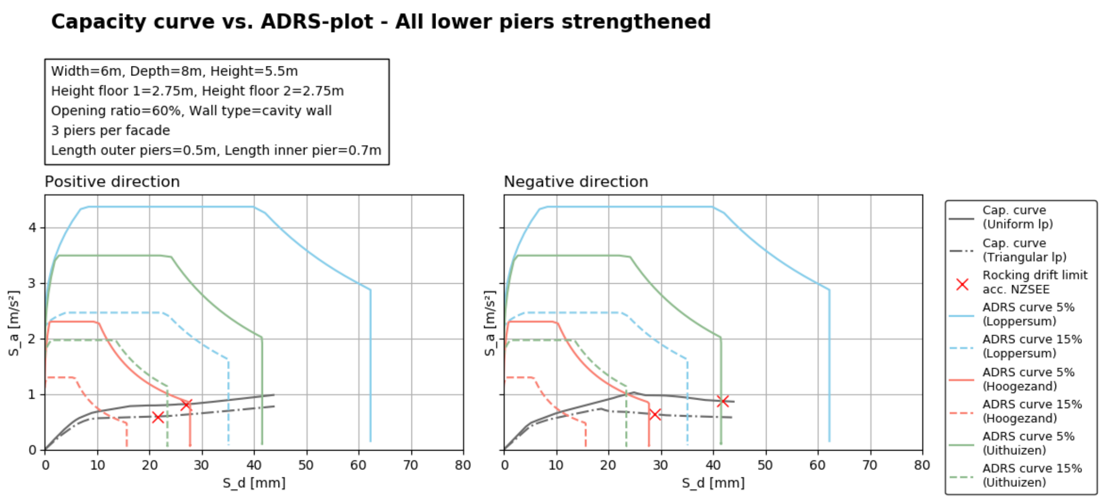

Figure X.16: Capacity curve of the same model with an opening ratio of 60% and all lower piers strengthened with timber frame shear walls and two WHT 620 anchors per pier. Assessed with the NZSEE rocking drift limits.

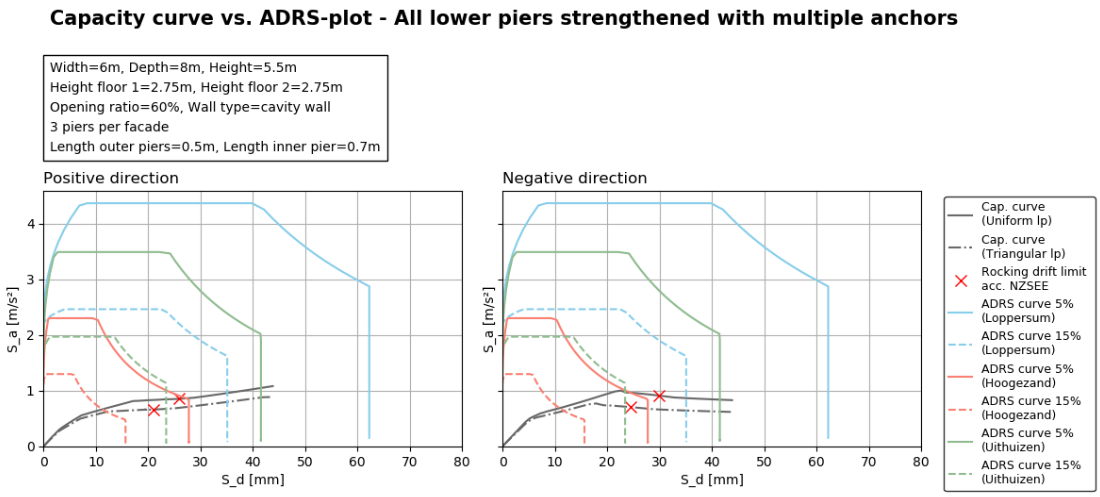

Figure X.17: Capacity curve of the same model with an opening ratio of 60% and all lower piers strengthened with timber frame shear walls and 10 WHT 620 anchors per pier. Assessed with the NZSEE rocking drift limits.

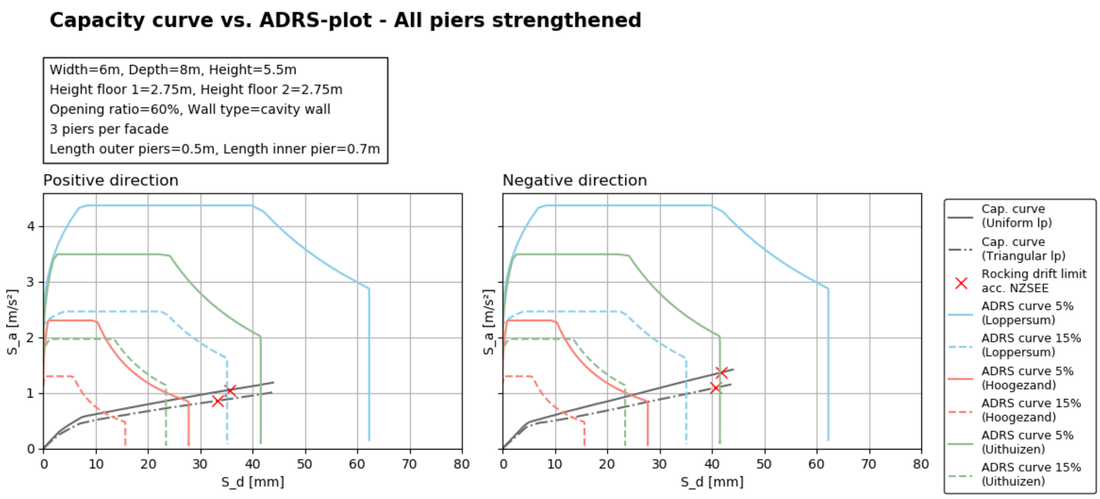

Figure X.18: Capacity curve of the same model with an opening ratio of 60% and all piers strengthened with timber frame shear walls and two WHT 620 anchors per pier. Assessed with the NZSEE rocking drift limits.

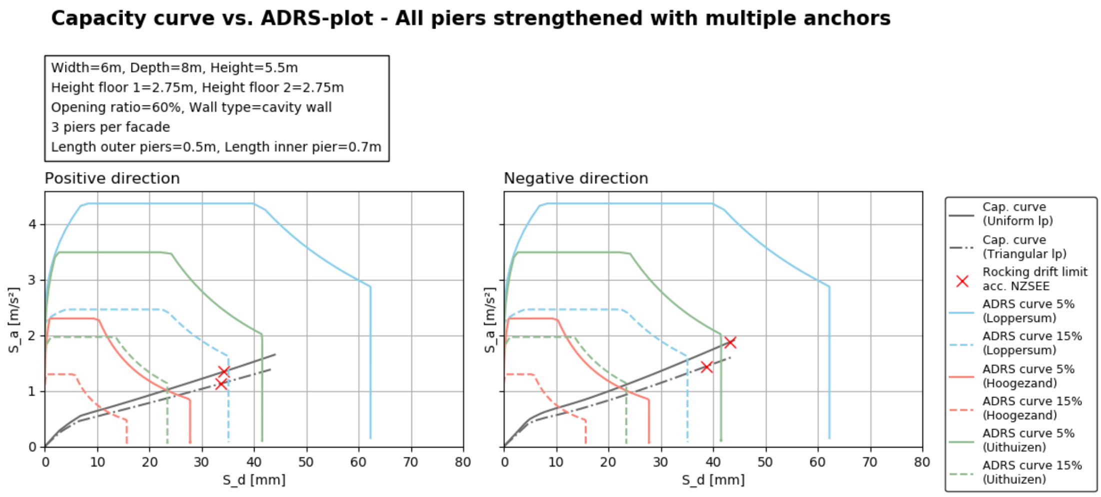

Figure X.19: Capacity curve of the same model with an opening ratio of 60% and all lower piers strengthened with timber frame shear walls and 10 WHT 620 anchors per pier. Assessed with the NZSEE rocking drift limits.

Y. Element forces strengthened models

Model with 60% opening ratio and height of 2,75 m

Presentation of forces in the structural elements due to gravity loading and the pushover analyses in both directions of a model with an opening ratio of 60%, an inter storey height of 2,75m, width of 6m and a depth of 8m, for which all piers are strengthened with a timber frame shear wall and two anchors per pier. The corresponding capacity curve is presented in Figure Y.1

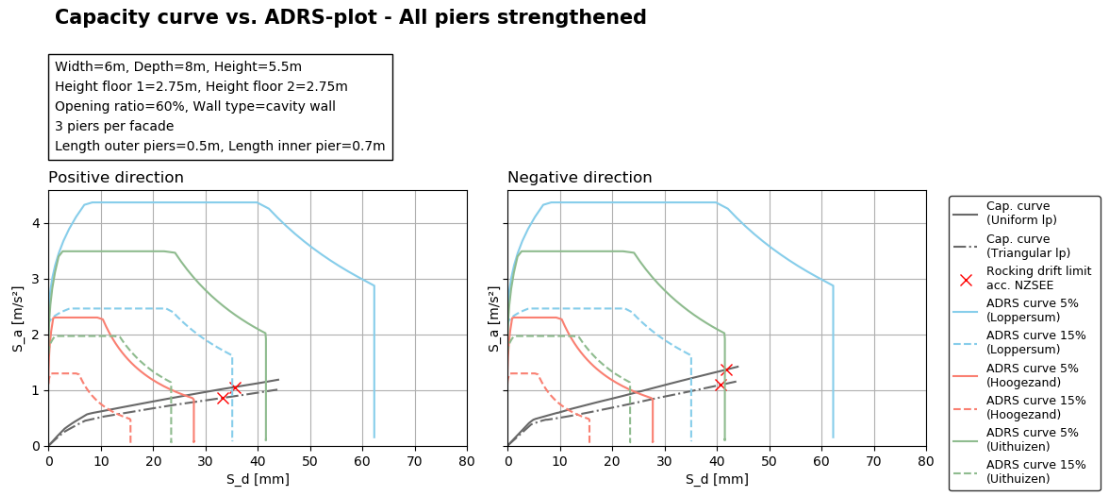

Figure Y.1: Capacity curve of a strengthened model with an opening ratio of the ground floor façade walls of 60%, an inter storey height of 2,75m, width of 6m and a depth of 8m.

Axial loads piers

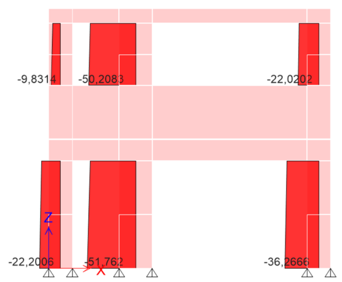

Figure Y.2: Axial forces due to gravity loading

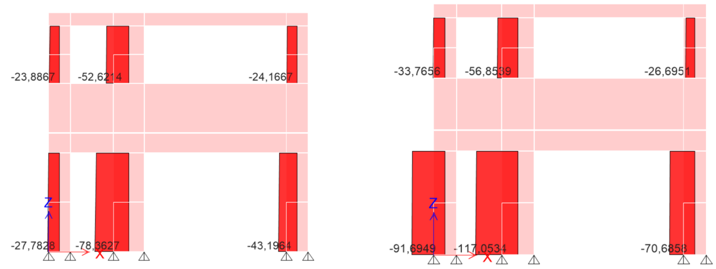

(a) Axial forces at end elastic phase

(b) Axial forces end capacity curve

Figure Y.3: Axial forces of piers pushed in positive direction

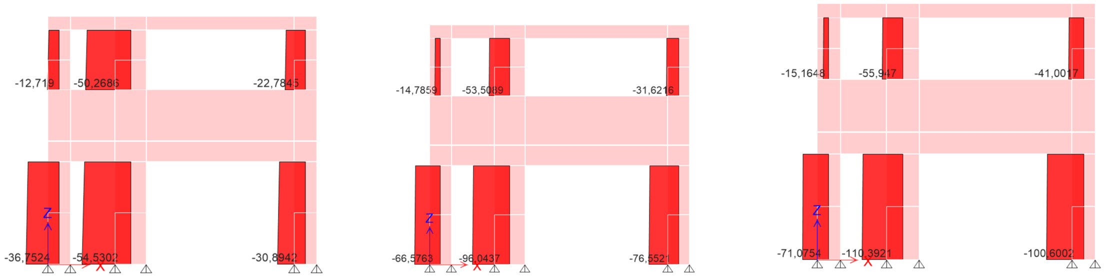

(a) Axial forces at end elastic phase

(b) Axial forces at step 60

(c) Axial forces at end capacity curve

Figure Y.4: Axial forces of piers pushed in negative direction

Shear forces piers

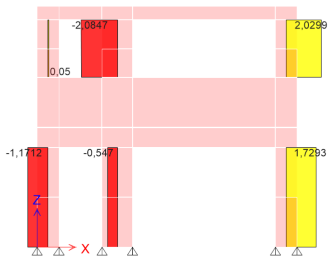

Figure Y.5: Shear forces of piers due to gravity loading

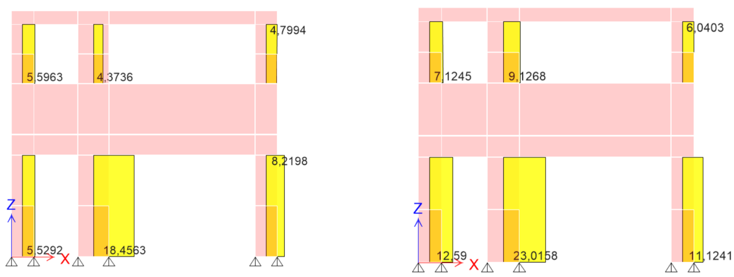

(a) Shear forces at end elastic phase

(b) Shear forces end of capacity curve

Figure Y.6: Shear forces of piers pushed in positive direction

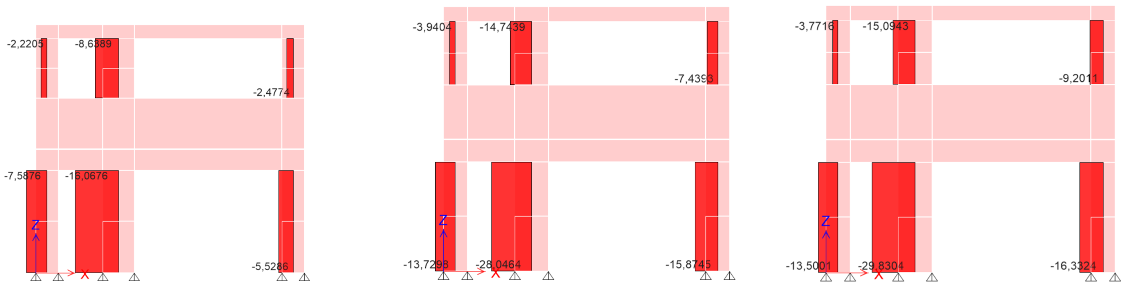

(a) Shear forces at end elastic phase

(b) Shear forces at step 60 capacity curve

(c) Shear forces end of capacity curve

Figure Y.7: Shear forces of piers pushed in negative direction

Shear forces spandrels

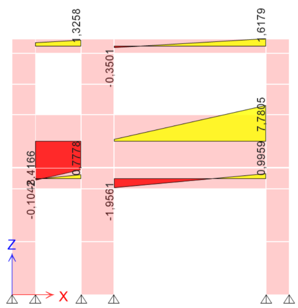

Figure Y.8: Shear forces of spandrels due to gravity loading

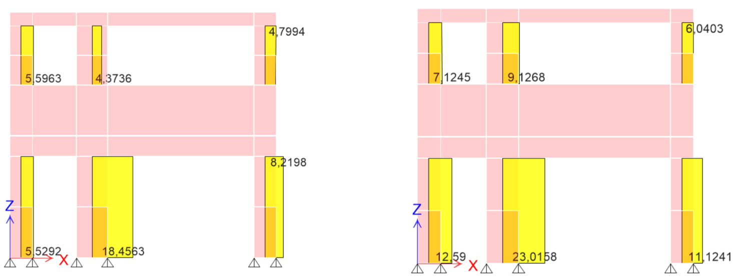

(a) Shear forces of spandrels at end elastic phase

(b) Shear forces of spandrels at end of capacity curve

Figure Y.9: Shear forces of spandrels pushed in positive direction

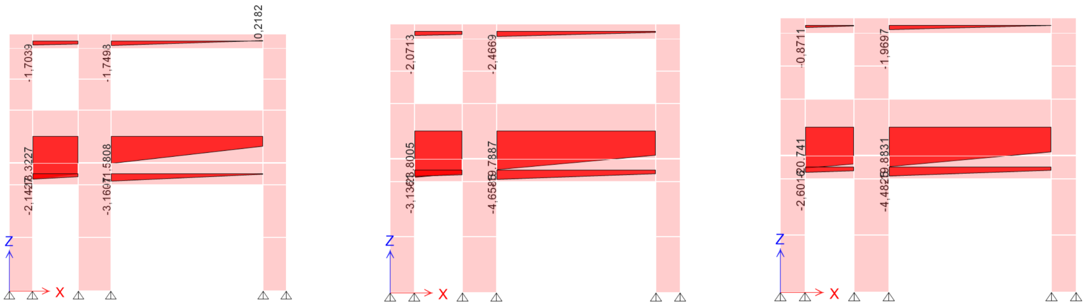

(a) Shear forces of spandrels at end elastic phase

(b) Shear forces of spandrels at step 60 of capacity curve

(c) Shear forces of spandrels at end of capacity curve

Figure Y.10: Shear forces of spandrels pushed in negative direction

Anchor forces

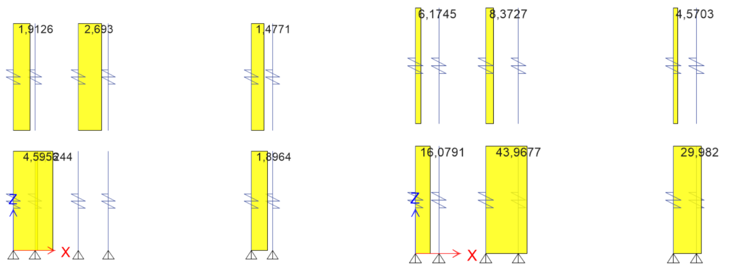

(a) Anchor forces of spandrels at end elastic phase

(b) Anchor forces of spandrels at end of capacity curve

Figure Y.11: Anchor forces of spandrels pushed in positive direction

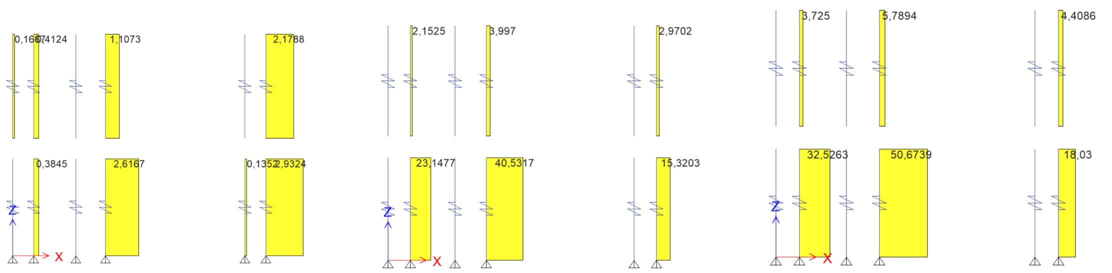

(a) Anchor forces of spandrels at end elastic phase

(b) Anchor forces of spandrels at step 60 of capacity curve

(c) Anchor forces of spandrels at end of capacity curve

Figure Y.12: Anchor forces of spandrels pushed in negative direction

Model with large middle piers

Presentation of forces in the structural elements due to gravity loading and the pushover analyses in both directions of a model with large middle piers, an inter storey height of 2,75m, width of 6m and a depth of 8m, for which only the lower piers are strengthened with a timber frame shear wall and two anchors per pier. The corresponding capacity curve is presented in Figure Y.13

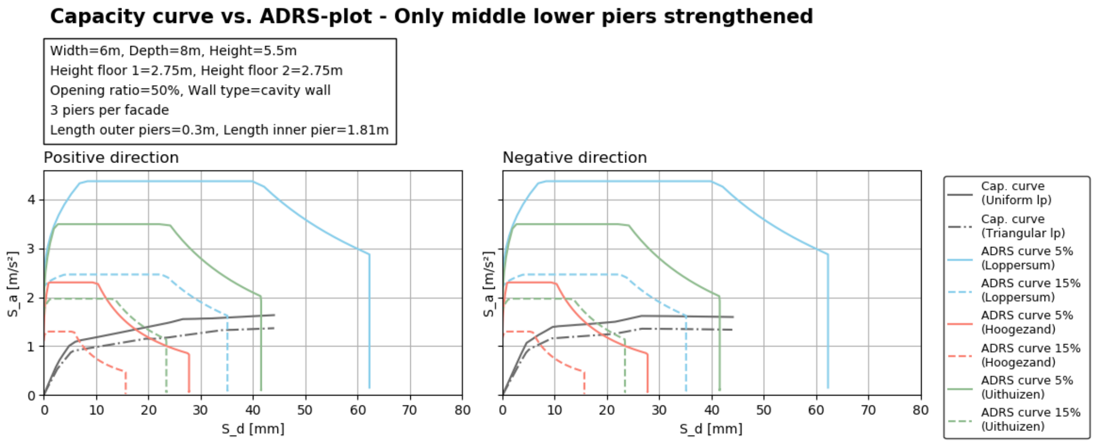

Figure Y.13: Capacity curve of a strengthened model with large middle piers, an inter storey height of 2,75m, width of 6m and a depth of 8m.

Axial loads piers

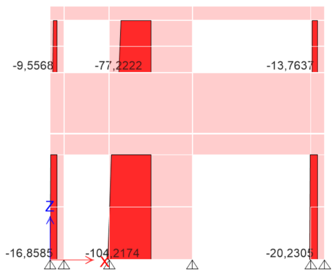

Figure Y.14: Axial forces due to gravity loading

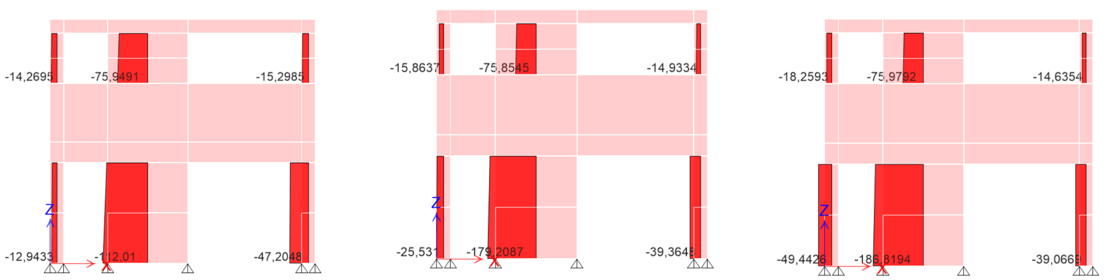

(a) Axial forces at end elastic phase (b) Axial forces at step 72 (c) Axial forces at end of capacity curve

Figure Y.15: Axial forces of piers pushed in positive direction of model with large middle piers

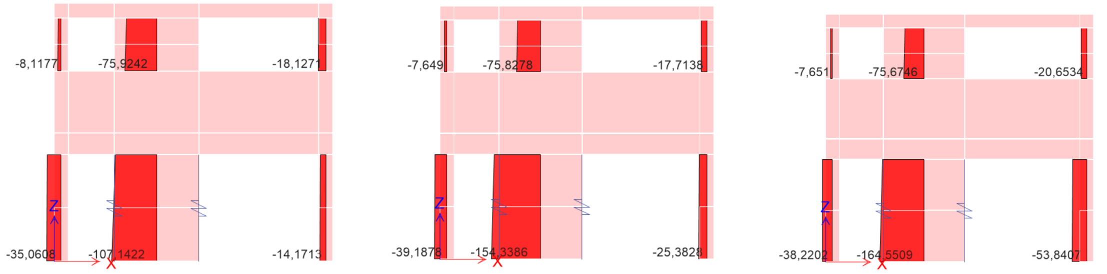

(a) Axial forces at end elastic phase

(b) Axial forces at step 60

(c) Axial forces at end of capacity curve

Figure Y.16: Axial forces of piers pushed in negative direction of model with large middle piers

Shear forces piers

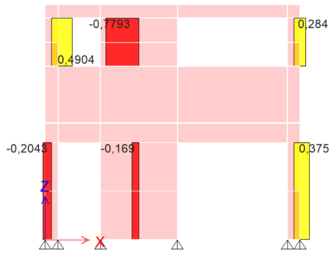

Figure Y.17: Shear forces of piers due to gravity loading

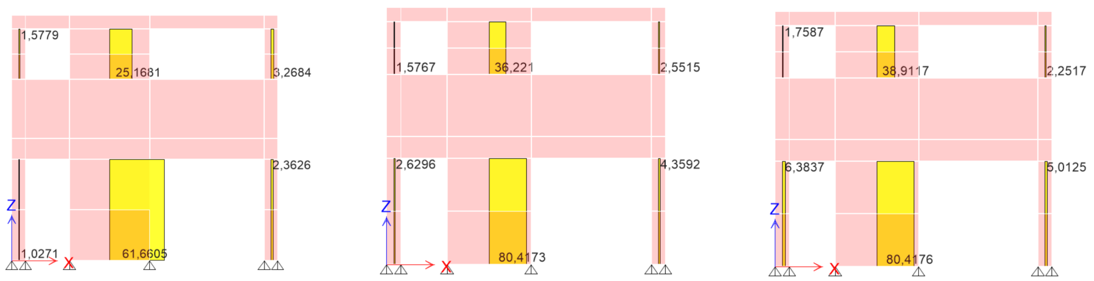

(a) Shear forces at end elastic phase

(b) Shear forces before failure middle piers

(c) Shear forces after failure middle piers

Figure Y.18: Shear forces of piers pushed in positive direction

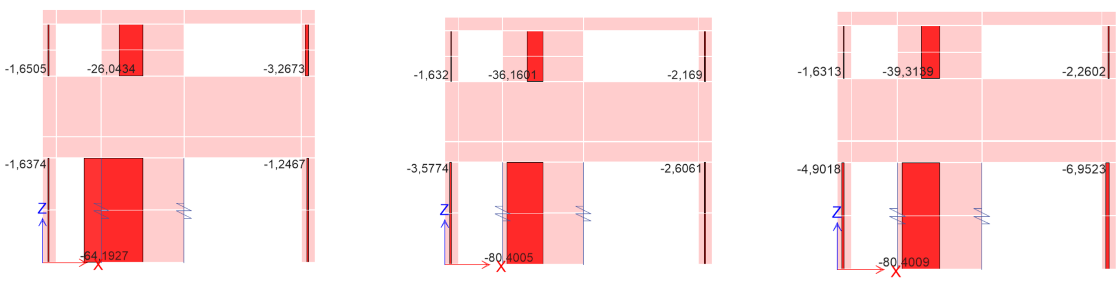

(a) Shear forces at end of elastic phase

(b) Shear forces before failure middle piers

(c) Shear forces after failure middle piers

Figure Y.19: Shear forces of piers pushed in negative direction

Shear forces spandrels

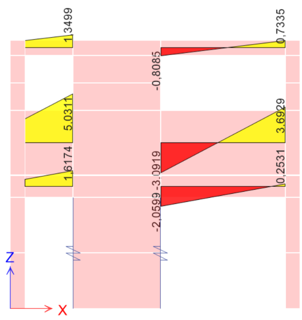

Figure Y.20: Shear forces of spandrels due to gravity loading

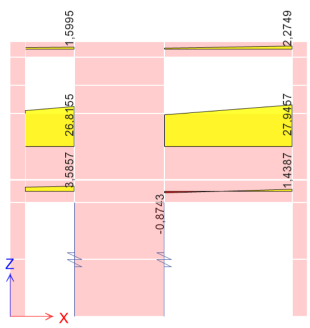

(a) Shear forces of spandrels at end elastic phase

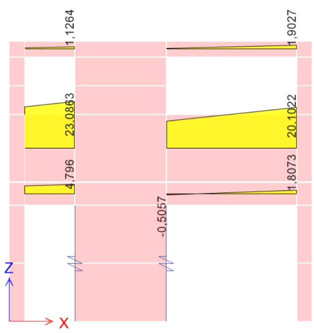

(b) Shear forces of spandrels at step 72 of capacity curve

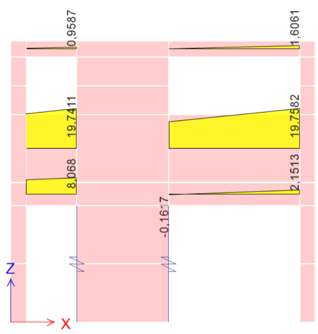

(c) Shear forces of spandrels at end capacity curve

Figure Y.21: Shear forces of spandrels pushed in positive direction

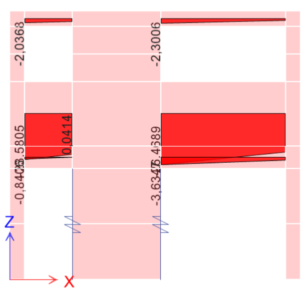

(a) Shear forces of spandrels at end elastic phase

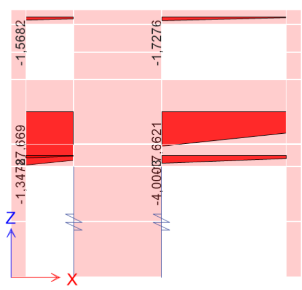

(b) Shear forces of spandrels at step 60

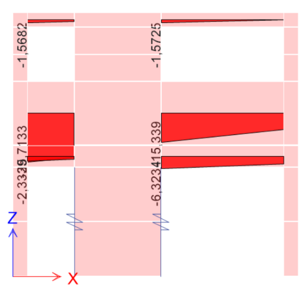

(c) Shear forces of spandrels at end capacity curve

Figure Y.22: Shear forces of spandrels pushed in negative direction

Anchor forces

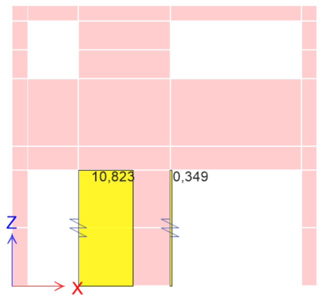

(a) Anchor forces of spandrels at end elastic phase

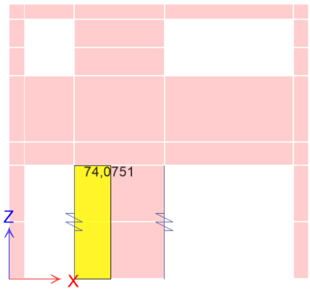

(b) Anchor forces of spandrels at step 72 of capacity curve

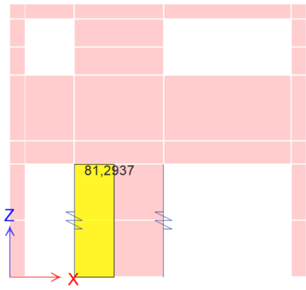

(c) Anchor forces of spandrels at end of capacity curve

Figure Y.23: Anchor forces of spandrels pushed in positive direction

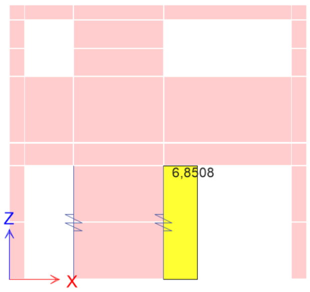

(a) Anchor forces of spandrels at end elastic phase

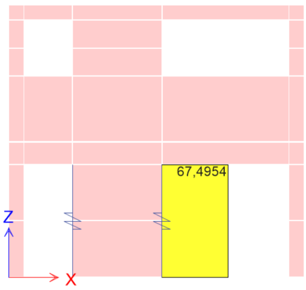

(b) Anchor forces of spandrels at step 72 of capacity curve

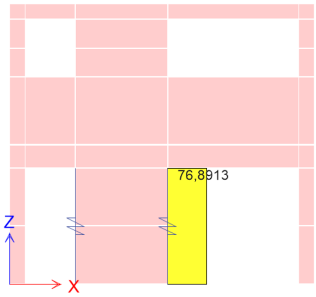

(c) Anchor forces of spandrels at end of capacity curve

Figure Y.24: Anchor forces of spandrels pushed in negative direction

Z. Calculation of timber shear wall behaviour

Timber retrofit applied to wide middle piers

Sheating-to-framing connection configuration

Material properties

OSB				
density	$\rho_{k,1}$	600	kg/m³	
thickness	t_{OSB}	20	mm	
Timber (C24)				
density	$\rho_{k,2}$	420	kg/m³	
thickness	t_{timber}	80	mm	
Nails				
diameter nail	d	4	mm	
head diameter nail	d_h	8	mm	
length	l	75	mm	
tensile strength steel	f_u	600	N/mm²	
type		non predrilled	-	
		round	-	
		non smooth shank	-	

Calculation

penetration depth 1	t_1	20	mm	
penetration depth 2	t_2	55	mm	
min. penetration depth	t_{min}	24	mm	
embedment strength 1 (OSB)	$f_{h,1,k}$	33,23	N/mm²	8.3.1.3(8.22)
embedment strength 2 (Timber)	$f_{h,2,k}$	22,72	N/mm²	8.3.1.1(5)
ratio embedment strength	β	0,68	-	
fastener yield moment	$M_{y,Rk}$	6617	Nmm	8.3.1.1(4)
material factor	$\gamma_{m,con}$	1,3	-	
modification factor OSB	$k_{mod,1}$	0,9	-	
modification factor timber	$k_{mod,2}$	0,9	-	
mean modification factor	k_{mod}	0,9	-	
withdrawal parameter 1	$f_{ax,1,k}$	7,20	N/mm²	8.3.2(4)
withdrawal parameter 2	$f_{ax,2,k}$	3,53	N/mm²	8.3.2(4)
head pullthrough parameter 1	$f_{head,1,k}$	25,20	N/mm²	8.3.2(4)
head pullthrough parameter 2	$f_{head,2,k}$	12,35	N/mm²	8.3.2(4)
axial withdrawal capacity fastener 1	$F_{ax,1,Rk}$	1584	N	
axial withdrawal capacity fastener 2	$F_{ax,2,Rk}$	776	N	
axial withdrawal capacity	$F_{ax,Rk}$	776	N	
Lateral capacity individual fastener (failure mode a)	$F_{v,Rk,a}$	2659	N	8.2.2(1)
Lateral capacity individual fastener (failure mode b)	$F_{v,Rk,b}$	4999	N	8.2.2(1)
Lateral capacity individual fastener (failure mode c)	$F_{v,Rk,c}$	1791	N	8.2.2(1)
	$F_{v,Rk,c2}$	1985	N	8.2.2(2)
Lateral capacity individual fastener (failure mode d)	$F_{v,Rk,d}$	1154	N	8.2.2(1)
	$F_{v,Rk,d2}$	1327	N	8.2.2(2)
Lateral capacity individual fastener (failure mode e)	$F_{v,Rk,e}$	1987	N	8.2.2(1)
	$F_{v,Rk,e2}$	2181	N	8.2.2(2)
Lateral capacity individual fastener (failure mode f)	$F_{v,Rk,f}$	1375	N	8.2.2(1)
	$F_{v,Rk,f2}$	1569	N	8.2.2(2)
Characteristic load-carrying capacity per shear plane per fastener	$F_{f,Rk}$	1327	N	

Figure Z.1: Calculation for the strength of the sheathing-to-framing connection of the timber frame shear wall applied to the lower wide middle piers. Formulas used according to Eurocode 5 [31], see references.

Parameters wall

number of panels		1	-	
number of sheets		1	-	
wall panel width	b_i	1800		
height wall	h	2750	mm	
reference width	b_0	1375	mm	
width ratio	c_i	1,00	-	
fastener spacing	s	50	mm	
width timber framing elements	h_2	70	mm	
thickness of timber framing elements	b_2	80	mm	
Characteristic racking load-carrying capacity of one wall panel	$F_{i,v,Rk}$	57336	N	9.2.3.1(2)
Total racking load-carring capacity	$F_{v,Rk}$	57336	N	
Design racking load-carrying capacity	$F_{v,Rd}$	39694	N	"= F_{04}"

Figure Z.2: Design racking load-carrying capacity of the sheathing-to-framing connection. Formulas used according to Eurocode 5 [31], see references.

Elastic horizontal displacement

General info

height	h_1	2750	mm	
width	b_1	1800	mm	
horizontal force	F	39694	N	"= F_{04}"
distributed load	q	0	N/mm	

Displacement due to sheathing-to-framing fastener

panel dimension ratio	α	1,53	-
parameter	η	0,93	-
parameter	ξ	1,91	-
shape function	λ	3,64	-
fastener spacing	s_c	50	mm
elastic stiffness of each fastener	k_c	1137	N/mm
displacement	Δ_{sh}	3,62	mm

Displacement due to rigid-body rotation

hold down stiffness	k_h	13250	N/mm
vertical elongation	v	4,6	mm
rotation angle	γ	0,003	-
horizontal displacement	Δ_h	7,0	mm

Displacement due to sheating panel shear deformation

shear modulus of panel	G_p	1080	N/mm²
panel thickness	t_p	20	mm
number of panels	n_{bs}	1	-
shear deformation	ζ	0,001021	
displacement	Δ_p	2,81	mm

Displacement due to rigid-body translation

stifness of angle brackets	ka	26093	N/mm
number of angle brackets	na	0	-
displacement	Δ_a	0,00	mm

Total horizontal elastic displacement

	$\Delta_{tot,el}$	13,4	mm

Figure Z.3: Total elastic horizontal displacement of the applied timber frame shear wall according to research by Casagrande et al. [32], see formulas of Appendix T

Backbone curve input ETABS

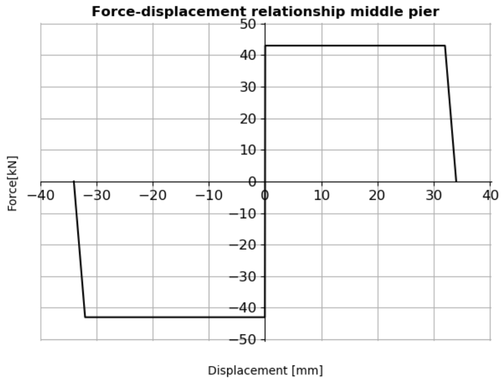

(a) Force-displacement relationship of large middle masonry piers governed by shear behaviour according to the NPR 9998:2018.

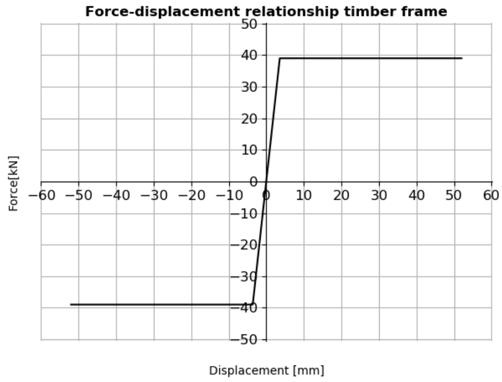

(b) Idealised backbone curve of a timber frame shear wall with configuration as calculated in Figure Z.1, based on Eurocode 5 [31]

Figure Z.4: Idealised force-displacement relationships of both masonry and timber walls.

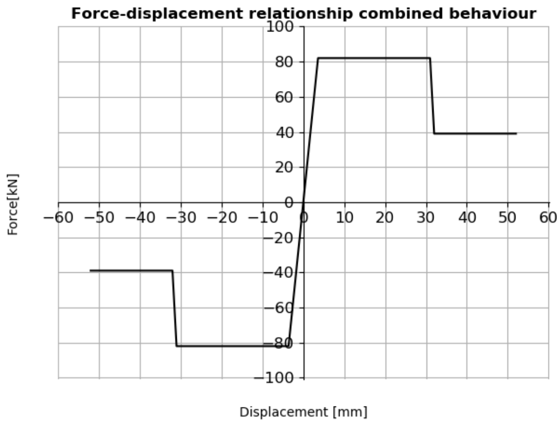

Figure Z.5: Proposed idealised combined masonry-timber shear behaviour for strengthened large middle pier, as input for ETABS.

Timber retrofit applied to model with CaSi element masonry

Sheating-to-framing connection configuration

Material properties

OSB				
density	$\rho_{k,1}$	600	kg/m³	
thickness	t_{OSB}	18	mm	
Timber (C24)				
density	$\rho_{k,2}$	420	kg/m³	
thickness	t_{timber}	70	mm	
Nails				
diameter nail	d	3,1	mm	
head diameter nail	d_h	6	mm	
length	l	70	mm	
tensile strength steel	f_u	600	N/mm²	
type		non predrilled	-	
		round	-	
		non smooth shank	-	

Calculation

penetration depth 1	t_1	18	mm	
penetration depth 2	t_2	52	mm	
min. penetration depth	t_{min}	18,6	mm	
embedment strength 1 (OSB)	$f_{h,1,k}$	39,31	N/mm²	8.3.1.3(8.22)
embedment strength 2 (Timber)	$f_{h,2,k}$	24,53	N/mm²	8.3.1.1(5)
ratio embedment strength	β	0,62	-	
fastener yield moment	$M_{y,Rk}$	3410	Nmm	8.3.1.1(4)
material factor	$\gamma_{m,con}$	1,3	-	
modification factor OSB	$k_{mod,1}$	0,9	-	
modification factor timber	$k_{mod,2}$	0,9	-	
mean modification factor	k_{mod}	0,9	-	
withdrawal parameter 1	$f_{ax,1,k}$	7,20	N/mm²	8.3.2(4)
withdrawal parameter 2	$f_{ax,2,k}$	3,53	N/mm²	8.3.2(4)
head pullthrough parameter 1	$f_{head,1,k}$	25,20	N/mm²	8.3.2(4)
head pullthrough parameter 2	$f_{head,2,k}$	12,35	N/mm²	8.3.2(4)
axial withdrawal capacity fastener 1	$F_{ax,1,Rk}$	907	N	
axial withdrawal capacity fastener 2	$F_{ax,2,Rk}$	445	N	
axial withdrawal capacity	$F_{ax,Rk}$	445	N	
Lateral capacity individual fastener (failure mode a)	$F_{v,Rk,a}$	2193	N	8.2.2(1)
Lateral capacity individual fastener (failure mode b)	$F_{v,Rk,b}$	3954	N	8.2.2(1)
Lateral capacity individual fastener (failure mode c)	$F_{v,Rk,c}$	1436	N	8.2.2(1)
	$F_{v,Rk,c2}$	1547	N	8.2.2(2)
Lateral capacity individual fastener (failure mode d)	$F_{v,Rk,d}$	866	N	8.2.2(1)
	$F_{v,Rk,d2}$	977	N	8.2.2(2)
Lateral capacity individual fastener (failure mode e)	$F_{v,Rk,e}$	1557	N	8.2.2(1)
	$F_{v,Rk,e2}$	1668	N	8.2.2(2)
Lateral capacity individual fastener (failure mode f)	$F_{v,Rk,f}$	919	N	8.2.2(1)
	$F_{v,Rk,f2}$	1030	N	8.2.2(2)
Characteristic load-carrying capacity per shear plane per fastener	$F_{f,Rk}$	977	N	

Figure Z.6: Calculation for the strength of the sheathing-to-framing connection of the timber frame shear wall applied to a model with CaSi element masonry. Formulas used according to Eurocode 5 [31], see references.

Parameters wall

number of panels		1	-	
number of sheets		1	-	
wall panel width	b_i	700		
height wall	h	2750	mm	
reference width	b_0	1375	mm	
width ratio	c_i	0,51	-	
fastener spacing	s	50	mm	
width timber framing elements	h_2	70	mm	
thickness of timber framing elements	b_2	80	mm	
Characteristic racking load-carrying capacity of one wall panel	$F_{i,v,Rk}$	8353	N	9.2.3.1(2)
Total racking load-carring capacity	$F_{v,Rk}$	8353	N	
Design racking load-carrying capacity	$F_{v,Rd}$	5783	N	"= F_{04}"

Figure Z.7: Design racking load-carrying capacity of the sheathing-to-framing connection. Formulas used according to Eurocode 5 [31], see references.

Elastic horizontal displacement

General info

height	h_1	2750	mm	
width	b_1	700	mm	
horizontal force	F	5783	N	"= F_{04}"
distributed load	q	0	N/mm	

Displacement due to sheathing-to-framing fastener

panel dimension ratio	α	3,93	-
parameter	η	2,13	-
parameter	ξ	20,35	-
shape function	λ	8,08	-
fastener spacing	s_c	50	mm
elastic stiffness of each fastener	k_c	927	N/mm
displacement	Δsh	3,57	mm

Displacement due to rigid-body rotation

hold down stiffness	k_h	13250	N/mm
vertical elongation	v	1,7	mm
rotation angle	γ	0,002	-
horizontal displacement	Δh	6,7	mm

Displacement due to sheating panel shear deformation

shear modulus of panel	G_p	1080	N/mm²
panel thickness	t_p	18	mm
number of panels	n_{bs}	1	-
shear deformation	ζ	0,00042	
displacement	Δp	1,17	mm

Displacement due to rigid-body translation

stifness of angle brackets	ka	26093	N/mm
number of angle brackets	na	0	-
displacement	Δa	0,00	mm

Total horizontal elastic displacement

	$\Delta_{tot,el}$	11,5	mm

Figure Z.8: Total elastic horizontal displacement of the applied timber frame shear wall according to research by Casagrande et al. [32], see formulas of Appendix T

Backbone curve input ETABS

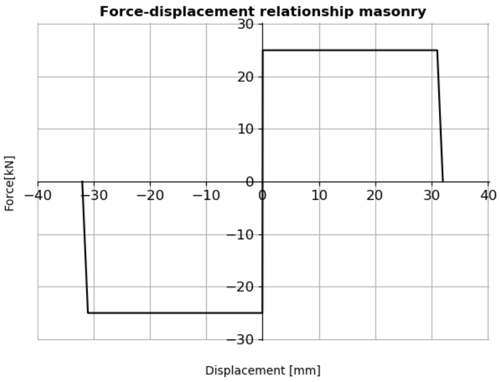

(a) Force-displacement relationship of masonry piers of model with CaSi element masonry.

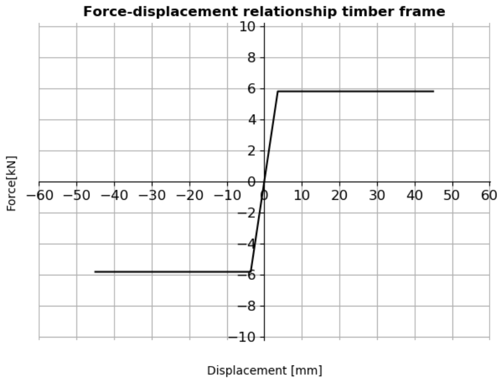

(b) Idealised backbone curve of a timber frame shear wall with configuration as calculated in Figure Z.6, based on Eurocode 5 [31]

Figure Z.9: Idealised force-displacement relationships of both masonry and timber walls.

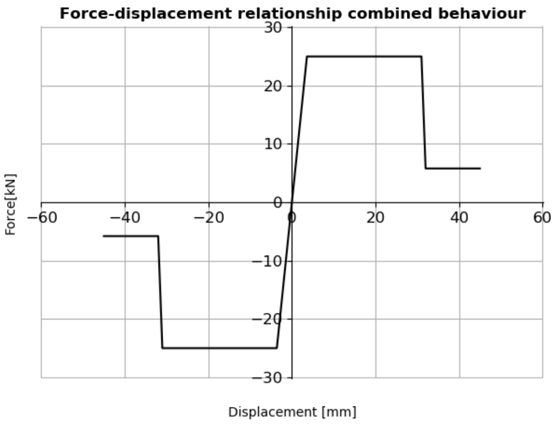

Figure Z.10: Proposed idealised combined masonry-timber shear behaviour for strengthened masonry piers of model with CaSi element, as input for ETABS.